Characterization of Neuromuscular Communication in the *C. elegans* Pharynx During Feeding

BY

ALENA KOZLOVA

B.S., Moscow State University, 2008

THESIS

Submitted as a partial fulfillment of the requirements
for the degree of Doctor of Philosophy in Biological Sciences
in the Graduate College of the
University of Illinois at Chicago, 2017

Chicago, Illinois

Defense Committee:

Teresa Orenic, Chair

Peter Okkema, Advisor

Janet Richmond

Ankur Saxena

Michael Ragozzino, Psychology

AKNOWLEDGEMENTS

First, I would like to thank my thesis advisor Peter Okkema for his continuous support, guidance, encouragement and inspiration over the years. Pete is an excellent scientist and dedicated mentor. He always has time to help and answer questions. I will always appreciate his patience, attention and interest towards research. His support and guidance was critical in helping me complete this dissertation.

I would like to that the members of my thesis committee: Teresa Orenic, Janet Richmond, Ankur Saxena and Michael Ragozzino for their time, advice and suggestions over the years.

I would like to thank the past and present members of the Okkema laboratory: Tom Ronan, Kalpana Ramakrishnan, Paul Huber and Angenee Milton for their friendship, ideas and advice. Their friendship provided a great work environment, which helped me to develop as a scientist.

I also want to thank all the members of Alfonso laboratory for providing ideas and suggestions for research. In addition, I would like to acknowledge the worm community for providing us strains and plasmids.

Finally, I want to thank my family for endless support, positive energy and enthusiasm that allowed me to finish my PhD. I want to thank my brother Denis for the encouragement and great ideas. I want especially thank my mother and father for their unconditional love and inspiration. I could never have succeeded without them.

TABLE OF CONTENTS

LIST OF TABLES

LIST OF FIGURES

LIST OF FIGURES (continued)

LIST OF ABBREVIATIONS

ACh	Acetylcholine
bp	base pairs
Ca^{2+}	calcium ions
cDNA	complimentary DNA
Co-IP	coimmunoprecipitation
cuEx	Extrachromosomal array generated in Okkema Lab
cuIs	Integrated transgenic strain generated in Okkema Lab
DIC	Differential Interference Contrast
DNA	Deoxyribonucleic acid
GECI	Genetically encoded calcium indicator
Gfp/GFP	green fluorescent protein
F1	First generation progeny in genetic cross
F2	Second generation progeny in genetic cross
F3	Third generation progeny in genetic cross
F4	Fourth generation progeny in genetic cross
L1-L4	Larval development stages in *C. elegans*
M	Molar
mg	milligram
ml	milliliter
mM	millimolar
mRNA	messenger RNA
ng	nanogram
OP50	*E. coli* strain
NGM	Nematode growth medium
PABP	poly(A) binding protein
PCR	Polymerase chain reaction
PO	Oligo nucleotides designed in Okkema Lab
pOK	Plasmid generated in Okkema Lab
RNA	Ribonucleic acid
RNAi	RNA mediated interference
rpm	revolutions per minute
rRNA	ribosomal RNA
°C	Degree Celsius

SUMMARY

Communication between motor neurons and their target muscles is crucial for proper muscle contraction and function. This communication is mediated by the neurotransmitter acetylcholine, which is released from the motor neuron and binds receptors embedded in the muscle cell membrane. Acetylcholine stimulates two very different types of contractions in adjacent muscle cells in the *C. elegans* pharynx, called pumping and peristalsis. The signaling mechanisms that stimulate pumping have been characterized, but we do not know how these mechanisms affect peristalsis. Here we used time-lapse imaging to examine muscle contractions and Ca^{2+} transients during peristalsis in wild-type animals and various mutants affecting acetylcholine signaling. We reported the surprising result that, while mutants affecting the *eat-2* nicotinic acetylcholine receptor exhibited reduced pumping, they also had hyperstimulated peristalses. This hyperstimulation depends on crosstalk with a muscarinic acetylcholine receptor, and we suggest crosstalk results from acetylcholine spillover from synapses that normally stimulate pumping to receptors in adjacent cells. This crosstalk underlies feeding defects in a nicotinic acetylcholine receptor mutant and contributes to the dietary restriction and extended adult lifespan observed in these animals.

The NK-2 family homeobox transcription factor CEH-28 is expressed exclusively in the M4 motor neuron. Mutants affecting *ceh-28* exhibit a loss of M4 polarity and defects in synapse morphology. Instead of having synapses only in the posterior isthmus, M4 forms abnormally sized and spaced synapses throughout the entire isthmus in *ceh-28* mutants. Here, we examined M4 activity and found that in wild-type animals Ca^{2+} transients were larger in the posterior part of the M4 where it forms synapses with isthmus muscles. In contrast, in *ceh-28* mutants Ca^{2+} transients were low and uniform along the entire length of M4. We also looked at Ca^{2+} transients in the pharyngeal isthmus muscles and found that *ceh-28* mutants have lower Ca^{2+} signals than wild-type animals. This indicates that function of M4 and the isthmus muscles is impaired in *ceh-28* mutants. We suggest that in *ceh-28* mutants abnormal morphology and

synaptic organization of the M4 motor neuron results in the reduced M4 activity and reduced function of the isthmus muscles, which eventually lead to the “stuffed pharynx” phenotype.

In conclusion, these studies provide a much more complete understanding of the neuromuscular communication between a motor neuron and a muscle cell, and consequences of signaling defects at the neuromuscular junction. These studies also describe powerful imaging tools for quantitative analyses of the neuronal and the pharyngeal muscle activity during peristalsis.

1 INTRODUCTION

1.1 Background

Signaling from a neuron to a muscle cell is essential for proper muscle contraction and the normal function of an entire organism. Neuromuscular communication occurs at structures called synapses, which play an important role in sending a message from the nervous system to the muscle cells.

Motor neurons are a special class of neurons within the nervous system, which are responsible for communicating with muscle cells via synapses. These neurons stimulate muscle contraction by releasing appropriate amounts of signaling molecules called neurotransmitters. Failure of motor neurons to function and communicate with muscle cells can lead to neurodegenerative disorders such as Amyotrophic lateral sclerosis (Wijesekera and Leigh, 2009), Huntington disease (Walker et al., 2007), as well as neuromuscular disease, such as myasthenia gravis (reviewed in (Gilhus, 2016)), and congenital myasthenic syndromes (Conti-Fine et al., 2006; Engel et al., 2015). Understanding the mechanisms of neurodegenerative and neuromuscular disorders is crucial to identifying better ways to treat these diseases.

Investigating the mechanisms for neuromuscular communication will help not only understand pathogenesis of the above mentioned disorders but may provide valuable insights regarding how motor neurons signal in the nervous system and how target muscles respond to this signaling in organisms with more complex nervous systems. Analyzing mechanisms that govern communication between neurons and muscles cells is a challenging task because of the complexity of the nervous system. The focus of this study is to understand mechanisms of neuromuscular communication in the *C. elegans* pharynx during feeding.

1.2 *C. elegans* as a great model to study neuromuscular communication

1.2.1 Overview of *C. elegans* nervous system

The nervous system of an adult *C. elegans* hermaphrodite is a very compact but complex organ (Hobert, 2005). It consists of 302 neurons and 56 glial cells, which makes the

nervous system an organ with the most cells. These neurons are part of two nervous systems: the somatic nervous system of 282 neurons and the much smaller pharyngeal nervous system of 20 neurons. The neurons of the nervous system are assigned to 118 different classes based on their topology and the connections they make through the synapses (Sulston and Horvitz, 1977; Sulston et al., 1983; White et al., 1986). Communication between neurons occurs via chemical synapses (6,400), gap junctions (900), and neuromuscular junctions (1,500).

The *C. elegans* nervous system is not only responsible for basic behaviors such as locomotion, feeding and defecation (de Bono and Maricq, 2005), but it allows animals to discriminate and move towards chemicals, odorants, food sources and detect the presence of other nematodes by pheromones (Golden and Riddle, 1982).

Depending on their circuitry, *C. elegans* neurons can be divided into four functional groups. The first group is motor neurons, which form synapses with muscle cells. Among 302 neurons in *C. elegans*, 113 belong to the group of motor neurons, which control movement such as crawling and swimming (White et al., 1976, 1986). The second group includes sensory neurons, which allow animals to sense chemical, thermal and oxygen gradients and move towards favorable surroundings. The third group is interneurons, which receive signals from upstream neurons and send them to other neurons. The fourth group includes polymodal neurons, which perform more than one type of circuit function (Bargmann, 2006; Bergamasco and Bazzicalupo, 2006; Chen et al., 2006; Hall et al., 2006).

C. elegans neuron shares similar functional organization with a vertebrate neuron. A typical neuron in vertebrates consists of a cell body (soma), dendrites and axons. The signal is usually received by dendrites from other neurons and then transported down the axon to the axonal terminal from where it is transmitted to another cell. In *C. elegans,* some neurons only have sensory functions and act as dendrites. Other neurons only send outputs (processes) and act as axons. Most of the neurons have mixed functions and can both receive and transmit a

signal. The cell bodies of most neurons in *C. elegans* are organized into ganglia, which contain cell clusters but few or no synapses (Hall et al., 2006; White et al., 1986).

1.2.2 Synapses – structure and function

Synapses are functional connections between two cells (neuron-neuron or neuron-muscle) through which "information" flows from one cell to another cell (Fatt, 1954; Katz, 2003). This "information" can be passed via either electrical or chemical signals. One neuron can form anywhere from a few to many thousands of synapses. At the synapse, the membrane of the presynaptic cell (sends a signal) connects with a target post-synaptic cell (receives a signal). The presynaptic part is localized on the axon and the postsynaptic part is found on a dendrite or soma.

There are two different types of synapses, electrical and chemical synapses. At the chemical synapse, a neuron releases neurotransmitter into the space between two cells, which is called the synaptic cleft. The neurotransmitter is packed inside synaptic vesicles (SVs) in the presynaptic cell and during neurotransmission is released in to the synaptic cleft via exocytosis. On the postsynaptic cell, neurotransmitter binds to the receptors resulting in a signal transduction. In some cases, the remaining neurotransmitter molecules are degraded by enzymes in the synaptic cleft or transported back in to the presynaptic cell (Johnson and Russell, 1983).

In *C. elegans*, chemical synapses occur between presynaptic and one or more postsynaptic cells. One of the postsynaptic cells may be a muscle cell. These synapses are made *en passant* ("in passing" from French) between two processes and characterized by the presence of an electron-dense presynaptic density approximately 50nm wide and 100-400 nm long. SVs are found near this density and form the "active zone" (Nakata et al., 2005; Rostaing et al., 2004; Weimer and Jorgensen, 2003; Zhen and Jin, 2004). The presynaptic region can vary in size even within the same neuron (Jin, 2005). Post-synaptic processes have post-synaptic receptor clusters very close to pre-synaptic release zone (Gally et al., 2004; Jin, 2005).

At the chemical synapses in *C. elegans*, a neuron releases monoamines, acetylcholine (ACh), gamma-aminobutyric acid (GABA) or glutamate, which are similar to neurotransmitters in other organisms used during rapid neurotransmission. There are usually 10 to 100 synaptic vesicles ready to be released. Docked vesicles are tightly attached to the presynaptic membrane within 75 nm from a presynaptic density. Precursor vesicles are produced in the cell body of the neuron before they are transported down the axon (Hall and Hedgecock, 1991). In addition to these neurotransmitters, there are more than 150 neuropeptides in *C. elegans* that are believed to modulate synaptic function and rapid neurotransmission through gated ion channels (Richmond and Broadie, 2002).

Neuromuscular junctions (NMJs) are the specialized chemical synapses where "information" flows from a neuron to a muscle cell. In *C. elegans*, body wall muscles extend long and thin processes, called arms, to make synapses with the motor neurons. Several muscle arms can form a "muscle plate" resulting in simultaneous stimulation of more than one muscle by vesicle release from a single axon (White et al., 1976, 1986). In contrast, pharyngeal muscles do not form arms, and presynaptic processes are embedded in the muscle soma. Electrical synapses (gap junctions) are generated by close contact between cells. In *C. elegans,* all tissues have gap junctions, and there are approximately 900 gap junctions in the nervous system. They are found between two neurons or two muscle cells. Gap junctions in *C. elegans* are formed by proteins called "innexins", which are orthologous to vertebrate "pannexins" (Altun et al., 2009; Phelan and Starich, 2001; Starich et al., 1996). Innexins may form homotypic, heterotypic and heteromeric gap junctions. Gap junctions function to synchronize neuronal activity, cross inhibit neighboring axons, transmit metabolic signals, synchronize neuron and muscle activities such as action potentials, calcium transients in the neurons and in the muscle cells, mediate electrical coupling for synchronous pharyngeal muscle contraction (Chuang et al., 2007; Li et al., 2003; Liu et al., 2011; Peters et al., 2007; White et al., 1986).

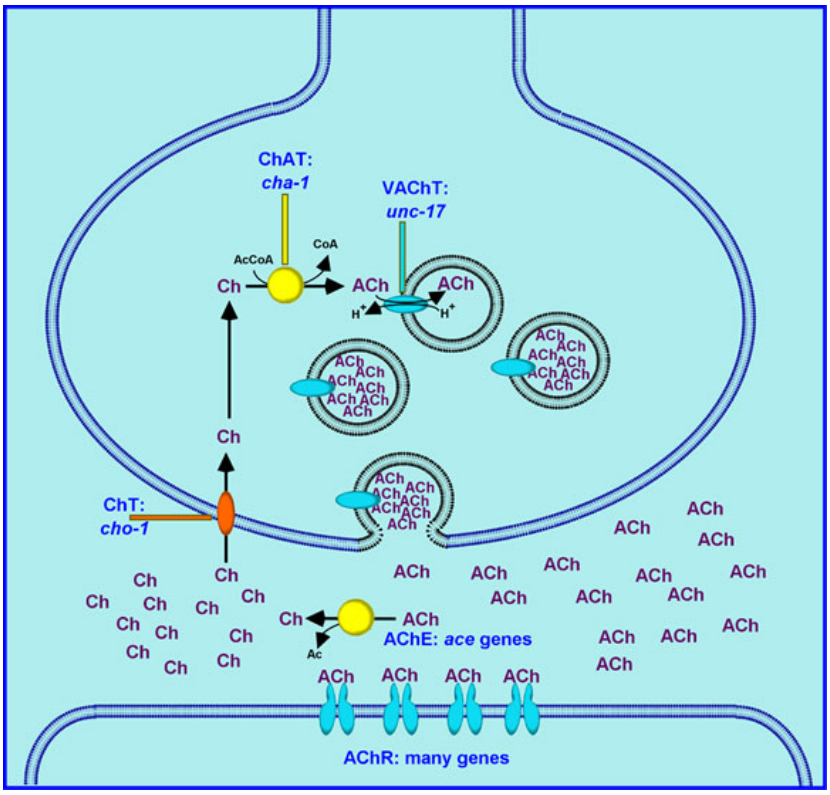

Figure 1 Synthesis of acetylcholine, cholinergic enzymes and transporters

Synthesis of ACh is catalyzed by choline acetyltransferase and involves acetylation of choline by acetyl-Coenzyme A. VAChT helps to package ACh into the synaptic vesicles. ACh then is released into the synaptic cleft, where it diffuses and binds to the AChRs located on the post synaptic membrane. Acetylcholinesterase terminates the action of ACh by hydrolyzing ACh into the choline and acetate. Choline is then transported back to the presynaptic cell where it is used for ACh synthesis. This figure is adapted from WormBook http://www.wormbook.org/chapters/www_acetylcholine/acetylcholine.html.

1.2.3 Acetylcholine as a major neurotransmitter at the neuromuscular junctions in *C. elegans*

ACh is used as a signaling molecule to transmit a signal by almost a half of the neurons in *C. elegans* (Pereira et al., 2015). The first neurotransmitter discovered was ACh, which was identified in *Ascaris* by Helen Mellanby (Mellanby, 1955). Choline acetyltransferase (ChAT) catalyzes the acetylation of choline by acetyl-Coenzyme A (Figure 1) (Rand and Russell, 1985). ACh is then packaged into the synaptic vesicles with the help of the vesicular acetylcholine transporter (VAChT), which is encoded by the *unc-17* gene (Alfonso et al., 1993). After being released into the synaptic cleft ACh diffuses and binds to the acetylcholine receptors (AChRs) located on the post synaptic membrane. Acetylcholinesterase terminates the action of ACh by hydrolyzing ACh into the choline and acetate (Johnson and Russell, 1983). Choline is then transported back to the presynaptic cell where it is used for ACh synthesis.

1.3 Pharyngeal structure and anatomy

1.3.1 Overview of the *C. elegans* pharynx

The pharynx is a bilobed tubular neuromuscular pump located in the head of the animal (Albertson and Thomson, 1976; Avery and Horvitz, 1989). It can be divided into the following parts: buccal cavity, procorpus, metacorpus (anterior bulb), isthmus, terminal bulb and pharyngeal-intestinal valve (Figure 2). There are 80 nuclei identified within the pharynx, which belong to seven types of pharyngeal cells: arcade cells, muscles, epithelia, neurons, glands, marginal cells and valves (Table I) (Albertson and Thomson, 1976; Sulston et al., 1983). Pharyngeal muscles and marginal cells have three-fold symmetry around the pharyngeal lumen (Figure 3B). There are eight types of pharyngeal muscle cells (pm1-pm8) and three types of marginal cells (mc1-mc3), which have characteristics of epithelia (Figure 3A). pm8 connects the pharynx to the intestine via pharyngeal intestinal valve posteriorly, and nine arcade cells connect the pharynx to the buccal cavity anteriorly. Five gland cells and twenty neurons are

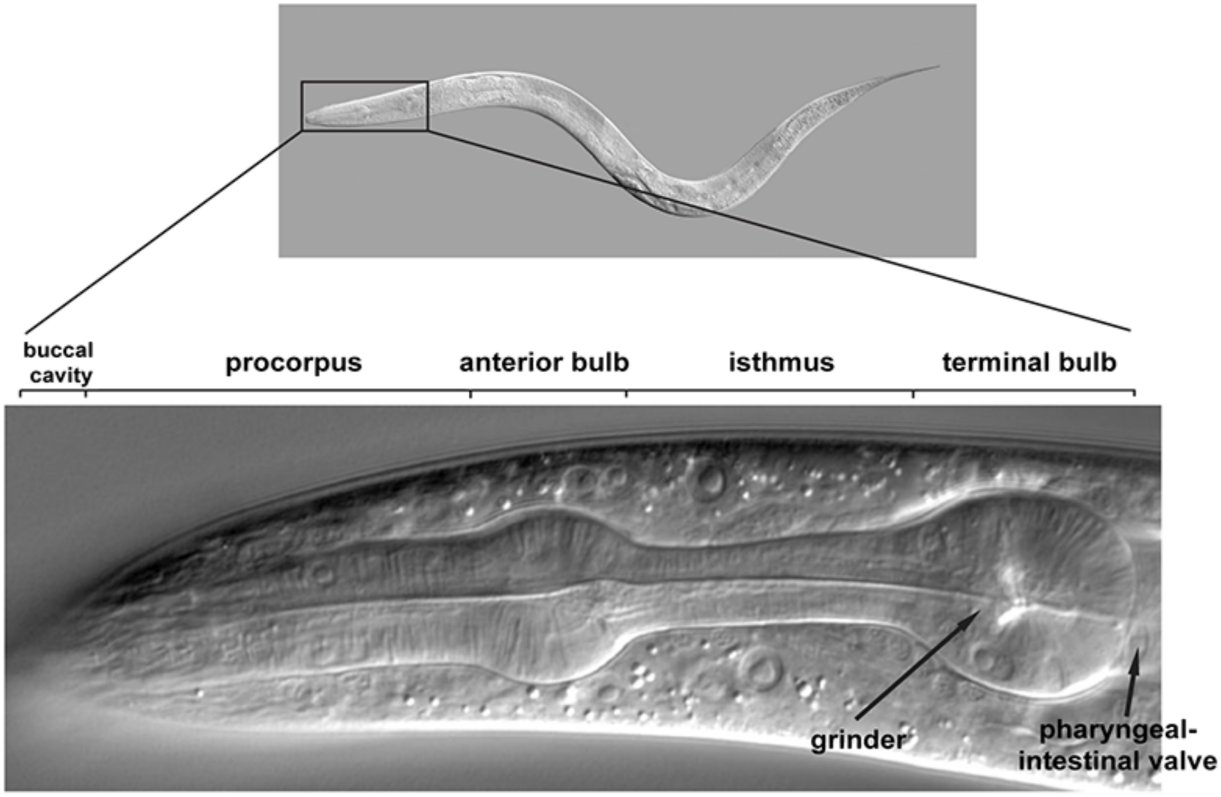

Figure 2 Morphology of the *C.elegans* pharynx

DIC images of the whole animal and the *C. elegans* pharynx. The top image shows a whole worm with the pharynx in the boxed region. The bottom image represents regions of the pharynx: buccal cavity, procorpus, anterior bulb (metacorpus), isthmus, terminal bulb and pharyngeal-intestinal valve. Anterior is to the left.

Table I: Number of cells and nuclei in the *C.elegans* pharynx

Cell type	Cells	Nuclei
muscles	20	37
neurons	20	20
glands	4	5
epithelial cells	9	9
marginal cells	7	9
Total	**60**	**80**

Table represents number of cells and number of nuclei of a particular cell type within the *C. elegans* pharynx.

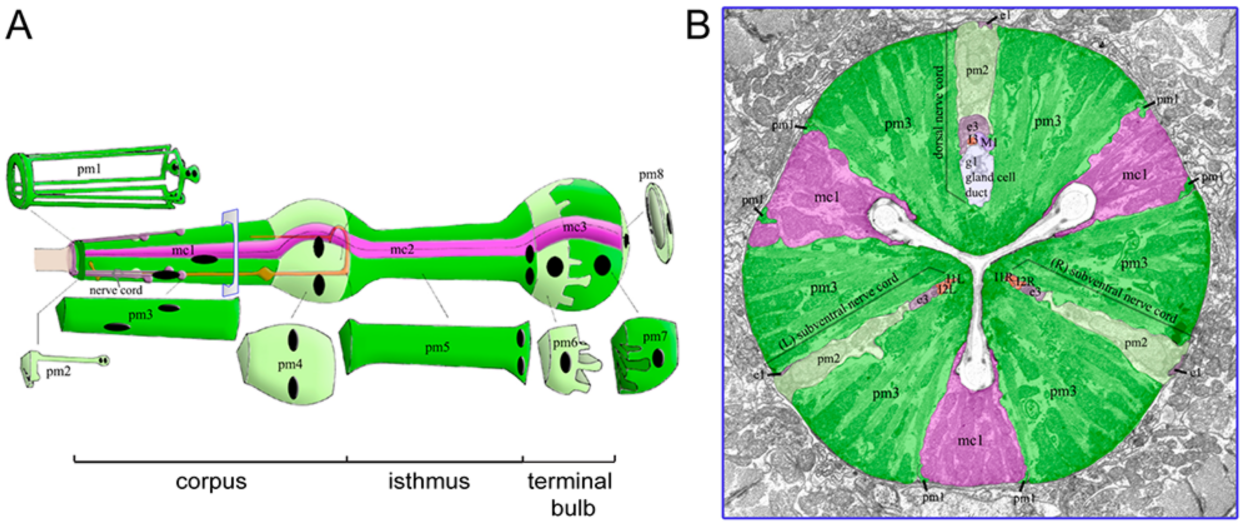

Figure 3 Anatomy of the *C. elegans* pharyngeal muscles

Schematic illustration of the *C.elegans* pharynx (left) and a micrograph of a TEM cross section (right). Pharyngeal muscles (pm1-pm8) are represented in green, marginal cells (mc1-mc3) in pink and muscle nuclei in black. Pharyngeal muscle cells and marginal cells are arranged around the circumference of the pharynx with a three-fold rotational symmetry as depicted in the cross section mid-way through the procorpus. This figure is adapted from WormBook (http://www.wormbook.org/chapters/www_organformation/organformation.html). WormBook content is licensed under a Creative Commons Attribution License https://creativecommons.org/licenses/by/2.5/.

located in clefts formed in the pharyngeal muscles cells. The cuticle lines the pharyngeal lumen and is continuous with body cuticle. The isthmus is a region of the pharynx, which connects the anterior bulb to the posterior bulb. The isthmus is composed of three pm5 cells, which extend throughout the entire isthmus region. The isthmus controls food transport from the corpus to the terminal bulb (Albertson and Thomson, 1976).

1.3.2 The pharyngeal nervous system

The pharyngeal nervous system includes 20 neurons, which are positioned entirely within the pharynx. There are five classes of motor neurons (M1, M2, M3, M4, M5), six classes of interneurons (I1, I2, I3, I4, I5, I6) and three classes are classified as other neurons (MI, NSM, MC) (Albertson and Thomson, 1976). Six neuron classes consist of two bilaterally symmetric cells, while others include single cells. Most of the neurons have their cell bodies located in one of the pharyngeal bulbs extending processes posteriorly and/or anteriorly along the pharynx in clefts within the pharyngeal muscles. Pharyngeal neurons do not have “synaptic terminals”, but instead form *en passant* synapses, which occur along the length of the neuron (White et al., 1976). The processes interact with other processes via synapses. The pharyngeal motor neurons also make synapses with pharyngeal muscle cells forming NMJs (Albertson and Thomson, 1976; Avery and Thomas, 1997).

The pharyngeal nervous system receives two inputs. The first input is external, somatic pharyngeal innervation through a pair of gap junctions between pharyngeal I1 neurons and extrapharyngeal RIP neurons. The other input is internal via mechanoreception by some of the pharyngeal neurons, which have free endings just under the pharyngeal cuticle of the pharyngeal lumen (Albertson and Thomson, 1976). The extrapharyngeal and pharyngeal nervous systems can function without interaction. A dissected pharynx retains its behavioral and electrophysiological characteristics. (Avery et al., 1995). Similarly, when 19 nonessential pharyngeal neurons are killed, the extrapharyngeal nervous system is not strongly affected (Avery and Horvitz, 1989).

Motor neuron M1 innervates the procorpus by making synapses on the pm1, pm2 and pm3. The pair of motor neurons M2 make synapses on pm4 and pm5. The M3 and MC motor neurons innervate pm4. The single cell motor neuron M4 forms NMJs with only pm5 in the isthmus. The M5 motor neuron innervates pm6 and pm7 in the terminal bulb (Albertson and Thomson, 1976).

The M3, M4 and MC motor neurons are necessary and sufficient for normal feeding. When all the pharyngeal neurons are ablated except these three, pharyngeal feeding is nearly normal. (Avery, 1993b; Raizen et al., 1995). Only the M4 pharyngeal motor neuron is necessary for viability, as animals with ablated M4 cannot feed and die of starvation (Avery and Horvitz, 1987).

1.4 There are two types of pharyngeal muscle contractions

Feeding is essential for life. It requires both proper development of the pharynx and its function. The *C. elegans* pharynx is a tubular organ, which is responsible for accumulating bacteria from outside, and subsequently concentrating and grinding them (Doncaster, 1962; Seymour et al., 1983). Pumping and peristalsis are two different feeding motions in *C. elegans* (Figure 4) (Albertson and Thomson, 1976; Avery and Horvitz, 1989).

1.4.1 Pharyngeal pumping

During a pump, muscles of the corpus and anterior isthmus simultaneously contract and then relax (Figure 4A, B). The liquid with suspended bacteria flows in and fills the lumen while the isthmus stays closed. At the same time, the muscles of terminal bulb contract and relax to grind the bacteria and pass debris into the intestine. Because the myofilaments in the pharyngeal muscle cells are radially oriented, pumping pulls the lumen open from its closed Y-shape to a triangular shape. Relaxation of the muscle of the corpus and anterior isthmus closes the lumen. Liquid is expelled from the lumen and the bacteria are trapped. A thick, rigid cuticle secreted by pm6 and pm7 muscle cells on their luminal surfaces forms the grinder in the

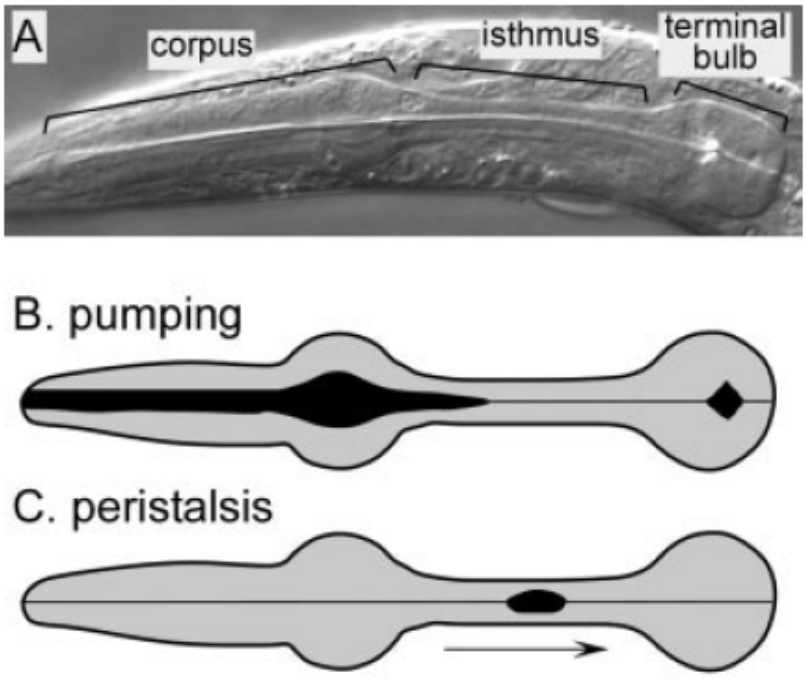

Figure 4 Pharyngeal muscle contractions

Representation of the pharyngeal muscle contraction during pumping and peristalsis. (A) DIC micrograph of the pharynx with corpus, isthmus and terminal bulb indicated. (B) Pharyngeal muscle contraction during a pump, which results in accumulation of food in the corpus and anterior isthmus. The open lumen is shown by the black regions. (C) Pharyngeal muscle contraction during a peristalsis, which transports food from anterior to the posterior isthmus. This figure is adapted from (Ray et al., 2008).

terminal bulb. The grinder has three segments, which are rotated during muscle contraction. Food is trapped between the segments, ground and passes to the intestine through the pharyngeal-intestinal valve. Relaxation of the muscles of the terminal bulb returns the grinder to its resting position (Doncaster, 1962). Pumping is very frequent event, and occurs on average 200 pumps/min (Avery and Horvitz, 1987).

1.4.2 Pharyngeal peristalsis

Isthmus peristalsis is the second feeding motion, which follows immediately after a pump, but does not occur after every pump (Figure 4A, C). In contrast to a pump, peristalsis is a wave like contraction and relaxation, which travels from the anterior to the posterior isthmus and carries the trapped bacteria to the terminal bulb (Doncaster, 1962). Peristalsis is not a frequent event, and only every fourth pump is followed by an isthmus peristalsis (Avery and Horvitz, 1987). Calcium transients were detected in the posterior isthmus after some pumps, but they have not been directly correlated with the isthmus muscle peristalsis (Shimozono et al., 2004). Isthmus peristalsis is absolutely dependent on the motor neuron M4, and M4 laser ablation leads to elimination of this contraction (Avery and Horvitz, 1987).

The isthmus functions as a double valve separating the high- and low-pressure parts of the pharynx (Avery and Shtonda, 2003). The region between the mouth and the middle isthmus is at low pressure, while regions between the anterior isthmus and terminal bulb, the terminal bulb and intestine are at high pressure. At the end of the pump, food is transferred from the anterior isthmus, which is at low pressure, to the middle isthmus, which is at high pressure (Riddle et al., 1997). This is supported by an observation of air bubbles in the pharynx, whose size remains unchanged in the corpus and anterior isthmus. They subsequently become smaller in size in the isthmus and vanish into the solution in the terminal bulb, which is indicative of high pressure (Doncaster, 1962).

1.4.3 Synchronization of pharyngeal muscle contraction

Pharyngeal contractions are believed to be synchronized by electrical coupling via gap

junctions. Contraction at the corpus, anterior isthmus and terminal bulb starts at the same time. This contraction remains synchronized even when all the pharyngeal neurons are killed, meaning that it does not require the pharyngeal nervous system (Avery and Horvitz, 1989; Raizen and Avery, 1994). Dye injected into one pharyngeal muscle soon appears in the other pharyngeal muscles (Starich et al., 1996). The *eat-5* gene, which encodes innexin, is necessary for synchronization of the muscles of the corpus and terminal bulb, as *eat-5* mutants have asynchronized contractions of the corpus and terminal bulb (Starich et al., 1996).

Posterior isthmus contractions do not occur in synchrony with those of the corpus and terminal bulb. Moreover, the anterior and posterior parts of the isthmus do not contract at the same time, even though isthmus muscle cells run along the entire length of the isthmus. Isthmus peristalsis is a wave of contraction followed by relaxation, which propagates from the anterior to posterior isthmus, resulting in a small portion of isthmus lumen being opened at a time. In addition, no electrophysiological signals were detected from the isthmus muscles. Peristaltic contraction of isthmus muscles allows the terminal bulb and the corpus to have different pressure (Riddle et al., 1997).

1.5 Pharyngeal muscle action potentials

Pharyngeal muscle action potentials resemble a vertebrate heart action potential. They are both long-lasting (~400 msec) and have three phases: excitation (E), plateau (P) and repolarization (R) (Figure 5) (Raizen and Avery, 1994). The action potential begins when the membrane potential rises from its resting level (-40 to -50 mV) to its depolarization level of +30 to +40 mV. Then it is followed by a plateau phase for about 150 msec, ending with the repolarization phase, during which the membrane potential decreases to a more negative value than the resting potential. After repolarization is over, the membrane potential recovers to its resting level. Every contraction-relaxation cycle corresponds to a single action potential. Contraction is detected 30 msec after excitation and proceeds during the plateau phase; and relaxation occurs right after repolarization (Doncaster, 1962; Raizen and Avery, 1994).

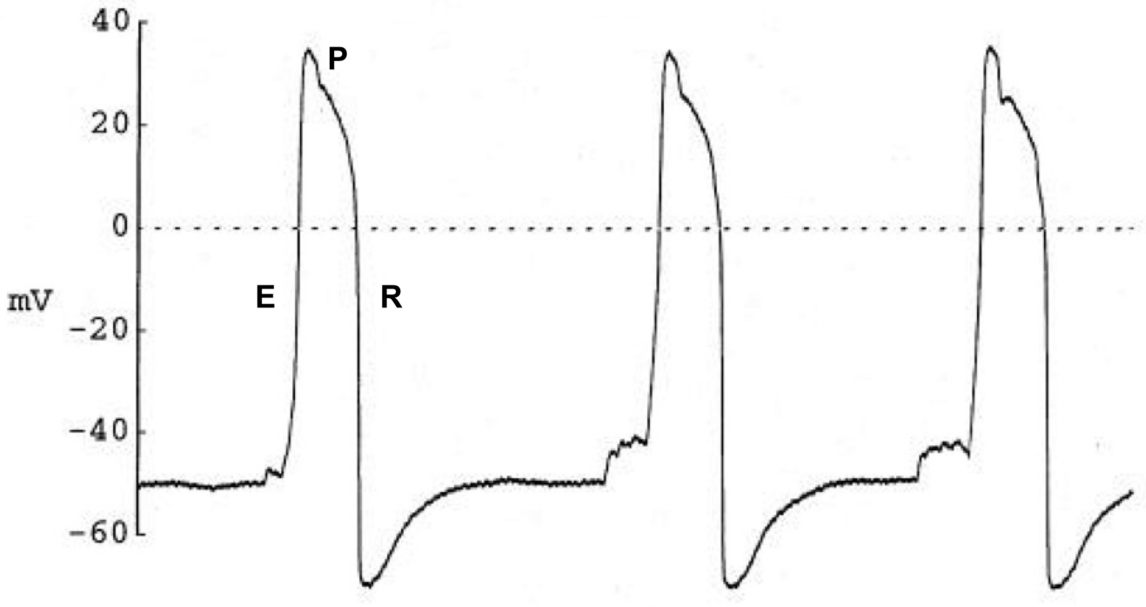

Figure 5 Electrical recordings from the pharyngeal muscles

Representation of intracellular recording from the muscle cell of the terminal bulb. Excitation phase is marked with “E” and characterized with a sharp rise of membrane potential from -50 mV to ~35 V, which initiates action potential within a muscle cell. Repolarization phase is marked with “R” and characterized by a drop in membrane potential, which leads to the end of the action potential. This figure is adapted from (Davis et al., 1995).

1.5.1 The MC motor neuron initiates action potentials via EAT-2 and is necessary for rapid pumping

The MC motor neuron is responsible for the fast depolarization of the pharyngeal muscles during rapid pumping. Each firing of MC initiates an action potential in the pharyngeal muscles (Raizen and Avery, 1994; Raizen et al., 1995). The MC motor neuron is a cholinergic neuron, and it releases ACh, which mediates fast neurotransmission at the NMJ (McKay et al., 2004; Raizen and Avery, 1994; Raizen et al., 1995) via EAT-2 (Figure 6). EAT-2 is a non-α nicotinic acetylcholine receptor (nAChR) subunit, and EAT-2::GFP specifically localizes to small puncta near the pm4 and pm5 pharyngeal muscles junction (McKay et al., 2004). This is the place where most-posterior of the MC processes form synapses with pm4 (Albertson and Thomson, 1976).

1.5.2 The T-type calcium channel CCA-1 boosts the action potential amplitude

T-type (or low threshold) calcium channels respond to small depolarizations and mediate low-threshold calcium spikes (Figure 6) (Perez-Reyes, 2003). *cca-1* encodes the T-type alpha subunit of the calcium channel, which becomes active at the start of the action potential and necessary for the efficient initiation of the action potential in the pharyngeal muscles. In the absence of *cca-1*, the action potential forms a plateau at -30 mV, which decreases a chance of efficient action potential triggered by MC signaling and reduces food uptake by an animal (Shtonda and Avery, 2005; Steger et al., 2005). Therefore, CCA-1 boosts the excitatory effect of synaptic input from the MC neuron resulting in a rapid depolarization of pharyngeal muscle.

1.5.3 The L-type calcium channel EGL-19 regulates muscle excitation and contraction

egl-19 encodes for the α1 subunit of an L-type voltage-gated calcium channel, which regulates the duration of the muscle action potential (Figure 6). Loss-of-function in *egl-19* leads to a loss of muscle contraction and subsequent lethality. Reduction-of-function in *egl-19* results in a decreased rate of muscle depolarization and weak contractions. Gain-of-function in *egl-19* results in prolonged muscle action potentials and muscle contractions (Lee et al., 1997).

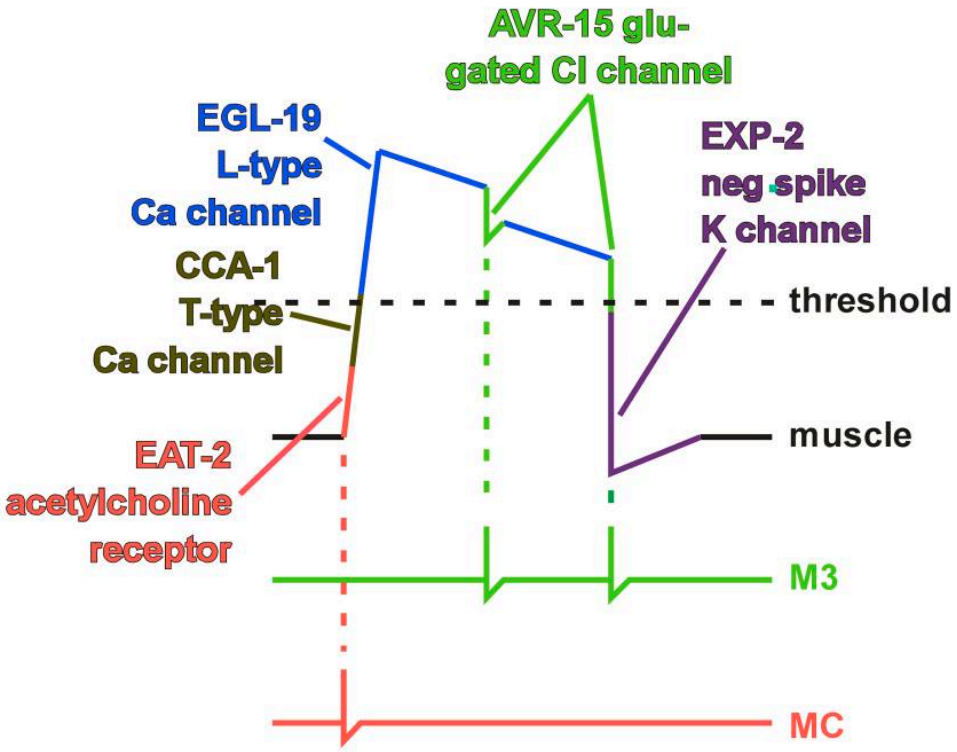

Figure 6 Action of ion channels during the muscle cell action potential

Schematic representation of a muscle cell action potential and action of ion channels. The MC motor neurons initiate a muscle action potentials by activating the EAT-2 nicotinic acetylcholine receptor. The T-type calcium channel CCA-1 boosts the excitatory effect of the MC input resulting in a rapid depolarization. The voltage-gated calcium channel EGL-19 regulates the duration of muscle action potential. The M3 motor neurons mediate muscle relaxation via the glutamate-gated AVR-15 chloride channels. Fast repolarization of the muscle cell membrane occurs via the voltage-gated potassium channel EXP-2. This figure is adapted from the WormBook http://www.wormbook.org/chapters/www_feeding/feeding.html.

1.5.4 M3s initiate inhibitory potentials

Appropriate relaxation of the pharyngeal muscle is crucial for normal feeding (Avery and Shtonda, 2003). M3 motor neurons forms synapses on the pm4 (Albertson and Thomson, 1976) and modulate the timing of pharyngeal muscle relaxation, and M3 ablation results in a delayed relaxation. M3s generate fast inhibitory postsynaptic potentials and ablation of M3s results in prolonged contraction of the pharyngeal muscles (Avery, 1993b; Raizen and Avery, 1994). *avr-15* encodes two alternatively spliced subunits of glutamate-gated chloride channels and mediates hyperpolarization of pharyngeal muscles via inhibitory glutamatergic neuromuscular transmission (Figure 6) (Dent et al., 1997).

1.5.5 The potassium channel EXP-2 mediates repolarization of pharyngeal muscles

exp-2 encodes a subunit of a voltage gated potassium channel that is necessary for the fast repolarization of the pharyngeal muscles (Figure 6) (Davis et al., 1999). Loss of *exp-2* results in a long-lasting action potential. When a membrane potential decreases below the threshold due to M3 signaling, EXP-2 opens and allows potassium to exit the cell. This results in a more negative membrane potential causing more EXP-2 to open (Davis et al., 1999; Shtonda and Avery, 2005). Therefore, EXP-2 mediates a fast and regenerative negative-going current spike.

1.6 The MC and M4 motor neurons stimulate pharyngeal muscle contractions

1.6.1 MC motor neurons control the rate of pumping

The MCs are excitatory motor neurons, which initiate action potential in the pharyngeal muscles and control frequency of pumping (Avery and Horvitz, 1989; Raizen et al., 1995). Animals with impaired signaling from MCs have a starved appearance because of slow pumping. Loss of *eat-2* also leads to the slow pumping phenotype indicating that MC controls rapid pumping by activating EAT-2 signaling in the pharyngeal muscles (McKay et al., 2004). In the absence of the MC motor neuron or *eat-2*, pharyngeal muscles are able to pump showing that neither MC (Raizen et al., 1995) nor *eat-2* (Avery and Horvitz, 1989) is necessary for this

contraction. In this case, pumping is generated by spontaneous action potentials within a muscle, and it is unknown how they are initiated. Among all the pharyngeal neurons, only I1 make chemical synapses onto the MCs (Albertson and Thomson, 1976). In the absence of I1, bacteria and serotonin can still activate MCs (Raizen et al., 1995). This indicates that in the presence of food, MC is the master regulator of rapid pumping.

The MC motor neurons are cholinergic neurons, and existing evidence strongly suggests they mediate rapid pumping by releasing ACh. First, the AChR inhibitor, curare, blocks MC neurotransmission (Raizen et al., 1995). Second, loss-of-function mutations in the *cha-1* and *unc-17* genes result in a slow pumping (Alfonso et al., 1993; Avery, 1993a; Varoqui et al., 1994). *cha-1* encodes for choline acetyltransferase, which is necessary for ACh synthesis, and *unc-17* encodes for the vesicular acetylcholine transporter. Both of these genes are necessary for cholinergic neurotransmission. *cha-1* null mutants do not pump at all (Chapter 3).

1.6.2 The M4 motor neuron is necessary for peristalsis

M4 is a polarized neuron, which has both dendritic and axonal characteristics. The cell body of the neuron is located dorsally in the anterior bulb, from where it sends two equivalent processes, which travel circumferentially around the nerve ring and then go posteriorly to the terminal bulb. Then they turn and run anteriorly to the middle of the isthmus (Figure 7). In the posterior isthmus, M4 forms synapses with pm5 (Albertson and Thomson, 1976). The anterior part of M4 is characterized as dendritic and receives signals from I3, I5, I6 and NSM neurons. The posterior part of M4 is axonic and transmits signals to the isthmus muscles. M4 also forms synapses with pm6 in the terminal bulb (Chiang et al., 2006).

Peristaltic contractions depend on M4 (Avery and Horvitz, 1987). Animals with a laser ablated M4 do not have peristalsis and eventually die of starvation. They are still able to pump slowly, but bacteria block the lumen of the corpus and are not transported down to the terminal bulb (Avery and Horvitz, 1987). When M4 ablated animals are treated with an ACh agonist, the lumen becomes clear of the food (Raizen et al., 1995).

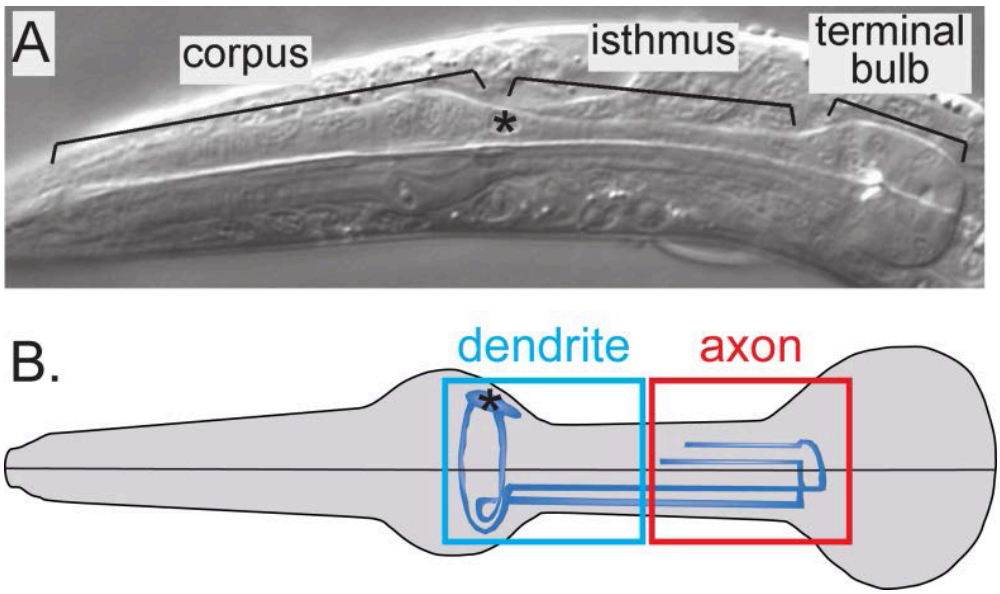

Figure 7 Morphology of the M4 motor neuron

(A) DIC micrograph of the pharynx with corpus, isthmus and terminal bulb indicated. (B) Schematic representation of the M4 motor neuron morphology. The cell body of the neuron (indicated with asterisk in A) is located dorsally in the anterior bulb. It extends two equivalent processes, which travel circumferentially around the nerve ring and then go subventrally to the terminal bulb. Then they turn dorsally and run anteriorly to the middle of the isthmus. M4 has both dendritic and axonic characteristics. The anterior part of M4 (blue) is characterized as dendritic and receives a signal. The posterior part of M4 (red) transmits a signal to the isthmus muscles. This figure is adapted from (Ray et al., 2008)

1.7 M4 is a multifunctional neuron

M4 is a cholinergic motor neuron, and existing evidence strongly suggests it stimulates isthmus peristalsis by releasing ACh (Avery and Horvitz, 1987; Duerr et al., 2008). First, it expresses *unc-17* (Alfonso et al., 1993; Avery and Thomas, 1997; Varoqui et al., 1994). Second, the ACh agoinst arecoline can stimulate isthmus muscle contraction in mutants with impaired M4 signaling (Ramakrishnan and Okkema, 2014; Ray et al., 2008).

M4 also functions as a neurosecretory cell, which is supported by the following evidence. First, it secrets the FMRFamide-like peptide neurotransmitter FLP-21 to modulate gustatory response in response to hypoxia (Pocock and Hobert, 2010). The hypoxia-inducible transcription factor upregulates serotonin expression, which promotes hypoxia-enhanced sensory perception through receptor SER-7 in M4. M4 then transmits this information back to the *C.elegans* CNS via secretion of FLP-21. Second, M4 secretes the insulin-like growth factor INS-10 to modulate anterior touch neuron sensitivity (Chen and Chalfie, 2014). M4 has been shown to contain a large number of dense core vesicles (Albertson and Thomson, 1976), which presumably package neuropeptides. Besides *flp-21*, M4 expresses other neuropeptide genes such as *flp-2* and *flp-5*, as well as growth factor *egl-17* (Burdine et al., 1998; Kim and Li, 2004). In *C. elegans*, *flp* genes are expressed in all neuronal cell types, including motor neurons, sensory neurons and interneurons. *flp*-expressing neurons play roles in many different behaviours, including feeding.

Finally, M4 functions as a neuroendocrine cell. It regulates gland cell morphology in the pharynx by secreting the TGF-ß-family growth factor DBL-1 (Ramakrishnan et al., 2014). *dbl-1* expression in M4 depends on the transcription factor CEH-28.

1.8 M4 function depends on a transcription factor CEH-28

ceh-28 encodes a homeodomain transcription factor, which belongs to NK-2 family. There are three more genes in the *C. elegans* genome (*ceh-22*, *ceh-24* and *ceh-27*), which also encode NK-2 transcription factors (Harfe and Fire, 1998; Okkema et al., 1997).

CEH-28 is expressed only in M4 from mid embryogenesis (Ray et al., 2008). It has a major role in synapse morphology and assembly in the M4 neuron. *ceh-28(cu11)* mutants show abnormally sized and mispositioned synapses (Figure 8). As a result animals lose the ability to efficiently feed, resulting in a highly penetrant stuffed pharynx phenotype, in which the lumen of the corpus and anterior isthmus is blocked with bacteria. Treatment of *ceh-28* mutants with the muscarinic AChR (mAChR) antagonist atropine leads to a suppression of feeding defects in these mutants. Similarly, wild-type animals treated with mAChR agonist arecoline phenocopies feeding defects observed in *ceh-28* mutants. This suggests that *ceh-28* phenotypes are presumably mediated through the mAChR, GAR-3.

1.9 Overview of acetylcholine receptors

AChRs are membrane proteins that respond to ACh binding. Ligand-gated AChRs can be divided into two major subtypes: ionotropic nicotinic receptors (nAChRs) (Changeux and Edelstein, 2001; Lindstrom, 1997) and metabotropic muscarinic receptors (mAChRs) (Ishii and Kurachi, 2006; Wess, 1996), which are activated by ACh and expressed in neuronal and nonneuronal cells (Albuquerque et al., 1995; Dani and Bertrand, 2007; Eglen, 2005; Gotti and Clementi, 2004).

1.9.1 Ion channels

One of the crucial characteristics of the cell membrane is to regulate ion transport and exchange (Armstrong and Hille, 1998; Doyle et al., 1998; Hodgkin and Huxley, 1952; Payandeh et al., 2011). All of the ion channels share similarities in structure such as that the pore in the center is formed by four or five transmembrane α helices.

Ligand-gated ion channels are activated upon binding of a chemical messenger. Once a chemical signal reaches the channel, it binds to its binding site resulting in a ‘gate’ opening. Usually the ‘gate’ and the binding site are not localized in close proximity on the channel. They are commonly located between two adjacent subunits.

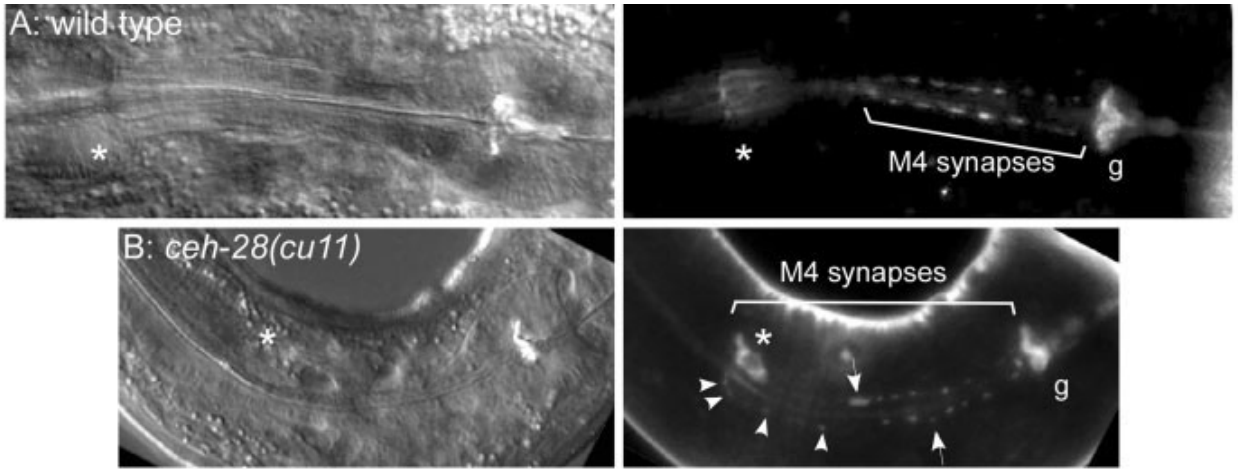

Figure 8 M4 synapses in wild type and *ceh-28* mutants

(A) DIC micrograph of the pharyngeal isthmus in a wild-type animal (left). The position of M4 cell body is indicated with an asterisk. GFP micrograph of the same wild-type animal, in which M4 synapses are localized in the posterior isthmus and marked with SNB::GFP (right). (B) DIC micrograph of the pharyngeal isthmus in a *ceh-28* animal (left). GFP micrograph of the same *ceh-28* animal, in which M4 synapses are localized throughout the entire length of the isthmus and also marked with SNB::GFP (right). Ectopic synapses in the anterior isthmus are marked with arrowheads, and abnormally sized synapses are marked with arrows. The grinder is autofluorescent and is marked (g). This figure is adapted from (Ray et al., 2008).

1.9.2 Role of nicotinic acetylcholine receptors in vertebrates

nAChRs are ligand-activated ion channels, which respond to ACh and drugs, such as the nicotinic receptor agonist nicotine. Binding of ACh or an agonist, such as nicotine, to nAChR allows ion flow through the channel resulting in a fast membrane depolarization.

Nicotinic receptors consist of five subunits, which have a symmetric arrangement around the pore (Figure 9). There are 17 types of vertebrate nAChR subunits: α subunits (α1-10), β subunits (β1-4), λ, δ and ε subunits. α subunits carry the main part of the ligand-binding sites (Lindstrom, 1997). Each subunit has the following: 1) an extracellular N-terminal domain of an approximate size of 200-220 amino acids, which bears the ligand-binding domain (Dennis et al., 1988; Galzi and Changeux, 1995); 2) four small (15-20 amino acids long) hydrophilic transmembrane domains (TM1-TM4) and two small hydrophilic loops, which link TM1-TM2 and TM2-TM3; 3) a cytoplasmic loop 100-150 amino acids long, which connects TM3 and TM4 (Huganir and Greengard, 1990); 4) a short extracellular C-terminal end (4-28 amino acids). nAChR subunits are classified as α- and non-α subunits. α-subunits are characterized by a Cys-Cys pairs near the entrance to TM1, which is important for agonist binding (Karlin et al., 1986). nAChRs are divided into muscle and neuronal subtypes depending on where they are expressed. Muscle nAChRs are found on muscle cells and mediate neuromuscular transmission at the NMJ. Neuronal nAChRs are found in the peripheral and central nervous systems. Vertebrate muscle nAChRs are composed of five subunits: $(\alpha1)_2\beta1\lambda\delta$ in a fetal muscle (Raftery et al., 1980) and $(\alpha1)_2\beta1\varepsilon\delta$ in an adult muscle (Mishina et al., 1986; Witzemann et al., 1987). ACh binding to α_λ (the α1 subunit next to the λ subunit) and α_δ sites leads to conformational changes in the α1 subunits and channel opening (Unwin et al., 2002). The β1 subunit plays a role in nAChR clustering (Wheeler et al., 1994).

Neuronal nAChRs are found in the peripheral and central nervous system as well as in nonexcitable cells, such as epithelial cells and cells of the immune system. There are nine α (α2- α10) and three β (β2-β4) subunits for neuronal nAChRs. α7-α10 form either

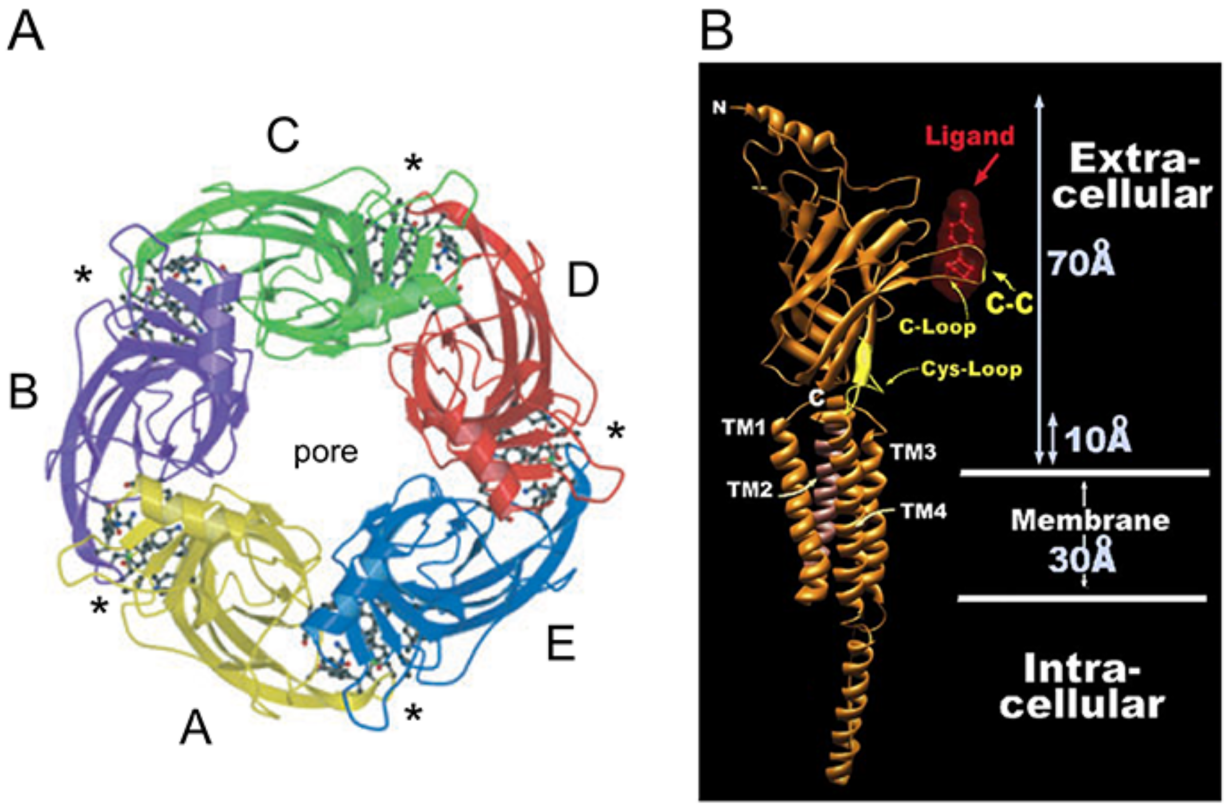

Figure 9 Structure of the nicotinic acetylcholine receptor

(A) Crystal structure of nAChR, top view. Each subunit is represented in a different color and a different letter (A-E). Between subunits there are ligand-binding sites, which are indicated with asterisks (Adapted from (Kalamida et al., 2007)). (B) The EM structure of the α subunit of nAChR. The extracellular domain is largely made up of β-sheets and TMs by α-helices. Cytoplasmic domain is represented as large α-helix. A C loop with Cys-Cys pair wrap a ligand projecting from the extracellular domain. This figure is adapted from (Albuquerque et al., 2009).

homopentamers or heteropentamers (Plazas et al., 2005). α2-α6 and β2-β4 subunits generate heteropentamers in 2:3 ratio. Homopentameric nAChRs have five ligand-binding sites per molecule and heteropentameric nAChRs have only two binding sites located between an α and a β subunit. Because calcium plays a crucial role in modulation of neuronal activity, neuronal nAChRs are highly selective to calcium (Adams and Nutter, 1992; Castro and Albuquerque, 1995). Due to the high calcium permeability of the neuronal nAChRs, calcium travels through the channel resulting in increased intracellular calcium, membrane depolarization and activation of VGCCs (Dajas-Bailador et al., 2002; Rathouz and Berg, 1994) or further release of calcium from intracellular stores (Beker et al., 2003; Dajas-Bailador et al., 2002). nAChRs composed of α7 subunits induce Ca^{2+} release from intracellular stores (Dajas-Bailador et al., 2002; Sharma and Vijayaraghavan, 2001). nAChRs containing α3- and/or β2 subunits in the brain activate primarily VGCC (Dajas-Bailador et al., 2002; Shoop et al., 2001).

1.9.3 Role of muscarinic acetylcholine receptors in vertebrates

mAChRs are prototypical members of the family-A G-protein-coupled receptors (GPCRs) with five molecularly distinct existing subtypes (M_1-M_5) (Caulfield, 1993; Caulfield and Birdsall, 1998; Wess, 1996). Each mAChR subtype is a protein with seven transmembrane domains, which belongs to one of two classes depending on what G-proteins it activates (Figure 10). M_2 and M_4 mAChRs activate G-proteins from the Gi family, resulting in inhibition of adenylyl cyclase and prolonged opening of potassium channel (Felder, 1995; Migeon et al., 1995). M_1, M_3 and M_5 mAChRs are coupled to Gq-type G-proteins. Activation of these receptors leads to production of 1,2-diacylglycerol (DAG) and inositol-1,4,5-trisphosphate (IP3) via activation of phospholipase C*β* (PCL*β*), and subsequent increases intracellular concentrations of calcium (Espada et al., 2009; Felder, 1995). In contrast to rapid depolarization in response to nAChRs, signaling through mAChRs results in a slower response via second messenger systems (Dutar and Nicoll, 1988).

Peripheral mAChRs mediate actions of ACh on organs and tissues that are innervated by parasympathetic nerves (reduction of heart rate and stimulation of smooth muscle contraction) (Caulfield, 1993). Central mAChRs play a major role in modulating behavioral, sensory, motor and cognitive functions. Altered signaling through central mAChRs is associated with major diseases of the central nervous system (CNS), such as depression and epilepsy, Alzheimer's and Parkinson's disease (Eglen et al., 1999; Felder et al., 2000). All organs and tissues have mAChRs (Caulfield, 1993; Levey, 1993; Vilaro et al., 1993; Wolfe and Yasuda, 1995). The M_1 mAChR is expressed in all regions of the forebrain, specifically in the striatum, cerebral cortex and in the hippocampal pyramidal neurons (Levey, 1993; Levey et al., 1995; Marino et al., 1998). M_1 receptors play a role in mediating learning processes and memory (Fisher et al., 1996; Iversen, 1997). M_2 receptors are found in the CNS (Vilaro et al., 1993; Wolfe and Yasuda, 1995) and also in the heart and smooth muscles (Brodde and Michel, 1999; Caulfield, 1993; Eglen et al., 1996).

Even though M_2 and M_4 receptors are coupled to G-proteins from the Gi family, M_4 receptors are preferentially expressed in the CNS (Vilaro et al., 1993; Wolfe and Yasuda, 1995) including the cortex, hippocampus and striatum (Hersch et al., 1994; Rouse et al., 1999). The M_3 receptor is expressed at low levels throughout the central nervous system (Yamada et al., 2001b) and peripheral organs and tissues that are innervated by parasympathetic nerves (Caulfield, 1993; Eglen et al., 1996). The exact role of the M_3 receptor is unknown, but it is predicted to mediate smooth muscle contraction and glandular function (Caulfield and Birdsall, 1998; Wess, 1996). M_5 receptors are expressed in low levels in both neuronal and non-neuronal cell (Eglen and Nahorski, 2000) controlling cerebral vasodilation and blood flow (Araya et al., 2006; Yamada et al., 2001a). M_5 receptors share ligand-binding properties with M_3 receptors.

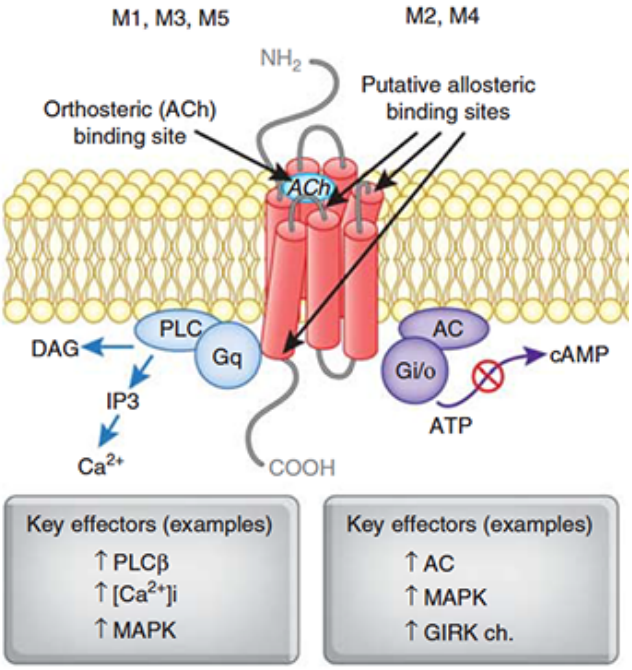

Figure 10 Structure and signaling of the muscarinic acetylcholine receptor

Each mAChR subtype is a seven TM protein, which belongs to one of the two functional classes. mAChRs M_2 and M_4 activate G-proteins of Gi-type, which leads to an inhibition of adenylyl cyclase and prolonged opening of a potassium cation. M_1, M_3 and M_5 are coupled to Gq-type G-proteins. Activation of these G proteins results in production of IP3 and DAG via activation of *PCLβ* and subsequent increase of intracellular calcium levels. Across species, mAChR subtypes share sequence homology, especially in the orthosteric ACh binding sites. This figure is adapted from (Jones et al., 2012).

1.9.4 Nicotinic acetylcholine receptors in C. elegans

In comparison to vertebrates, which have fewer than 20 nAChR subunit genes, the *C. elegans* genome has 27 nAChR encoding genes. nAChR subunits are divided into five classes based on a sequence similarity: UNC-38, UNC-29, ACR-8, ACR-16 and DEG-3 (Jones and Sattelle, 2004; Mongan et al., 1998; Mongan et al., 2002), each of each contains three to nine members of both α and non-α subunits. The UNC-38 class has three α subunits, which resemble insect subunits. The UNC-29 has four subunits, which are similar to vertebrate skeletal muscle non-α subunits. The ACR-16 class includes α and non-α subunits, which resemble vertebrate α7 subunits. The ACR-8 and DEG-3 subunits are nematode specific, where ACR-8 contains three α subunits and DEG-3 both α and non-α subunits. *C. elegans* body wall muscles express nAChR subunits, which respond to either levamisole or nicotine. The levamisole-sensitive nAChRs are heteromeric and include three subunits: UNC-38, UNC-29 and UNC-63 (Culetto et al., 1999; Fleming et al., 1997; Richmond and Jorgensen, 1999). The nicotine receptors sensitive to nicotine are homomeric and contain the α subunit from ACR-16 class (Francis et al., 2005; Touroutine et al., 2005).

The EAT-2 receptor, which is a focus of this thesis, is a non-α nAChR subunit as discussed previously in 1.5.1. It belongs to the ACR-16 class of nAChRs, and it is unknown which other subunits EAT-2 interacts with to form a heteropentameric channel. Along with *eat-2,* nAChRs *acr-6, acr-7, acr-10, acr-14* and *acr-16* are also expressed in the pharyngeal muscles (Okkema, Moerman and Waterston, unpublished).

1.9.5 Role of muscarinic acetylcholine receptors in *C. elegans*

There are three mAChR encoding genes in *C. elegans* genome: *gar-1*, *gar-2* and *gar-3* (Park et al., 2003; Park et al., 2000; Suh et al., 2001). GAR-3 mAChR is the most similar to the vertebrate muscarinic receptors, based on its pharmacological profile. It binds the antagonist scopolamine, and the agonists carbachol and arecoline (Hwang et al., 1999; Park et al., 2003; Steger and Avery, 2004). Overexpression of GAR-3 results in arecoline hypersensitivity (Steger

and Avery, 2004). The *gar-3* promoter drives expression in the pharyngeal muscles (Steger and Avery, 2004). Signaling through GAR-3 results in an increase of pharyngeal muscle contractions by increasing the duration of the muscle action potentials, strength and length of contraction (Ramakrishnan and Okkema, 2014; Ray et al., 2008; Steger and Avery, 2004). GAR-3 expression in heterologous systems activates PLC and Protein kinase C (PKC), which indicates that GAR-3 functions in the pharyngeal muscle as a Gq coupled receptor (Lee et al., 2001; Min et al., 2000).

gar-1 and *gar-2* do not have any function in the pharynx. First, *gar-1* and *gar-2* are expressed outside of the pharynx in the extrapharyngeal nervous system, motor neurons in the ventral cord and the HSN motor neuron (Lee et al., 2000). Second, the GAR-1 receptor binds atropine, but not scopolamine (Lee et al., 1999), and GAR-2 does not bind either of those (Lee et al., 2000). Third, *gar-1* and *gar-2* mutations have no effects on arecoline hypersensitivity (Tarawneh, Kozlova and Okkema, unpublished).

2 MATERIALS AND METHODS

2.1 The *C. elegans* strains, plasmids and oligonucleotides used in this study are listed in Appendices G - I

2.2 General methods

2.2.1 Handling nematodes

C. elegans strains were grown under standard conditions (Lewis and Fleming, 1995) on nematode growth media (NGM) plates seeded with the OP50 strain of *E. coli* and maintained in 16-25°C incubators. To passage, 4-6 L4 hermaphrodites were picked to a new plate every 5-7 days depending which temperature they were maintained. Worms were kept in liquid nitrogen for the long-term storage. First, the worms were starved on five 60 mm NGM plates and then harvested from each plate with 2 ml of a 1:1 mixture of M9 buffer (20mM KH_2PO_4, 40mM Na_2HPO_4, 30mM NaCl, 1mM $MgSO_4$) and freezing buffer (100 mM NaCl, 50mM KH_2PO_4, 30% glycerol, 140mM NaOH, 0.6 mM $MgSO_4$). Then animals were aliquoted into five separate cryostorage Nunc vials and frozen at -80°C. The next day, the strains were validated by thawing out one vial of the frozen animals to four or five 60 mm NGM plates seeded with OP50. The following day, the plates were checked for the presence of the viable animals. After validation, the rest of the vials were transferred to the liquid nitrogen tank.

2.2.2 Germline transformation in *C. elegans*

Using the standard techniques (Mello and Fire, 1995), the germline transformations were performed by coinjecting a plasmid of interest and pRF4 plasmid that contains the *rol-6(su1006)* gene (Kramer et al., 1990). *rol-6(su1006)* encodes for a mutated collagen protein, which results in a rolling phenotype instead of sinusoidal movement when is expressed in animals. Each injected animals was placed on an individual 60 mm NGM plate seeded with OP50. Animals who survived microinjection were let to produce F1, which was then screened for rollers. Rolling F1 animals were cloned on individual plates and let to produce F2. If F2 progeny had rollers then the line was established as permanent. The presence of rolling phenotype in F2 generation

showed that the extrachromosomal array was stable within the line and could be passed from one generation to the next.

2.2.3 Integration of transgenes using ultraviolet and trimethylprosalen

Transgenes were randomly integrated into the chromosomes from multi-copy extrachromosomal arrays using ultraviolet and trimethylprosalen (UV-TMP) (Kage-Nakadai et al., 2014). Long-wavelength UV irradiation (356 nm) in combination with TMP treatment lead to a higher mutation frequency and a lower frequency of rearrangements of chromosomes comparing to short-wavelength UV irradiation (254 nm). TMP containing solutions were always kept covered with aluminum foil. One mg of TMP (Fisher, Catalog# AC2299881000) was dissolved in 1 ml of DMSO (Fisher, Catalog# BP231) at 37°C for 3 hours with continuous rocking. TMP was used within 2-3 weeks and stored at -20°C. Twenty µl of 1 mg/ml TMP was added to 380 µl M9 buffer resulting in a final concentration of 50 µg/ml. Forty-fifty extrachromosomal array-containing rolling L4s were added into the 400 µl of 50 µg/ml TMP. The worms were incubated in the solution for 15 min at the room temperature. Then, animals were transferred to the unseeded 10 cm NGM plate in the dark and the plate was covered with the aluminum foil. The foil was removed and the worms were exposed to 350 µJ(x100) long wave UV Stratalinker 1800 for 2 min and 200 µl of OP50 was added to the plate. The plate was covered with foil and worms were maintained on the plate for 5 hours at the room temperature or overnight at 16°C. From this point OP50 seeded 60 mm NGM plates were used. After incubation, 3 rolling L4 animals were picked per plate for 10 plates as P0s. In 3 days, 10 F1s from each plate were picked and placed one animal per plate resulting in 100 plates total. In 3 days, 2 F2s were picked from each plate and places one animals per plate resulting in 200 plates total. In 3 days, these plates were scored for 100% rollers.

2.2.4 Microscopy

A Zeiss AxioImager microscope was used to visualize animals and capture differential interference contrast (DIC) and fluorescence microscopy images. Images were collected with an

MRm camera or Q-Imaging Rolera EM-C^2 EMCCD camera and ZEN Software. Still images or time-lapse images were processed using ZEN software, Adobe Photoshop, Adobe Illustrator and Fiji (Schindelin et al., 2012). Time-lapse recordings of calcium transients, pumping and peristalsis were performed using methods described in detail in 2.4.4 and 2.5.7.

2.3 Methods for manipulating nucleic acids

2.3.1 Isolation of plasmid DNA

Two-three ml of 2xTY growth media (16g Tryptone, 10g Yeast extract, 5g NaCl and dH_2O to 1 L) containing the appropriate amount of antibiotic was inoculated with a single colony and incubated overnight at 37°C at 220 rpm. DNA was isolated from the overnight culture using commercially available Promega minipreps DNA Purification Kit (Catalog# A1460) and the manufacturer's protocol.

2.3.2 Digestion with restriction endonuclease and DNA gel electrophoresis

Digestion of DNA was performed with the restriction enzymes supplied by commercial manufacturers (New England Biolabs, Fermentas). Usually, 4-5 µl of plasmid DNA (300-500 ng) was digested with 0.5 Units of the enzyme in the recommended for this enzyme buffer for an hour at the recommended temperature in the water bath. Total volume of the restriction digest reaction was 30 µl.

To visualize the products of DNA restriction digest, 0.8%-1.2% agarose gel was made using 1X TAE buffer (40 mM Tris base, 30 mM acetic acid, 5mM sodium acetate and 1 mM EDTA) containing 0.3 µg/ml Ethidium Bromide (EtBr). 6X gel loading buffer was added to 1X concentration to the restriction digest, which was then loaded on the agarose gel along with DNA ladder and ran at 100 mV. The agarose gel apparatus consisted of Thermo EC, Maxicell Primo EC340 electrophoretic gel boxes that were connected to a Thermo 105 power supply. The agarose gel was analyzed on the Alpha Imager using UV light to visualize DNA. Images of the gel were saved as TIFF files. Different DNA ladders were used depending on the size of the expected DNA fragments: DNA ladders from commercial manufacturers (Invitrogen 100bp

ladder 1kb ladder and 1kb plus ladder) and DNA ladder, which was generated by digesting Lambda DNA (New England Biolabs) with HindIII and KpnI.

2.3.3 Purification of DNA fragments using agarose gel electrophoresis

To improve the efficiency of the cloning process, PCR products or DNA fragments of a particular size generated by restriction digest were purified using agarose gel electrophoresis. This helped to eliminate undigested DNA and DNA fragments of unwanted size, which usually is a cause of background colonies during transformation. DNA, which was going to be gel purified, was run on 0.8% agarose gel in 1X TAE containing 0.3 µg/ml EtBr and the products were visualized using UV trans-illuminator. A new razor blade was used to excise the desired band from the gel and placed in 1.5 ml microfuge tube. The DNA was extracted from the gel slice using the Promega Gel and PCR Purification Kit (Promega, Catalog# A9281) and the manufacturer's protocol.

2.3.4 Quantification of nucleic acids

A nanodrop (ND-1000) was used for quantification of DNA and RNA samples according to the manufacturer's protocol. For the instrument calibration, dH_2O or relevant buffer, which was used to dissolve DNA, served as a blank solution.

2.3.5 Primer design and preparation

Mac Vector software was used to design primers, which were then purchased from Integrated DNA technologies. The lyophilized primers were dissolved in the dH_2O to the concentration of 1 µg/µl and stored for long-term at -20°C. Working stocks were prepared by diluting the master stock to arrive the desired concentrations, usually 0.1 µg/µl.

2.3.6 Single worm PCR

Single worm PCR was performed by picking 1 animal from each genotype onto the individual PCR tubes containing 2.5 µl of worm 1X lysis buffer (50mM KCl, 10 mM Tris pH 8.3, 2.5 mM $MgCl_2$, 0.45% Triton X-100, 0.45% Tween 20,0.1% gelatin) and 0.1 mg/ml Proteinase K (Roche Biochemicals). Following the transfer, each tube was observed under the Zeiss

dissecting microscope to make sure that the worm was in the solution. The tubes were then placed in DNA Engine PTC-200 (Peltier Thermal Cycler) and worms were lysed using the following program: (1) 60°C - 1 hr, (2) 95°C - 15 min, (3) 4°C - forever. Lysed worms were used as DNA template for the PCR. PCR reaction contained 2.5 µl of 10X PCR buffer (Invitrogen, Catalog# 10966034), 0.75 µl of 50 mM $MgCl_2$ (Invitrogen, Catalog# 10966034), 0.4 µl of each 25 mM dNTP (Invitrogen, Catalog# 10297018), 0.1 µg/µl of each primer used for genotyping and 2.5 Units of Platinum Taq polymerase (Invitrogen, Catalog# 10966034). The tubes were then placed in DNA Engine PTC-200 using appropriate PCR program.

2.3.7 DNA ligations

Ligation reaction was performed to ligate two purified DNA fragments: an insert and a vector. Total volume of ligation reaction usually was 10 µl. It contained 1:5 or 1:3 molar ratios of the insert to the vector along with 1 Unit of T4 DNA ligase (Invitrogen, Catalog# 15224-917) and 2 µl of 5X ligase buffer (Invitrogen, Catalog# 46300-018). When necessary, the vector was dephosphorylated using Calf intestinal alkaline phosphatase (CIAP) (Invitrogen, Catalog# 18009-019) to prevent religation of the vector to itself. The ligation reaction was incubated at 16°C overnight and transformed into the competent DH5 alpha *E. coli* cells.

2.3.8 Preparation of competent DH5 alpha *E. coli* cells

Three ml of 2X TY were inoculated with a single DH5 alpha colony and the culture was incubated overnight at 37°C at 220 rpm. The next day 100 ml of 2X TY was added to 500 ml flask and inoculated with 0.5 ml of overnight culture. The culture was grown at 37°C at 220 rpm until OD_{600} = 0.6. The culture was incubated on ice for 15 min and bacteria were pelleted by centrifugation at 4,000 rpm at 4°C for 4 min. The supernatant was aspirated and the bacteria pellets were resuspended in 2 ml of ice cold Buffer 1 (10 mM MES pH 6.2, 100 mM $RbCl_2$, 10 mM $CaCl_2$, 50 mM $MnCl_2$) and combined in one tube. Additional 14 ml of Buffer 1 was added to the tube followed by incubation on ice for 15 min. The bacterial cells were pelleted by centrifugation at 4,000 rpm at 4°C for 4 min. The supernatant was aspirated and the pellet was

resuspended in 1.6 ml of ice cold Buffer 2 (10 mM MOPS, 75 mM $CaCl_2$, 10 mM $RbCl_2$, 15% glycerol). The tube was incubated on ice for 15 min. Aliquots of 100-200 µl were frozen in a dry ice ethanol bath and stored at -80°C.

2.3.9 DNA transformations

DNA was transformed into the competent DH5 alpha *E. coli* cells by the heat shock method of transformation. The cells were first thawed on ice and the ligation mixture or plasmid DNA was incubated with 100 µl of the competent cells on ice for 30 min. Cells were heat shocked at 42°C for 40 sec, returned to ice immediately after the heat shock and incubated on ice for 2 min. The cells were recovered by adding 250 µl of 2X TY media and incubated by shaking at 220 rpm at 37°C for 1 hour. Then, the cells were spread on the 2X TY plates (16g Tryptone, 10g Yeast extract, 5g NaCl, 18g of agar and dH_2O to 1 L) containing appropriate amount of antibiotic needed for the selection. The plates were incubated overnight at 37°C and checked the next day for the presence of single colonies.

2.3.10 DNA sequencing

DNA plasmids were sequenced using Sanger sequencing method at the DNA services facility at the University of Illinois at Chicago (RRC center) using custom designed or standard sequencing primers provided by RRC.

2.4 Analyzing feeding behavior and drug studies

2.4.1 Generation of *eat-2(ok3528)* strain OK1023

eat-2(ok3528) was derived from the strain VC2820 carrying *eat-2(ok3528)/mT1 ; +/mT1[dpy-10(e128)].* The segregation of this strain was initially described as wild type, arrested mT1 aneuploids, sterile Dpys (mT1 homozygotes), and *ok3528* homozygotes (arrest stage/phenotype undetermined). While maintaining VC2820, *ok3528* homozygotes were able to grow to adulthood and were used to establish OK1234. Animals were subjected to PCR to confirm that they were homozygous for *eat-2(ok3528)*. Worms were lysed as described in 2.3.6. The PCR reaction was described in 2.3.6. The PCR program used to identify *eat-2(ok3528)* was

(1) 94°C - 2 min, (2) 94°C - 45 sec, (3) 58.6°C - 45 sec, (4) 72°C - 30 sec, (5) go to step 2 - 39 times, (6) 72°C - 5 min, (7) 12°C – forever. The PCR primers used for *eat-2(ok3528)* PCR were PO1423 [TGCGTGGTAGAGGGATAGTG], PO1424 [TCTCGACGAGACCTACGTTG] and PO1425 [ACAGCTACAGTACCTCGCAC]. Under these conditions, a wild type *eat-2* amplified a 333 bp fragment and *eat-2(ok3528)* homozygote amplified a 385 bp fragment, which was visualized on 1.5% agarose gel.

2.4.2 Construction of *eat-2(ok3528); gar-3(gk305)* strain OK1064

The OK1064 strain containing *eat-2(ok3528); gar-3(gk305)* was generated using the following steps. In the P0, N2 males were mated with VC657 hermaphrodites carrying *gar-3(gk305)* to generate an adequate number of *gar-3(gk305)*/+ males. In the F1 generation, *gar-3(gk305)*/+ males were mated with *eat-2(ok3528)* mutants. In the F2 generation, cross progeny, 10 hermaphrodites, which were supposed to be double heterozygous for *gar-3(gk305)* and *eat-2(ok3528)* (genotype: *eat-2(ok3528)*/+*; gar-3(gk305)*/+) were cloned into individual plates and allowed to lay eggs. F2 moms were subjected to two separate PCRs to confirm that they were *eat-2(ok3528)*/+*; gar-3(gk305)*/+. Using a worm pick, F2 moms were transferred into the individual PCR tubes containing 5 µl of worm 1X lysis buffer (50mM KCl, 10 mM Tris pH 8.3, 2.5 mM $MgCl_2$, 0.45% Triton X-100, 0.45% Tween 20,0.1% gelatin) and 0.1 mg/ml Proteinase K (Roche Biochemicals). Following the transfer, each tube was observed under the Zeiss dissecting microscope to make sure that the worm was in the solution. The tubes were then placed in DNA Engine PTC-200 (Peltier Thermal Cycler) and worms were lysed using the following program: (1) 60°C x 1 hr, (2) 95°C x 15 min, (3) 4°C hold. Lysed worms were used as DNA template for the PCR to identify *eat-2(ok3528)* and *gar-3(gk305)*. The PCR reaction was described in 2.3.6. PCR conditions, program and primers used to identify *eat-2(ok3528)* were described in 2.4.1. The PCR program used to identify *gar-3(gk305)* was (1) 94°C - 2 min, (2) 94°C - 45 sec, (3) 59°C - 45 sec, (4) 72°C - 30 sec, (5) go to step 2 - 39 times, (6) 72°C - 5 min, (7) 12°C - forever. The PCR primers used for *gar-3(gk305)* were PO1426

[TAATAGGTTCGGCCCAGAGC], PO1427 [GTGATCGTTTGCTGGGAAGC] and PO1428 [CGAAGCTCAGAATGTCAGTAACG]. Under these conditions, a wild type *gar-3* amplified a 294 bp fragment and *gar-3(gk305)* homozygote amplified a 472 bp fragment, which was visualized on 1% agarose gel. Approximately 90 F3 hermaphrodites from the *eat-2(ok3528)*/+*; gar-3(gk305)*/+ F2 plates were cloned to individual plates and allowed to lay eggs at 20°C overnight. F3 moms were subjected to two separate PCRs to identify animals homozygous for *eat-2(ok3528)* and *gar-3(gk305).*

2.4.3 Construction of *ace-3(dc2); gar-3(gk305)* strain OK1081

The OK1081 strain containing *ace-3(dc2); gar-3(gk305)* was generated using the following steps. In the P0, N2 males were mated with hermaphrodites from the VC657 carrying *gar-3(gk305)* to generate an adequate number of *gar-3(gk305)*/+ males. In the F1 generation, *gar-3(gk305)*/+ males were mated with *ace-3(dc2)* mutants. In the F2 generation, cross progeny, 10 hermaphrodites, which were suppose to be double heterozygous for *ace-3(dc2)* and *gar-3(gk305)* (genotype: *ace-3(dc2)*/+*; gar-3(gk305)*/+) were cloned into individual plates and allowed to lay eggs. F2 moms were subjected to two separate PCRs to confirm that they were *ace-3(dc2)*/+*; gar-3(gk305)*/+. F2 moms were lysed as described in 2.3.6. The PCR reaction was described in 2.3.6. PCR conditions, program and primers used to identify *gar-3(gk305)* were described in 2.4.2. The PCR program used to identify *ace-3(dc2)* was (1) 94°C - 2 min, (2) 94°C - 45 sec, (3) 57°C - 45 sec, (4) 72°C - 30 sec, (5) go to step 2 - 39 times, (6) 72°C - 5 min, (7) 12°C – forever. The PCR primers used were PO1435 [CAAGGATACAGAGTACACGGCA], PO1436 [CAAGCCCGCAAATTGAACTGA] and PO1437 [GCAAGTGGCAAGCGAGAATA]. Under these conditions, a wild type *ace-3* amplified a 256 bp fragment and *ace-3(dc2)* homozygote amplified a 323 bp fragment, which was visualized on 1.5% agarose gel. Approximately 90 F3 hermaphrodites from *ace-3(dc2)*/+*; gar-3(gk305)*/+ F2 plates were cloned to individual plates and allowed to lay eggs at 20°C overnight. F3 moms were lysed as described in 2.4.1 and subjected to PCR to identify animals homozygous for *ace-*

3(dc2) and gar-3(gk305).

2.4.4 Analysis of pharyngeal muscle contractions in untreated L1 animals

Ten adult hermaphrodites were bleached on an unseeded 60 mm NGM plate and incubated overnight at 20°C. To make 1 ml of the bleach solution, 133 µl of 4N NaoH, 200 µl of Sodium hypochlorite and 667 µl of M9 buffer were mixed together. Next day, 20 hatched L1 larvae were identified and mounted on a 2% agarose pad in 5 µl of M9 buffer containing OP50. Cover slip was places immediately on the top of the swimming worms. Individual N2 or mutant animals that pumped were recorded at 25 frames/sec for 1 min using a Zeiss AxioImager microscope (63X magnification) with an MRm camera and ZEN Software. For each genotype the feeding behavior was analyzed in at least 5 animals (~500 pumps/per animal). Time-lapse images were exported and processed using Fiji (Schindelin et al., 2012) to generate time-lapse movies.

2.4.5 Analysis of pharyngeal muscle contractions in arecoline and nicotine treated animals

Ten adult hermaphrodites were bleached on an unseeded 60 mm NGM plate and incubated overnight at 20°C. The next day, 20 hatched L1 larvae were identified and mounted on a 2% agarose pad in 7 µl of arecoline (Acros Organics, Cat# CAS: 300-08-3) or nicotine (Sigma, Cat# N5260-25G) containing OP50. Animals were incubated for 15 minutes before the cover slip was placed on the top of the worms. Individual N2 or mutant animals that pumped were recorded at 25 frames/sec for 1 min using a Zeiss AxioImager microscope (63X objective) with an MRm camera and ZEN Software. For each drug treatment the feeding behavior was analyzed in at least 5 animals (~500 pumps/per animal). Time-lapse images were exported and processed using Fiji (Schindelin et al., 2012) to generate time-lapse movies. A stock of 1 M arecoline was made and stored at -20°C. At the day of the experiment, a dilution of a desired arecoline concentration was prepared to use for the treatment. The nicotine solution of a desire concentration was made freshly at the day of the experiment.

2.4.6 Analysis of pharyngeal muscle contractions in *cha-1(ok2253)* mutants

Strain VC1836 carries *cha-1(ok2253); nT1[qIs51]. cha-1(ok2253)* homozygotes arrest as L1s. Homozygous lethal deletion chromosome is balanced by GFP-marked translocation. The strain segregated as following: wild type expressing the pharyngeal *myo-2::GFP*, heterozygotes expressing *myo-2::GFP*, arrested *nT1[qIs51]* aneuploids and GFP negative arrested *cha-1(ok2253)* homozygotes. To analyze pharyngeal muscle contractions in *cha-1(ok2253)* homozygotes, newly hatched L1s were examined on the plates. Animals with sick appearance were used for mounting on a slide as described in 2.4.4 and 2.4.5. The time-lapse recordings of pharyngeal muscle contractions were performed as described in 2.4.4 and 2.4.5 only in animals, which were not expressing *myo-2::GFP*.

2.4.7 Quantification of pumping and peristalsis

The pharyngeal muscle contractions in every animal were recorded at 25 frames/sec for 1 min. A region of recorded time-lapse movie of 500 frames was selected, during which animal was consistently pumping. A relative time, which calculated a time for each frame, was extracted from this region. These values were imported into Excel spreadsheet. Within chosen region, the pumping frequency, the peristalsis frequency, the percentage of pumps followed by peristalsis and the duration of peristalsis were measured.

The pumping frequency was calculated using following formula: total number of pumps (n)/ total time for (n) pumps. The peristalsis frequency was calculated using following formula: total number of peristalses (n)/ total time for (n) peristalses. The percentage of pumps followed by peristalsis was calculated as a percent of pumps followed by peristalsis using the formula: total number of peristalses x 100/ total number of pumps. The duration of peristalsis was measured as a time between opening of middle isthmus and closing of posterior isthmus. The average, standard error of mean and p value for all the measurements mentioned above was calculated using Microsoft Excel. p value was calculated by running two-tailed Student's t-test.

2.5 Analyzing calcium transients in pharyngeal muscles during pumping and peristalsis

2.5.1 Generating *myo-2::GCaMP3* reporter pOK294.04

A 50 µl reaction containing 2 µg of pPD 96.48 (*myo-2* promoter containing plasmid) was incubated with 5 µl of 10X NEB buffer #4, 2 Units of HindIII and 2 Units MscI for 3 hours at 37°C. This reaction excised *myo-2* promoter sequence 1177bp long, which served as an insert. At the same time, a 50 µl reaction containing 2 µg of pOK290.02 (*str-2::GCaMP3*) was also incubated with 5 µl of 10X NEB buffer #4, 2 Units of HindIII and 2 Units MscI for 3 hours at 37°C. This reaction excised GCaMP3 sequence 4755 bp long, which served as a vector. The digested products were purified by gel electrophoresis and eluted in 30 µl of dH_20. Then, the insert was ligated into the vector with 1:3 (vector : insert) ratio to generate a plasmid pOK294.04. 30 µl ligation reaction contained 73.6 ng of the insert, 34.5 ng of the vector, 6µl of 5X ligase buffer and 0.5 Units of T4 DNA ligase. The ligation reaction was incubated at 16°C overnight. The next day, the entire ligation mix was transformed into the 100 µl of the competent DH5 alpha *E. coli* cells using methods described in 2.3.9, and all the cells were spread on the 2X TY plate containing 100 ng/µl ampicillin. A tube with 2X TY growth media was inoculated with a colony from the plate. Total ten colonies were picked into ten tubes and incubated overnight at 37°C at 225 rpm. The plasmid DNA was isolated from these cultures next day using methods described in 2.3.1. Purified plasmid DNA was digested separately with HindIII, SphI and EcoRV to confirm that it contained *myo-2::GCaMP3* sequence. The plasmid DNA was subjected to sequencing as described in 2.3.10.

2.5.2 Construction of *cuIs36[myo-2::GCaMP3]* strain OK1020

Germline transformations were performed by microinjection using pRF4 (100 ng/µl) containing *rol-6(su1006)* as a transformation marker and the *myo-2::GCaMP3* reporter pOK294.04 (20 ng/µl) using methods described in 2.2.2. The extrachromosomal *myo-*

2::GCaMP3 transgene *cuEx804* was chromosomally integrated by UV-TMP mutagenesis using methods described in 2.2.3 and outcrossed to form OK1020 carrying *cuIs36[myo-2::GCaMP3]*.

2.5.3 Construction of *eat-2(ok3528); cuIs36[myo-2::GCaMP3]* strain OK1063

The OK1063 strain containing *eat-2(ok3528); cuIs36[myo-2::GCaMP3]* was generated using the following steps. In the P0, N2 males were mated with rolling hermaphrodites from the OK1020 carrying *myo-2::GCaMP3* reporter to generate an adequate number of *cuIs36[myo-2::GCaMP3]*/+ rolling males. In the F1 generation, *cuIs36[myo-2::GCaMP3]*/+ rolling males were mated with *eat-2(ok3528)* mutants. In the F2 generation, cross progeny, 3 rolling hermaphrodites, which were double heterozygous for the *cuIs36[myo-2::GCaMP3]* transgene and *eat-2(ok3528)* (genotype: *eat-2(ok3528)*/+; *cuIs36[myo-2::GCaMP3]*/+) were cloned into individual plates and allowed to have progeny at 20°C for three days. Approximately 30 F3 rolling hermaphrodites from each F2 plate (total 60 hermaphrodites) were cloned to individual plates and allowed to lay eggs at 20°C overnight. F3 moms were lysed as described in 2.3.6. The tubes were frozen at -20°C. In the F4 generation, the plates were screened for 100% rollers homozygous for *cuIs36[myo-2::GCaMP3]*. F3 moms from the plates with *cuIs36[myo-2::GCaMP3]* homozygotes were subjected to PCR to identify animals homozygous for *eat-2(ok3528)* as described in 2.3.6 and 2.4.1.

2.5.4 Construction of *gar-3(gk305); cuIs36[myo-2::GCaMP3]* strain OK1062

The OK1062 strain containing *gar-3(gk305); cuIs36[myo-2::GCaMP3]* was generated using the following steps. In the P0, N2 males were mated with rolling hermaphrodites from the OK1020 carrying *myo-2::GCaMP3* reporter to generate an adequate number of *myo-2::GCaMP3*/+ rolling males. In the F1 generation, *cuIs36[myo-2::GCaMP3]*+ rolling males were mated hermaphrodites from the VC657 carrying *gar-3(gk305)* mutants. In the F2 generation, cross progeny, 3 rolling hermaphrodites, which were double heterozygous for the *cuIs36[myo-2::GCaMP3]* transgene and *gar-3(gk305)* (genotype: *gar-3(gk305)*/+; *cuIs36[myo-2::GCaMP3]*/+) were cloned into individual plates and allowed to have progeny at 20°C for three

days. Approximately 30 F3 rolling hermaphrodites from each F2 plate (total 60 hermaphrodites) were cloned to individual plates and allowed to lay eggs at 20°C overnight. F3 moms were lysed as described in 2.3.6. The tubes were frozen at -20°C. In the F4 generation, the plates were screened for 100% rollers homozygous for *cuIs36[myo-2::GCaMP3].* F3 moms from the plates with *cuIs36[myo-2::GCaMP3]* homozygotes were subjected to PCR to identify animals homozygous for *gar-3(gk305)* as described in 2.3.6 and 2.4.2.

2.5.5 Construction of *eat-2(ok3528); gar-3(gk305); cuIs36[myo-2::GCaMP3]* strain OK1075

The OK1075 strain containing *eat-2(ok3528); gar-3(gk305); cuIs36[myo-2::GCaMP3]* was generated using the following steps. In the P0, N2 males were mated with rolling hermaphrodites from the OK1020 carrying *myo-2::GCaMP3* reporter to generate an adequate number of *cuIs36[myo-2::GCaMP3]*/+ rolling males. In the F1 generation, *cuIs36[myo-2::GCaMP3]*/+ rolling males were mated with *eat-2(ok3528); gar-3(gk305)* mutants. In the F2 generation, cross progeny, 6 rolling hermaphrodites, which were triple heterozygous for the *cuIs36[myo-2::GCaMP3]* transgene, *eat-2(ok3528)* and *gar-3(gk305)* (genotype: *eat-2(ok3528)*/+*; gar-3(gk305)*/+; *cuIs36[myo-2::GCaMP3]*/+) were cloned into individual plates and allowed to have progeny at 20°C for three days. Approximately 20 F3 rolling hermaphrodites from F2 plates (total 120 hermaphrodites) were cloned to individual plates and allowed to lay eggs at 20°C overnight. F3 moms were lysed as described in 2.3.6. The tubes were frozen at -20°C. In the F4 generation, the plates were screened for 100% rollers homozygous for *cuIs36[myo-2::GCaMP3].* F3 moms from the plates with *cuIs36[myo-2::GCaMP3]* homozygotes were subjected to two separate PCRs to identify animals homozygous for *eat-2(ok3528); gar-3(gk305).* PCR reaction was described in 2.3.6. PCR conditions, programs and primers to identify *eat-2(ok3528)* and *gar-3(gk305)* were described in 2.4.1 and 2.4.2 respectively.

2.5.6 Construction of *ceh-28(cu11); cuIs36[myo-2::GCaMP3]* strain OK1059

The OK1059 strain containing *ceh-28(cu11); cuIs36[myo-2::GCaMP3]* was generated

using the following steps. In the P0, N2 males were mated with hermaphrodites from *ceh-28(cu11)* strain to generate an adequate number of *ceh-28(cu11)*/0 males. In the F1 generation, *ceh-28(cu11)*/0 males were mated with rolling hermaphrodites from the OK1020 strain carrying *cuIs36[myo-2::GCaMP3]* reporter. In the F2 generation, cross progeny, 15 rolling hermaphrodites, which had either *ceh-28(cu11)*/+*; cuIs36[myo-2::GCaMP3]*/+ or +/+*; cuIs36[myo-2::GCaMP3]*/+ genotypes, were cloned into individual plates and allowed to lay eggs. Once laid eggs, these animals subjected to PCR to identify *ceh-28(cu11)*/+ heterozygotes. F2 moms were lysed as described in 2.3.6. The PCR reaction was described in 2.3.6. The PCR program was (1) 94°C - 2 min, (2) 94°C - 45 sec, (3) 54°C - 45 sec, (4) 72°C - 2 min, (5) go to step 2 - 39 times, (6) 72°C - 5 min, (7) 12°C – forever. The PCR primers used were PO640 [CCCAATGCAATCTACGCAG], PO641 [GAATCAAACCGCCAACCAG] and PO642 [CCCAGCGTGTCATACATGG]. Under these conditions, a wild type *ceh-28* amplified a 269 bp fragment and *ceh-28(cu11)* homozygote amplified a 516 bp fragment, which were visualized on 1.5% agarose gel. The rolling progeny from F2 moms who were *ceh-28(cu11)*/+*; cuIs36[myo-2::GCaMP3]*/+ were cloned (total 60 hermaphrodites) into individual plates and allowed to have progeny at 20°C for three days. F3 moms were lysed as described in 2.3.6. The tubes were frozen at -20°C. In the F4 generation, the plates were screened for 100% rollers homozygous for *cuIs36[myo-2::GCaMP3]*. F3 moms from the plates with *cuIs36[myo-2::GCaMP3]* homozygotes were subjected to PCR to identify animals homozygous for *ceh-28(cu11)* as described above in the paragraph.

2.5.7 Calcium imaging in the pharyngeal muscles

10-12 young adult animals were incubated in 7 µl of 20mM serotonin (Sigma, Cat# H7752-5G) for 10 min on 2% agarose pad. Then worms were immobilized using 1.5 µl Polystyrene 0.10 micron microspheres (Polysciences, Inc, Cat# 00876) by applying them directly in the drop of serotonin. A coverslip was very gently placed on the top of the animals immediately after applying microspheres.

GCaMP3 imaging was performed on a Zeiss AxioImager microscope using a Q-Imaging Rolera EM-C^2 EMCCD camera. Individual animal that pumped was recorded at 25-30 frames/sec for 1 min using ZEN software, 63X magnification, GFP filter and 2x2 binning function. Exposure time to the blue light (475-485nm) was set so that the isthmus region was not overexposed. Time-lapse recording was started as soon as blue light was on, because it inhibits the pharyngeal muscle contractions.14-bit TIFF images were exported from time-lapse recording.

2.5.8 Analyzing calcium imaging in the pharyngeal muscles

Animals pumping with a frequency less than 100 pumps/min were analyzed. For quantification, the pharynx was straightened with CellProfiler (Kamentsky et al., 2011) and aligned using StackReg Fiji plugin (Thevenaz et al., 1998) (Appendix L). The isthmus was cropped and two regions of interest (ROI) were drawn as 10 pixel (2.54 μm) wide lines in the center and posterior isthmus respectively. Fluorescence measurements were analyzed using custom Matlab scripts or using Micrsoft Excel. Total fluorescence was measured within the ROI and normalized for each GCaMP3 peak using formula: normalized $\Delta F=(Fmax-Fmin)/Fmin*100\%$ (where Fmax is maximum fluorescence of GCaMP3 peak and Fmin is a minimum fluorescence immediately before GCaMP3 increase). Peak duration was quantified as a width of GCaMP3 fluorescence at half peak height. Rise time was quantified as time that it took for each fluorescence peak to reach its maximum using Matlab scripts (Appendix K). A Student t-test was used to compare GCaMP3 fluorescence measurements between different genotypes, and boxplots were generated using the Matlab *boxplot* command. Peak delay was calculated as time between the maximum increase in GCaMP3 fluorescence in the center and posterior isthmus using the Matlab *diff* command (Appendix K).

2.6 Analyzing calcium transients in the M4 motor neuron during pumping and peristalsis

2.6.1 Generation *ser-7b::GCaMP3* reporter pOK290.02

A 50 µl reaction containing 1 µg of pOK197.03 (*ser-7b* promoter containing plasmid) was incubated with 5 µl of 10X NEB buffer #2, 0.5 µl of 100X BSA, 1 Unit of SphI and 1 Unit of XbaI for 3 hours at 37°C. This reaction excised *ser-7b* promoter sequence 2126 bp long, which served as an insert. At the same time, a 50 µl reaction containing 0.75 µg of pOK270.01 (*str-2::GCaMP3* plasmid) was incubated with 5 µl of 10X NEB buffer #2, 0.5 µl of 100X BSA, 1 Unit of SphI and 1 Unit of XbaI for 3 hours at 37°C. This reaction excised GCaMP3 sequence 4748 bp long, which served as a vector. To dephosphorylate two ends of linearized vector and prevent religation of the vector to itself, the vector was dephosphorylated with CIAP. After the restriction digestion was over, 0.5 Units of CIAP were added directly to the restriction digest mix, which contained pOK270.01 plasmid and incubated for 1 hour at 37°C. EDTA was added at the final concentration 0.4mM to stop dephosphorylation and incubated for 15 min at 65°C. The digested products were purified by gel electrophoresis and eluted in 30 µl of dH_20. Then, the insert was ligated into the vector with 1:3 (vector : insert) ratio to generate a plasmid pOK290.02 of 6910 bp total size. 10 µl ligation reaction contained 42.52 ng of the insert, 31.7 ng of the vector, 2µl 5X of ligase buffer and 0.5 Units of T4 DNA ligase. The ligation reaction was incubated at the room temperature for 2 hours. The entire ligation mix was transformed into the 100 µl of the competent DH5 alpha *E. coli* cells using methods described in 2.3.9, and all the cells were spread on the 2X TY plate containing 100 ng/µl ampicillin. A tube with 2X TY growth media was inoculated with a single colony from the plate. Ten colonies were picked into ten tubes and incubated overnight at 37°C while shaking. The plasmid DNA was isolated from these cultures next day using methods described in 2.3.1. Purified plasmid DNA was digested with HindIII to confirm that it contained *ser-7b::GCaMP3* sequence. The plasmid DNA was subjected to sequencing as described in 2.3.10.

2.6.2 Construction of *cuIs32[ser-7b::GCaMP3]* strain OK0991

Germline transformations were performed by microinjection using pRF4 (50 ng/µl) containing *rol-6(su1006)* as a transformation marker and the *ser-7b::GCaMP3* reporter pOK290.02 (80 ng/µl) using methods described in 2.2.2. The extrachromosomal *ser-7b::GCaMP3* transgene *cuEx791* was chromosomally integrated by UV-TMP mutagenesis using methods described in 2.2.3 and outcrossed to form OK0991 carrying *cuIs32[ser-7b::GCaMP3]*.

2.6.3 Construction of *ceh-28(cu11); cuIs32[ser-7b::GCaMP3]* strain OK1022

The OK1022 strain containing *ceh-28(cu11); cuIs32[ser-7b::GCaMP3]* was generated using the following steps. In the P0, N2 males were mated with hermaphrodites from *ceh-28(cu11)* strain to generate an adequate number of *ceh-28(cu11)*/0 males. In the F1 generation, *ceh-28(cu11)*/0 males were mated with rolling hermaphrodites from the OK0991 strain carrying *cuIs32[ser-7b::GCaMP3]* reporter. In the F2 generation, cross progeny, 15 rolling hermaphrodites, which had either *ceh-28(cu11)*/+*; cuIs32[ser-7b::GCaMP3]*/+ or +/+*; cuIs32[ser-7b::GCaMP3]*/+ genotypes, were cloned into individual plates and allowed to lay eggs. Once laid eggs, these animals subjected to PCR to identify *ceh-28(cu11)*/+ heterozygotes. F2 moms were lysed as described in 2.3.6. and subjected to PCR to identify *ceh-28(cu11*)/+ as described in 2.5.6. The PCR reaction was described in 2.3.6. The progeny from F2 moms who were *ceh-28(cu11)*/+*; cuIs32[ser-7b::GCaMP3]*/+ were cloned (total 60 hermaphrodites) into individual plates and allowed to have progeny at 20°C for three days. F3 moms were lysed as described in 2.3.6. The tubes were frozen at -20°C. In the F4 generation, the plates were screened for 100% rollers homozygous for *cuIs32[ser-7b::GCaMP3]*. F3 moms from the plates with *cuIs32[ser-7b::GCaMP3]* homozygotes were subjected to PCR to identify animals homozygous for *ceh-28(cu11)* as described in 2.5.6. The PCR reaction was described in 2.3.6.

2.6.4 Calcium imaging in the M4 motor neuron

10-12 young adult animals were incubated in 7 µl of 20mM serotonin (Sigma, Cat# H7752-5G) for 10 min on 2% agarose pad. Then worms were immobilized using 1.5 µl Polystyrene 0.10 micron microspheres (Polysciences, Inc, Cat# 00876) by applying them directly in the drop of serotonin. Coverslip was very gently placed on the top of the animals immediately after applying microspheres.

GCaMP3 imaging was performed on a Zeiss AxioImager microscope using a Q-Imaging Rolera EM-C^2 EMCCD camera. Individual animal that pumped was recorded at 25-30 frames/sec for 1 min using ZEN software, 63X magnification, FITC filter and 2x2 binning function. Exposure time to the blue light (475-485nm) was set so that the processes of the M4 motor neuron were not overexposed. Time-lapse recording was started as soon as blue light was on, because it inhibits the pharyngeal muscle contractions.14-bit TIFF images were exported from time-lapse recording.

2.6.5 Analyzing calcium imaging in the M4 motor neuron

Animals pumping with frequency less than 100 pumps/min were analyzed. For quantification, the pharynx was straightened with CellProfiler (Kamentsky et al., 2011) and aligned using StackReg Fiji plugin (Thevenaz et al., 1998) (Appendix L). The isthmus was cropped and three regions of interest (ROI) were drawn as identical boxes in anterior, middle and posterior regions of M4 processes. Fluorescence measurements were analyzed using custom Matlab scripts or using Micrsoft Excel. Total fluorescence was measured within the ROI and normalized for each GCaMP3 peak using formula: normalized $\Delta F=(Fmax-Fmin)/Fmin*100\%$ (where Fmax is maximum fluorescence of GCaMP3 peak and Fmin is a minimum fluorescence immediately before GCaMP3 increase). A two-tailed Student's t-test was used to compare GCaMP3 fluorescence measurements between different genotypes, and boxplots were generated using the Matlab *boxplot* command (Appendix K). Peak delay was calculated as time between the maximum increase in GCaMP3 fluorescence in either middle

and anterior or middle and posterior parts of M4 using the Matlab *diff* command.

2.7 Construction of *cuEx794[eat-5::GFP]* strain OK0988

Germline transformations were performed by microinjection using pRF4 (100 ng/µl) containing *rol-6(su1006)* as a transformation marker and the *eat-5::GFP* reporter pOK295.01 (15 ng/µl) using methods described in 2.2.2 to form OK0988 strain carrying *cuEx794[eat-5::GFP]*.

2.8 Construction of *cuEx796[inx-3::GFP]* strain OK0990

Germline transformations were performed by microinjection using pRF4 (100 ng/µl) containing *rol-6(su1006)* as a transformation marker and the *inx-3::GFP* reporter pOK295.02 (15 ng/µl) using methods described in 2.2.2 to form OK0990 strain carrying *cuEx796[inx-3::GFP]*.

2.9 Growth assay

20 adult hermaphrodites were allowed to lay eggs on two OP50 seeded NGM plates for 8 hours at 25°C. Embryos were transferred to freshly seeded plates forming a crescent around *E. coli* and incubated at 20°C for 16 hours (overnight). Next day, unhatched embryos were counted, and hatched L1s were allowed to grow an additional three days. Adult animals were counted and removed on day 5. *eat-2(ok3528)* and *eat-2(ok3528); gar-3(gk305)* were allowed to grow for an additional day to quantify slow growing adults. For each genotype, two plates were set up with 50 embryos each.

2.10 Adult life span assay

Life span assay was performed according to previously published protocol (Sutphin and Kaeberlein, 2009). For this assay NGM plates were freshly seeded with OP50 and then *E. coli* cells were UV-killed using following steps. The lids were removed from the plates and the plates were placed inside Stratagene UV Stratalinker 1800. Energy was set to '9999' and the plates were exposed to UV for approximately 5 min. Plates with UV-killed OP50 could be stored at 4°C for up to 1 month. For each genotype tested 4 plates with 30 L4 worms were set up. 1 plate was an extra plate to replace missing animals. Plates were incubated at 20°C during life span assay.

30 L4 worms were transferred to NGM plates with UV-killed OP50. Early in their life span they were transferred to the new plates two times a week (every three days) to prevent counting their grown progeny. Occasionally, animals would move to the edge of the plate and desiccate there. These animals were called 'missing' and every time the plates were checked for dead animals they were also checked for missing worms by tilting the plate and looking at the edges. The missing animals were replaced by the animals of the same age that had been maintained in parallel. The dead animals were removed and scored. To make sure that the animal was dead the head of the worm was tapped with platinum wormpick. The worm was scored as dead if it did not respond by moving its head. The date and the number of worms that were alive were recorded and the plates were returned to 20°C. When animals entered a reproductively non-active period and stopped laying eggs, they were kept on the same plates without transferring. The plates were monitored until all worms have died. Kaplan Meier Survival Analysis was used to generate survival plots by entering the total number of animals on 3 plates at the beginning of the experiment and number of survived animals at different time points (GraphPad Prism 5). Median life span was calculated and Chi-square statistical analysis was performed for each genotype tested.

2.11 Determining the M4 gene expression profile in wild type and *ceh-28(cu11)* mutants

2.11.1 Immunostaining using anti-FLAG antibodies to confirm transgene function

2.11.1.1 Animals harvesting and fixation

Antibody staining was performed according to the Finney-Ruvkun protocol (Finney and Ruvkun, 1990). Strains N2, OK0793 *unc-119(ed3); culs30 [ser-7b::3XFLAG::PABP]* and OK0828 *ceh-28(cu11); culs30* were grown on two 60mm NGM plates seeded with OP50 *E. coli* until plates were full of worms of a mixed population. Animals from each plate were washed with 2ml of H_2O and transferred to the eppendorf tubes. Once animals settled down, they were spun down at 2000 rpm for 2 min and supernatant was gently aspirated. All the following centrifugations were performed at 2000 rpm for 2 min followed by gentle aspiration of a

supernatant. 1 ml of H_2O was added into then eppendorf tube with worms and previous step was repeated. To fix the animals, 1.25 ml of freshly prepared fixative solution was added, which contained 1X Modified Ruvkun's Witches Brew (80mM KCl, 20mM NaCl, 10mM EGTA, 5mM Spermidine, 30mM PIPES at pH 7.4, 50% Methanol) and 1% formaldehyde. Animals were gently mixed by inversions. The tube with worms was immersed in dry ice/ethanol to freeze. Then the tube was thawed on ice and incubated on ice with occasional agitation for 30 min.

2.11.1.2 Reduction of disulfide linkages

Animals were spun down and supernatant was gently aspirated. Worms were resuspended in 1 ml of 1X TTB (100mM Tris HCl at pH 7.4, 1% Triton-X 100, 1mM EDTA) and 1% 2-mercaptoethanol following by incubation at 37°C for 2 hours with gentle shaking. After this point the worms were fragile and were handled very gently. Animals were spun down and supernatant was gently aspirated. Then they were resuspended in 1 ml of 1X Borate buffer at pH 9.2 (25mM H_3BO_3, 12.5mM NaOH) and spun down. Animals were again resuspended in 1 ml of 1X Borate buffer containing 10mM DTT and incubated at room temperature for 15 min while shaking. Then they were spun down again.

2.11.1.3 Oxidation of –SH groups

1 ml of 1X Borate buffer was added following by spinning. Worms were resuspended in 1 ml of 1X Borate buffer containing 0.3% H_2O_2 and incubated at room temperature for 15 min. Animals were spun down, washed with 1 ml of 1X Borate buffer and spun down again. Worms were resuspended in 1 ml of Antibody buffer B (1X PBS, 0.2% BSA, 0.5% Triton-X 100, 0.05% NaN3, 1mM EDTA) and incubated for 15 min. Then animals were spun down and resuspended in 1 ml of Antibody buffer A (1X PBS, 1% BSA, 0.5% Triton-X 100, 0.05% NaN3, 1mM EDTA).

2.11.1.4 Antibody staining

20 µl of worms were transferred to eppendorf tube and anti-FLAG primary antibodies (Sigma, Catalog# F3165-0.2MG) at 1:1000 dilution were added in 200 µl of Antibody buffer A. Animals were incubated at room temperature for 2 hours with gentle shaking and spun down.

Then, the animals were resuspended in 500 µl of Antibody buffer B and spin was repeated. Worms were resuspended again in the same volume of Antibody buffer B and incubated at room temperature for 2 hours with gentle shaking. Animals were spun down followed by aspiration of supernatant. Texas Red labeled goat anti-mouse secondary antibodies at 1:250 dilution and DAPI at 1:1000 dilution were added. Then tubes were wrapped into the aluminum foil and were incubated at room temperature for 2 hours with gentle shaking. Animals were washed by spinning down and resuspending in 500 µl of Antibody buffer B. Previous step was repeated one more time followed by incubation at room temperature for 2 hours with gentle shaking. Animals were spun down, resuspended in 500 µl of Antibody buffer A, spun down again and most of the supernatant was removed. 100 µl of Antibody buffer A was added and 10 µl of worms was pipetted on the glass slide. A cover slip was placed on top and sealed with nail polish. Worms were visualized on a Zeiss AxioImager microscope equipped for fluorescence microscopy and DIC. Images were captured with an MRm camera and ZEN Software.

2.11.2 Coimmunoprecipitation of poly(A) mRNA from M4

Coimmunoprecipitation of poly(A) mRNA from M4 was performed according to modified Poly-A binding protein protocol provided by David Miller.

2.11.2.1 Preparation of the HB101 bacterial culture

To obtain 15 ml of concentrated of *E. coli* strain HB101, 3 L of Luria Bertani growth media (10g Tryptone, 5g Yeast extract, 10g NaCl and dH_2O to 1 L) were inoculated with a single HB101 colony using aseptic techniques. The inoculated culture was incubated at 37°C overnight. The next day, the culture was spun down at 3000 rpm for 30 min at 4°C and precipitated bacteria were gently resuspended on ice by pipetting in 15 ml of cold M9 buffer using 25 ml sterile plastic pipette. The HB101 stock culture was stored for a week at 4°C.

2.11.2.2 Worm growth in a liquid culture

From an unstarved 60mm NGM plate, 20 L4 worms were placed on each of eight 100mm plates seeded with 200 µl of OP50 and grown until just clear of bacteria. Worms from

each plate were washed with 2 ml S-basal and added into the 2 L flask containing 500 ml S-basal. To make 1L of S-basal, 5.85 g NaCl, 50 ml 1M potassium phosphate buffer at pH 6.0 (98g KH2PO4, 48g K2HPO4 and dH_2O to 1 L) were mixed in dH_2O added to 1 L and sterilized by autoclaving. Once the medium cooled down, 2ml of 5 mg/ml cholesterol was added. 5 ml of concentrated HB101, 100 µl of nystatin (final concentration 2,000Units/ml) and 100 µl of streptomycin (final concentration 10 µg/ml) were added to the worm liquid culture. The flask was put on a shaker at 20°C with vigorous shaking, so that the culture is well oxygenated. The worm culture was incubated for 6 days until was full of adults. The same amount of HB101, streptomycin and nystatin was added to the worm culture every day.

2.11.2.3 Worm harvesting and bleaching

Animals were harvested by centrifugation in 50 ml conical tubes (all centrifugations were at 2500 rpm for 3 min at 4°C unless is stated otherwise). After every spin, supernatant was aspirated and worm culture was added until all worms were pelleted. Next, animals were washed 3 times by centrifugation with cold M9 buffer until supernatant is clear. Animals were bleached for 4 min by continuously inverting the tubes. Then the tubes were spun down for 1 min and supernatant was quickly removed. Fresh Bleach solution was added to the animals and tubes were inverted for another 4 min (solution turned yellow when most of the animals were lysed). For 1 ml of pelleted animals 10 ml of Bleach solution (2 ml of sodium hypochlorite, 0.5 ml 10N NaOH and 7.5 ml dH_2O) was used. The released embryos were spun down for 1 min and supernatant was quickly removed. The embryos were washed 3 times by centrifugation with 10 ml of cold M9.

2.11.2.4 Sucrose flotation

Sucrose flotation was performed to separate live embryos from dead embryos and dead animals. Embryos were combined in 15 ml conical tubes. The total volume of pelleted embryos in one tube did not exceed 500 µl. Embryos were resuspended in 5 ml cold dH_2O and 5 ml 60% sucrose was added. The tube was inverted several times to mix the embryos with sucrose

solution and centrifuged at 1200 rpm for 6 min at 4°C. The floated embryos were carefully collected into the 5 ml of cold dH_2O with sterile plastic pipette and washed 3 times with 10 ml cold of M9 buffer. The floated embryos on the top were mostly alive and all the dead embryos along with dead animals were collected on the bottom of the tube.

2.11.2.5 Worm synchronization and fixation

300 µl to 1ml of pelleted embryos were resuspended in 50ml room temperature M9 and then this volume was divided between two 50ml conical tubes. Embryos were allowed to hatch by incubating at 20°C for 15 hours at 200 rpm. The next day, hatched L1s were collected by centrifugation. Packed L1s were resuspended in 100 ml of S-basal and incubated at 20°C for 6 hours at 200 rpm. After recovery, L1 animals were washed 3 times with cold M9 buffer by centrifugation. 20% paraformaldehyde (PFM) solution was freshly made by resuspending PFM powder in 4.5X weight (in mg) µl of 5mM NaOH and heating at 65°C with occasional mixing until PFM was dissolved. Worms were fixed with 0.5% PFM by incubating for 1 hour at 4°C on a nutator. L1s' pellets of 300 µl pellets and less were fixed in 10 ml 0.5% PFM. L1s' pellets between 300 µl and 1 ml were fixed in 30 ml of 0.5% PFM. Animals were washed 4 times with cold M9 buffer by centrifugation and flash frozen in liquid nitrogen. At this point L1s can be stored at -80°C.

2.11.2.6 Obtaining L1 lysates

100 µl of pelleted L1 animals were washed once with 1 ml of cold homogenization buffer (HB) by centrifugation at 2500 rpm for 2.5 min at 4°C. HB buffer (150mM NaCl, 50mM HEPES, pH 7.6, 10mM $MgCl_2$, 1mM EGTA, 15mM EDTA, 0.6 mg/ml heparin, 10% glycerol, 0.1% DEPC-H_2O) contained Protease Inhibitor Cocktail Tablet (Roche, Catalog# 11836153001), 1mM DTT, 50U/ml RNasin (Promega Cataog# N2111), 8mM ribonucleoside vanadyl complex (VRC, New England BioLabs, Catalog# S1402S). Because VRC collects at the bottom of the tube, HB was inverted a few times before using. Pelleted L1s were resuspended in 250 µl cold HB and then homogenized by sonication [12 rounds, 8 sec each round = (0.9 sec-pulse on + 0.1 sec-pulse

off) x 8 times]. The tube was placed in ice bath for 15 sec after each round of sonication to prevent overheating. Worm lysate was recovered by centrifugation at 18000 g for 20 min at 4°C, aliquoted and kept -80°C until ready to use.

2.11.2.7 Extraction of total RNA with Trizol

Thirty µl of L1 lysate was used to determine yield of total RNA. 270 µl of Trizol (ThermoFisher Scientific, Catalog# 15596026) was added to the lysate, mixed well by inverting several times and incubated at room temperature for 5 min. Sixty µl of chloroform was added, shaken for 15 sec and incubated at room temperature for 10 min. The tubes were spun down at 14000 rpm for 15 min at 4°C. An aqueous layer was removed to a new eppendorf tube. An equal volume of isopropanol was added, mixed well by inverting several times and at the room temperature for 10 min. The tubes were spun down at 14000 rpm for 25 min at 4°C. The pellet was washed with 1 ml of 75% ethanol by spinning down at 7500 rpm for 5 min at 4°C. The pellet was washed one more time with 1 ml of 100% ethanol by spinning down at 7500 rpm for 5 min at 4°C. The pellet was air dried for 5 min and resuspended in 20 µl of DEPC-H_2O. Total RNA concentration was determined by using Nanodrop as described in 2.3.4.

2.11.2.8 Immunoprecipitation of mRNA/FLAG-PABP

Eighty µl of suspended anti-FLAG M2 beads (Sigma, Catalog# F2426) were prepared by washing 2 times in 0.1M glycine (made in DEPC-H_2O, pH 3.5) and 4 times in 1ml of cold HB (all centrifugations were performed at 3500 rpm for 5 min at 4°C unless stated otherwise). An amount of lysate corresponding to 200 µg of total RNA was added to 50 µl of prepared beads. Cold 4°C HB containing 400U/ml RNasin and 1.6mM VRC was added up to 1 ml. This lysate was incubated with beads for 2 hours at 4°C on a nutator. Then beads were quickly washed 2 times with of 1ml low-salt HB. The beads were washed additional 2 times by incubating for 30 min each time while rotating on a nutator. The beads were spun down for 3 min after each wash. Low-salt HB contained 25 mM NaCl, 20 mM HEPES at pH 7.6, 1mM EGTA, 1mM EDTA,

0.6 mg/ml heparin, 10% glycerol, 0.1% DEPC-H_2O and stored at 4°C. After the final wash, supernatant was removed and beads were ready for elution.

2.11.2.9 Elution of mRNA/FLAG-PABP and mRNA extraction

Elution buffer (50mM Tris at pH 8.0, 10 mM EDTA at pH 8.0 and 1.3% SDS) was preheated at 65°C before using. 100 µl of elution buffer, which contained 40U/ml RNasin, was added to the beads and incubated 15 min at 65°C while rotating in hybridization oven. After incubation beads were spun down (all centrifugations were performed at 3500 rpm for 5 min at 4°C unless stated otherwise) and eluate was removed to a new eppendorf tube. 100 µl of an elution buffer was added again and elution step was repeated 3 more times. Eluates were pooled together and incubated with Proteinase K at the final concentration 0.16mg/ml (New England BioLabs, Catalog# P8107S) for 1 hour at 65°C to remove a crosslink between mRNA and FLAG-PABP. mRNA was extracted from pooled eluates using Qiagen RNeasy Micro Kit (cat# 74004) and stored at -80°C until ready to submit for library preparation and sequencing.

2.11.3 Reverse transcription PCR (RT-PCR)

To synthesize single-stranded cDNA form purified mRNA the High Capacity cDNA Reverse Transcription Kit was used (ThermoFisher Scientific, Catalog# 4368814). RT reaction of total volume 20 µl included 10 µl of 20 ng RNA, 2 µl of 10X RT Buffer, 0.8 µl of 25X dNTP mix, 2 µl of 10X Random Primers, 1 µl of MultiScribe Reverse Transcriptase (50 Units), 1 µl of RNasin (40 Units) and 3.2 µl of Nuclease free H_2O. In the negative control for the RT reaction MultiScribe Reverse Transcriptase was substituted with 1µl Nuclease free H_2O. Tubes with RT reaction were loaded into the Thermal Cycler and following conditions were programed: (1) 25°C – 10 min, (2) 37°C – 120 min, (3) 85°C – 5 min, (4) 4°C - Forever.

PCR primers were designed for *ceh-28* and *ser-7* and *ama-1* and when possible primers spanned two exons to avoid amplification of genomic DNA that may be present. Primers for *ceh-28* PCR were PO0643 (ACAACAGCAGAAGAGAAAACCGAG) and PO0644 (GCTAACCGCTTGCATTTGTATCG). Primers for *ser-7* PCR were PO1401

(CTTTTTCGTGGGGCTCGTTG) and PO1402 (GTGCATAGCGTTAGGTCGGA). Primers for *ama-1* PCR were PO1061 (AGGCGAAGGATGTGTTGTG) and PO1062 (TCACCGTGTTCTTTGGGTC). The PCR conditions used for amplification and product sizes for each gene are indicated Table VIII.

2.11.4 Library preparation and RNA sequencing

The Quant seq protocol was used to prepare a library close to 3' end of mRNA (Moll et al., 2014). QuantSeq generates strand-specific next-generation sequencing (NGS) libraries close to the 3′ end of poly(A) RNAs. Sequencing of 3' end of mRNA makes easier counting transcripts and perfect in our case of recovering partially degraded RNA after performing Co-IP and purification steps. QuantSeq allows generation of one fragment per transcript, directly linking gene expression to the number of reads mapping a gene. NGS reads are generated towards the poly(A) tail and directly correspond to the mRNA sequence. QuantSeq library preparation and Illumina RNA sequencing was performed by the University of Illinois RRC.

2.11.5 Analysis of RNA-seq data

Analysis of RNA-seq data was performed by Core of Research Informatics (CRI) at University of Illinois and included the following steps. Bowtie2 was used to align the sequences with *C. elegans* genome, HTseq to count the number of reads per sample and EdgeR to perform differential analysis (Anders et al., 2013; Anders et al., 2015; Trapnell et al., 2012).

3 Crosstalk between acetylcholine receptors affects signaling at the neuromuscular junction in the *Caenorhabditis elegans* pharynx

3.1 Abstract

Precise signaling at the neuromuscular junction (NMJ) is essential for proper muscle contraction. In the *C. elegans* pharynx, acetylcholine (ACh) released from the MC and M4 motor neurons stimulate two different types of contractions in adjacent muscle cells, termed pumping and isthmus peristalsis. MC stimulates rapid pumping through the nicotinic ACh receptor EAT-2, which is tightly localized at the MC NMJ, and *eat-2* mutants exhibit a slow pump rate. Surprisingly, we found that *eat-2* mutants also hyperstimulated peristaltic contractions, and these are characterized by increased and prolonged Ca^{2+} transients in the isthmus muscles. This hyperstimulation depends on crosstalk with the GAR-3 muscarinic acetylcholine receptor as *gar-3* mutation specifically suppressed the prolonged contraction and increase Ca^{2+} observed in *eat-2* mutant peristalses. GAR-3 dependent hyperstimulation was also observed in mutants lacking the *ace-3* acetylcholinesterase, and we suggest that NMJ defects in *eat-2* and *ace-3* mutants result in ACh spillover that stimulates extrasynaptic GAR-3 receptors in adjacent isthmus muscles. *gar-3* mutation also suppressed slow larval growth and prolonged lifespan phenotypes that result from dietary restriction in *eat-2* mutants, indicating that crosstalk with the GAR-3 receptor has a long-term impact on feeding behavior and *eat-2* mutant phenotypes.

3.2 Introduction

Communication between motor neurons and their target muscles is crucial for proper muscle contraction and function. This communication is mediated by the neurotransmitter acetylcholine (ACh), which is released from the motor neuron and binds receptors embedded in the muscle cell membrane. In vertebrate skeletal muscle, these receptors are nicotinic acetylcholine receptors (nAChRs), which are homo- or hetero-penatmeric, ligand-gated ion channels [reviewed in (Albuquerque et al., 2009)]. In smooth and cardiac muscle, the receptors are typically muscarinic acetylcholine receptors (mAChRs), which are 7-pass transmembrane, G-protein coupled receptors [reviewed in (Wess, 2004)]. nAChRs are fast-acting receptors that rapidly and directly depolarize muscle cells to stimulate contraction in response to ACh, while mAChRs act more slowly by activating downstream signal transduction cascades and can either stimulate or inhibit contraction. A number of inherited and acquired diseases affecting communication at the neuromuscular junction in human skeletal muscle exhibit defects in nAChRs and other proteins required for their function, including myasthenia gravis and congenital myasthenic syndromes [reviewed in (Engel et al., 2015);(Gilhus, 2016)].

We are examining the mechanisms controlling contractions of the pharyngeal muscles of *Caenorhabditis elegans*. The pharynx is a tubular organ with large muscle cells positioned around a central lumen (Figure 11A) (Albertson and Thomson, 1976). The myofilaments in these muscles are oriented radially, so that contraction opens the pharyngeal lumen and relaxation closes this lumen. During feeding, these muscles perform two distinct types of contractions, termed pumping and peristalsis [reviewed in (Avery and You, 2012)]. Pumping occurs frequently (~200/min), and it is a simultaneous contraction of muscles in the corpus and anterior isthmus that ingests bacteria into the lumen and concentrates this material in the anterior region of the isthmus, while at the same time contraction of muscles in the terminal bulb crushes bacteria and expels the debris into the intestine (Figure 11B). Peristalsis occurs relatively infrequently and

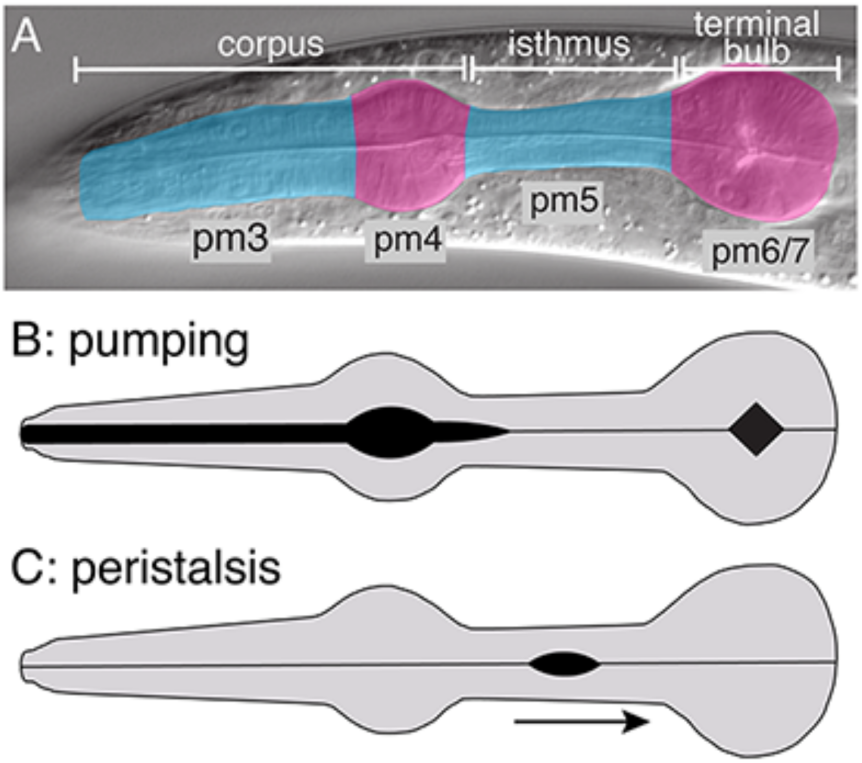

Figure 11 Pharyngeal anatomy and contractions

(A) DIC micrograph of an adult pharynx indicating anatomical regions (white bars) and colored to indicate the location of pharyngeal muscle cells (pm). The pharynx exhibits 3-fold rotational symmetry, and there are three of the pm3-pm7 muscle cells surrounding the central lumen (Albertson, 1976). pm5 cells extend the length of the isthmus and are the primary focus of this work. (B, C) Diagrams indicating pharyngeal muscle contractions during pumping and peristalsis. The black regions indicate open lumen, and the arrow indicates the direction of the peristaltic contraction. This figure is adapted from (Ray et al., 2008).

always following a pump. Peristalsis is a wave-like contraction followed by rapid relaxation traveling through the pm5 muscle that transports a bolus of ingested bacteria from the anterior isthmus to the terminal bulb (Figure 11C). The contractions in the pm5 muscle are remarkably complex. Three pm5 muscles are arranged around the circumference of the pharyngeal lumen, and each of these cells extends through the entire length of the isthmus (Figure 11A) (Albertson and Thomson, 1976). During a pump, the anterior portion of the pm5 cells contracts to open the lumen in the anterior isthmus, but the posterior half of these cells remain relaxed. In contrast, during peristalsis, the anterior portion of pm5 remains relaxed, while a wave-like contraction followed by relaxation travels from the center to posterior isthmus.

Rapid pumping is stimulated by the two MC neurons that form synapses on the muscles near the junction of the pm4 and pm5 muscles (McKay et al., 2004), and laser ablation of the MCs results in a slow pump rate (Avery and Horvitz, 1989). The MCs stimulate a nAChR containing the non-alpha subunit EAT-2 that clusters at the MC synapses, and *eat-2* mutants exhibit the same slow pump rate observed in MC ablated animals (McKay et al., 2004; Raizen and Avery, 1994). EAT-2 stimulation initiates an increase in cytoplasmic Ca^{2+} concentration in the pharyngeal muscles that is mediated by the voltage-activated Ca^{2+} channels CCA-1 and EGL-19 leading to muscle contraction (Kerr, 2006; Shtonda and Avery, 2005; Steger and Avery, 2004). MC does not synapse on the terminal bulb, but simultaneous contraction of corpus and terminal bulb is mediated by electrical coupling (Starich et al., 1996). In the absence of MC or EAT-2, pumping occurs slowly, and it is thought that these contractions are generated autonomously within the muscle.

Peristalsis is stimulated by the single M4 motor neuron that extends processes through the isthmus and synapses on the muscles in the posterior half of pm5, and ablation of M4 eliminates peristalsis (Avery and Horvitz, 1987). The receptors that respond to M4 to produce a peristalsis are unknown, but our previous studies of M4 defective mutants have implicated mAChRs (Ramakrishnan and Okkema, 2014; Ray et al., 2008). While other studies suggest that

peptide neurotransmitters secreted from other neurons may also be involved (Song and Avery, 2012). The *C. elegans* genome contains three genes encoding mAChRs, *gar-1, gar-2,* and *gar-3*, but only *gar-3* is expressed in pharyngeal muscles (Dittman and Kaplan, 2008; Lee et al., 2000; Steger and Avery, 2004), and the muscarinic agonist arecoline can stimulate pumping through GAR-3 (Steger and Avery, 2004).

Here we examine the roles nAChRs and mAChRs play in peristalsis in wild-type animals and mutants defective in ACh synthesis or response, using both direct observation and imaging the genetically encoded Ca^{2+} indicator GCaMP3 (Tian et al., 2009). We find that treatment of mutants lacking endogenous ACh with either nicotinic or muscarinic agonists stimulated both pumping and peristaltic contractions, and the response to these agonists depends on the nAChR subunit EAT-2 and the mAChR GAR-3, respectively. Surprisingly, in the absence of exogenous agonist, *eat-2* mutants exhibited hyperstimulated isthmus muscle peristalses and increased isthmus muscle Ca^{2+} concentrations, and this hyperstimulation depends on crosstalk with the GAR-3 receptor. This relationship between EAT-2 and GAR-3 affected feeding behavior throughout the life of the animal, as *gar-3* mutation suppressed the slow larval growth and prolonged lifespan phenotypes resulting from dietary restriction in *eat-2* mutants (Avery, 1993a; Lakowski and Hekimi, 1998). *ace-3* acetylcholinesterase mutants similarly exhibited hyperstimulated isthmus peristalses that were dependent on *gar-3*, and we hypothesize that, in the absence of EAT-2 or ACE-3, unbound ACh spills over from the synapse and stimulates extrasynaptic GAR-3 in the isthmus muscles.

3.3 Materials and Methods

3.3.1 Nematode handling, transformation and strains

C. elegans strains were grown under standard conditions (Lewis and Fleming, 1995). Germline transformations were performed by microinjection using pRF4 (200 ng/µl) containing *rol-6(su1006)* as a transformation marker and the *myo-2::GCaMP3* reporter pOK294.04 (20

ng/µl) (Mello and Fire, 1995). The extrachromosomal *myo-2::GCaMP3* transgene *cuEx804* was chromosomally integrated by UV/TMP mutagenesis and outcrossed to form *cuIs36*.

The following strains were generated by the *C. elegans* Gene Knockout Consortium (Consortium, 2012): VC1836 *cha-1(ok2253); nT1[qIs51],* VC657 *gar-3(gk305),* FX863 *acr-7(tm863),* RB918 *acr-16(ok789),* VC2661 *acr-10(ok3118),* RB2294 *acr-6(ok3117),* VC2820 *eat-2(ok3528)/mT1; +/mT1*.

The following strains were constructed by others: wild-type strain N2 (Brenner, 1974), RB1132 *acr-14(ok1155)* (Ruaud and Bessereau, 2006), DA1116 *eat-2(ad1116)* (Raizen et al., 1995), DA465 *eat-2(ad465)* (Avery, 1993a), *ace-3(dc2)* (Combes et al., 2000), *ace-2(g72); ace-1(p1000)* (Culetto et al., 1999; Talesa et al., 1995), *eat-18(ad820)* (Raizen et al., 1995).

The following strains were constructed in this study: OK1020 *cuIs36[myo-2::GCaMP3]*, OK1062 *gar-3(gk305); cuIs36*, OK1063 *eat-2(ok3528); cuIs36*, OK1064 *eat-2(ok3528); gar-3(gk305),* OK1075 *eat-2(ok3528); gar-3(gk305); cuIs36, ace-3(dc2); gar-3(gk305)*, OK1023 *eat-2(ok3528).*

3.3.2 General methods for nucleic acid manipulations and plasmid construction

Standard methods were used to manipulate all DNAs (Ausubel, 1990), and plasmids sequences are available from the authors. The *myo-2* promoter from plasmid pPD 96.48 was cloned into HindIII and MscI digested *str-2::GCaMP3* plasmid (Chalasani et al., 2007) to generate pOK294.04.

3.3.3 Genotyping

Individual animals were genotyped for *eat-2(ok3528)*, *gar-3(gk305)* and *ace-3(dc2)* alleles by PCR (Beaster-Jones and Okkema, 2004). Primers for genotyping *eat-2(ok3528)* were PO1423 (TGCGTGGTAGAGGGATAGTG), PO1424 (TCTCGACGAGACCTACGTTG), PO1425 (ACAGCTACAGTACCTCGCAC). Primers for genotyping *gar-3(gk305)* were PO1426 (TAATAGGTTCGGCCCAGAGC), PO1427 (GTGATCGTTTGCTGGGAAGC), PO1428 (CGAAGCTCAGAATGTCAGTAACG). Primers for genotyping *ace-3(dc2)* were PO1435

(CAAGGATACAGAGTACACGGCA), PO1436 (CAAGCCCGCAAATTGAACTGA), PO1437 (GCAAGTGGCAAGCGAGAATA).

3.3.4 Analysis of feeding behavior and drug studies

To analyze pharyngeal muscle contractions, L1 larvae hatched in the absence of food were suspended in 5 µl of M9 buffer containing OP50 and imaged on a 2% agarose pad under a coverslip. For drug treatments, either arecoline (Acros Organics, Cat# CAS: 300-08-3) or nicotine (Sigma, Cat# N5260-25G) was included and animals were treated for 15 min prior to adding a coverslip. Individual N2 or mutant animals that pumped were recorded at 25 frames/sec for 1 min (*cha-1* mutants were recorded for 5 min) using a Zeiss AxioImager microscope with an MRm camera and ZEN Software. For each genotype and drug treatment the feeding behavior was analyzed in at least 5 animals (~500 pumps/per animal). Time-lapse images were exported and processed using Fiji (Schindelin et al., 2012) to generate time-lapse movies. Acquisition times were exported from ZEN and quantifications were performed using Microsoft Excel.

3.3.5 Calcium imaging

Young adult animals were incubated in 5 µl of 20mM serotonin (Sigma, Cat# H7752-5G) for 10 min on 2% agarose pad and then immobilized using 1.5 µl Polystyrene 0.10 micron microspheres and a coverslip (Polysciences, Inc, Cat# 00876). GCaMP3 imaging was performed on a Zeiss AxioImager microscope using a Q-Imaging Rolera EM-C^2 EMCCD camera. Time-lapse movies were captured at 25-30 frames/sec using ZEN software and 14-bit TIFF images were exported. Animals pumping with frequency less than 100 pumps/min were analyzed. For quantification, the pharynx was straightened with CellProfiler (Kamentsky et al., 2011) and aligned using StackReg Fiji plugin (Thevenaz et al., 1998). The isthmus was cropped and two regions of interest (ROI) were drawn as 10 pixel (2.54 µm) wide lines in the center and posterior isthmus respectively. Fluorescence measurements were analyzed using custom Matlab scripts or using Micrsoft Excel. Total fluorescence was measured within the ROI and

normalized for each GCaMP3 peak using formula: normalized ΔF=(Fmax-Fmin)/Fmin*100% (where Fmax is maximum fluorescence of GCaMP3 peak and Fmin is a minimum fluorescence immediately before GCaMP3 increase). Peak duration was quantified as a width of GCaMP3 fluorescence at half peak height. Rise time was quantified as time that it took for each fluorescence peak to reach its maximum. A Student t-test was used to compare GCaMP3 fluorescence measurements between different genotypes, and boxplots were generated using the Matlab *boxplot* command. Peak delay was calculated as time between the maximum increase in GCaMP3 fluorescence in the center and posterior isthmus using the Matlab *diff* command.

3.3.6 Growth assay

Adult hermaphrodites were allowed to lay eggs for 8 hours at 25˚C, and embryos were transferred to freshly seeded plates and incubated at 20˚C for 16 hours. Unhatched embryos were counted, and hatched L1s were allowed to grow an additional three days. Adult animals were counted and removed on day 5. *eat-2(ok3528)* and *eat-2(ok3528); gar-3(gk305)* were allowed to grow for an additional day to quantify slow growing adults. For each genotype, two plates were set up with 50 embryos each.

3.3.7 Life span assay

Life span assays were performed according to previously published protocol (Sutphin and Kaeberlein, 2009). Assays were performed starting with 30 L4 worms fed with UV-killed OP50 *E. coli* at 20˚C, and dead or missing animals were replaced by animals of the same age. For each experiment, triplicate plates of each genotype were assayed, and representative results of 3 or more experiment are shown. Kaplan Meier Survival Analysis was used to generate survival plots and calculate median life span, and for statistical analysis (GraphPad Prism 5).

3.4 Results

3.4.1 Pumping and isthmus peristalsis can be stimulated through both nicotinic and muscarinic receptors

We are interested in the signaling mechanisms that produce productive pharyngeal muscle contractions during feeding. M4 and the MCs are cholinergic motor neurons that express choline acetyltransferase encoded by *cha-1* (Pereira et al., 2015; Raizen et al., 1995; Ramakrishnan and Okkema, 2014), and strong *cha-1* mutants have reduced pharyngeal contractions and arrest as severely uncoordinated L1s (Avery and Horvitz, 1990; Rand, 1989). Previous studies have shown that stimulation of nicotinic acetylcholine receptors (nAChRs) with nicotine or muscarinic acetylcholine receptors (mAChRs) with arecoline could induce pharyngeal muscle contractions, but these studies did not specifically examine peristalses in the absence of endogenous acetylcholine (Avery and Horvitz, 1990; Raizen et al., 1995; Ramakrishnan and Okkema, 2014).

To extend this work, we examined the effect of nicotine or arecoline treatment on *cha-1(ok2253)* mutant L1 animals. *cha-1(ok2253)* is a previously uncharacterized null allele containing a 1.7 kb deletion that eliminates the catalytic histidine (His341) required for ACh synthesis (Consortium, 2012). Untreated *cha-1(ok2253)* homozygotes completely lacked pharyngeal muscle contractions, but mutant animals treated with either nicotine or arecoline exhibited both pumping and peristalsis (Figure 12). These results indicate that acetylcholine is necessary for pumping and peristalsis, and that activation of either nAChRs or mAChRs can stimulate these contractions. Notably we observed occasional animals treated with either agonist that exhibited peristaltic contractions in the posterior isthmus without a preceding pump (2/10 animals treated with 10 mM arecoline; 2/40 animals treated with 5 mM nicotine), consistent with previous observations that peristalsis can be uncoupled from pumping by directly stimulating receptors in the isthmus muscles (Ramakrishnan and Okkema, 2014). In addition, while higher arecoline concentrations increased the percentage of animals exhibiting

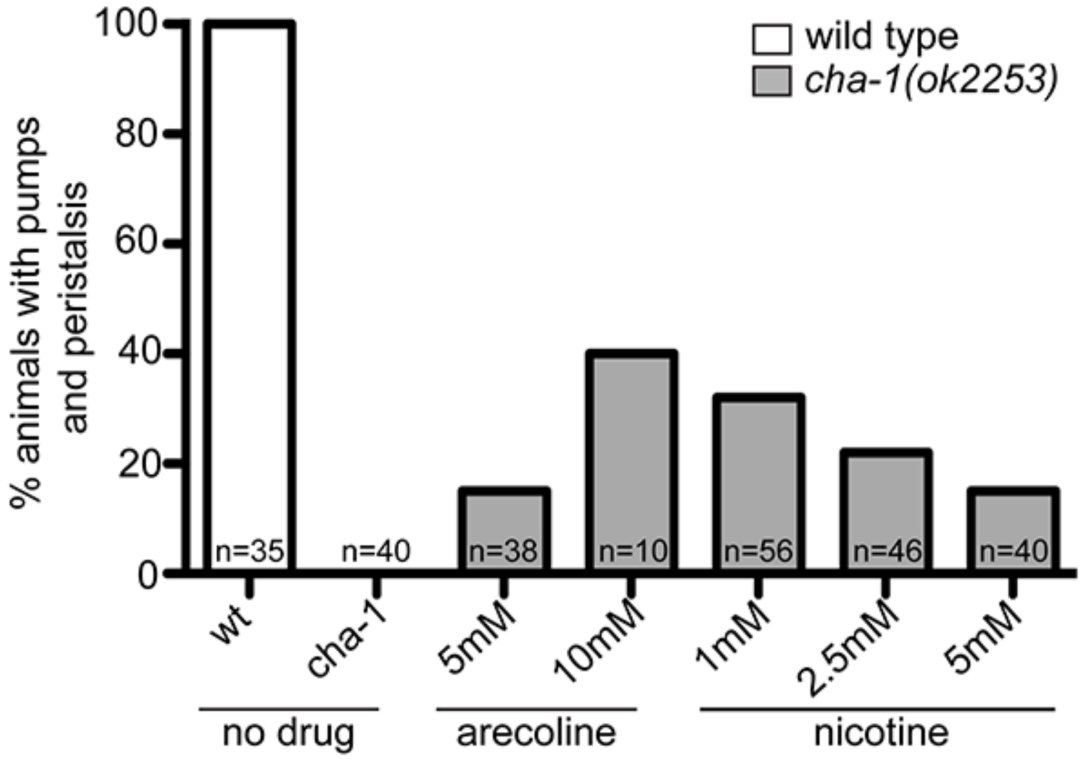

Figure 12 Muscarinic and nicotinic receptor agonists stimulate pharyngeal muscle contractions in *cha-1* mutants

The percent of wild-type or *cha-1(ok2253)* L1 animals exhibiting pharyngeal muscle pumping and peristalses, either untreated or treated with the indicated concentrations of arecoline or nicotine. Animals were visualized for 5 min each, and the number of animals observed (n) is indicated.

pharyngeal muscle contractions, higher nicotine concentration progressively decreased the percentage of animals exhibiting pharyngeal muscle contractions. This decrease may result from hyperstimulation of nAChRs as has been previously reported (Avery and Horvitz, 1990), although we did not observe the tetanic contractions previously observed in animals treated with nicotine.

3.4.2 EAT-2 and GAR-3 mediate the response to agonists

The results above indicate that activation of either mAChRs or nAChRs can stimulate pumping and peristaltic contractions in the pharynx. To identify the receptors involved in these responses, we asked if mutants affecting receptors expressed in the pharyngeal muscles become insensitive to agonists.

To examine the role mAChR signaling plays in pharyngeal muscle contractions, we characterized these contractions in *gar-3(gk305)* mutants (Consortium, 2012). *gar-3(gk305)* is a 452 bp deletion that would remove the C-terminal 151 aa of the receptor, including a portion of the third intracellular loop that mediates interaction with G-protein effectors (Kubo et al., 1988). *gar-3(gk305)* mutants are viable, look healthy and grow normally. Pharyngeal muscle contractions in *gar-3(gk305)* L1s were similar to those in wild type (Table II). Neither the rate of pumping nor the frequency or duration of peristalsis was significantly different between wild-type and *gar-3(gk305)* animals. In comparison to wild-type animals, *gar-3(gk305)* animals were almost completely insensitive to exogenously applied arecoline (Table II). Wild-type animals treated with arecoline exhibited a strongly reduced pump rate ($p < 10^{-5}$), and each of these pumps was followed by a peristalsis that was prolonged compared to untreated animals ($p < 10^{-6}$). In contrast, *gar-3(gk305)* mutants were largely unaffected by arecoline. The pump rate was unaffected in *gar-3(gk305)*, and, although these animals did exhibit a small decrease in the duration of peristaltic contractions when treated with arecoline ($p < 10^{-4}$), we note that this change is the opposite of the prolonged peristalses observed in arecoline treated wild-type animals. Thus, GAR-3 mediates the response to arecoline, but loss of this receptor has no

Table II: Quantification of pharyngeal muscle contractions

genotype (treatment)	pump rate (pumps/min ± sem)	peristalsis rate (peristalsis/min ± sem)	% pumps followed by peristalsis	duration of isthmus peristalsis (ms ± sem)
wild type [a]	218 ± 11	31 ± 3	14%	113 ± 4
wild type + arecoline [b]	13 ± 2	13 ± 2	100%	696 ± 92
gar-3(gk305) [c]	183 ± 15	32 ± 6	18%	146 ± 6
gar-3(gk305) + arecoline [d]	173 ± 13	18 ± 4	10%	119 ± 5
eat-2(ad465) [e]	66 ± 17	39 ± 11	59%	236 ± 11
eat-2(ad1116) [f]	32 ± 5	18 ± 2	63%	246 ± 9
eat-2(ok3528) [g]	27 ± 4	24 ± 3	86%	398 ± 12
eat-2(ok3528); gar-3(gk305) [h]	20 ± 2	15 ± 3	75%	227 ± 7
eat-18(ad820) [i]	19 ± 3	18 ± 3	92%	378 ± 26
ace-2(g72); ace-1(p1000) [j]	132 ± 38	20 ± 6	16%	191 ± 12
ace-3(dc2) [k]	128 ± 30	14 ± 2	14%	305 ± 14
ace-3(dc2); gar-3(gk305) [l]	235 ± 20	36 ± 7	15%	82 ± 1

[a] 17 N2 L1s were recorded for 19-20 s and a total of 1194 pumps were analyzed.

[b] Six N2 L1s treated with 5 mM arecoline were recorded for 34-46 s and a total of 48 pumps were analyzed.

[c] Six *gar-3(gk305)* L1s were recorded for 19-21 s and a total of 361 pumps were analyzed.

[d] Six *gar-3(gk305)* L1s treated with 5 mM arecoline were recorded for 19-21 s and a total of 342 pumps were analyzed.

[e] Five *eat-2(ad465)* L1s were recorded for 21-22 s and a total of 75 pumps were analyzed.

[f] Five *eat-2(ad1116)* L1s were recorded for 20-21 s and a total of 65 pumps were analyzed.

[g] Twelve *eat-2(ok3528)* L1s were recorded for 24-25 s and a total of 121 pumps were analyzed.

[h] Seven *eat-2; gar-3* L1s were recorded for 32-33 s and a total of 75 pumps were analyzed.

[i] Six *eat-18* L1s were recorded for 32-33 s and a total of 59 pumps were analyzed.

[j] Five *ace-2; ace-1* L1s were recorded for 23-24 s and a total of 258 pumps were analyzed.

[k] Five *ace-3* L1s were recorded for 20-21 s and a total of 226 pumps were analyzed.

[l] Six *ace-3; gar-3* L1s were recorded for 19-20 s and a total of 468 pumps were analyzed.

strong effect on pharyngeal muscle contractions in the absence of this drug.

We then focused on *eat-2*, which encodes the only nAChR subunit known to function in the pharyngeal muscles (McKay et al., 2004; Raizen et al., 1995). To test if *eat-2* is necessary to respond to nicotine, we compared wild-type animals and *eat-2(ok3528)* mutants treated with nicotine at the L1 stage. Like *cha-1* mutants, wild-type animals treated with increasing concentrations of nicotine exhibited a dose-dependent decrease in pharyngeal muscle contractions (Figure 13), but *eat-2* animals were not significantly affected by this treatment. Thus the pharyngeal muscle response to nicotine depends on EAT-2 containing nAChRs.

3.4.3 *eat-2* mutants exhibit prolonged pumps and peristalses

To understand how EAT-2 affects muscle contractions, we examined three strong *eat-2* mutants at the L1 stage. *eat-2(ad465)* and *eat-2(ad1116)* are point mutations introducing an early stop codon and affecting a splice site, respectively (McKay et al., 2004)(WormBase WBVar00000089), while *eat-2(ok3528)* contains a 614 bp deletion predicted to cause a frameshift mutation upstream of the transmembrane domains (Consortium, 2012). As expected, the rate of pumping in all three mutants was significantly reduced compared to wild type ($p<10^{-5}$) (Table II) (Avery, 1993a; Raizen et al., 1995). However, the duration of peristaltic contractions in the posterior isthmus was unexpectedly increased up to nearly 4-fold ($p < 10^{-20}$), with relaxation of the posterior region of the isthmus muscles particularly delayed. The percent of pumps that were followed by a peristalsis was also increased in *eat-2* mutants, but as the pump rate was decreased in these animals, the absolute rate of peristalsis was similar in wild-type animals and *eat-2* mutants. Notably, *eat-2(ok3528)* mutants exhibited the strongest phenotypes, suggesting it is a null allele.

To corroborate our observations in *eat-2* mutants, we also examined pharyngeal muscle contractions in *eat-18* mutants. *eat-18* encodes a novel transmembrane protein required for

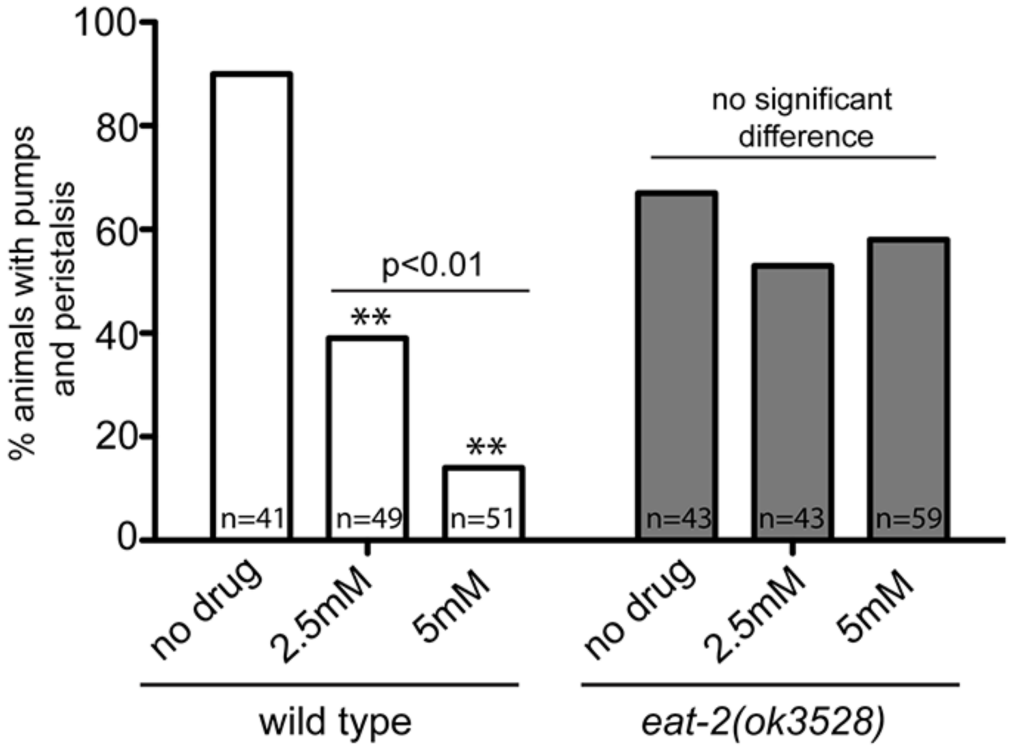

Figure 13 *eat-2* mutants are insensitive to exogenous nicotine

Percentage of wild-type or *eat-2(ok3528)* L1 animals exhibiting pharyngeal muscle pumping and peristalses, either untreated or treated with the indicated concentrations of nicotine. ** indicates significantly different than untreated animals ($p < 0.0001$), and the bar indicates significant difference between wild-type animals treated with increasing concentrations of nicotine. Animals were visualized for 5 min each, and the number of animals observed (n) is indicated.

function of EAT-2 and other nAChRs in the pharynx, and *eat-18* mutants share the reduced pump rate with *eat-2* mutants (McKay et al., 2004; Raizen et al., 1995). We found *eat-18(ad820)* animals also exhibit prolonged peristalses with almost all pumps followed by peristalses (Table II). In contrast, mutants affecting several other nAChR subunits reported to be expressed in the pharyngeal muscles, including *acr-6(ok3117), acr-7(tm863), acr-10(ok3118), acr-14(ok1155)*, and *acr-16(ok789)* (Saur et al., 2013), did not exhibit significant changes in pumping frequency, peristalsis frequency, or the duration of peristalsis (Table III).

Taken together these results indicate that loss of the EAT-2 nAChR subunit results in slow pumping and prolonged peristalses that occur after nearly every pump. Paradoxically the *eat-2* mutant defects in peristalsis are opposite those in pumping, indicating that, while wild-type EAT-2 stimulates rapid pumping, it also limits the duration of peristaltic contractions in the isthmus muscles.

3.4.4 *gar-3* mutation suppresses the peristalsis defects in *eat-2* mutants.

Pharyngeal muscle contractions in *eat-2* mutants are strikingly similar to those of wild-type animals treated with arecoline (Table II), suggesting that some of the *eat-2* mutant phenotypes are related to mAChR signaling. Since GAR-3 is the mAChR responding to arecoline in the pharynx, we examined pharyngeal muscle contractions in *eat-2(ok3528); gar-3(gk305)* double mutants.

We found that *gar-3* mutation partially suppressed the prolonged peristalses observed in *eat-2* single mutants. The duration of peristalses in *eat-2(ok3528); gar-3(gk305)* double mutants was strongly reduced compared to *eat-2(ok3528)* single mutants ($p < 10^{-24}$), although they were still longer than those in wild-type animals or *gar-3(gk305)* single mutants ($p < 10^{-14}$). In contrast, the reduced pumping frequency and increased frequency of peristalsis observed In *eat-2(ok3528)* single mutants was not suppressed in *eat-2(ok3528); gar-3(gk305)*. Thus, *eat-2* loss-of-function affects pumping and peristalsis by different mechanisms, and only the prolonged peristalsis phenotype depends on crosstalk with functional GAR-3 receptor.

Table III: Quantification of pharyngeal muscle contractions in *acr* mutants

genotype	pump rate (pumps/min ± sem)	peristalsis rate (peristalses/min ± sem)	% pumps followed by peristalsis	duration of isthmus peristalsis (ms ± sem)
wild type [a]	218 ± 11	31 ± 3	14%	113 ± 4
acr-6(ok3117) [b]	221 ± 14	12 ± 4	6%	115 ± 13
acr-7(tm863) [c]	198 ± 3	14 ± 4	7%	119 ± 7
acr-10(ok3118) [d]	199 ± 29	20 ± 6	12%	96 ± 3
acr-14(ok1155) [e]	199 ± 29	21 ± 6	12%	96 ± 4
acr-16(ok789) [f]	184 ± 9	20 ± 2	12%	118 ±7

[a] 17 N2 L1s were recorded for 19-20 s and a total of 1194 pumps were analyzed.

[b] Six *acr-6* L1s were recorded for 19-20 s and a total of 428 pumps were analyzed.

[c] Six *acr-7* L1s were recorded for 19-20 s and a total of 392 pumps were analyzed.

[d] 21 *acr-10* L1s were recorded for 20-21 s and a total of 1190 pumps were analyzed.

[e] Five *acr-14* L1s were recorded for 19-20 s and a total of 325 pumps were analyzed.

[f] Six *acr-16* L1s were recorded for 19-20 s and a total of 364 pumps were analyzed.

3.4.5 Ca^{2+} transients in the pharyngeal isthmus parallel the contractile phenotypes in *eat-2* and *gar-3* mutants

To characterize isthmus muscle excitation in wild-type animals and mutants, we constructed strains expressing the genetically encoded Ca^{2+} indicator (GECI) GCaMP3 using the pharyngeal muscle-specific *myo-2* promoter (Okkema et al., 1993; Tian et al., 2009). GCaMP3 fluorescence increases in muscle cells as cytoplasmic Ca^{2+} concentrations increase during excitation contraction coupling [reviewed (Bers, 2002)]. Similar to previous analyses of GECIs in the pharynx, we characterized adult animals treated with serotonin to stimulate pharyngeal muscle contractions and focused on animals pumping slowly to resolve individual excitation events (<100 pumps/min; <1.67 Hz) (Kerr, 2006; Shimozono et al., 2004).

We observed changes in Ca^{2+} concentration in the isthmus muscles that were very dynamic (Figure 14). As reported in previous studies, we observed that wild-type animals displayed an increase in Ca^{2+} throughout the central isthmus during pumping followed by a longer and delayed increase in Ca^{2+} in the posterior isthmus during peristalsis (Figure 15A, B) (Shimozono et al., 2004). We found that this Ca^{2+} signal during peristalsis exhibited a wave-like increase and decrease that traveled in an anterior to posterior direction through the posterior isthmus and resembled the progression of open pharyngeal lumen during peristalsis. While Ca^{2+} waves have not been previously described in the *C. elegans* pharynx (Shimozono et al., 2004), similar waves of Ca^{2+} can be observed in individual cardiac muscle cells, which are generated by progressive release of Ca^{2+} released from adjacent sites in the sarcoplasmic reticulum [reviewed in (Stuyvers et al., 2000)]. This mechanism may also underlie the wave-like contraction of pm5 during peristalsis.

To compare Ca^{2+} transients in the center and posterior isthmus in wild-type animals to those in various mutants, we quantified for each pump and peristalsis the normalized change in fluorescence ($\Delta F/F_o$), the width of each peak at 50% maximum fluorescence (peak duration),

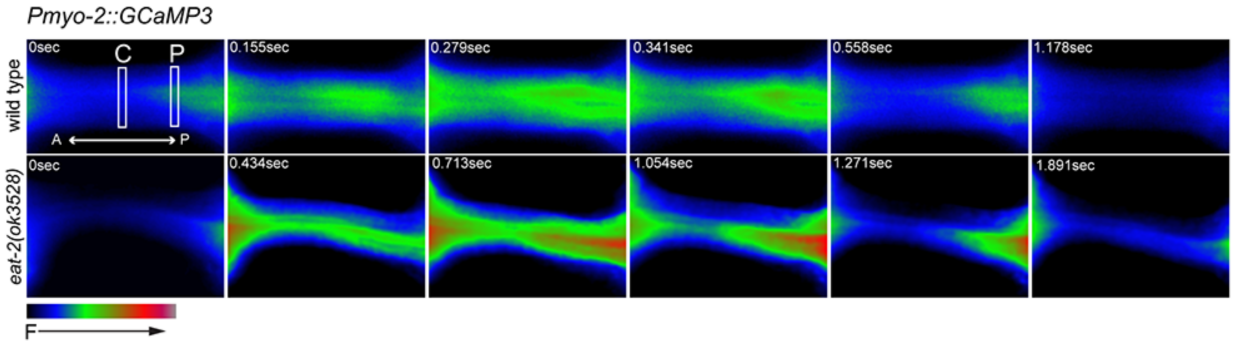

Figure 14 Dynamic changes in Ca^{2+} levels in the isthmus muscles

Time-lapse fluorescence images of the pharyngeal isthmus of a wild-type (top) or *eat-2(ok3528)* (bottom) adults expressing the GECI GCaMP3 in the pharyngeal muscles. Images are false colored as indicated at the lower left, and one pump and peristalsis are shown. Boxes indicate the regions where fluorescence levels were quantified in the center (C) and posterior (P) isthmus. The amount of time after fluorescence begins increasing are indicated, and the frames indicating maximum fluorescence in wild-type and *eat-2(ok3528)* are shown at 0.279 sec and 0.713 sec, respectively.

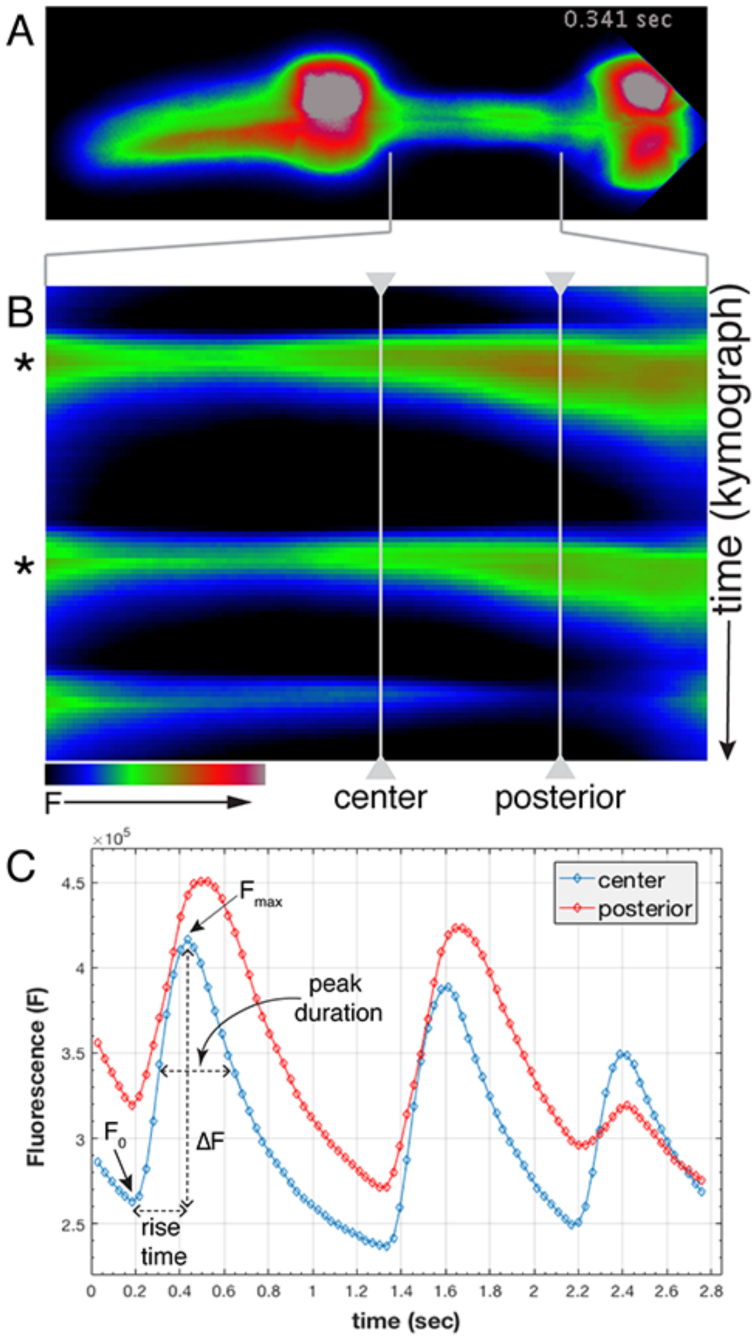

Figure 15 Characterization of GCaMP3 fluorescence in the pharyngeal isthmus

A) False colored fluorescence image of a wild-type animal expressing GCaMP3 in the pharyngeal muscles (anterior is left). B) Kymograph of maximum GCaMP3 fluorescence intensity in the isthmus region (indicated by brackets in A and B). Two pumps with peristalsis marked with asterisks are followed by a pump without a peristalsis. C) Normalized fluorescence levels ($\Delta F/F_o$) in the center and posterior isthmus plotted vs time (sec) for the contractions in panel B. Time points for time-lapse imaging (circles) and example measurements for ΔF, peak duration and rise time are indicated.

and the time that it took for fluorescence to reach its maximum (rise time) (Figure 15B, C; Table IV). In addition we calculated the time delay between the maximum increase in GCaMP3 fluorescence in the center and posterior isthmus (peak delay).

We found changes in GCaMP3 fluorescence in the pharyngeal isthmus that paralleled many of the defects we observed in peristaltic contractions in various mutants (Figure 16; Table IV). *eat-2(ok3528)* mutants, which have prolonged peristalses, also exhibited significantly increased $\Delta F/F_o$, peak duration and rise time in both the center and posterior isthmus ($p < 10^{-7}$). In addition, the peak delay was increased 2-fold ($p < 10^{-4}$). In comparison, *gar-3(gk305)* mutants, which have normal duration of peristalses, exhibited $\Delta F/F_o$ and rise times that were similar to those of wild-type animals, with a small decrease in $\Delta F/F_o$ only in the posterior isthmus, as well as a small decrease in peak duration in both the center and posterior isthmus ($p < 0.05$). However, the most striking change in these animals was a strongly decreased peak delay between the center and posterior isthmus ($p < 10^{-5}$). Finally, *eat-2(ok3528); gar-3(gk305)* double mutants, which suppress the prolonged peristalses observed in *eat-2(ok3528)* single mutants, exhibited decreases in $\Delta F/F_o$, peak duration, rise time, and peak delay compared to *eat-2(ok3528)* single mutants ($p < 10^{-5}$), although only $\Delta F/F_o$ was reduced to wild-type levels. Taken together, these results show that the level, duration, and rise time of Ca^{2+} increases in both the center and posterior isthmus best correlate with the duration of peristaltic contractions. Loss of *eat-2* increases these Ca^{2+} signals and produces prolonged peristalses that depend on wild-type *gar-3*.

3.4.6 *ace-3* mutants exhibit prolonged peristalses that depend on GAR-3

It is surprising that *eat-2* loss leads to a reduced pump rate, while at the same time hyperstimulating peristalsis and increased cytoplasmic Ca^{2+} concentration in the isthmus muscles. One hypothesis for these unexpected effects is that, in *eat-2* mutants, ACh released from MC cannot bind synaptic nAChRs, and instead, this unbound ACh spills over from the synapses and stimulates GAR-3 receptors located in the isthmus muscles. To examine this

Table IV: Quantification of GCaMP3 fluorescence dynamics

genotype	isthmus position	normalized ΔF	peak duration (ms±sem)	rise time (ms±sem)	peak delay (ms±sem)
wild type [a]	center	52±2	329±7	256±5	
	posterior	40±2	376±10	279±6	33±4
eat-2(ok3528) [b]	center	78±3	598±30	432±9	
	posterior	63±3	666±39	426±12	67±7
gar-3(gk305) [c]	center	51±3	310±11	258±8	
	posterior	34±2	345±14	281±10	7±3
eat-2; gar-3 [d]	center	57±2	414±12	315±6	
	posterior	36±2	485±17	346±8	26±4

[a] 15 wild-type young adults were recorded and an average of 130 pumps were analyzed.

[b] Six *eat-2(ok3528)* young adults were recorded and an average 56 pumps were analyzed.

[c] Five *gar-3(gk305)* young adults were recorded and an average of 31 pumps were analyzed.

[d] 12 *eat-2; gar-3* young adults were recorded and an average of 94 pumps were analyzed.

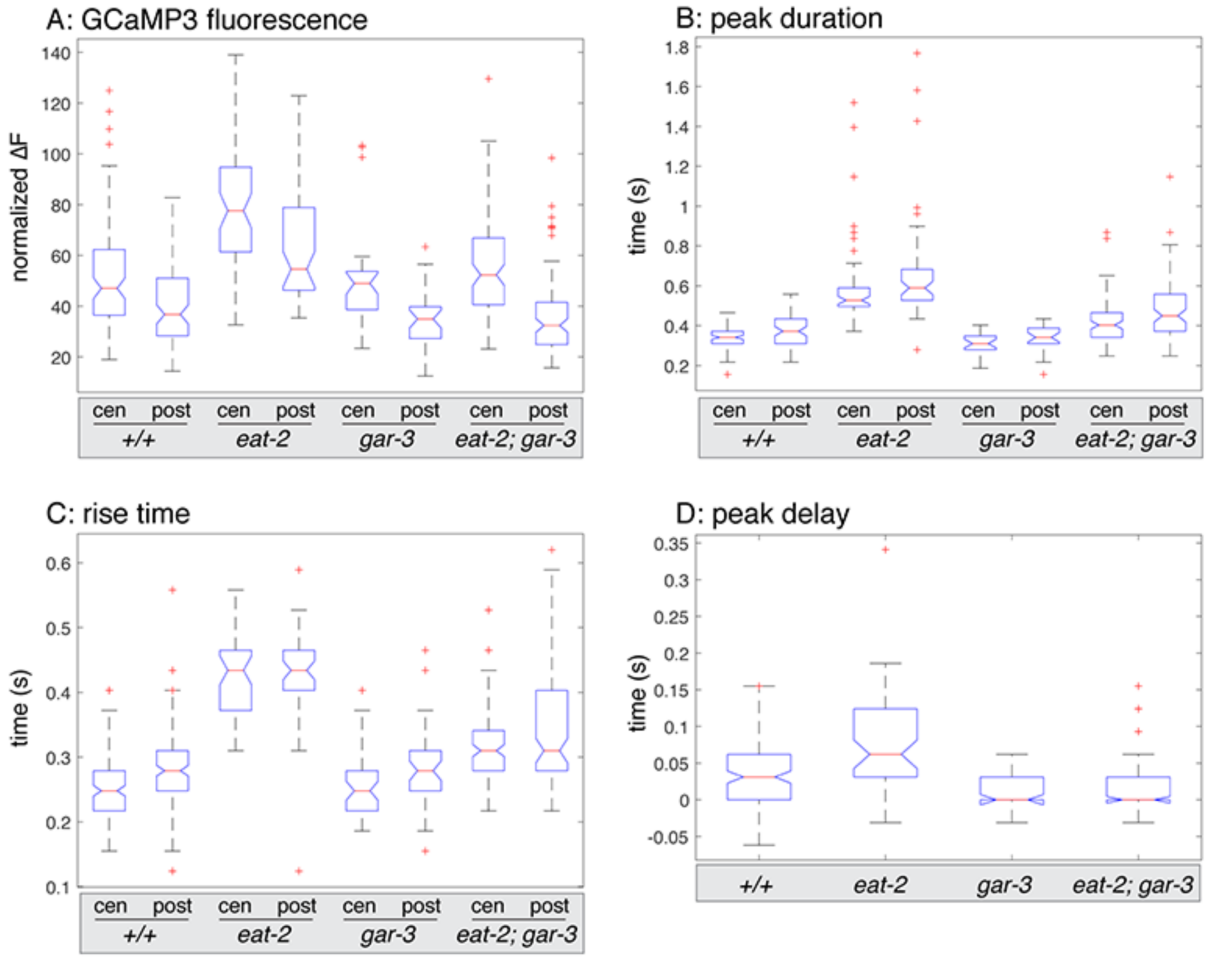

Figure 16 Quantification of GCaMP3 fluorescence in wild-type animals and mutants

Box and whisker plots comparing values measured from time-lapse imaging of GCaMP3 fluorescence during pumps followed by peristalses: (A) normalized GCaMP3 fluorescence levels ($\Delta F/F_o$), (B) peak duration, (C) peak rise time, (D) peak delay between the center and posterior isthmus. Genotypes and measurements in the center (cen) and posterior (post) isthmus are indicated. The central bar (red) denotes the median value with a notch indicating the 95% confidence for this median, the box indicates the interquartile range (IQR, 25th to 75th percentile), and the whiskers indicating values within 1.5 times the IQR. Suspected outlier values are indicated as red '+'.

hypothesis, we characterized pharyngeal muscle contractions in *ace* mutants defective in acetylcholinesterases that normally hydrolyze ACh and have increased unbound ACh in the synapse (Combes et al., 2000);Johnson, 1988 #1687}. *ace-3(dc2)* mutants exhibited significantly prolonged peristalses ($p < 10^{-9}$), which were similar to those of *eat-2* mutants (Table II). In comparison, *ace-2(g72); ace-1(p1000)* double mutants exhibited only mildly prolonged peristalses ($p < 0.02$). Both of these strains also exhibited a small decrease in the pump rate, but this was not significantly different from wild type, indicating that MC can effectively stimulate pumping in *ace* mutants.

To ask if the prolonged peristalses were suppressed by *gar-3* mutation, we examined *ace-3(dc2); gar-3(gk305)* double mutants and found that these animals exhibited peristalses that were similar to wild type. Thus the prolonged peristalses in *ace-3* mutants depend on crosstalk with wild-type GAR-3 receptor similar to what we observed in *eat-2* mutants.

3.4.7 *gar-3* suppresses the slow growth and extended life span of *eat-2* mutants

As *gar-3* mutation suppresses the peristalsis defects in *eat-2* mutants, we wanted to determine if this mutation also affects the persistent feeding defects in *eat-2* mutants. *eat-2* mutants exhibit slow larval growth and a prolonged adult life span, which result from dietary restriction (Avery, 1993a; Lakowski and Hekimi, 1998). We found that *gar-3* mutation at least partially suppressed both of these phenotypes.

While nearly all wild-type animals and *gar-3(gk305)* single mutants reached adulthood after 5 days at 20˚C, *eat-2* mutants grew much more slowly, and, even after 6 days, only 30% had reached adulthood (Figure 17A). *eat-2(ok3528); gar-3(gk305)* double mutants also grew slower than wild type and *gar-3(gk305)*, but they grew faster than *eat-2(ok3528)* single mutants, and 100% of these animals reached adulthood within 6 days.

Likewise, *eat-2* mutants have previously been shown to exhibit a longer adult life span than wild type animals (Lakowski and Hekimi, 1998), and we found that both *eat-2(ad1116)* and

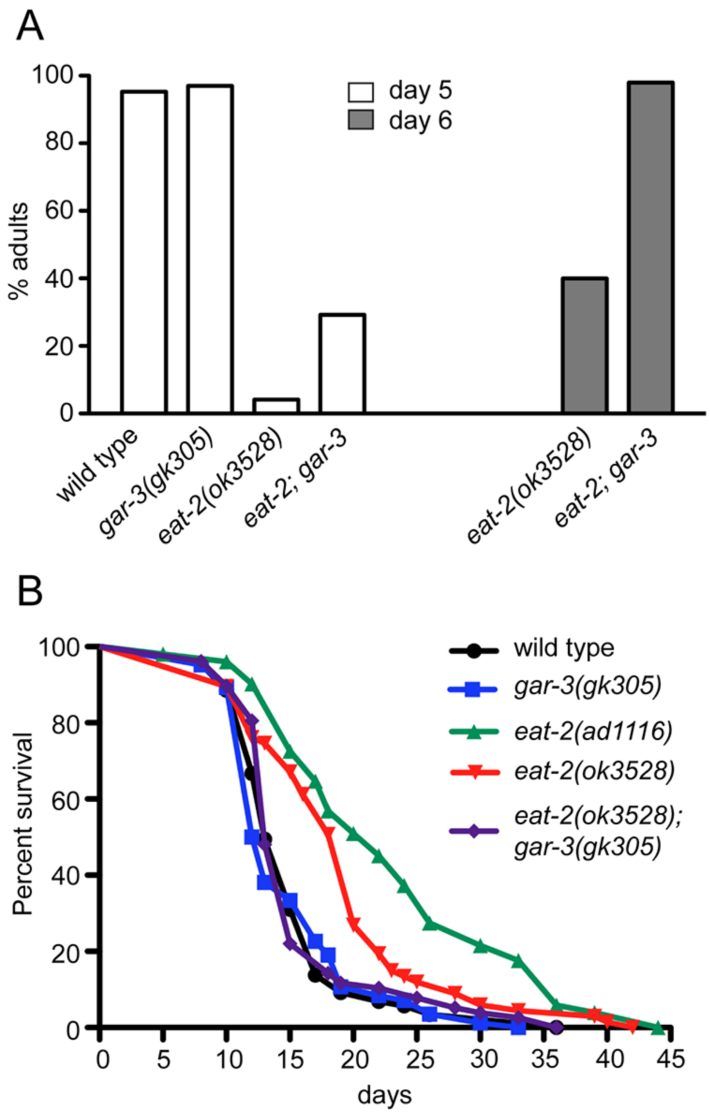

Figure 17 ***gar-3* mutation suppresses the slow growth and prolonged life span of *eat-2* mutants**

A) Bar graphs indicating the percent animals of the indicated genotypes reaching adulthood by day 5 or day 6 at 20˚C. B) Adult survival curves for animals of the indicated genotypes. Averages of representative triplicate assays performed on plates containing UV-killed *E. coli* as a food source. Nearly identical results were obtained in assays with living *E. coli*.

eat-2(ok3528) mutants exhibited significantly extended life spans (median adult survival 22 and 20 days, respectively) (Figure 17B). In comparison, the life span of *gar-3(gk305); eat-2(ok3528)* double mutants was indistinguishable from that of wild-type animals and *gar-3(gk305)* single mutants [median adult survival: N2 (13 days), *gar-3(gk305)* (12.5 days), *gar-3(gk305); eat-2(ok3528)* (13 days)].

Thus *gar-3(gk305)* suppresses both the slow larval growth and extended life span phenotypes of *eat-2(ok3528)* mutants, and we suggest this suppression is the result of improved isthmus peristalsis and feeding.

3.5 Discussion

In this work we show that crosstalk between the nAChR EAT-2 and the mAChR GAR-3 affects peristaltic muscle contractions in the isthmus of the *C. elegans* pharynx. Under normal circumstances, GAR-3 has a relatively minor role in these contractions, but in *eat-2* mutants, GAR-3 can stimulate increased cytoplasmic Ca^{2+} levels and peristalses that are prolonged compared to those of wild-type animals. We suggest this GAR-3 dependent stimulation of peristalsis results from ACh spillover from synapses between MC and the pharyngeal muscles in *eat-2* mutants, and consistent with this suggestion, acetylcholinesterase mutants similarly exhibit prolonged peristalses that are dependent on GAR-3. Crosstalk with GAR-3 contributes to the slow larval growth and extended life span phenotypes observed in *eat-2* mutants, indicating that this crosstalk has a long-term impact on *C. elegans* feeding.

3.5.1 *eat-2* mutants exhibit different effects on pumping and peristalsis

eat-2 mutants have a reduced pump rate, indicating that EAT-2 plays an excitatory role in pumping (Avery, 1993b; Raizen et al., 1995). In comparison, *eat-2* mutants exhibit prolonged peristalses, indicating EAT-2 does not excite isthmus muscle contractions. Rather it is necessary for rapid relaxation. These peristalsis phenotypes are similar to previous observations demonstrating that *eat-2* mutation leads to prolonged depolarization and contraction of the terminal bulb muscles during pumping (Steger and Avery, 2004).

The EAT-2 receptor is specifically localized at the sites where MC forms synapses near the junction of the pm4 and pm5 pharyngeal muscles, and it is necessary for MC to directly stimulate rapid pumping (McKay et al., 2004). Because MC does not synapse on either the posterior isthmus or the terminal bulb (Albertson and Thomson, 1976; McKay et al., 2004), the prolonged contraction of these muscles is likely an indirect effect of loss of EAT-2 containing receptors.

3.5.2 GAR-3 stimulates prolonged peristalsis in *eat-2* mutants

The prolonged peristalses in *eat-2* mutants depend on the GAR-3 receptor. *gar-3* mutation partially suppressed the prolonged peristaltic contraction of *eat-2* mutants, as well as the increased and prolonged Ca^{2+} transients in the isthmus muscles of these animals. This suppression demonstrates that GAR-3 receptor activation contributes to the *eat-2* mutant peristaltic phenotypes. Previous studies demonstrated that *gar-3* mutation similarly suppressed the prolonged contraction of the terminal bulb muscles in *eat-2* mutants (Steger and Avery, 2004). In comparison, *gar-3* single mutants have relatively minor defects in peristalsis. The duration of peristalsis was similar to wild-type animals. However, these mutants exhibited a sharp decrease in the peak delay between Ca^{2+} transients in the center and posterior isthmus and a decreased $\Delta F/F_o$ in the posterior isthmus. Thus, in wild-type animals, GAR-3 contributes to the spatially and temporally dynamic changes in Ca^{2+} concentration in the isthmus muscles, but this did not produce recognizable changes in the duration of peristalsis. These observations demonstrate that GCaMP3 may be a more sensitive assay for muscle excitation.

In contrast to its effect on peristalsis, *gar-3* mutation did not suppress reduced pump rate observed in *eat-2* mutants (Steger and Avery, 2004). Thus, the pumping and peristalsis defects in *eat-2* mutants arise via different mechanisms. Reduced pump rate results directly from loss of EAT-2 excitatory activity stimulated by the MC neuron, while the prolonged peristalsis results from excitation that depends on GAR-3.

3.5.3 ACh spillover may produce prolonged peristalses in *eat-2* mutants

We suggest that in *eat-2* mutants ACh spillover from synapses between MC near the junction of the pm4 and pm5 muscles activates slow-acting metabotropic GAR-3 receptors in pm5. GAR-3 activation stimulates increased and prolonged Ca^{2+} transients in the isthmus, which lead to prolonged peristalsis. GAR-3 is known to regulate Ca^{2+}-dependent processes in the pharyngeal muscles, and increased GAR-3 signaling produces prolonged pharyngeal muscle contractions during pumping (Steger and Avery, 2004). Because *gar-3* mutation only partially suppresses the prolonged peristalsis in *eat-2* mutant, other mechanisms must also contribute to the prolonged peristalsis in *eat-2* mutants. For example, voltage activated K^+ channels such as EXP-2 might not be efficiently activated in *eat-2* mutants for rapid repolarization of the isthmus muscles (Davis et al., 1999; Shtonda and Avery, 2005).

Neurotransmitter spillover is well characterized in glutamatergic, GABAergic, and dopaminergivc synapses [reviewed in (Diamond, 2002; Gassmann and Bettler, 2012; Rice and Cragg, 2008)]. At cholinergic synapses, unbound ACh is normally degraded by acetylcholinesterases located at the synapse [reviewed in (Rotundo, 2003)]. However, ACh spillover has been observed when quantal content is increased or when acetylcholinesterases are inhibited (Petrov et al., 2014; Stanchev and Sargent, 2011). We have similarly observed that *C. elegans ace-3* mutants with reduced acetylcholinesterase activity produce prolonged peristalses that are dependent on GAR-3.

We do not know if spillover in *eat-2* mutants occurs directly due to ACh diffusion from the synapses due to reduced binding *eat-2* mutants, or whether loss of *eat-2* leads to developmental defects during synaptogenesis that allow ACh spilover. Interestingly, loss of the gamma-subunit of the nAChR leads to a diffuse distribution of acetylcholinesterase clusters during development of mouse diaphragm muscles (Liu et al., 2008), and we speculate that a similar defect in acetylcholinesterase localization in *eat-2* mutants could underlie spillover from the MC synapses on the pharyngeal muscles.

Increased cytoplasmic Ca^{2+} levels in muscle cells have been observed in a number of human neuromuscular disorders, including myotonic dystrophies, Duchenne muscular dystrophy, as well as in *CoIQ* and slow-channel myasthenic syndromes [reviewed in (Engel et al., 2015; Vallejo-Illarramendi et al., 2014)]. This increased Ca^{2+} has been suggested to be a primary cause of muscle degradation in these disorders. In particular, myotonic dystrophies are initially characterized by delayed relaxation of muscles after contraction, and this resembles the prolonged peristalsis that we have observed in *eat-2* and other mutants. While we have not observed pharyngeal muscle degradation in these mutants, they provide a new model to characterize the immediate effects of Ca^{2+} dysregulation in muscle cells.

4 CEH-28 mediates Ca^{2+} activity of the M4 motor neuron and the pharyngeal isthmus muscles

4.1 Abstract

C. elegans pharyngeal behavior consists of two distinct types of muscle contractions called pumping and isthmus peristalsis. Peristalsis is a wave-like contraction in the posterior isthmus of the pharynx. It is stimulated by the pharyngeal motor neuron M4, which synapses with muscles specifically in the posterior isthmus. Mutants lacking the M4 specific transcription factor CEH-28 have abnormal and mispositioned synapses throughout the entire isthmus and exhibit a stuffed pharynx phenotype similar to that of animals lacking the M4 neuron. We are interested in understanding how synaptic defects in *ceh-28* mutants contribute to the stuffed pharynx phenotype. Using an M4-specific GCaMP3, we compared Ca^{2+} transients in this cell during peristalsis in wild-type animals and *ceh-28* mutants. In wild type, Ca^{2+} concentration increases preferentially in the posterior half of M4, where it forms synapses with the isthmus muscles. In contrast, *ceh-28* mutants exhibit Ca^{2+} increases that are both uniform along the entire length of M4 and reduced relative to wild type. Thus, Ca^{2+} concentrations increase in the regions where synapses are localized in both wild-type animals and *ceh-28* mutants, and we suggest reduced and improperly localized vesicle release underlies the feeding defects in *ceh-28* mutants. We also compared Ca^{2+} transients in the isthmus muscles in wild-type animals and *ceh-28* mutants. We found that *ceh-28* mutants have reduced Ca^{2+} signaling in the isthmus muscles. This suggests that the M4 synaptic defects in *ceh-28* mutants underlie reduced and improperly localized vesicle release from M4 in the isthmus muscle. This results in weak isthmus muscle contractions and the “stuffed pharynx” phenotype.

4.2 Introduction

Neurons are highly polarized cells that are specialized in information flow. They are composed of dendrites, which contain post-synaptic components that receive signals from other neurons, and axons, which contain synaptic vesicles necessary for signaling to other cells at synaptic regions. Neuronal polarity and proper synapse formation is essential for neuronal function. Loss of neuronal polarity and synaptic dysfunction are implicated in schizophrenia (SCZ), autism spectrum disorders (ASD) (Faludi and Mirnics, 2011; Pocklington et al., 2014; Spooren et al., 2012), depression (Duman and Aghajanian, 2012), Alzheimer's disease (Eldar-Finkelman, 2002; Hanger et al., 1992; Mandelkow et al., 1992; Skaper et al., 2017) and Parkinson's disease (Cappelletti et al., 2005; Cartelli et al., 2013).

The *C. elegans* nervous system is remarkably simple and well characterized. In adult hermaphrodites, the nervous system consists of only 302 cells that can be divided into a pharyngeal nervous system made up of 20 cells, and a somatic nervous system composed of 282 cells. By comparison, the human brain is estimated to contain more than 80 billion neurons. The limited number of neurons in *C. elegans* has enabled all neural connections to be identified using electron microscopy, and mapped out in the worm's connectome. (Albertson and Thomson, 1976; White et al., 1986). Although many studies demonstrate how the *C. elegans* nervous system senses the environment and controls different types of behavior (Ardiel and Rankin, 2010; Avery and You, 2012), (Schafer, 2005), it remains unknown how such a simple nervous system exhibits so many complex functions.

The pharyngeal motor neuron M4 stimulates contraction of muscles in a region of the pharynx called the isthmus (Avery and Horvitz, 1989). M4 is a polarized neuron with well-characterized morphology (Figure 18) (Albertson and Thomson, 1976). Its cell body is located in the anterior bulb of the pharynx, and it extends two equivalent processes around the circumference of the pharynx, which then travel along the length of the isthmus. Unlike bipolar

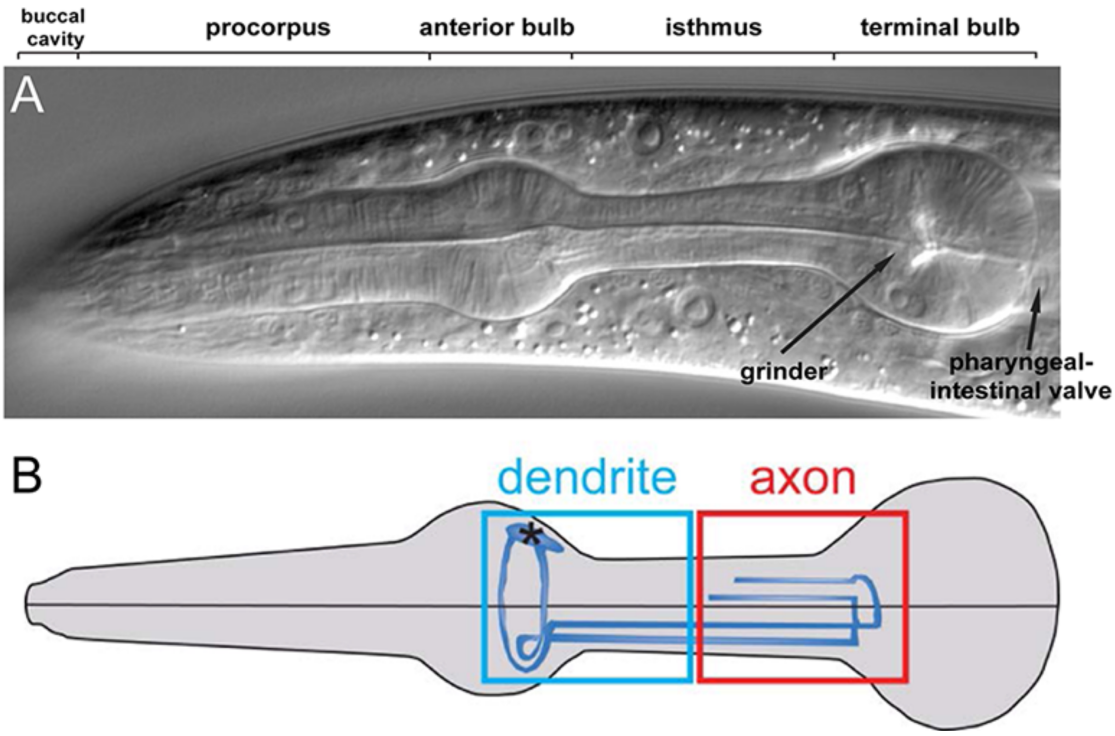

Figure 18 Morphology of the M4 motor neuron

(A) DIC micrograph of the pharynx with corpus, isthmus and terminal bulb indicated. (B) Schematic representation of the M4 motor neuron morphology. The cell body of the neuron (indicated with asterisk in A) is located dorsally in the anterior bulb. It extends two equivalent processes, which travel circumferentially around the nerve ring and then go subventrally to the terminal bulb. Then they turn dorsally and run anteriorly to the middle of the isthmus. M4 has both dendritic and axonic characteristics. Anterior part of M4 (blue) is characterized as dendritic and receives a signal. The posterior part of M4 (red) transmits the signal to the isthmus muscles. Anterior is to the left. Figure is adapted from (Ray et al., 2008).

neurons in many animals, each of the M4 processes is polarized and has distinct regions exhibiting dendritic and axonal properties. The anterior region of M4 is characterized as dendritic and receives input from other neurons, while a presynaptic axonal region of M4 forms *en passant* synapses with the posterior isthmus muscle (Figure 19A) (Albertson and Thomson, 1976; Chiang et al., 2006; Ray et al., 2008). M4 is necessary for peristalsis, in which the pharyngeal isthmus muscle contracts. Laser ablation of M4 leads to slow pumping, elimination of peristalsis and a "stuffed pharynx" phenotype, in which *E. coli* blocks the lumen of the corpus and anterior isthmus. M4 ablated worms do not survive beyond the L1 stage (Avery and Horvitz, 1987).

The NK-2 family homeobox transcription factor CEH-28 is expressed exclusively in the M4 motor neuron. Mutants affecting *ceh-28* exhibit a loss of M4 polarity and defects in synapse morphology. Instead of having synapses only in the posterior isthmus, the M4 cell in *ceh-28* mutants forms abnormally sized and spaced synapses throughout the entire isthmus (Figure 19B). Moreover, loss of *ceh-28* leads to the "stuffed pharynx" phenotype (Figure 20), due to inefficient transport of food through the isthmus (Ray et al., 2008). This phenotype is not as severe as M4 ablation, and the animals grow slowly to adulthood.

Here, we examine M4 activity in wild-type animals and *ceh-28* mutants by imaging the genetically encoded Ca^{2+} indicator (GECI) GCaMP3 (Tian et al., 2009). We found that in wild-type animals, Ca^{2+} transients were larger in the posterior part of the M4 neuron, where it forms synapses with the isthmus muscles. In contrast, Ca^{2+} transients in *ceh-28* mutants were low and uniform along the entire length of M4. This is consistent with previous observations of abnormally sized and spaced synapses that M4 forms in these mutants (Ray et al., 2008). We also examined Ca^{2+} transients in the pharyngeal isthmus muscles and found that *ceh-28* mutants have lower Ca^{2+} signals than wild-type animals. This indicates that in *ceh-28* mutants, isthmus muscle function is reduced. We suggest that in *ceh-28* mutants, abnormal morphology

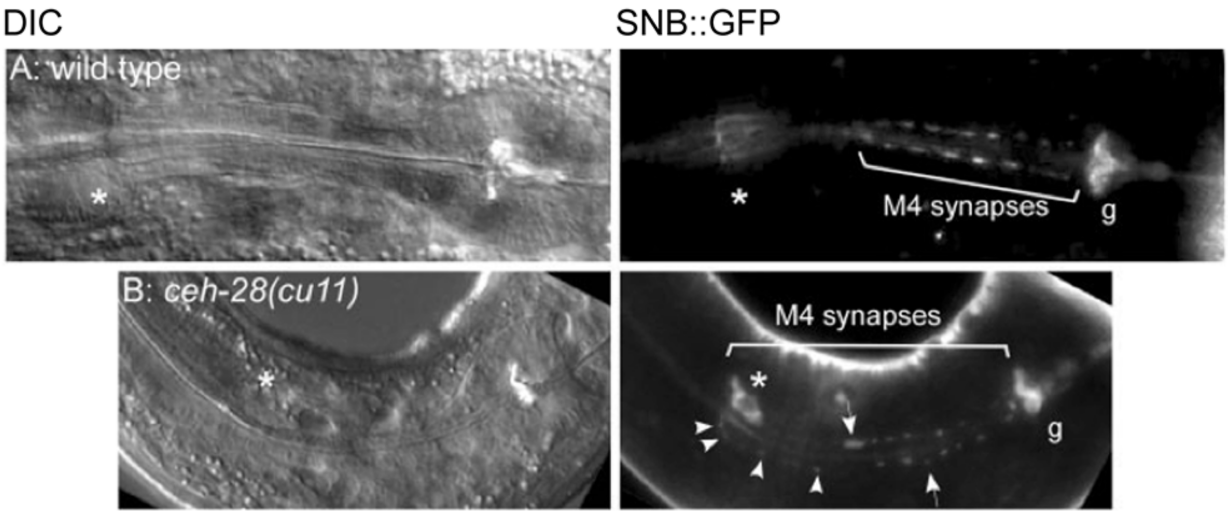

Figure 19 M4 synapses in wild type and *ceh-28* mutants

(A) DIC micrograph of the pharyngeal isthmus in wild-type animal (left). The position of M4 cell body is indicated with asterisk. GFP micrograph of the same wild-type animal, in which M4 synapses are localized in the posterior isthmus and marked with SNB::GFP (right). (B) DIC micrograph of the pharyngeal isthmus in *ceh-28* animal (left). GFP micrograph of the same *ceh-28* animal, in which M4 synapses are localized throughout the entire length of the isthmus and also marked with SNB::GFP (right). Ectopic synapses in the anterior isthmus are marked with arrowheads, and abnormally sized synapses are marked with arrows. The grinder is autofluorescent and is marked (g). Anterior is to the left. Figure is adapted from (Ray et al., 2008).

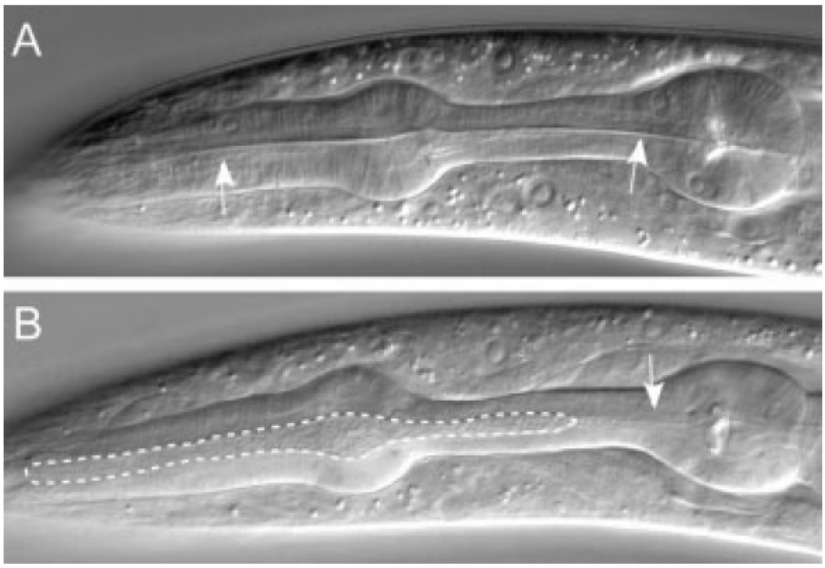

Figure 20 Stuffed pharynx in *ceh-28* mutants

(A) Wild-type animal with closed lumen indicated with arrows. (B) *ceh-28(cu11)* mutant with trapped *E. coli* cells in the corpus and anterior half of the isthmus (enclosed in a dashed line). Posterior half of the isthmus is unstuffed and indicated with an arrow. Anterior is to the left. Figure is adapted from (Ray et al., 2008).

and synaptic organization of the M4 motor neuron results in weak M4 activity and isthmus function, which eventually lead to the “stuffed pharynx” phenotype.

4.3 Materials and Methods

4.3.1 Nematode handling, transformation and strains

C. elegans strains were grown under standard conditions (Lewis and Fleming, 1995). Germline transformations were performed by microinjection using pRF4 (50 ng/µl) containing *rol-6(su1006)* as a transformation marker, the *ser-7b::GCaMP3* reporter pOK290.02 (80 ng/µl) and the *myo-2::GCaMP3* reporter pOK294.04 (20 ng/µl) (Mello and Fire, 1995). The extrachromosomal *ser-7b::GCaMP3* transgene *cuEx791* and *myo-2::GCaMP3* transgene *cuEx804* were chromosomally integrated by UV/TMP mutagenesis and outcrossed to form *culs32* and *culs36* respectively.

The following strains were used in this study: *ceh-28(cu11) X* (Ray et al., 2008), OK0991 *culs32[ser-7b::GCaMP3],* OK1022 *ceh-28(cu11) X; culs32,* OK1020 *culs36[myo-2::GCaMP3]*, OK1059 *ceh-28(cu11) X; culs36.*

4.3.2 General methods for nucleic acid manipulations and plasmid construction

Standard methods were used to manipulate all DNAs (Ausubel, 1990), and plasmids sequences are available from the authors. The *ser-7b* promoter from plasmid pOK197.03 was cloned into SphI and XbaI digested *GCaMP3::gfp* plasmid pOK270.01 to generate pOK290.02. The *myo-2* promoter from plasmid pPD 96.48 was cloned into HindIII and MscI digested *GCaMP3::gfp* plasmid 290.02 to generate pOK294.04.

4.3.3 Genotyping

Individual animals were genotyped for *ceh-28(cu11)* allele by PCR (Ray et al., 2008). Primers for genotyping were PO640 (CCCAATGCAATCTACGCAG), PO641 (GAATCAAACCGCCAACCAG), PO642 (CCCAGCGTGTCATACATGG).

4.3.4 Analysis of feeding behavior

To analyze pharyngeal muscle contractions young adults were incubated in 5 µl of

20mM serotonin (Sigma, Cat# H7752-5G) for 10 min on 2% agarose pad and then immobilized using 1.5 µl Polystyrene 0.10 micron microspheres and a coverslip (Polysciences, Inc, Cat# 00876). Individual animals that pumped were recorded at 25 frames/sec for 1 min using a Zeiss AxioImager microscope with an MRm camera and ZEN Software. For each genotype the feeding behavior was analyzed in at least 5 animals (~500 pumps/per animal). Time-lapse images were exported and processed using Fiji (Schindelin et al., 2012) to generate time-lapse movies. Acquisition times were exported from ZEN and quantifications were performed using Microsoft Excel.

4.3.5 Calcium imaging

Young adult animals were incubated in 5 µl of 20mM serotonin for 10 min on 2% agarose pad and then immobilized by using 1.5 µl of Polystyrene 0.10 micron microspheres. GCaMP3 imaging was performed on a Zeiss AxioImager microscope using a Q-Imaging Rolera EM-C^2 EMCCD camera. Time-lapse movies were captured at 25-30 frames/sec using ZEN software and 14-bit TIFF images were exported. Animals pumping with frequency less than 100 pumps/min were analyzed. Pharynx was straightened with CellProfiler (Kamentsky et al., 2011) and aligned using StackReg Fiji plugin (Thevenaz et al., 1998). The isthmus was cropped and regions of interests (ROI) were determined. For analysis of GCaMP3 in M4 three ROIs were drawn as boxes in the anterior, middle and posterior parts of M4. For analysis of GCaMP3 in the isthmus, two ROIs were drawn as 10 pixel (2.54 µm) wide lines in the center and posterior isthmus respectively. Fluorescence measurements were analyzed using custom Matlab scripts or using Micrsoft Excel. Total fluorescence was measured within the ROI and then normalized for each GCaMP3 peak using formula: normalized $\Delta F=\Delta F(Fmax-Fmin)/Fmin*100\%$ (where Fmax is maximum fluorescence of GCaMP3 peak and Fmin is a minimum fluorescence immediately before GCaMP3 increase). The student t test was used to compare GCaMP3 fluorescence between different wild-type animals and *ceh-28* mutants. Boxplots were generated using the Matlab *boxplot* command. Peak delay in M4 was calculated as time between the

maximum increase in GCaMP3 fluorescence in either anterior and middle or middle and posterior parts of M4 using the Matlab *diff* command. Peak delay in the isthmus was calculated as time between the maximum increase in GCaMP3 fluorescence in the center and posterior isthmus using the Matlab *diff* command.

4.4 Results

4.4.1 A GCaMP3 reporter demonstrates M4 depolarization during peristalsis

Isthmus peristalsis requires the M4 motor neuron. However, there is no direct evidence that this neuron depolarizes during peristalsis (Avery and Horvitz, 1987). To examine M4 activity, we constructed a strain expressing the GECI GCaMP3 specifically in M4 from a chromosomally integrated *ser-7b::GCaMP3* reporter (Hobson et al., 2003). GCaMP3 fluorescence increases as cytoplasmic Ca^{2+} concentrations increase during neuronal depolarization (Tian et al., 2009). GCaMP3 fluorescence was observed in the M4 body and the processes that extend through the pharyngeal isthmus, and fluorescence levels increased during the pharyngeal muscle contractions, indicating that GCaMP3 can be used effectively to image M4 depolarization (Figure 21A).

We used time-lapse imaging to examine GCaMP3 fluorescence in the M4 processes in young adult animals, and found that M4 depolarization was coincident with the isthmus peristalsis. For these experiments, animals were treated with serotonin to stimulate pharyngeal muscle contraction, as fluorescence imaging suppresses these contractions. In control experiments, serotonin stimulated both pumping and peristalsis in wild-type animals, and most pumps were followed by peristalsis (Table V). During peristalsis, increased GCaMP3 fluorescence in M4 was accompanied by a separation of the processes in the posterior isthmus indicative of the wave-like opening of the pharyngeal lumen (Figure 21A, compare the 0.279 sec and 0.403 sec time points). In some cases, pumps without peristalses could be recognized by movement of the autofluorescent grinder located in the terminal bulb of the pharynx, and these

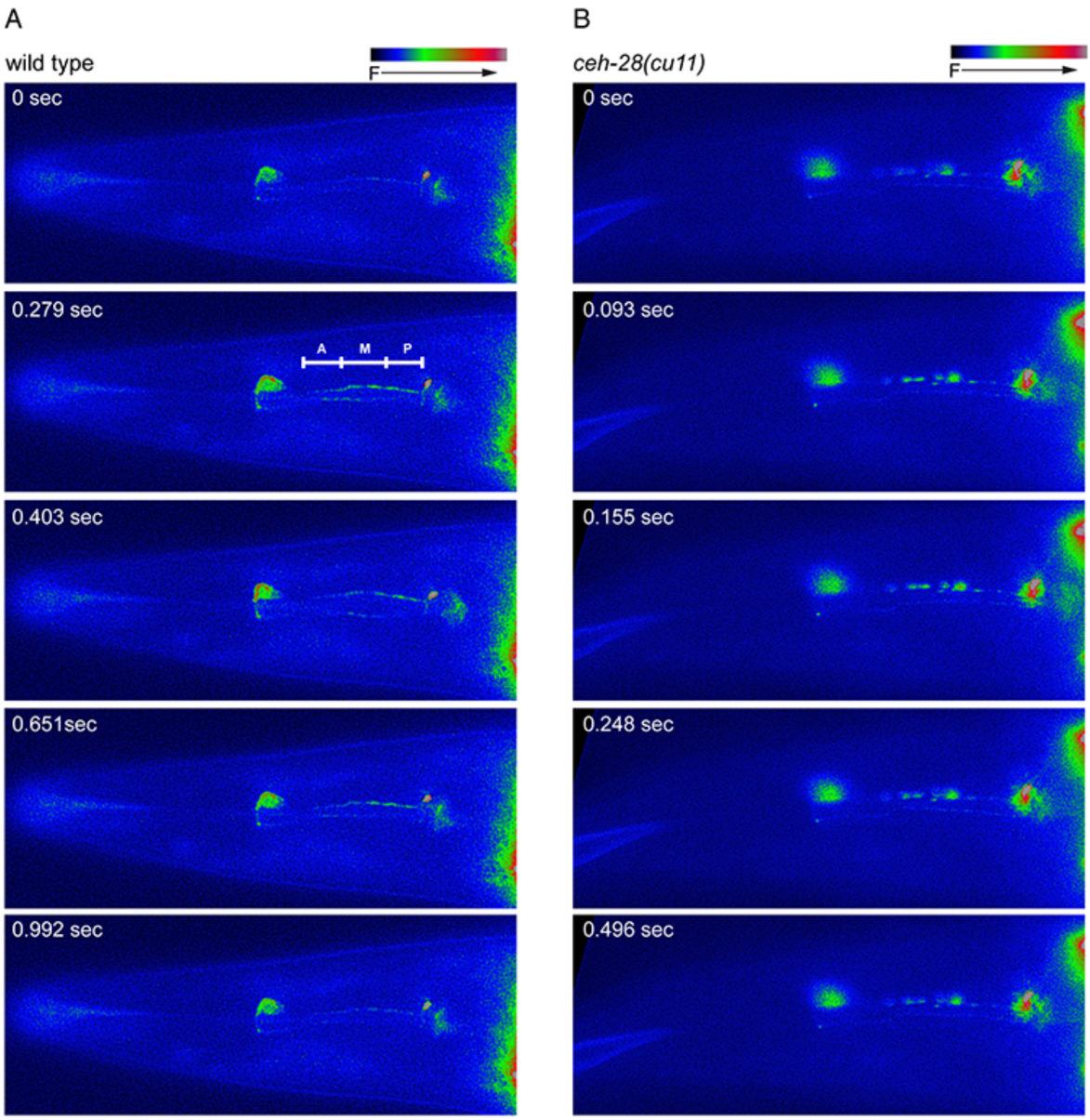

Figure 21 Changes in GCaMP3 fluorescence in the M4 motor neuron

Time-lapse fluorescence images of the M4 motor neuron of a wild-type animal (A) and *ceh-28(cu11)* mutant (B) expressing GCaMP3 specifically in M4 (anterior is left). Images are false colored as indicated at the top right for each panel, and one pump and peristalsis are shown for wild type and *ceh-28(cu11)* mutant. Brackets on the “0.279 sec” wild-type image indicate the regions where fluorescence levels was quantified in the anterior (A), middle (M) and posterior (P) compartments of M4. The amount of time after fluorescence begins increasing are indicated, and the frames indicating maximum fluorescence in wild-type and *ceh-28(cu11)* are shown at 0.279 sec and 0.155 sec, respectively.

Table V: Quantification of pharyngeal muscle contractions

genotype	pump rate (pumps/min ± sem)	peristalsis rate (peristalsis/min ± sem)	% pumps followed by peristalsis	duration of isthmus peristalsis (ms ± sem)
wild type [a]	107 ± 19	75 ± 10	74%	159 ± 5
ceh-28 (cu11) [b]	152 ± 20	137 ± 18	85%	108 ± 3

[a] Nine N2 young adults were recorded for 13-14 sec and a total of 206 pumps were analyzed.

[b] Nine *ceh-28 (cu11)* young adults were recorded for 15-16 sec and a total of 278 pumps were analyzed.

pumps were not associated with increased GCaMP3 fluorescence and M4 depolarization. Thus, we conclude that isthmus peristalsis occurs when M4 depolarizes.

We next measured the change in GCaMP3 fluorescence ($\Delta F/F_o$) in the M4 processes in the anterior, middle, and posterior regions of M4 during depolarization (Figure 21A). We found that fluorescence increased much more in the middle ($p<0.001$) and posterior ($p<10^{-5}$) region of M4 than in the anterior portion of M4 (Figure 22A, C; Table VI). This makes sense because this is where the synapses are located. We also found that GCaMP3 fluorescence increased simultaneously in the anterior, middle, and posterior isthmus indicating that Ca^{2+} increases simultaneously throughout the entire length of M4 during neuronal depolarization. To test this, we quantified a time delay between the maximum increase in GCaMP3 fluorescence in the middle/anterior and posterior/anterior compartments of M4 (M4 peak delay). Wild-type animals did not show M4 peak delay in both compartments of M4 (Table VI). We conclude that the wave-like contraction during peristalsis is stimulated by uniform release of ACh from M4 synapses in the middle and posterior isthmus.

4.4.2 *ceh-28* mutants exhibit weak peristalsis

ceh-28(cu11) mutants exhibit a stuffed pharynx phenotype, in which food blocks the lumen of the pharynx (Ray et al., 2008). We first examined pharyngeal muscle contractions in these mutants for any defects. We found that there is an increase in pumps that are followed by peristalsis in *ceh-28* mutants as compared to wild type animals ($p<0.01$). However, the duration of peristalsis was shorter in the mutants ($p<10^{-16}$) (Table V). We also examined peristalsis in general and found that 56% of *ceh-28* mutants (n = 9) exhibit weaker peristalsis compared to wild type where as 100% of the animals show strong peristalsis (n = 10). During weak peristalsis, the isthmus lumen does not open as wide as in wild-type animals.

4.4.3 *ceh-28* mutants exhibit low and uniform Ca^{2+} transients in M4

To determine whether there were any defects in M4 activity in *ceh-28* mutants, we examined Ca^{2+} transients in M4 by measuring changes in GCaMP3 fluorescence in these

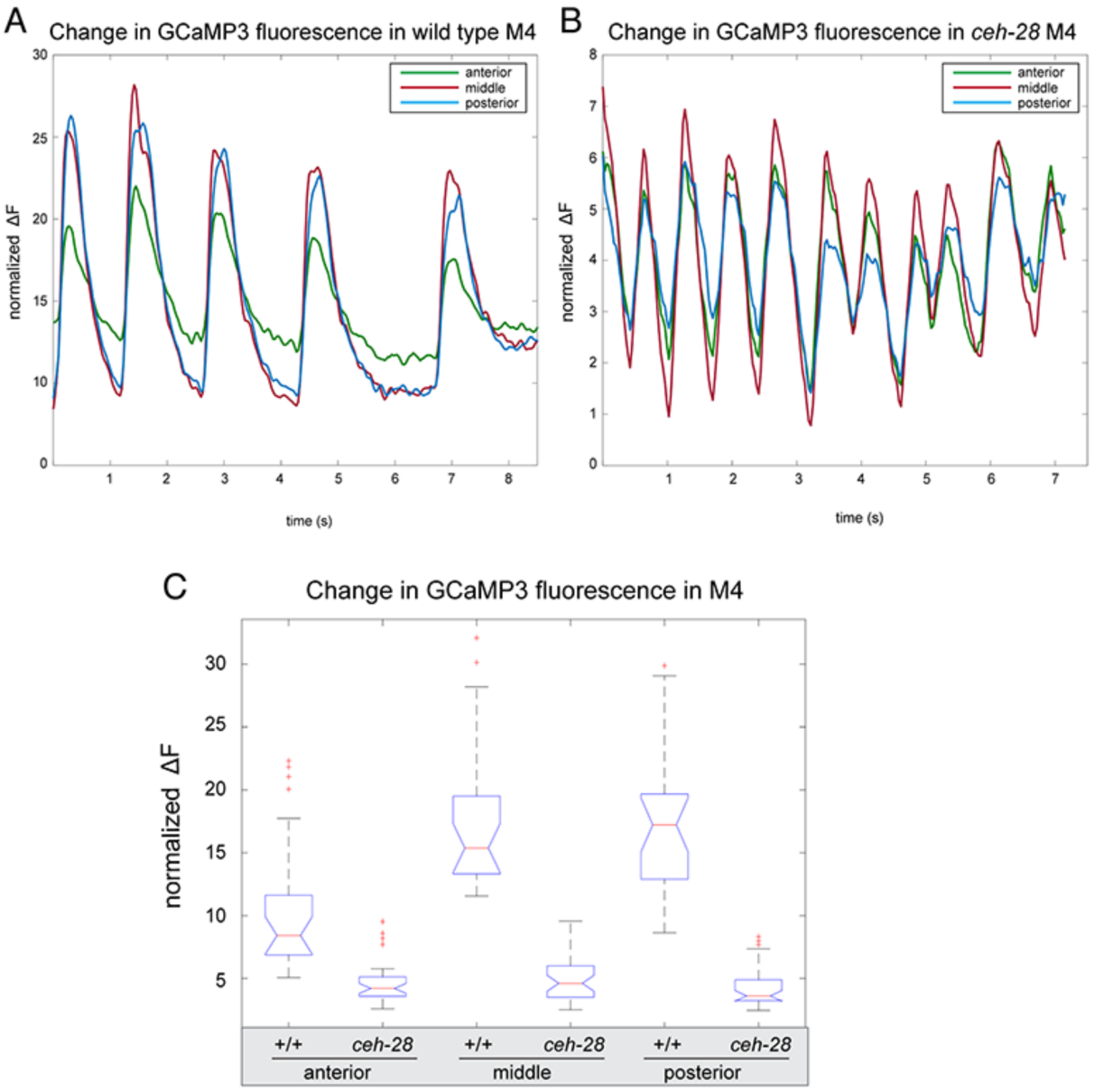

Figure 22 Characterization of GCaMP3 fluorescence in the M4 motor neuron

Normalized fluorescence levels ($\Delta F/F_o$) in the anterior, middle and posterior compartments of M4 plotted vs time (sec) in a wild-type (+/+) animal (A) and *ceh-28(cu11)* mutant (B). (C) Box and whisker plot comparing normalized GCaMP3 fluorescence levels in three compartments of M4 in wild-type animals and *ceh-28(cu11)* mutants. $\Delta F/F_o$ was measured from time-lapse imaging of GCaMP3 fluorescence during pumps followed by peristalses. Five wild type young adults were recorded and a total of 27 pumps with peristalsis were analyzed. Five *ceh-28(cu11)* young adults were recorded and a total of 41 pumps with peristalsis were analyzed. The central bar (red) denotes the median value with a notch indicating the 95% confidence for this median, the box indicates the interquartile range (IQR, 25th to 75th percentile), and the whiskers indicating values within 1.5 times the IQR. Suspected outlier values are indicated as red '+'.

Table VI: Quantification of GCaMP3 fluorescence dynamics in M4

genotype	isthmus position	average of normalized ΔF	peak delay (ms±sem)
wild type [a]	anterior	11±1	
	middle	18±1	-6±5
	posterior	17±1	7±4
ceh-28(cu11) [b]	anterior	5±0.5	
	middle	5±0.5	2±2
	posterior	4±0.5	2±2

[a] Five wild type young adults were recorded and a total of 27 pumps with peristalsis were analyzed.

[b] Five *ceh-28(cu11)* young adults were recorded and a total of 41 pumps with peristalsis were analyzed.

mutants. We hypothesized that lack of *ceh-28* leads to a decrease in Ca^{2+} levels in mutants affecting M4 activity. First, we found that *ceh-28* mutants have varicosities of different sizes along the length of the M4 processes (Figure 23). This was consistent with abnormally sized varicosities and synapses previously found in these mutants (Ray et al., 2008). In contrast to wild-type animals, in which GCaMP3 fluorescence increased much more in the middle and posterior M4 than in the anterior M4, changes in GCaMP3 fluorescence were lower and uniform throughout the entire length of the M4 in *ceh-28* mutants (Figure 22B, C; Table VI). These observations were consistent with our hypothesis: loss of *ceh-28* results in reduced Ca^{2+} transients.

Similar to wild-type animals, GCaMP3 fluorescence increased simultaneously in the anterior, middle, and posterior M4 in *ceh-28* mutants. When we quantified M4 peak delay in *ceh-28* mutants, we found that these mutants did not show the M4 peak delay in the middle and the posterior compartments of the M4 neuron. This indicates that Ca^{2+} increases simultaneously throughout the entire length of M4 during neuronal depolarization. (Table VI).

4.4.4 *ceh-28* mutants exhibit low and uniform Ca^{2+} transients in the isthmus muscles

To understand if there are any functional defects in the isthmus muscles of *ceh-28* mutants, we examined Ca^{2+} transients in pm5 muscles in response to M4 depolarization. To do so, we expressed GCaMP3 specifically in the pharyngeal muscles using the *myo-2* promoter both in wild type and *ceh-28* mutants (Okkema et al., 1993; Tian et al., 2009). We characterized adult animals treated with serotonin to stimulate pharyngeal muscle contractions and to resolve individual excitation events focused on animals pumping slowly (<100 pumps/min; <1.67 Hz) (Kerr, 2006; Shimozono et al., 2004). Wild-type animals exhibited changes in Ca^{2+} concentration in the isthmus muscles that were very dynamic. We observed that animals displayed an increase in Ca^{2+} throughout the central isthmus during pumping followed by a longer and delayed increase in Ca^{2+} in the posterior isthmus during peristalsis. This Ca^{2+} signal during peristalsis exhibited a wave-like increase and decrease that traveled through the posterior

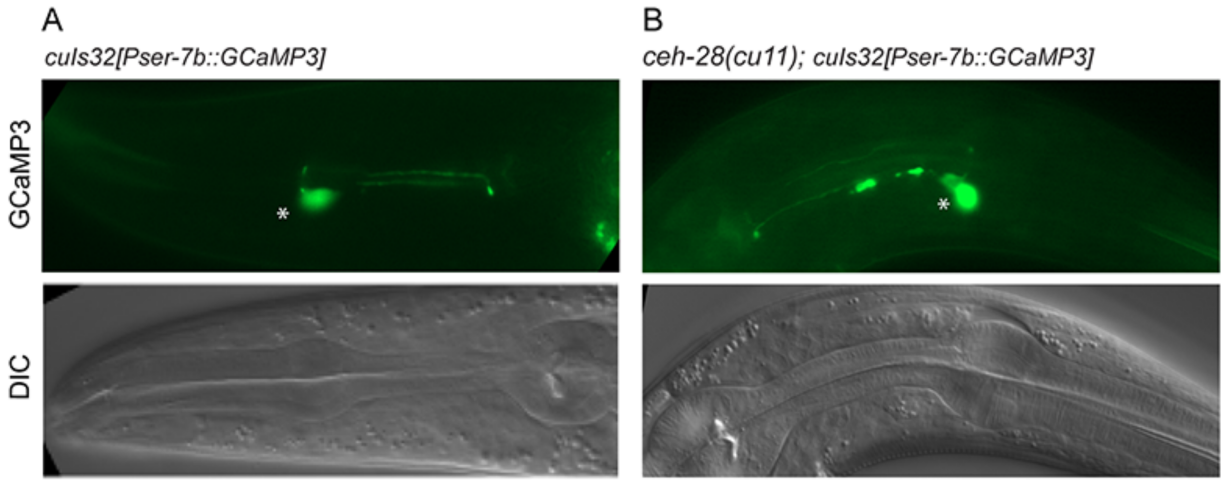

Figure 23 GCaMP3 fluorescence in M4 in wild type and *ceh-28* mutant

(A) GCaMP3 micrograph of a wild-type animal expressing *Pser-7b::GCaMP3*, in which two equivalent processes extend from the cell body and travel along the isthmus (top). DIC micrograph of the same wild-type animal (bottom). Anterior is to the left. (B) GCaMP3 micrograph of the *ceh-28(cu11)* mutant expressing *Pser-7b::GCaMP3*, in which the varicosities of different sizes are present in the anterior half of the M4 processes (top). DIC micrograph of the same *ceh-28(cu11)* mutant (bottom). Anterior is to the right. The position of M4 cell body is indicated with asterisk in A and B.

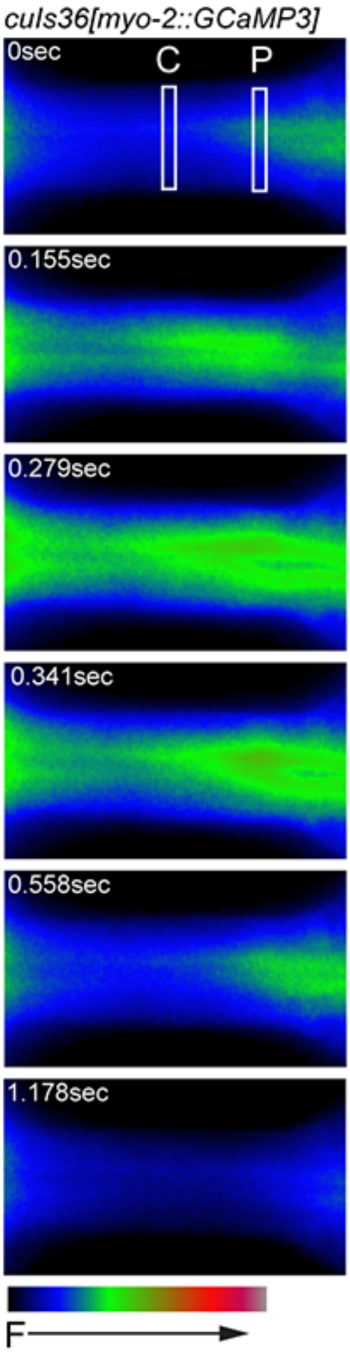

Figure 24 Dynamic changes in Ca^{2+} levels in the isthmus muscles

Time-lapse fluorescence images of the pharyngeal isthmus of a wild-type animal expressing GCaMP3 in the pharyngeal muscles. Images are false colored as indicated at the lower left, and one pump and peristalsis are shown. Boxes indicate the regions where fluorescence levels were quantified in the center (C) and posterior (P) isthmus. The amount of time after fluorescence begins increasing are indicated, and the frame indicating maximum fluorescence is shown at 0.279 sec.

isthmus and resembled the progression of open pharyngeal lumen during peristalsis consistent with our previous data (Figure 24).

To compare Ca^{2+} signals in wild-type animals with *ceh-28* mutants, we quantified $\Delta F/F_o$ and the time delay between the maximum increase in GCaMP3 fluorescence in the center and posterior isthmus (isthmus peak delay) for each pump and peristalsis. Similar to what we observed in M4, *ceh-28* mutants exhibited significantly decreased $\Delta F/F_o$ in the center ($p<10^{-10}$) and posterior ($p<10^{-6}$) of the isthmus muscles compared to wild-type animals (Figure 25; Table VII). These observations were in parallel with the weak peristalsis we observed in the mutant animals (Table V). In addition, *ceh-28* mutants did not have the isthmus peak delay ($p<0.001$) compared to wild-type animals (Table VII). This was consistent with abnormally localized synapses along the entire length of the M4 processes. Thus, when the signal is received uniformly from M4, Ca^{2+} concentration increases simultaneously throughout the isthmus muscles in *ceh-28* mutants. Taken together, both low and decreased dynamic Ca^{2+} transients in *ceh-28* mutants generated in response to low and uniform M4 signaling result in a weak peristalsis observed in these mutants.

4.5 Discussion

Peristaltic contractions are controlled by the cholinergic motor neuron M4 (Avery and Horvitz, 1987). In this work we show that the NK-2 homeobox gene *ceh-28* functions to control M4 activity by affecting its Ca^{2+} dynamics. We hypothesize that in the absence of *ceh-28*, levels of Ca^{2+} are decreased in M4 affecting its activity and the isthmus muscle contraction. As a result, *ceh-28* mutant animals develop feeding defects, which lead to the stuffed pharynx phenotype.

4.5.1 Peristalsis occurs when M4 depolarizes

Isthmus peristalsis is absolutely dependent on the M4 motor neuron; however, a direct connection between peristaltic contraction and M4 depolarization has not been established (Avery and Horvitz, 1987). We hypothesize that peristalsis occurs only if M4 fires an action

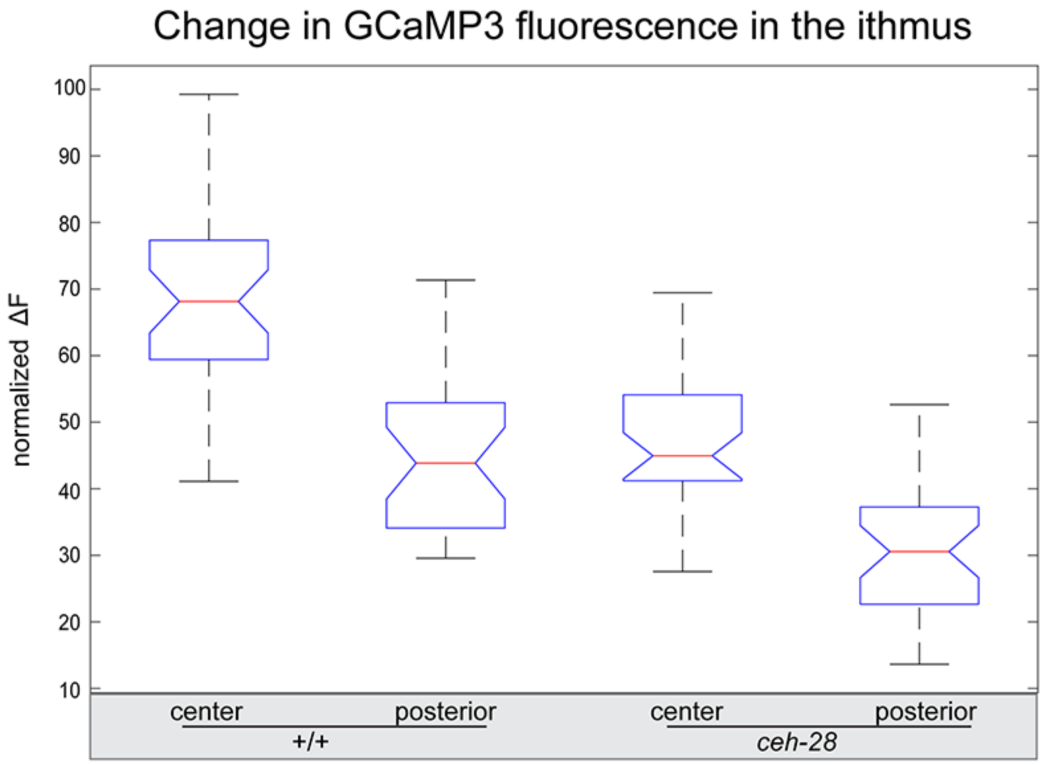

Figure 25 Quantification of change in GCaMP3 fluorescence in the isthmus

Box and whisker plot comparing change in GCaMP3 fluorescence ($\Delta F/F_o$) in the center and posterior isthmus in wild type (+/+) and *ceh-28(cu11)* mutants. ($\Delta F/F_o$) was measured from time-lapse imaging of GCaMP3 fluorescence during pumps followed by peristalses. Seven wild type young adults were recorded and the total of 37 pumps were analyzed. Five *ceh-28(cu11)* young adults were recorded and the total 40 pumps were analyzed. The central bar (red) denotes the median value with a notch indicating the 95% confidence for this median, the box indicates the interquartile range (IQR, 25th to 75th percentile), and the whiskers indicating values within 1.5 times the IQR. Suspected outlier values are indicated as red '+'.

Table VII: Quantification of GCaMP3 fluorescence dynamics in the isthmus muscles

genotype	isthmus position	average of normalized ΔF	peak delay (ms±sem)
wild type [a]	center	68±2	
	posterior	46±3	72±12
ceh-28(cu11) [b]	center	43±2	
	posterior	26±2	19±5

[a] Seven wild type young adults were recorded and the total of 37 pumps were analyzed.

[b] Five *ceh-28(cu11)* young adults were recorded and the total 40 pumps were analyzed.

potential. The action potential in *C. elegans* neurons is dependent on Ca^{2+} currents (Goodman et al., 1998). Therefore, changes in Ca^{2+} concentrations we observe in M4 correlate with its depolarization. Here we demonstrate that the isthmus peristalsis occurs only when Ca^{2+} concentrations increase in the M4 processes. Although we did not have a way to perform DIC and GCaMP3 imaging simultaneously, we clearly observed that increased GCaMP3 fluorescence in M4 was accompanied by a separation of the processes in the posterior isthmus. This is indicative of the wave-like opening of the pharyngeal lumen during peristalsis contractions of isthmus muscles during Ca^{2+} transients in M4. This is the first evidence of the isthmus peristalsis being associated with M4 depolarization.

4.5.2 M4 activity is decreased in *ceh-28* mutants

Interestingly, Ca^{2+} transients in M4 do not have a wave-like characteristic in contrast to peristaltic contractions. Ca^{2+} concentration increases simultaneously along the entire length of the M4 processes, eventually producing a wave-like peristalsis. One explanation may be that changes in Ca^{2+} concentration occur so quickly that it is hard to detect them in M4 during its depolarization. Another explanation could be that the isthmus muscles do not require gradual release of ACh to generate the wave-like peristalsis.

Activation of the voltage-gated Ca^{2+} channels (VGCC) by membrane depolarization results in an influx of Ca^{2+} through the presynaptic membrane. This initiates synaptic vesicle fusion with the plasma membrane and release of a neurotransmitter from a neuron (Katz and Miledi, 1967). There are many mechanisms that regulate the function of these Ca^{2+} channels, and therefore modulate synaptic transmission (Catterall, 2000; Dunlap et al., 1995; Tedford and Zamponi, 2006). Third or fourth power of Ca^{2+} entry is involved in neurotransmitter release (Augustine et al., 1987; Dodge and Rahamimoff, 1967; Katz and Miledi, 1970; Zucker and Regehr, 2002). Therefore, whenever we observed increases in Ca^{2+} concentrations in M4, we correlated it with both the M4 depolarization and ACh release as well.

The larger Ca^{2+} transients we observed in the posterior half of M4 correlate with the synapses in the posterior half of the isthmus in wild-type animals. In *ceh-28* mutant animals these Ca^{2+} transients were low and uniform, which is consistent with abnormal and mispositioned synapses in these mutants. First, this indicates that ACh release is decreased in *ceh-28* mutants. Second, *ceh-28* controls levels of Ca^{2+} in the presynaptic M4. Two possible mechanisms of how CEH-28 controls M4 activity are by regulating synaptogenesis or levels of cytoplasmic Ca^{2+}. We suggest that lack of *ceh-28* leads to a decreased concentration of Ca^{2+} in M4 and decreased ACh release from the abnormal synapses, which overall results in impaired M4 activity. One of the mechanisms for controlling Ca^{2+} concentration could be by regulating VGCC EGL-19 or UNC-2. In *ceh-28* mutants, the function of Ca^{2+} channels may be downregulated, resulting in low intracellular Ca^{2+}, which is not enough to release appropriate amounts of synaptic vesicles for the strong stimulation of the isthmus muscles.

4.5.3 *ceh-28* mutants have weak M4 activity and isthmus muscle contractions

ceh-28 mutants display the stuffed pharynx phenotype, which is characterized by blockage of the pharyngeal lumen with *E. coli* cells (Ray et al., 2008). We suggest that reduced M4 activity in *ceh-28* mutants results in a weak contraction of the isthmus muscles, leading to the stuffed pharynx. This statement is supported by a few observations. First, *ceh-28* mutant adults have weak muscle contraction and lower Ca^{2+} transients in the isthmus muscles. Second, in wild-type animals, changes in Ca^{2+} concentration are very dynamic, exhibiting a wave-like increase and decrease that travels through the posterior isthmus with the isthmus peak delay between the posterior and center of the isthmus. In contrast, in *ceh-28* mutants, Ca^{2+} transients are not as dynamic, and lack the wave-like characteristic and the isthmus peak delay. Reduced M4 activity in *ceh-28* mutants is likely not enough to generate wave-like Ca^{2+} transients in the isthmus muscle. Alternatively, wave-like changes in Ca^{2+} levels are so low that they are very hard to detect.

Motor neurons are an essential class of neurons that are important in establishing connections with muscles. Many neurodegenerative diseases such as Amyotrophic lateral sclerosis (Wijesekera and Leigh, 2009) and Huntington's disease (Walker et al., 2007) are associated with a failure of motor neuron function and signaling. In this study we used the *C. elegans* pharynx as an *in vivo* model, in which a single motor neuron communicates with a single muscle cell. We demonstrated that lack of *ceh-28* affects M4 neuronal function by decreasing levels of Ca^{2+} concentrations, which eventually results in weak isthmus muscle contractions. Investigating neuromuscular communication between M4 and the isthmus muscles may provide valuable insights regarding how motor neurons signal in the nervous system and how target muscles respond to this signaling in organisms with more complex nervous systems.

5 Identifying potential targets of CEH-28 by performing M4 RNA-sequencing

5.1 Abstract

Neurons are highly polarized cells and are specialized to receive and transmit signals within an organism. Characterizing a neuron's specific gene expression profile is important for understanding how the neuron functions within a nervous system, neuronal development and signaling. The *C. elegans* single cell motor neuron M4 is a polarized cell, which has both dendritic and axonal characteristics. M4 forms synapses with the pharyngeal isthmus muscle and is responsible for isthmus peristalsis. Proper synapse formation is crucial for information flow from M4 to the isthmus muscle and efficient pharyngeal muscle contractions. The NK-2 homeodomain transcription factor CEH-28 is expressed exclusively in M4 and regulates its proper synapse formation and morphology. *ceh-28* mutants exhibit abnormally sized and positioned synapses, which leads to inefficient peristaltic contractions and feeding. We hypothesize that CEH-28 regulates genes responsible for synapse development and positioning in M4. To find targets of CEH-28, we performed M4 RNA-sequencing using an mRNA-tagging technique. We identified 39 potential targets of CEH-28, which are enriched in the M4 motor neuron and downregulated in *ceh-28* mutants. Only three genes are expressed in the pharynx and there is no available information for the remaining 31 genes. Therefore, further analysis is required to test whether potential targets of CEH-28 are expressed in M4 and if their expression is lost in *ceh-28(cu11)* mutants.

5.2 Introduction

Neurons are polarized cells that are specialized for information flow. They receive and transmit signals. Understanding the transcript profile of a single neuron provides information on how a particular single neuron functions within the nervous system. Neuronal specific gene expression profiles show functional and biochemical characteristics of an individual neuron, which are important for understanding neuronal development and signaling. Moreover, comparing gene expression in wild type and mutants can reveal the molecular basis of mutant phenotypes.

C. elegans is a great model for performing gene expression profiles on a single neuron. The nervous system of *C. elegans* is relatively small and very well characterized (Albertson and Thomson, 1976; White et al., 1986). In the adult hermaphrodite, the nervous system consists of 302 neurons, which belong to two separate subgroups. 282 neurons belong to the somatic nervous system, and 20 neurons are part of the pharyngeal nervous system.

The single cell motor neuron M4 is responsible for isthmus peristalsis, one of the pharyngeal muscle contractions. Peristaltic contractions are essential for proper feeding. The motor neuron M4 is a polarized cell. The anterior region of the M4 motor neuron has characteristics of a dendrite and receives signals, whereas the posterior region of M4 has characteristics of an axon and transmits signals. Two processes of M4 extend throughout the isthmus from anterior to posterior to form synapses with the posterior isthmus muscles (Albertson and Thomson, 1976). Proper synapse formation and signaling from M4 are required for efficient feeding behavior (Avery and Horvitz, 1987).

The NK-2 homeodomain transcription factor CEH-28 is expressed exclusively in M4 and regulates proper synapse formation and morphology (Ray et al., 2008). The M4 motor neuron in *ceh-28* mutants loses its polarity and exhibits abnormally sized and spaced synapses throughout the entire length of M4, which leads to inefficient peristaltic contractions and feeding. Also, *ceh-28* mutants have decreased Ca^{2+} signaling both in M4 and isthmus muscles (Chapter

4). We hypothesized that CEH-28 regulates genes required for normal synaptogenesis, neuronal polarity and Ca^{2+} signaling, and as a result, for normal feeding. We are interested in identifying the transcriptional targets of CEH-28.

There are a few downstream targets regulated by CEH-28 that have been previously identified and include *dbl-1*, *egl-17*, *flp-5* and *flp-2* (Ramakrishnan and Okkema, 2014; Ramakrishnan et al., 2014). *dbl-1(ev580)* mutants exhibit normal synapses and do not have any of the feeding defects, that are observed in *ceh-28(cu11)* mutants. *flp-2(gk1039), egl-17(n1377)* or *flp-5(gk3123)* mutants do not have the stuffed pharynx phenotype associated with *ceh-28(cu11)*. This indicates that none of these secreted proteins is necessary for normal feeding.

To identify additional targets of CEH-28, we used an mRNA tagging technique to enrich mRNA from the M4 neuron. This method has been previously used to enrich transcripts from a small number of neurons (Kunitomo et al., 2005; Takayama et al., 2010; Von Stetina et al., 2007). Briefly, poly(A) binding protein tagged with FLAG (FLAG-PABP) is expressed in the neuron using a cell specific promoter, where PABP binds to 3' end of poly(A) mRNA. Then, PABP-mRNA complex is immunoprecipitated from the neuron by using anti-FLAG beads. Purified mRNA is then submitted for RNA sequencing (RNA-seq).

Here we report the results from RNA-seq performed on transgenic wild-type animals and *ceh-28(cu11)* mutants expressing FLAG-PABP in M4, and non transgenic wild type animals. The analysis of the RNA-seq data revealed a list of 39 potential targets of CEH-28. Based on information from the literature, only three genes are expressed in the pharynx. Five genes have known expression pattern and they are not expressed in the pharynx. None of the genes have any known neuronal function. Expression patterns for the rest of the 31 genes are unknown. Therefore, further analysis is required to confirm whether potential targets of CEH-28 are expressed in M4 and if their expression is lost in *ceh-28(cu11)* mutants.

5.3 Materials and Methods

5.3.1 Nematode handling and strains

C. elegans strains were grown under standard conditions (Lewis and Fleming, 1995). The following strains were used in this study: wild-type strain N2 (Brenner, 1974), OK0793 *unc-119(ed3); cuIs30 [ser-7b::3XFLAG::PABP]*, OK0828 *ceh-28(cu11); cuIs30* (Ramakrishnan, 2014).

5.3.2 Immunostaining using anti-FLAG antibodies to confirm transgene function

Immunostaining with anti-FLAG antibodies was performed according to the Finney-Ruvkun protocol (Finney and Ruvkun, 1990). The detailed protocol is described in 2.9.1. Strains N2, OK0793 and OK0828 were grown on two 60mm NGM plates seeded with OP50 *E. coli* until plates were full of worms of a mixed population. Animals from each plate were washed with 2 ml of dH_2O and transferred to Eppendorf tubes. Animals were fixed with 1.25 ml of freshly prepared fixative solution. Next, they were incubated in 1 ml of 1X TTB buffer containing DTT, and then in 1 ml of 1X Borate buffer containing 3% H_2O_2 for 15 minutes for each incubation. Expression of PABP was detected by staining with anti-FLAG primary antibody (1:1000 dilution) and a Texas Red labeled goat anti-mouse secondary antibody (1:250 dilution). Animals were also stained with DAPI (1:1000 dilution) to detect nuclei. Worms were mounted on a slide containing a 2% agarose pad. A cover slip was placed on top and nail polish was used to seal. Worms were imaged on a Zeiss AxioImager microscope equipped with DIC and fluorescence microscopy. Images were captured with an MRm camera and ZEN Software.

5.3.3 Coimmunoprecipitation of poly(A) mRNA from M4

Coimmunoprecipitation of poly(A) mRNA from M4 was performed according to modified Poly-A binding protein protocol provided by David Miller, which is described in details in 2.9.2.

5.3.3.1 Preparation of the HB101 bacterial culture

To obtain 15 ml of concentrated of *E. coli* strain HB101, 3 L of LB growth media was inoculated with a single HB101 colony. The inoculated culture was incubated at 37°C overnight.

The next day, the bacteria was precipitated and gently resuspended on ice in 15 ml of cold M9 buffer. HB101 stock culture was stored for a week at 4°C.

5.3.3.2 Worm growth and synchronization

From unstarved 60mm NGM plates, 20 L4 worms were placed on eight 100mm plates seeded with OP50 and grown until just clear of bacteria. Worms from each plate were washed with 2 ml S-basal and added into a 2 L flask containing 500 ml S-basal. 5 ml of concentrated HB101, 100 µl of nystatin (final concentration 2,000Units/ml) and 100 µl of streptomycin (final concentration 10 µg/ml) were added to the worm liquid culture. The flask was put on a shaker at 20°C with vigorous shaking and the worm culture was incubated for 6 days until full of adults. The same amount of HB101, streptomycin and nystatin were added to the worm culture every day.

5.3.3.3 Worm harvesting and bleaching

Animals were harvested by centrifugation in 50 ml conical tubes. Next, animals were washed 3 times by centrifugation with cold M9 buffer until the supernatant was clear. Animals were bleached for 4 min by continuously inverting the tubes. Then, the tubes were spun down for 1 min and supernatant was quickly removed. Fresh bleach solution was added to the animals, and tubes were inverted for another 4 min. For 1 ml of pelleted animals, 10 ml of bleach solution was used. Embryos were washed 3 times by centrifugation with 10 ml of cold M9.

5.3.3.4 Sucrose flotation

Sucrose flotation was performed to separate live embryos from dead embryos and dead animals. Embryos were combined in 15 ml conical tubes. Embryos were resuspended in 5 ml cold dH_2O and 5 ml 60% sucrose was added. The tube was inverted several times to mix the embryos with sucrose solution and centrifuged at 1200 rpm for 6 min at 4°C. The floated embryos were carefully collected into 5 ml of cold dH_2O with sterile plastic pipettes and washed 3 times with 10 ml of cold M9 buffer.

5.3.3.5 Worm synchronization and fixation

Embryos were allowed to hatch by incubating at 20°C for 15 hours at 200 rpm. The next day, hatched L1s were collected by centrifugation, resuspended in 100 ml of S-basal and incubated at 20°C for 6 hours at 200 rpm. After recovery, L1 animals were washed 3 times with cold M9 buffer by centrifugation. Worms were fixed with 0.5% PFM by incubating for 1 hour at 4°C on a nutator. Animals were washed 4 times with cold M9 buffer by centrifugation and flash frozen in liquid nitrogen. At this point, L1s can be stored at -80°C.

5.3.3.6 Obtaining L1 lysates

100 µl of pelleted L1 animals were washed once with 1 ml of cold HB buffer, which contained 1mM DTT, 50U/ml RNasin and 8mM VRC. Pelleted L1s were resuspended in 250 µl cold HB and then homogenized by sonication. Worm lysate was recovered by centrifugation at 18000 g for 20 min at 4°C, aliquoted and kept -80°C until ready to use. 30 µl of L1 lysate was subjected for RNA isolation using Trizol to determine concentration of total RNA.

5.3.3.7 Immunoprecipitation of mRNA/FLAG-PABP

80 µl of unpacked anti-FLAG M2 beads were prepared by washing 2 times in 0.1M glycine and 4 times in 1ml of cold HB. Amount of lysate corresponding to 200 µg of total RNA was added to 50 µl of prepared beads. Cold HB containing 400U/ml RNasin and 1.6mM VRC was added up to 1 ml. Lysate was incubated with beads for 2 hours at 4°C on a nutator. Then, beads were quickly washed 2 times with 1ml of low-salt HB. The beads were washed an additional 2 times by incubating for 30 min each, while rotating on a nutator. After the final wash, supernatant was removed and beads were ready for elution.

5.3.3.8 Elution of mRNA/FLAG-PABP and mRNA extraction

100 µl of elution buffer was added to the beads and incubated for 15 minutes at 65°C while rotating. After incubation, the beads were spun down and eluate was removed to a new Eppendorf tube. 100 µl of elution buffer was added again, and the elution step was repeated 3 more times. Eluates containing mRNA/FLAG-PABP were pooled together and incubated with

ProK at a final concentration 0.16mg/ml for 1 hour at 65°C to remove a crosslink between mRNA and FLAG-PABP. mRNA was extracted from pooled eluates using the Qiagen RNeasy Micro Kit and stored at -80°C until ready to submit for library preparation and sequencing.

5.3.4 Reverse transcription PCR (RT-PCR)

To synthesize single-stranded cDNA form purified mRNA, a High Capacity cDNA Reverse Transcription Kit was used (ThermoFisher Scientific, Catalog# 4368814). The RT reaction of a total volume of 20 µl included 10 µl of 20 ng RNA, 2 µl of 10X RT Buffer, 0.8 µl of 25X dNTP mix, 2 µl of 10X Random Primers, 1 µl of MultiScribe Reverse Transcriptase (50 Units), 1 µl of RNasin (40 Units) and 3.2 µl of Nuclease free H_2O. In the negative control for the RT reaction MultiScribe Reverse Transcriptase was substituted with 1µl Nuclease free H_2O. Tubes with RT reaction were loaded into the Thermal Cycler and the following conditions were programed: (1) 25°C – 10 min, (2) 37°C – 120 min, (3) 85°C – 5 min, (4) 4°C - Forever.

PCR primers were designed for *ceh-28*, *ser-7* and *ama-1,* and when possible, primers spanned two exons to avoid amplification of genomic DNA that may be present. Primers for the *ceh-28* PCR were PO0643 (ACAACAGCAGAAGAGAAAACCGAG) and PO0644 (GCTAACCGCTTGCATTTGTATCG). Primers for *ser-7* PCR were PO1401 (CTTTTTCGTGGGGCTCGTTG) and PO1402 (GTGCATAGCGTTAGGTCGGA). Primers for *ama-1* PCR were PO1061 (AGGCGAAGGATGTGTTGTG) and PO1062 (TCACCGTGTTCTTTGGGTC). The PCR conditions used for amplification and product sizes for each gene are indicated in Table VIII.

5.3.5 Library preparation and RNA sequencing

The Quant seq protocol was used to prepare a library close to the 3’ end of the mRNA (Moll et al., 2014). The Quant seq protocol was used to prepare a library close to 3’ end of mRNA (Moll et al., 2014). QuantSeq generates strand-specific next-generation sequencing (NGS) libraries close to the 3′ end of poly(A) RNAs. Sequencing of 3’ end of mRNA makes easier counting transcripts and perfect in our case of recovering partially degraded RNA after

performing Co-IP and purification steps. QuantSeq allows generation of one fragment per transcript, directly linking gene expression to the number of reads mapping a gene. NGS reads are generated towards the poly(A) tail, and directly correspond to the mRNA sequence. QuantSeq library preparation and Illumina RNA sequencing was performed by the University of Illinois RRC.

5.3.6 Analysis of RNA-seq data

Analysis of RNA-seq data was performed by the Core of Research Informatics (CRI) at the University of Illinois, and included the following steps. Bowtie2 was used to align the sequences with the *C. elegans* genome, HTseq to count the number of reads per sample, and EdgeR to perform differential analysis (Anders et al., 2013), (Anders et al., 2015), (Trapnell et al., 2012).

Table VIII: Conditions for performing RT-PCR of the genes expressed in M4

Step / Gene	*ceh-28*	*ser-7*	*ama-1*
1	94°C for 2 min		
2	94°C for 30 sec		
3	55.3°C for 30 sec	54.9°C for 30 sec	52.9°C for 30 sec
4	72°C for 30 sec	72°C for 30 sec	72°C for 20 sec
5	Go to Step 2 39 times		
6	72°C for 5 min		
7	12°C for ∞		
Product size	189 bp	117 bp	99 bp

3 genes were used in RT-PCR to validate coimmunoprecipitated RNA. The PCR conditions as well as product sizes amplified are listed.

5.4 Results

5.4.1 Performing immunoprecipitation of PABP-mRNA from M4

CEH-28 has been previously reported to have a role in synapse development in the M4 neuron. *ceh-28* mutants exhibit abnormal and mispositioned synapses (Ray et al., 2008). Based on this finding, we hypothesize that CEH-28 regulates target genes involved in synapse formation and positioning in M4. To identify targets of CEH-28, we compared the gene expression profile of M4 in wild-type animals with *ceh-28* mutants by performing RNA-seq.

Strains specifically expressing chromosomally integrated FLAG-PABP under the *ser-7b* promoter in wild-type animals and *ceh-28* mutants have been previously generated (Ramakrishnan, 2014). We performed staining with anti-FLAG antibodies to confirm the functionality of the transgene. We found that 100% of both wild-type animals (n=30) and *ceh-28* mutants (n=30) exhibit expression of PABP in the M4 neuron (Figure 26). Occasional animals exhibited staining of PABP outside the pharynx in one to two cells in the head: 10% of wild-type animals (n=30) and 12% of *ceh-28* mutants (n=30). The non-pharyngeal cells that expressed PABP varied among the animals.

To identify genes that are differentially regulated by CEH-28, we performed coimmunoprecipitation (Co-IP) of M4 specific mRNA from transgenic wild-type animals (wild-type (Tg)), *ceh-28* mutants (*ceh-28* (Tg)) expressing FLAG-PABP, and from non-transgenic wild-type animals (wild-type (nTg)). The latter strain served as a negative control for non-specific binding to the anti-FLAG beads. The integrity of RNA was confirmed by loading a small aliquot on a gel before performing Co-IP. Two bands corresponding to 28S and 18S ribosomal RNA were clearly visible on the gel, indicating that the total RNA used for Co-IP was intact (Figure 27). 200 µg of total RNA was used for Co-IP of poly(A)-mRNA from each genotype. We expected to coimmunoprecipitate poly(A)-mRNA only from the wild-type (Tg) and *ceh-28* (Tg) samples. Surprisingly, some poly(A)-mRNA was pulled down from the wild-type (nTg) sample as well. This indicates that the mRNA expression profile for wild-type (Tg) and *ceh-28* (Tg)

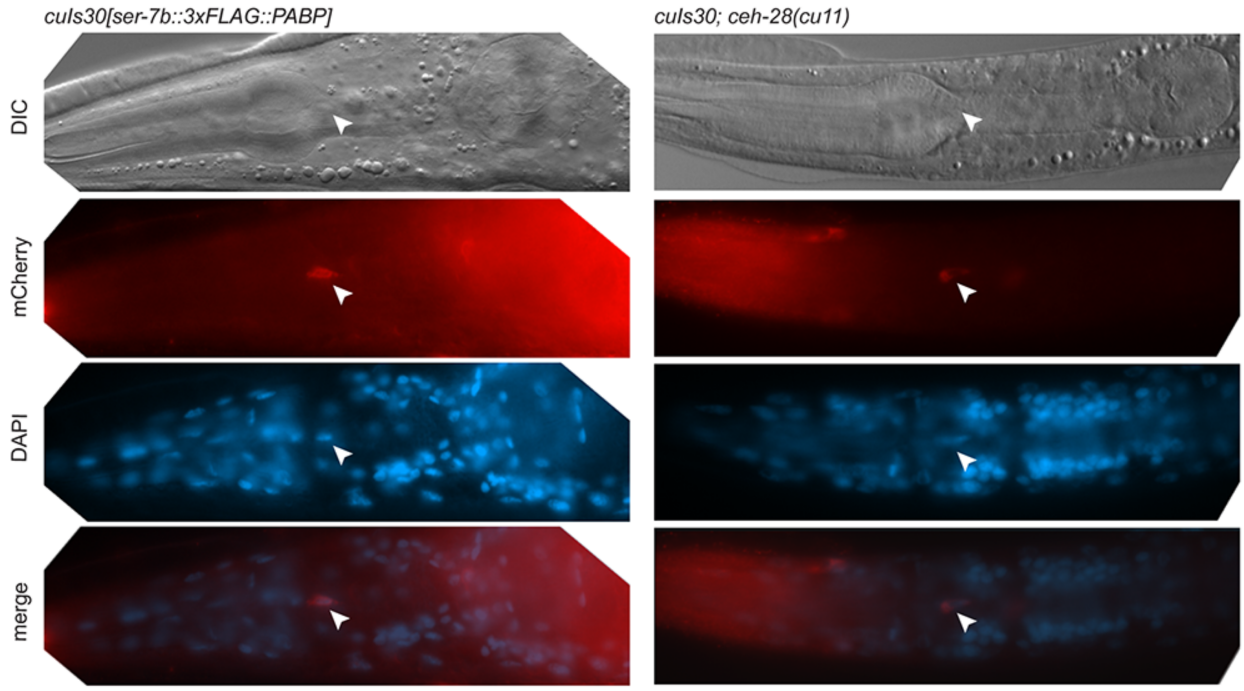

Figure 26 Expression of PABP in M4 using anti-FLAG antibodies

PABP expression is detected in the M4 neuron in a strain containing *culs30[ser-7b::3xFLAG::PABP]* in a wild-type (left panel) and *ceh-28(cu11)* mutant (right panel) background. Arrowhead indicates location of M4 cell body. Anterior is to the left, and ventral is at the bottom.

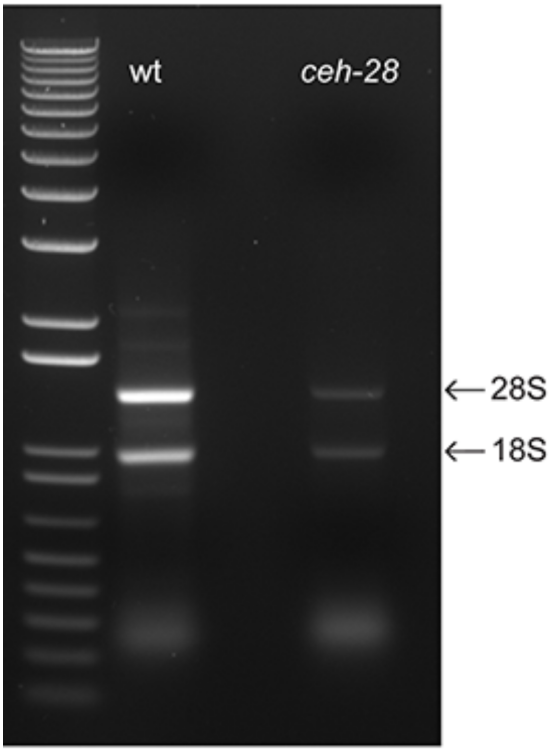

Figure 27 Total RNA purified from transgenic wild-type animals and *ceh-28(cu11)* mutants

Agarose gel stained with ethidium bromide, showing RNA purified from whole worm lysate from wild type carrying *cuIs30[ser-7b::3xFLAG::PABP]* (wt) and *ceh-28(cu11); cuIs30[ser-7b::3xFLAG::PABP]* (*ceh-28*). RNA in both samples is intact with two bands indicating 28S and 18S ribosomal RNA. The ladder is 1 kb Plus DNA ladder.

would include transcripts not specific to the M4 neuron. As a result of the Co-IP experiment, we were able to pull down on average 31 ng of mRNA from wild-type (Tg), 22 ng from *ceh-28* (Tg) and 15 ng from wild-type (nTg). Four replicates were performed for wild-type (Tg) and *ceh-28* (Tg), and three replicates for wild-type (nTg).

5.4.2 Validation of coimmunoprecipitated poly(A)-mRNA

To assess the integrity and quality of coimmunoprecipitated mRNA, we used the TapeStation 2200 at UIC RRC. TapeStation gives an assessment of RNA quality and quantity in a single step. Tape Station revealed the presence of RNA heterogeneous in size, which indicated a partial degradation of coimmunoprecipitated mRNA (Figure 28). Also, Tape Station showed two peaks of 28S and 18S rRNAs, indicating that mRNA samples contained ribosomal RNAs.

To examine whether coimmunoprecipitated mRNA contained RNAs that are present in the M4 neuron, we performed RT-PCR. We expected to detect the presence of *ser-7*, *ceh-28,* and *ama-1* RNAs in the wild-type (Tg) and *ceh-28* (Tg) samples. *ama-1* is necessary for mRNA transcription and encodes the amanitin-binding subunit of RNA polymerase II. *ama-1* is a housekeeping gene and is expressed in all *C. elegans* cells. *ser-7* encodes 5-HT7 serotonin receptor. *ser-7* is expressed in M4, and in a few other neurons located in the head, the tail and the pharynx. *ceh-28* is exclusively expressed in the M4 motor neuron. We were able to detect the presence of *ser-7*, *ceh-28* and *ama-1* RNAs in wild-type (Tg) (Figure 29) and *ceh-28* (Tg) (data not shown). Surprisingly, we also found these RNAs in the wild-type (nTg) sample (data not shown). This indicates that there was nonspecific binding to the anti-FLAG beads during Co-IP experiment.

5.4.3 Library preparation and mRNA sequencing

The QuantSeq protocol was used to prepare a library close to the 3’ end of the mRNA (Moll et al., 2014). QuantSeq generates strand-specific next-generation sequencing (NGS) libraries close to the 3′ end of poly(A) RNAs. Library preparation starts with annealing oligo-dT

primers to poly(A)-RNA. Next, the first strand of cDNA is synthesized and RNA is removed. A complementary second strand of cDNA is synthesized using random primers. At this point, primers introduce Illumina-specific linkers. Double-stranded cDNA is purified using magnetic beads and amplified by PCR. Adapters for Illumina sequencing and external barcodes are introduced at this step. Sequencing of the 3' end of mRNA makes it easier to count transcripts and perfect in this experiment for recovering partially degraded RNA after performing Co-IP and purification steps. QuantSeq allows generation of one fragment per transcript, directly linking gene expression to the number of reads mapping a gene. NGS reads are generated towards the poly(A) tail and directly correspond to the mRNA sequence. The QuantSeq library preparation and Illumina RNA sequencing was performed at the UIC RRC.

5.4.4 Analysis of the RNA-seq data

Quadruplicate RNA samples of wild-type (Tg), *ceh-28* (Tg) and triplicate RNA samples of wild-type (nTg) were sequenced. We received on average 11.5 million reads per sample. Analysis of the RNA-seq data was performed in our laboratory and at the UIC by CRI. Analysis included the following steps. Bowtie2 was used to align the sequences with *C. elegans* genome, HTseq to count the number of reads per sample and EdgeR to perform differential analysis (Anders et al., 2013; Anders et al., 2015; Trapnell et al., 2012). The results of both analyses were similar, and we decided to choose a gene list obtained from RRC for the further analysis.

We first compared wild-type (Tg) to wild-type (nTg) to identify a list of genes, which are enriched in the M4 pull down samples and found 1275 protein coding genes (FDR<0.05, logFC range is 0.76-8.19) (Figure 30).

We next compared wild-type (Tg) to *ceh-28* (Tg) to identify genes, which are downregulated in *ceh-28(cu11)*, and found 111 protein coding genes (FDR<0.05, logFC range is 1.1-9.19) (Figure 30). These genes may be directly or indirectly regulated by CEH-28.

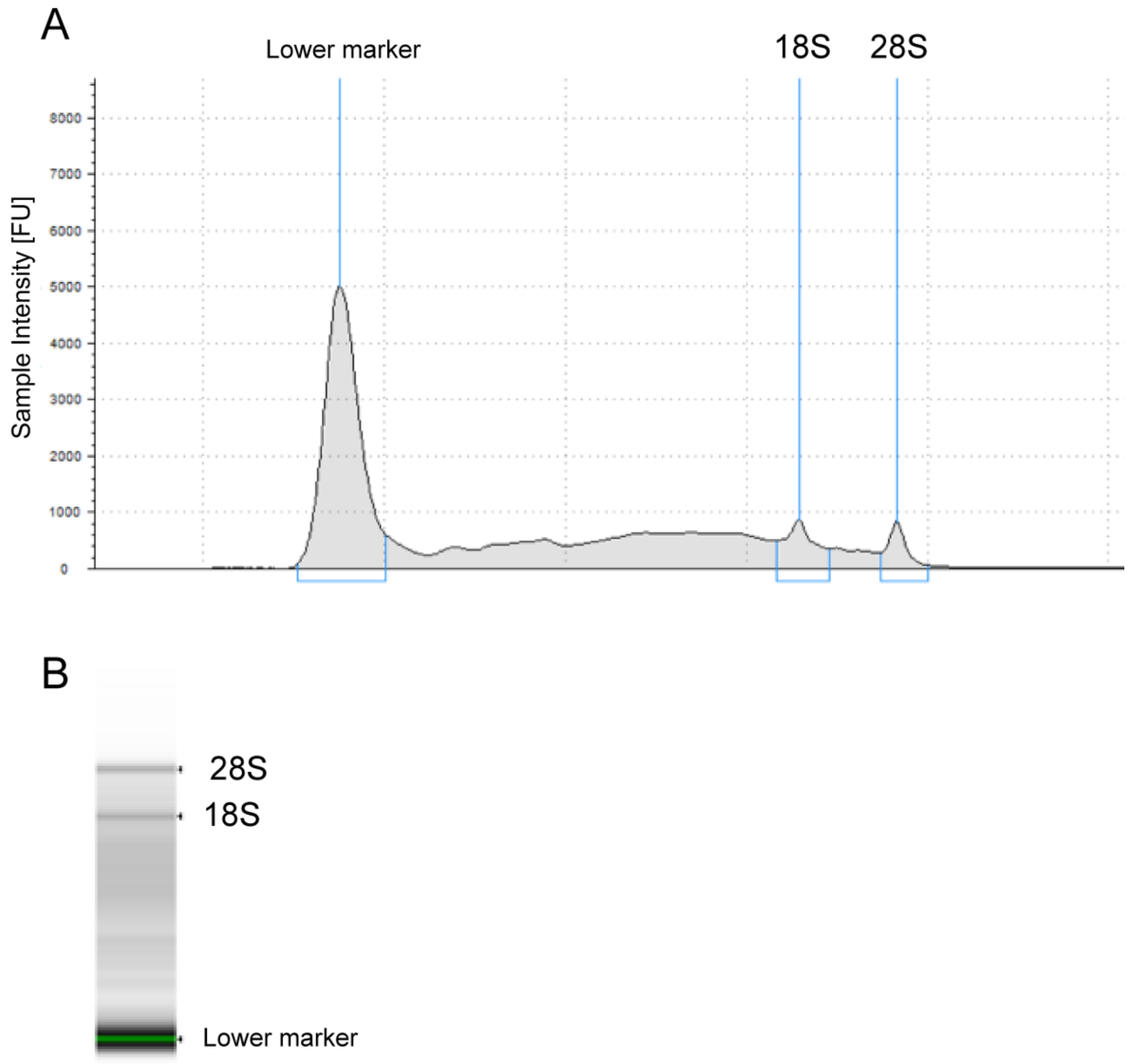

Figure 28 Assessment of RNA quality using TapeStation 2200

TapeStation 2200 was used to examine integrity of coimmunoprecipitated mRNA. (A) Representative electropherogram of RNA from wild-type (Tg) indicates that the sample contains RNA heterogeneous in size. Three peaks in the electropherogram represent lower marker, 18S (18S rRNA) and 28S (28S rRNA). The RNA integrity number (RIN) of the sample is 3.6. (B) Gel image representing RNA from the same sample. Similar to the electropherogram, it shows that the sample consists of RNA heterogeneous in size. Three bands represent lower marker, 18S rRNA and 28S.

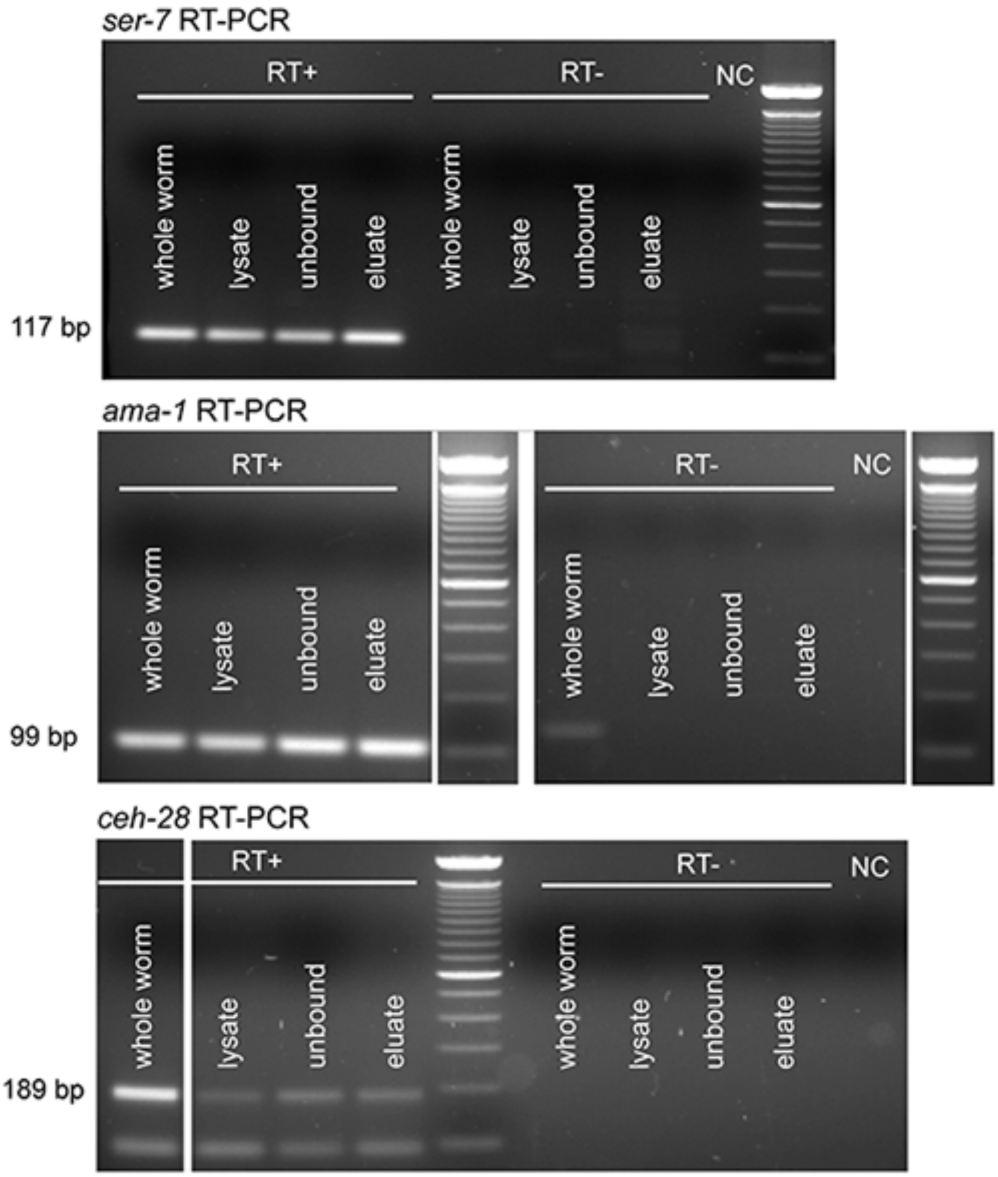

Figure 29 RT-PCR of genes expressed in M4

Agarose gels stained with ethidium bromide showing the results of RT-PCR for *ser-7*, *ama-1* and *ceh-28* genes. The expected sizes of *ser-7* is 117 bp, *ama-1* is 99 bp and *ceh-28* 189 bp. The product of the correct size is present in eluate fraction for all genes tested. NC indicates negative control for PCR, where cDNA was substituted with dH_2O. The ladder is 1 kb DNA ladder. There are two separate gels representing *ama-1* RT+ and RT- PCRs. Each gel has irrelevant lanes excised between the RT samples and the ladder. The irrelevant lanes between "whole worm" and the rest of the *ceh-28* RT-PCR gel were excised. Description of the lanes is following:

- "whole worm" - RNA isolated from whole worm lysate
- "lysate" - RNA isolated from lysate obtained after sonication
- "unbound fraction" - RNA purified from unbound fraction after performing Co-IP
- "eluate" - RNA purified from eluate

Finally, we compared genes enriched in the M4 motor neuron to genes downregulated in *ceh-28* mutants to identify a list of genes that are potential targets of CEH-28 in M4. We found 39 protein coding genes (FDR<0.05, logFC range is 1.16-5.16) (Figure 30), and called this list of 39 genes “Potential targets of CEH-28”.

We asked two questions. Is there any evidence in the literature whether the “Potential targets of CEH-28” are expressed in the M4 motor neuron or in the pharynx? Are any of the “Potential targets of CEH-28” involved in neuronal polarity and/or neuronal function? We found that 3 genes (*mlp-1*, *tag-290, gst-4*) are expressed in the pharynx. There is no evidence whether they are expressed in M4 or have neuronal function (Table IX). For the 5 genes (*anc-1, cyp-13A7, col-12, grd-14, phat-2*) the expression pattern was described, and they do not have any function in the pharynx or neuronal function. The expression pattern for the rest of the 31 genes is not known.

Importantly, in the RNA-seq analysis we did not detect genes, that have been previously identified as targets of CEH-28 in M4, such as *dbl-1*, *egl-17*, *flp-5* and *flp-2*.

5.5 Discussion

5.5.1 Identification of the 39 candidate genes regulated by CEH-28

After performing RNA-seq data analysis, we identified 39 protein coding genes, which are enriched in wild-type (Tg) vs wild-type (nTg) and downregulated in *ceh-28(cu11)* vs wild-type (Tg). We first examined the literature to determine the expression pattern of these genes. We found that some of are expressed in the pharynx, some are not, and for most of the genes there is no available information about the expression pattern.

The genes that are expressed in the pharynx are *mlp-1*, *tag-290* and *gst-4* (Table IX). However, they have not been reported to be expressed in M4 and do not have any clear neuronal function. *gst-4* encodes for a putative glutathione-requiring prostaglandin D synthase. It is a major cellular detoxification enzyme and deals with oxidatively damaged cellular components (Leiers et al., 2003). *mlp-1* encodes for LIM domain-containing protein that is a

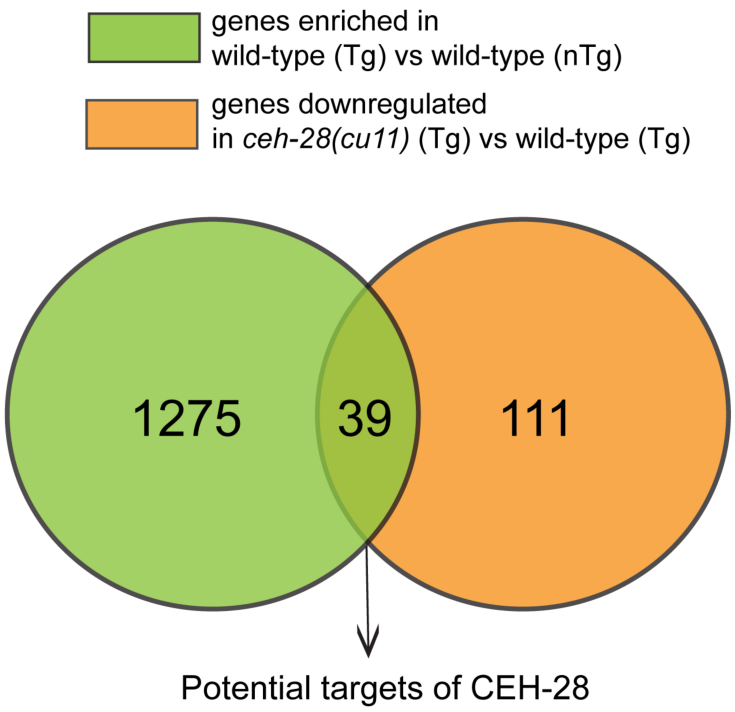

Figure 30 Differential analysis of RNA-seq data

Schematic Venn diagram representing number of genes obtained during deferential analysis of the RNA-seq data. 1275 protein coding genes are enriched in wild-type (Tg) vs wild-type (nTg) (green circle). 111 protein coding genes are downregulated in *ceh-28(cu11)* vs wild-type (Tg) (orange circle). Overlap between green and orange circles represents 39 protein coding genes, which are potential targets of CEH-28 and maybe regulated by CEH-28 in M4.

member of the MLP/CRP family of muscle LIM domain proteins. It plays a role in cytoskeleton organization, mediates protein-protein interactions (McKay et al., 2003). *tag-290* is an ortholog of human TFPI (tissue factor pathway inhibitor) and TFPI2 (tissue factor pathway inhibitor 2) (McKay et al., 2003). It is possible that the expression in the M4 neuron was obscured by a broad expression of the gene in the pharynx. Moreover, the function of the gene is often studied in a tissue of interest, and cells in different tissues are not specifically described.

There are 5 genes that have a described expression pattern, however there is no evidence of them being expressed in the pharynx and having any neuronal function. These genes are *anc-1, cyp-13A7, col-12, grd-14, phat-2* (Table IX).

The expression pattern is unknown for the rest of 31 genes and there is no evidence of them having a neuronal function (Table IX).

As a result of the analysis, nothing stands out from the list of 39 genes as definite potential candidates, which are expressed in M4, and have neuronal function, or play a role in neuronal polarity and synapse formation. Importantly, for the majority of the genes, there is no available information about their expression pattern. Some of these genes may potentially be good CEH-28 targets.

There are a few possible explanations why previously identified targets of CEH-28 such as *dbl-1*, *egl-17*, *flp-5* and *flp-2* were not detected in RNA-seq analysis. First, the Co-IP experiment we performed was clearly nonspecific, because RNA from the wild-type (nTg) sample was pulled down. Non specifically coimmunoprecipitated RNA could obscure any changes in genes expression in the M4 neuron. For example, *dbl-1* is expressed in M4 and in many other neurons as well. Nonspecific coimmunoprecipitation of *dbl-1* from these other neurons could mask any changes in *dbl-1* expression in M4 when comparing wild-type (Tg) to *ceh-28(cu11)*. Second, there were problems with the quality of distilled water in the research building at the time when Co-IP was conducted including high levels of bacterial contamination. This could possibly have interfered with the technically challenging experiment we performed

because in the “Potential targets of CEH-28” there a few genes, that encode for fungus-induced proteins.

5.5.2 Future experiments

Nonspecific binding is a common problem during pull downs. To understand what the ratio of the nonspecific binding to the specific binding is, a quantitative RT-PCR (qRT-PCR) could be performed. For example, the ratio of *ceh-28*/*ama-1* transcripts in the wild-type (Tg) and wild-type (nTg) samples can be measured using qRT-PCR. *ama-1* is a housekeeping gene, which is expressed in all cells of the organism, and *ceh-28* is exclusively expressed in M4. If there is an enrichment in the M4 transcripts such as *ceh-28* during pull down, then we expect that the *ceh-28*/*ama-1* ratio in wild-type (Tg) would be greater than in wild-type (nTg).

There are several different ways theough which RNA-seq data can be analyzed. We specifically focused on 39 genes, that represent genes that are expressed in M4 and regulated by CEH-28. The RNA-seq data analysis could be expanded with a focus on larger sets of genes in parallel: (1) 1275 genes expressed in M4 and (2) 111 genes regulated by CEH-28 (Figure 31). First, we would like to know how many genes have neuronal function using one of the Gene Ontology analyses, such as the David Functional annotation tool (Huang da et al., 2009), (Huang et al., 2007). In parallel, the promoter regions of the genes would be scanned for CEH-28 homeodomain binding sites with the JASPAR motif (Ramakrishnan and Okkema, 2014). The NK-2 homeodomain transcription factors bind a particular consensus sequence. It has been shown previously that *dbl-1* expression in M4 depends on a site that matches this consensus sequence (Ramakrishnan et al., 2014). Genes that have both neuronal function and CEH-28 binding sites would be further analyzed. Mutants for these genes would be evaluated for *ceh-28* mutant phenotypes, including stuffed pharynx. If the mutants are not available, then RNAi would be performed on these genes. Because we are looking for the targets of CEH-28, that are involved in synapse formation and/or positioning, we would only be interested if the mutant

animals (or RNAi treated) have a stuffed pharynx and/or abnormal synapse morphology. In parallel, *gfp* fusions would be generated to examine the expression pattern of these genes.

Identifying targets of CEH-28 involved in synapse formation or/and positioning would lead to an understanding of the mechanisms controlling neuronal polarity and synaptogenesis. Because both neuronal polarity and abnormal synapse assembly are causes for many neurodegenerative diseases (Okouchi et al., 2007), it would likely identify genes that can be investigated as biomarkers and possible therapeutic targets for these devastating diseases.

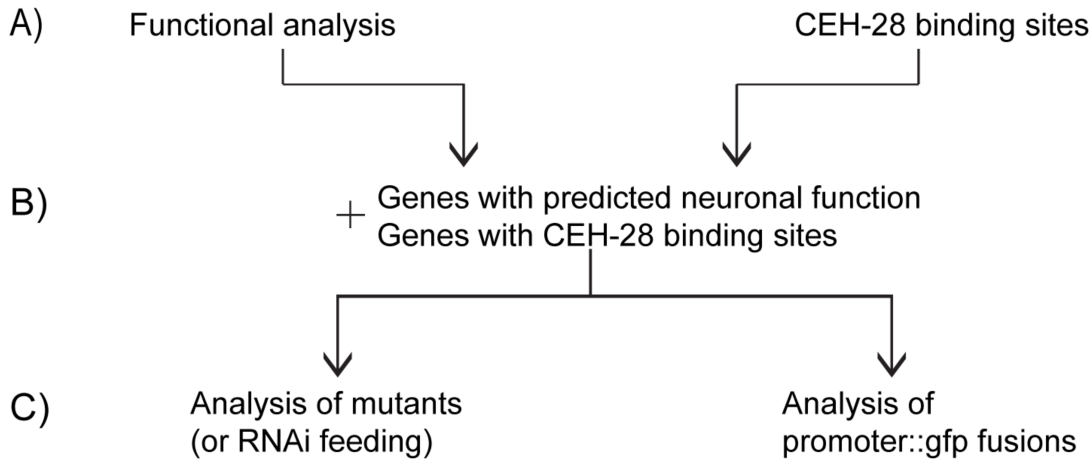

Figure 31 Alternative analysis of RNA-seq data

Flow chart represents alternative steps for the RNA-seq data analysis. 1275 genes enriched in the M4 neuron and 111 genes regulated by CEH-28 would be processed in parallel. (A) Perform functional analysis. In parallel, screen the promoter regions of the genes for the NK-2 consensus sequence. (B) Identify genes with neuronal function and the NK-2 binding sites. (C) Analyze mutants of these genes for the *ceh-28* mutant phenotypes. In parallel, generate promoter::gfp fusions to examine expression patterns

Table IX: The 39 potential targets of CEH-28 identified by RNA-seq

Genes	Published expression pattern	Description
mlp-1	Adult: pharynx, intestine, rectal gland cells, body wall muscle, vulval muscle, spermatheca, body wall muscle, hypodermis, gonad sheath cells, neurons along body, head neurons and tail neurons. Larva: pharynx, intestine, rectal gland cells, body wall muscle, body wall muscle, head neurons, tail neurons. (McKay et al., 2003)	Encodes for protein containing LIM domain that is a member of the muscle LIM proteins. It plays role in cytoskeleton organization, mediates protein-protein interactions.
tag-290	Adult: pharynx; arcade cells. Larva: pharynx; arcade cells. Can see expression in the isthmus and TB on the image. (McKay et al., 2003)	An ortholog of human TFPI (tissue factor pathway inhibitor) and TFPI2; is predicted to have serine-type endopeptidase inhibitor activity, based on protein domain information.
gst-4	Adult: muscle fibers, hypodermis and the cells surrounding the pharynx, nervous system, reproductive system, vuvla muscle, head neuron, body wall muscles, intestine. L3: isthmus and terminal bulb, hypodermis. (Leiers et al., 2003)	Encodes a putative glutathione-requiring prostaglandin D synthase. It is a major cellular detoxification enzyme and deal with oxidatively damaged cellular components. There is a direct correlation between concentration of GST-4 and the resistance to oxidative stress (Leiers et al., 2003).

anc-1	Expressed in a variety of cells, body wall muscles, vulval muscle. ANC-1 was localized with antibdies to the cytoplasm of postembryonic somatic cells. ANC-1 localization in the nuclear periphery was detected in different cells, including uterine cells. Subcellular localization: cytoplasm, perinuclear (Starr and Han, 2002).	Encodes a protein, orthologous to Drosophila MSP 300 and mammalian SYNE1 and SYNE2 proteins. ANC-1 anchors nuclei by connecting the nucleus to the actin cytoskeleton (Starr and Han, 2002).
cyp-13A7	Intestine (Chakrapani et al., 2008)	Encodes a homolog of cytochrome P450 proteins (CYP), which are membrane proteins with a heme prosthetic group that catalyze steroid hormones the, and also detoxify foreign substances such as xenobiotic compounds *C. elegans*. Most drugs induce the CYP enzymes expression, which results in reduction of the bioavailability of the drug (Chakrapani et al., 2008).
col-12	Cuticle (Johnstone and Barry, 1996) Expressed throughout development but expression is increased when new cuticle is secreted and after the L4 to adult larval molt.	Encodes a member of the collagen superfamily containing collagen triple helix repeats (20 copies).

grd-14	Adult: seam cells, hypodermis, intestine; uterine. L1 through adulthood: rectal epithelial cells Larval Expression: intestine; head mesodermal cell; hypodermis; seam cells. (Hao et al., 2006)	Encodes a hedgehog-like protein containing. GRD-14 is necessary for vulval morphogenesis, locomotion normal growth.
phat-2	Gland cells (Ghai et al., 2012)	Encodes mucin-like proteins that are secreted into the pharyngeal lumen to facilitate the transport of bacteria through the pharynx
nhr-265	No info	Is predicted to have activity of DNA binding transcription factor, steroid receptor activity, zinc ion binding activity, and sequence-specific, based on protein domain information.
cut-2	No info	Encodes a secreted protein which is a component of cuticlin, the insoluble residue of nematode cuticles; CUT-2 contributes to the external cortical layer of the cuticle of all larval stages.
his-26	No info	Encodes an H4 histone.
his-51	No info	Encodes an H2A histone.
his-53	No info	Encodes an H2A histone.
lec-1	No info	Encodes a galectin. Galectin domain homologous to vertebrate 14-kDa-type galectins.
str-154	No info	Seven TM receptor
fipr-7	No info	FIP (Fungus-Induced Protein) Related
fipr-6	No info	FIP (Fungus-Induced Protein) Related
fipr-5	No info	FIP (Fungus-Induced Protein) Related
fipr-9	No info	FIP (Fungus-Induced Protein) Related
nduo-5	No info	Mitochondrial genome encoded NADH - (NaDh) Ubiquinone Oxidoreductase chain homolog.

dos-1	No info	Encodes an unfamilar protein with no clear orthologs outside of nematodes.
srbc-15	No info	Serpentine receptor class bc (Srbc), 7TM GPCR
irld-35	No info	Insulin/EGF-Receptor L Domain protein.
irld-53	No info	Insulin/EGF-Receptor L Domain protein.
clec-209	No info	Same as F56A4.2, C-type LECtin
cct-8	No info	Encodes a putative theta subunit of the eukaryotic cytosolic ('T complex') chaperonin, CCT-8 is necessary for transgene repression, fertility, distal tip cell migration, locomotion, vulval development, and rapid growth.
C31H5.6	No info	C31H5.6 is an ortholog of human BAAT (bile acid CoA:amino acid N-acyltransferase), ACOT4 (acyl-CoA thioesterase 4), ACOT2 (acyl-CoA thioesterase 2) and ACOT1 (acyl-CoA thioesterase 1); C31H5.6 is predicted to have thiolester hydrolase activity, based on protein domain information.
C35B1.5	No info	C35B1.5 is an ortholog of human NXNL1 (nucleoredoxin-like 1) and NXNL2 (nucleoredoxin-like 2).
C02E7.6	No info	
C02E7.7	No info	
C26F1.1	No info	
C35B1.8	No info	
F56A4.3	No info	F56A4.3 is an ortholog of human GSTP1 (glutathione S-transferase pi 1).
F09F9.2	No info	
F56A4.2	No info	
Y65B4A.6	No info	An ortholog of human EIF4A3 (eukaryotic translation initiation factor 4A3); Y65B4A.6 is involved in embryo development, germ cell development, hermaphrodite genitalia

		development, locomotion, the molting cycle, nematode larval development, oviposition, regulation of cell proliferation and regulation of meiotic nuclear division.
Y19D10A.10	No info	
Y69A2AR.22	No info	
Y43F8B.22	No info	

39 genes are enriched in wild-type (Tg) versus wild-type (nTg) and downregulated in *ceh-28* (Tg) versus wild-type (Tg). Expression pattern and gene description is shown in if available.

6 DISCUSSION AND CONCLUSIONS

6.1 GCaMP3 is a powerful tool to monitor calcium transients in live *C. elegans*

Ca^{2+} is an ubiquitous second messenger which is involved in many aspects of cell signaling, especially in neurons and other excitable cells (Burgoyne, 2007). Small molecule calcium sensitive dyes and genetically encoded calcium indicators (GECI) are used to detect changes in intracellular concentrations of Ca^{2} (Yasuda et al., 2004), (Mank and Griesbeck, 2008). The advantage of using of GECI is that it allows for a noninvasive way of detecting Ca^{2+} dynamics within a cell. GECI GCaMP is based on circularly permuted GFP (cpGFP), calmodulin (CaM), which is the calcium-binding protein and CaM-interacting peptide M13 (Nakai et al., 2001), (Akerboom et al., 2009). A few variants of GCaMP have been engineered, with GCaMP6 as the latest variant. GCaMP6, compared to the earlier variants of GCaMP, has enhanced sensitivity, increased the dynamic range of the fluorescence response, and increased Ca^{2+} affinity and brightness (Chen et al., 2013). To detect even slight changes in Ca^{2+} transients in the pharyngeal muscles cells, the more sensitive GCaMP6 could be used.

The color palette of GECI was also extended with engineering of RCaMP, which is based on red fluorescent proteins. This allows multi-color imaging of Ca^{2+} transients simultaneously in different cells or cell compartments (Akerboom et al., 2013). For example, expression of RCaMP in the M4 neuron and GCaMP3 in the pharyngeal muscles would allow simultaneous imaging of Ca^{2+} transients in M4 and the pharyngeal muscles. Generation of RCaMP also allows integration of GECIs into optogenetic experiments. Activation of the light-modulated ion protein channelrhodopsin-2 (ChR2) excites most GECIs because of excitation spectral overlap (Nagel et al., 2003), (Nagel et al., 2005). Optogenetic manipulation using ChR2 combined with imaging of RCaMP overcomes this problem, and could elucidate interactions both between two excitable cells and within single cells.

One of the caveats of using GECI is that they act as calcium buffers. Expression of GECI in a cell changes the spatio-temporal dynamics of calcium. Calcium buffers affect

intracellular free calcium to a certain degree based on the following factors: its concentration, mobility and affinity (Zhou and Neher, 1993), (Neher, 1995), (Helmchen et al., 1996). To decrease buffering, GECI with a reduced number of calcium binding sites per sensor has been generated and could be used to overcome this problem (Thestrup et al., 2014).

GFP based calcium sensors use a single channel for recording fluorescence. Recording from a single channel is simpler than from two channels. All photons emitted from a probe are collected without any loss from emission filters or beam splitters. Fluorescence resonance energy transfer (FRET)-based calcium sensors are ratiometric and require recording from two channels separately. Measurement of Ca^{2+} concentrations is based on the ratio of the two emission channel intensities, which is independent from the expression levels of the indicator. FRET-based ratiometric sensors include yellow cameleons (Nagai et al., 2004), (Lutcke et al., 2010), (Horikawa et al., 2010), D3cpv (Palmer et al., 2006) and TN-XXL (Mank et al., 2008). FRET-based indicators are less influenced by changes in optical path length and fluctuations in excitation light intensity. Ratiometric imaging is very useful when movement artifacts may be present such as tissue or the animal's movement, because these artifacts affect both channels and are cancelled out during processing. Moreover, the resting ratio of the FRET-based indicator is used to measure the resting level of calcium. The immobilization method we used here was not perfect, and sometimes a movement of an animal was present. In this case, the animal was disregarded and not used for GCaMP3 recording. FRET-based GECI could be a solution to this problem while monitoring Ca^{2+} transients within the pharyngeal muscles cells.

Here, we developed a GCaMP3-based tool, which detects Ca^{2+} transients in the M4 motor neuron and pharyngeal muscles in live *C. elegans*. To monitor calcium dynamics, we performed a recording from a single channel using an epifluorescent microscope equipped with a camera, which is able to collect time-lapse images at 25-30 frames/sec.

Pharyngeal GCaMP3 is ideally suited for better understanding any mutants, which affect contractile behavior of the pharynx. In Chapter 3, we describe in detail characterized Ca^{2+}

transients in the isthmus muscles of *gar-3(gk305)* mutants. As we reported, these mutants do not have any defects in pharyngeal isthmus peristalsis. The frequency of peristaltic contractions, the percentage of pumps followed by peristalsis and the duration of peristalsis look similar in *gar-3(gk305)* mutants to what we observed in wild-type animals. Surprisingly, when we looked at the Ca^{2+} transients in *gar-3(gk305)* mutants, we found that there is no peak delay in GCaMP3 fluorescence between the center and posterior isthmus. Even though these mutants do not have any pharyngeal contractile defects, their pharyngeal Ca^{2+} transients differ from that observed in wild type. In this case, the pharyngeal GCaMP3 helped us to understand the *gar-3(gk305)* mutant phenotype, and gave better understanding of the model. This demonstrates that the pharyngeal GCaMP3 tool provides much deeper understanding of the mutant phenotype on the molecular level even if this mutant does not exhibit any visible contractile defects.

6.2 *eat-2* mutants as a model for neuromuscular disorders

Using GCaMP3 specifically expressed in pharyngeal muscles, we observed increased Ca^{2+} transients in the isthmus of *eat-2(ok3528)* mutants: increased $\Delta F/F_o$, peak duration and rise time (Table III). We also showed that loss of *eat-2* results in the prolonged peristalses that depends on wild-type *gar-3*.

Increased Ca^{2+} transients in muscle cells have been reported in a number of neuromuscular disorders, including myotonic dystrophies, Duchenne muscular dystrophy, as well as in *ColQ* and slow-channel myasthenic syndromes (Tang et al., 2012), (Vallejo-Illarramendi et al., 2014), (Engel et al., 2015). In particular, myotonic dystrophies are characterized by an inability of the muscles to relax after a contraction, which resembles the prolonged peristaltic contraction we observed in *eat-2* mutants. There are a few proposed mechanisms for the increased Ca^{2+}. One mechanism is associated with an increase in sensitivity of the voltage gated calcium channel $Ca_V1.1$. The other mechanism is associated with mutations in acetylcholinesterase *ColQ* resulting in excessive Ca^{2+} enter into the muscle cells due to the extended residence of ACh in the synaptic space (Engel et al., 1977), (Hutchinson et

al., 1993). Mutations in ligand-binding or pore domains of nAChR have also been shown to be a cause of congenital myasthenic syndromes (Engel et al., 1982), (Ohno et al., 1995), (Engel et al., 2015). These mutations result in abnormal signal transmission from a neuron to a muscle cell, but these mutations have not been associated with increased Ca^{2+} in muscle cells. It is unclear whether *eat-2* defects underlie any of these disorders, but *eat-2* mutants provide a new model to study the immediate effects of Ca^{2+} dysregulation in muscle cells.

6.3 Identification of the receptor responsible for isthmus peristalsis

The receptor necessary for the isthmus peristalsis has not been identified yet. Both *eat-2(ok3528)* and *gar-3(gk305)* single mutants have peristaltic contractions, suggesting that neither EAT-2 nor GAR-3 are necessary for peristalsis. Therefore, we initially hypothesized that EAT-2 and GAR-3 play redundant roles in isthmus peristalsis. To test this hypothesis, we generated *eat-2(ok3528); gar-3(gk305)* double mutants and characterized pharyngeal muscle contractions in these animals. We found that these mutants are still able to produce both pumping and peristalsis, indicating that there must be some other receptor involved in isthmus peristalsis.

We then expanded our research to five nAChR subunit genes (*acr-6*, *acr-7*, *acr-10*, *acr-14* and *acr-16*). These genes, along with *eat-2*, show enriched expression in embryonic pharyngeal muscles based on RNA-seq data (Okkema, Moerman and Waterston, unpublished). None of these receptor mutants have any defects in pharyngeal muscle contractions under both untreated and arecoline treated conditions. The *C. elegans* genome encodes 27 nAChR subunit genes, and it is very time consuming to test all of these genes one by one by examining receptor mutant phenotypes.

We showed that mAChR GAR-3 is the receptor, which mediates the response to arecoline in the pharyngeal muscles (Table II). Although it has been shown that the other two mAChRs genes *gar-1* and *gar-2* do not have any function in the pharynx, we also examined the pharyngeal muscle contractions in *gar-1(ok755)* and *gar-2(ok520)* mutants, both untreated and treated with arecoline (Lee et al., 2000), (Lee et al., 1999), (Lee et al., 2000), (Tarawneh,

Kozlova and Okkema, unpublished). We did not find any defects in the isthmus peristalsis, indicating that GAR-1 and GAR-2 are not necessary for the isthmus peristalsis.

To identify the receptor necessary for peristalsis, RNA sequencing on whole pharynxes dissected from adult animals could be performed to obtain the pharyngeal transcriptome. Alternatively, RNA sequencing on the pharyngeal muscle cells could be performed. The pharyngeal muscle cells expressing *myo-2::GFP* could be collected by using fluorescence-activated cell sorting (FACs). Then, the whole pharyngeal or pharyngeal muscle transcriptome could be screened for the genes encoding nAChRs. Next, mutants for these nAChR genes could be examined for the defects in peristaltic contractions such as frequency and duration of peristalsis. If receptor mutants have defects in isthmus peristalsis, then Ca^{2+} transients could be characterized to better understand mutant phenotype.

EAT-2 is non-α nAChR subunit that belongs to the ACR-16 class of nAChRs. Non-α subunits associate with α subunits to form heteropentameric channels. Obtaining the pharyngeal muscle transcriptome could help to identify which α subunit EAT-2 could potentially associate with to form a functional nAChR.

6.4 Identification of GAR-3 receptor localization in the pharyngeal muscles

According to the spillover model proposed in Chapter 3, in *eat-2(ok3528)* mutants, unbound ACh diffuses from the synapse and binds to the GAR-3 receptor on the isthmus muscles, resulting in prolonged peristalsis. We hypothesized that GAR-3 is localized to the isthmus muscles. To test this hypothesis, the expression pattern of fluorescently tagged GAR-3 fusion protein could be examined. The expression of GFP-tagged GAR-3 fusion protein (GAR-3-GFP) has been previously described (Chan et al., 2013). Fluorescence was observed in the ventral nerve cord and in body wall muscles. Unfortunately, this strain, which carries GAR-3-GFP, also has *myo-2::GFP* as a coinjection marker and could not be used to test if GAR-3-GFP is expressed in the pharyngeal muscle. Therefore, a different strain expressing GAR-3-GFP could be generated, which carries pRF4 plasmid as a coinjection marker.

6.5 Examination of MC motor neuron morphology in *eat-2* mutants

We do not know if the spillover in *eat-2* mutants occurs directly due to ACh diffusion from the synapses because of reduced binding to EAT-2 in *eat-2* mutants, or whether loss of *eat-2* leads to developmental defects during synaptogenesis that allows ACh spillover. For example, it has been previously reported that loss of the gamma-subunit of the nAChR leads to a diffuse distribution of acetylcholinesterase clusters during development of mouse diaphragm muscles (Liu et al., 2008).

One read out of a developmental defect in synaptogenesis may be abnormal morphology. Therefore, if loss of *eat-2* leads to developmental defects in the MC motor neuron, the morphology of this neuron may appear abnormal in *eat-2* mutants. *ceh-19* encodes a homeobox protein, which shares similarity to Bar-like homeoproteins from vertebrates and Drosophila. *ceh-19* is required for proper specification of the MC motor neuron and expressed in three pairs of neurons: MC motor neurons, ADF sensory amphid neurons and PHA phasmid neurons (Feng and Hope, 2013). To test if the MC motor neuron has morphological defects in *eat-2* mutants, the expression pattern of *ceh-19::gfp* could be characterized in these mutants and compared to wild type. If the MC processes exhibit morphological abnormalities, MC synapses could be examined by expressing fluorescent synaptic markers *snb::gfp* or *rab-3::gfp* fusion genes in MC using the *ceh-19* promoter (Sieburth et al., 2005).

6.6 Identifying additional targets of CEH-28

Sequencing of mRNA coimmunoprecipitated from M4 using the mRNA tagging technique did not reveal any clear potential targets, which are expressed in the pharynx and have neuronal function (Table IX). As described in Chapter 5, alternative analysis of RNA-seq data could be performed to expand the list of potential targets (Figure 31). In the pull down we performed, there was non-specific binding of RNA to the anti-FLAG beads, which resulted in background during RNA-seq data analysis. This background likely obscured the changes in gene expression in the M4 neuron when compared wild type (Tg) to *ceh-28* (Tg).

To decrease the noise in the RNA-seq data, the FACS technique could be used to isolate RNA specifically from the M4 neuron. This method has been previously used for RNA purification from M4 in our laboratory (Ramakrishnan, 2014). However, an insufficient quantity of M4 cells was collected during flow cytometry. Growing animals in liquid culture could help obtain larger quantities of animals, and a larger amount of M4 cells collected during FACS. Once a synchronous population of L1s is obtained, the larval cells are isolated by dissociation using SDS-DTT and Pronase E (Zhang et al., 2011). Dissociated cells from wild type and *ceh-28* mutants expressing GFP are subjected to cell sorting using FACS. Cells isolated from N2 animals serve as a negative control. Ideally, only GFP expressing cells (M4 cells) are collected during flow cytometry. RNA is purified from the sorted cells and submitted for sequencing. Genes differentially expressed between wild type and *ceh-28* mutants would be considered as potential targets of CEH-28. Next, mutants for these genes would be examined for the *ceh-28* phenotypes, including ‘stuffed pharynx’. We anticipate that this method of RNA isolation from M4 would produce less background compared to the mRNA tagging technique, because only GFP positive M4 cells would be used for RNA purification.

7 APPENDICES

7.1 Appendix A: GAR-3 does not act via the voltage gated calcium channel EGL-19

7.1.1 *egl-19(n582)* mutants do not exhibit defects in pharyngeal muscle contractions

Ca^{2+} influx through the voltage-gated calcium channel EGL-19 contributes to an increase in an intracellular concentration of Ca^{2+} necessary for the membrane depolarization and muscle contraction (Catterall, 2000; Katz and Miledi, 1967). We have shown (Chapter 3) that signaling through the GAR-3 receptor results in an increase of calcium concentrations in the isthmus muscles and prolonged peristaltic contractions. We would like to understand how signaling via GAR-3 leads to an increase of calcium concentrations inside the muscle cell.

We hypothesized that GAR-3 acts via EGL-19 in the isthmus muscles. *egl-19* expression has been detected in the isthmus muscles (Lee et al., 1997). To test our hypothesis we quantified the pharyngeal muscle contractions in *egl-19(n582)* mutants. *egl-19(n582)* is a point mutation introducing an early stop codon (Lee et al., 1997). *egl-19(n582)* is a reduction of function mutation, which generally reduces EGL-19 channel activity. The null mutants die as embryos, because *egl-19* is essential gene necessary for the muscle contraction. Frequency of pumping and peristalsis, percentage of pumps followed by peristalsis and duration of peristalsis in *egl-19(n582)* mutants were similar to those in wild-type animals (Table X). These observations were not surprising because *gar-3(gk305)* mutants also do not show defects in pharyngeal muscle contractions. It is also possible that some of the *egl-19* function is retained in *egl-19(n582)* mutants contributing to the normal pharyngeal muscle contractions.

7.1.2 *egl-19(n582)* mutants treated with arecoline exhibit hyperstimulated peristalsis

Wild-type animals treated with arecoline have frequent and prolonged peristalsis. We showed that *gar-3(gk305)* mutants are not sensitive to arecoline treatment and exhibit normal frequency and duration of peristalsis (Table III). If GAR-3 acts via EGL-19, then *egl-19(n582)* mutation should be also insensitive to arecoline treatment. Arecoline treated *egl-19(n582)* mutants, similar to the arecoline treated wild-type animals, exhibit less frequent pumping,

frequent and prolonged peristalsis (Table X). This indicates that in the absence of EGL-19, GAR-3 is able to hyperstimulate the isthmus muscle peristalsis. Thus, we conclude that GAR-3 does not act through EGL-19.

Table X: Quantification of the pharyngeal muscle contractions in *egl-19, unc-2, egl-19; unc-2* and *sca-1* mutants

genotype	pump rate (pumps/min ± sem)	peristalsis rate (peristalses/min ± sem)	% pumps followed by peristalsis	duration of isthmus peristalsis (ms ± sem)
wild type [a]	209 ± 18	20 ± 4	10%	132 ± 5
wild type + arecoline [b]	13 ± 2	13 ± 2	100%	696 ± 92
egl-19(n582) [c]	213 ± 21	15 ± 5	8%	142 ± 9
egl-19(n582) + arecoline [d]	19 ± 1	14 ± 1	74%	427 ± 40
unc-2(lj1) [e]	56 ± 18	22 ± 6	59%	212 ± 17
egl-19(n582); unc-2(lj1) [f]	29 ± 2	22 ± 4	76%	289 ± 9
sca-1(tm5339) [g]	161 ± 22	18 ± 6	12%	179 ± 9

[a] Five N2 L1s were recorded for 19-20 s and a total of 347 pumps were analyzed.

[b] Six N2 L1s treated with 5 mM arecoline were recorded for 34-46 s and a total of 48 pumps were analyzed.

[c] Five *egl-19(n582)* L1s were recorded for 19-20 s and a total of 356 pumps were analyzed

[d] Five *egl-19(n582)* L1s treated with 5 mM arecoline were recorded for 34-45 s and a total of 48 pumps were analyzed.

[e] Seven *unc-2(lj1)* L1s were recorded for 30-31 s and a total of 159 pumps were analyzed.

[f] Five *egl-19(n582); unc-2(lj1)* L1s were recorded for 17-18 s and a total of 51 pumps were analyzed.

[g] Five *sca-1(tm5339)* L1s were recorded for 20-21 s and a total of 281 pumps were analyzed.

7.2 Appendix B: *unc-2(lj1)* mutants exhibit hyperstimulated peristalsis

unc-2 encodes an alpha subunit of a calcium channel, which is similar to the human N, P/Q and R-type voltage-gated calcium channel (Bargmann, 1998; Mathews et al., 2003; Schafer and Kenyon, 1995). Transcriptional fusion of the *unc-2* promoter region to GFP is expressed in the pharyngeal muscles (Mathews et al., 2003). We hypothesized that GAR-3 acts via UNC-2 in the isthmus muscles. To test our hypothesis we quantified pharyngeal muscle contractions in *unc-2(lj1)* mutants. *unc-2(lj1)* contains a 1547 bp deletion predicated to cause a frameshift mutation after exon 12. Surprisingly, the rate of pumping was significantly reduced in these mutants compared to wild type ($p < 10^{-3}$) (Table X). However, the duration of peristaltic contractions in the posterior isthmus increased up to 2-fold ($p < 10^{-5}$). The percent of pumps followed by peristalsis was also increased in *unc-2(lj1)* mutants ($p<0.01$), but as the pump rate was decreased in these animals, the absolute rate of peristalsis was similar in wild-type animals and *unc-2(lj1)* mutants. The defects in pharyngeal muscle contractions in *unc-2(lj1)* mutants are similar to those we observed in *eat-2(ok3528)* mutants (Table III). *eat-2(ok3528)* mutants also exhibit reduced pump rate, increased percent of pumps followed by peristalsis and increased duration of peristalsis.

We also examined *egl-19(n582); unc-2(lj1)* double mutants, and they show even more severe defects in the pharyngeal muscle contractions (Table X). This indicates that EAT-2 and UNC-2 may work together to produce proper pharyngeal isthmus peristalsis.

7.3 Appendix C: *sca-1(tm5339)* mutants have prolonged peristaltic contractions

During depolarization of a muscle cell calcium is released from a sarcoplasmic reticulum (SR) via ryanodine receptors (RyR) [reviewed in (Berchtold et al., 2000)]. This leads to an increase of an intracellular Ca^{2+}, which binds troponin subunit and this activated a muscle contraction. During relaxation, Ca^{2+} is translocated back to the SR resulting in a decrease of Ca^{2+} concentration within a cell. This process is mediated by the Sarco-Endoplasmic Reticulum Calcium ATPase (SERCA).

In *C. elegans* genome, SERCA is encoded by *sca-1* gene (Zwaal et al., 2001). We hypothesized that SCA-1 is essential for isthmus peristalsis. To test this hypothesis, we examined pharyngeal muscle contractions in *sca-1(tm5339)* mutants. Pumping rate and rate of peristalsis looked similar in *sca-1(tm5339)* mutants when compared to wild-type animals (Table X). However, the duration of peristalsis was somewhat prolonged in the mutants ($p < 10^{-5}$). This suggests that SCA-1 affects the duration of the peristaltic contractions.

7.4 Appendix D: *eat-5* and *inx-3* are expressed in the pharyngeal muscles

To express GCaMP3 specifically in the isthmus muscle we searched for the promoters specifically expressed in the pm5. *eat-5* and *inx-3* encode for innexins required for synchronized pharyngeal muscle contractions (Avery, 1993a; Li et al., 2003; Starich et al., 1996). Previous evidence suggest that *eat-5* and *inx-3* are expressed in the isthmus muscles but it is not clear whether these genes are also expressed in other parts of the pharynx (Altun et al., 2009). To examine expression patterns of *eat-5* and *inx-3*, we generated OK0988 strain carrying *cuEx794[Peat-5::gfp]* and OK0990 strain carrying *cuEx796[Pinx-3::gfp]*.

We found that expression of *eat-5* localizes to the isthmus muscle and the muscles of the terminal bulb (Figure 32A). Expression in the anterior bulb was much stronger than in the isthmus. Expression of *inx-3* was only found in the muscles of the terminal bulb (Figure 32B).

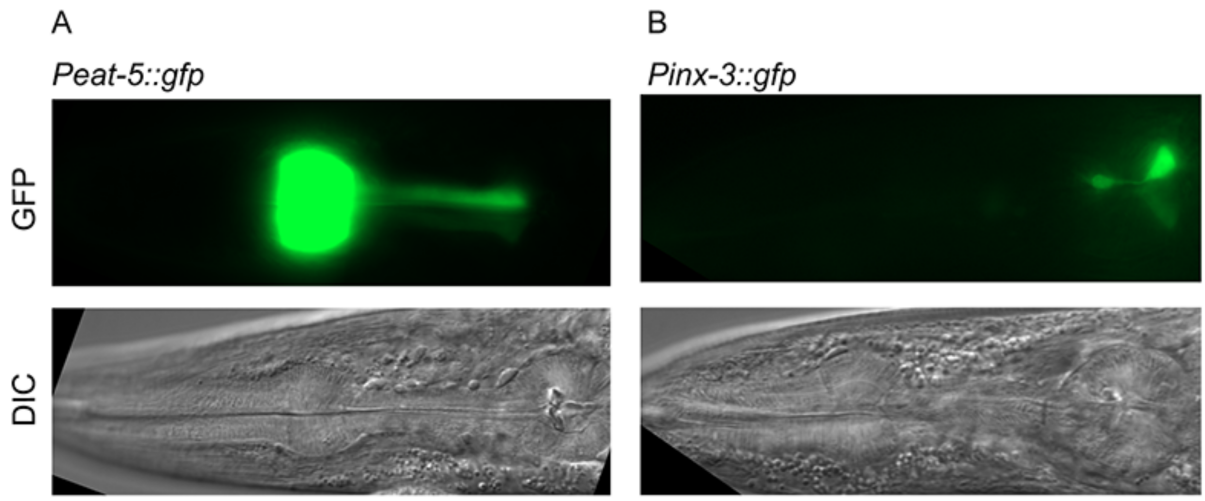

Figure 32 *eat-5* and *inx-3* are expressed in the pharyngeal muscles

(A) GFP micrograph of the wild-type animal expressing *Peat-5::gfp* in the isthmus muscles and muscles of the anterior bulb (top). DIC micrograph of the pharynx in the same wild-type animal (bottom). (B) GFP micrograph of the wild-type animal expressing *Pinx-3::gfp* in the muscles of the terminal bulb (top). DIC micrograph of the pharynx in the same wild-type animal (bottom). Anterior is to the left.

7.5 Appendix E: Examining pharyngeal muscle contractions in *ceh-28(cu11)* L1 mutant animals

Previous observations in *ceh-28(cu11)* L1 mutant animals show that they hyperstimulate isthmus muscle contractions (Ray et al., 2008). 100% of these mutants (n=5) have frequent and prolonged peristalsis, when prolonged peristaltic contractions occur after every pump. In contrast, when I looked at these mutants, I observed prolonged peristalsis only in 20% of the animals (n=50) during a time period of 1 min. The rest of the animals had normal peristaltic contractions. It is still possible that 100% of these mutants exhibit prolonged peristalsis, but not at all times. Prolonged peristalsis may be followed by normal peristalsis, which is then again followed by prolonged peristalsis. In this case, I probably imaged *ceh-28(cu11)* mutants during a time period when they had normal peristalsis. Therefore, pharyngeal muscle contractions in *ceh-28(cu11)* L1 mutant animals have to be examined more carefully. Frequency of pumping and peristalsis as well as duration of peristalsis has to be quantified at separate time periods within the same animal.

7.6 Appendix F: Testing different immobilization techniques

Serotonin stimulates pharyngeal pumping and peristalsis. We treated adult animals with serotonin to stimulate pharyngeal muscle contractions while imaging GCaMP3 fluorescence (Chapter 3 and 4). Therefore, all the GCaMP3 measurements were made in the animals under the serotonin conditions. 70% of the serotonin treated animals were also immobilized (n=30). Unfortunately, we were not able to find a different way to immobilize animals and stimulate pharyngeal muscle contractions, so we could image them under non-serotonin conditions. To test different immobilization techniques, we varied the thickness of the agarose pad, tried different type of Sephadex (G-15, G-25, G-50), glass beads and a worm glue (Table XI). Among them, only Sephadex G-15 and worm glue efficiently immobilized animals. Animals immobilized with Sephadex G-15 did not have any pharyngeal muscle contractions (n=30). Only 20% of animals immobilized with the worm glue (n=30), had pumping and peristalsis.

We have also tried custom made microfluidic device to immobilize animals and image them under non-serotonin conditions (Hulme et al., 2007). We were able to trap worms within the device but none of them exhibited any pumping and peristalsis (n=50). The device with different dimensions has to be constructed, so that animals can exhibit pharyngeal muscle contraction while being immobilized within the microfluidic device.

Table XI: Testing different immobilization techniques

Immobilization method	% of immobilized animals	% of animals with pumping	Number of animals tested
Serotonin	70	90	30
Thin agarose pad	0	70	30
Thick agarose pad	0	20	40
Sephadex G-15	90	0	30
Sephadex G-25	0	40	30
Sephadex G-50	0	20	30
Glass beads	0	40	35
Worm glue	100	20	30
Microfluidic device	100	0	50

7.7 Appendix G: List of Plasmids

Table XII: List of Plasmids

Plasmid	Description	Chapter
pOK290.02	*Pser-7b::GCaMP3* GCaMP3 under control of M4 promoter *ser-7b*. *ser-7b* promoter SphI-XbaI fragment from pOK197.03 was inserted into SphI-XbaI digested pOK270.01	4
pOK294.04	*Pmyo-2::GCaMP3* GCaMP3 under control of pharyngeal muscles promoter *myo-2*. *myo-2* promoter HindIII-MscI fragment from pPD96.48(L2531) was inserted into HindIII-MscI digested pOK290.02	3
pOK295.01	*Peat-5::gfp* wp423(*Peat-5::gfp*) received from Zhao-Wen Wang and Bojun Chen	Appendix D
pOK295.02	*Pinx-3::gfp* wp403(*Pinx-3::gfp*) received from Zhao-Wen Wang and Bojun Chen	Appendix D

7.8 Appendix H: List of Oligos

Table XIII: List of Oligos

Oligo	Sequence 5' – 3'	Description
PO640	CCCAATGCAATCTACGCAG	Forward primer for genotyping *ceh-28(cu11)* mutants
PO641	GAATCAAACCGCCAACCAG	Forward primer for genotyping *ceh-28(cu11)* mutants
PO642	CCCAGCGTGTCATACATGG	Reverse primer for genotyping *ceh-28(cu11)* mutants
PO643	ACAACAGCAGAAGAGAAAACCGAG	Forward primer for genotyping *ceh-28(cu11)* mutant
PO644	GCTAACCGCTTGCATTTGTATCG	Reverse primer for genotyping *ceh-28(cu11)* mutant
PO1061	GTGCATAGCGTTAGGTCGGA	Forward primer for amplifying *ama-1* exons by RT-PCR
PO1062	TCACCGTGTTCTTTGGGTC	Reverse primer for amplifying *ama-1* exons by RT-PCR
PO1401	CTTTTTCGTGGGGCTCGTTG	Forward primer used to amplify SER-7 orf by RT-PCR
PO1402	GTGCATAGCGTTAGGTCGGA	Reverse primer used to amplify SER-7 orf by RT-PCR
PO1423	TGCGTGGTAGAGGGATAGTG	Reverse primer for genotyping *eat-2(ok3528)* mutant
PO1424	TCTCGACGAGACCTACGTTG	Forward primer for genotyping *eat-2(ok3528)* mutant
PO1425	ACAGCTACAGTACCTCGCAC	Forward primer for genotyping *eat-2(ok3528)* mutant
PO1426	TAATAGGTTCGGCCCAGAG	Forward primer for genotyping *gar-3(gk305)* mutant
PO1427	GTGATCGTTTGCTGGGAAGC	Forward primer for genotyping *gar-3(gk305)* mutant

PO1428	CGAAGCTCAGAATGTCAGTAACG	Reverse primer for genotyping *gar-3(gk305)* mutant
PO1435	CAAGGATACAGAGTACACGGCA	Forward primer for genotyping *ace-3(dc2)* mutant
PO1436	CAAGCCCGCAAATTGAACTGA	Reverse primer for genotyping *ace-3(dc2)* mutant
PO1437	GCAAGTGGCAAGCGAGAATA	Reverse primer for genotyping *ace-3(dc2)* mutant
M13F-20	GTAAAACGACGGCCAGT	Standard sequencing primer to sequence inserts
M13R -27	AACAGCTATGACCATG	Standard sequencing primer to sequence inserts

7.9 Appendix I: List of Strains

Table XIV: List of Strains

Strain	Genotype	Description	Chapter
OK0499	*ceh-28(cu11)* X	Strain carrying a mutation in *ceh-28*. Homozygous viable deletion length 1266 bp.	4
OK0793	*unc-119(ed3); cuIs30[ser7b::3XFLAG::PABP]*	*unc-119(ed3)* worms carrying *ser-7b* (pOK271.13) promoter driving expression of FLAG tagged PolyA Binding Protein (PABP) obtained by micro particle bombardment).	5
OK0828	*ceh-28(cu11); cuIs30[ser7b::3XFLAG::PABP]*	Strain obtained by crossing OK0499 carrying *ceh-28(cu11)* with *cuIs30[ser7b::3XFLAG::PABP]*	5
OK0988	*cuEx794*	Extrachromosomal array containing 15 ng/µl of pOK295.01 [*eat-5::GFP*] and 100ng/ul of pRF4.	Appendix D
OK0990	*cuEx796*	Extrachromosomal array containing 15 ng/µl of pOK295.01 [*inx-3::GFP*] and 100ng/ul of pRF4.	Appendix D
OK0991	*cuIs32*	Integrated strain expressing *ser-7b::GCaMP3* (pOK290.02). Integrated by UV/TMP irradiation of *cuEx791*. Outcrossed four times. GCaMP3 fluorescence is very weak at 16'C. To detect GCaMP3 fluorescence passage at 25'C.	4
OK0996	*cuEx804*	Extrachromosomal array containing 20 ng/µl of pOK294.04 [*Pmyo-2::GCaMP3*] and 100ng/ul of pRF4.	3
OK1020	*cuIs36*	Integrated strain expressing *myo-2::GCaMP3* (pOK294.04). Integrated by UV/TMP irradiation of *cuEx804*. Grow at 16°C. Outcrossed two times.	3, 4
OK1022	*ceh-28(cu11)* X; *cuIs32*	Strain obtained from cross of OK0499 carrying *ceh-28(cu11)* and OK1022 carrying *cuIs32*.	4
OK1059	*ceh-28(cu11)* X; cuIs36	Strain obtained from cross of OK0499 carrying *ceh-28(cu11)* and OK1020 carrying *cuIs36*.	4
OK1062	*gar-3(gk305)* V; *cuIs36*	Strain obtained from cross of VC657 carrying *gar-3(gk305)* and OK1020 carrying *cuIs36*.	3
OK1063	*eat-2(ok3528)* II; cuIs36	Strain obtained from cross of OK1023 carrying *eat-2(ok3528)* and OK1020 carrying *cuIs36*.	3

OK1071	*kyIs140I; unc-2(lj1)*	Strain carries 1547 bp deletion in *unc-2* gene (two exons are deleted). It also has a GFP marker for AWC (kyIs140I). Strain was obtained from Dr. Chiou-Fen, who initially requested it from Cori Bargmann's lab	Appendix B
OK1075	*eat-2(ok3528)*; *gar-3(gk305)*; *culs36*	Strain obtained from cross of OK1064 carrying *eat-2(ok3528); gar-3(gk305)* and OK1020 carrying *culs36*.	3
OK1081	*ace-3(dc2)*; *gar-3(gk305)*	Strain obtained from cross of VC657 carrying *gar-3(gk305)* and PR1300 carrying *ace-3(dc2)*.	3
VC657	*gar-3(gk305)*	Line carrying a mutation in mAChR GAR-3. Putative null mutation. Mutation deletes 452 bp (exons 8 and 9) creating a premature stop codon before translation of the last exon. Deletion affects transmembrane domains 6 and 7.	3
VC1836	*cha-1(ok2253)*; *nT1[qIs51]*	Strain carrying a mutation in ChAT *cha-1*. Homozygous lethal deletion (1712bp, exons 2-7) chromosome, which is balanced by GFP-marked translocation. Heterozygous animals are wild type with pharyngeal GFP. They segregate wild type GFP, arrested *nT1[qIs51]* aneuploids, and GFP negative *ok2253*.	3
VC2661	*acr-10(ok3118)*	*acr-10* encodes an alpha-7-like homomer-forming subunit of the nAChR. Line carries 418 bp deletion (deletes three exons).	3
VC2820	*eat-2(ok3528)/ mT1*; *+/mT1[dpy-10(e128)]*	Homozygous lethal deletion chromosome, which is balanced by *dpy-10*-marked translocation. Heterozygous animals are wild type. They segregate as wild type, arrested mT1 aneuploids, sterile Dpys (mT1 homozygotes), and *ok3528* homozygotes (arrest as L1s).	3
DA465	*eat-2(ad465)*	Line carries a substitution in a coding exon, which results in nonsense mutation (W to amber stop).	3
DA1116	*eat-2(ad1116)*	Line carries a substitution in an intron, which results in a splice-site.	3
RB756	*gar-2(ok520)*	*gar-2* encodes a novel, seven transmembrane-domain G protein-coupled AChR. Line carries 1159 bp deletion in coding exon, UTR 5, intron (deletes three exons, ~30% of the gene).	3

RB896	*gar-1(ok755)*	*gar-1* encodes a G protein-linked mAChR. Line carries a 1264 bp deletion in coding exon, intron (deletes four exons, ~20% of the gene).	3
RB918	*acr-16(ok789)*	*acr-16* encodes a subunit of the nAChR. Line carries 1082 bp deletion (deletes five exons).	3
RB1132	*acr-14(ok1155)*	*acr-14* encodes a subunit of the nAChR. Line carrying a 965bp deletion, which removes all transmembrane domains and therefore is most likely to be a null allele. The resulting proteins truncates prematurely at amino acid 227.	3
RB2294	*acr-6(ok3117)*	*acr-6* encodes a nAChR alpha subunit, which belongs to the UNC-38 subgroup. Line carries 328bp deletion in a coding exon, intron.	3
FX863	*acr-7(tm863)*	*acr-7* encodes a subunit of the nAChR superfamily. Line carries an insertion (GCTTCAG) and 625 bp deletion (deletes four exons) in a coding exon, intron resulting in a frame shift.	3
MT1212	*egl-19(n582)*	Line carrying a loss of function mutation in L-type voltage gated calcium channel (VGCC) *egl-19*. Mutation is a substitution in coding exon 9, which results in missense mutation (change of amino acid R899H). Egg laying defective. Retains late stage eggs. Slow and Floppy; Long.	Appendix A
JER1369	*sca-1(tm5339)*	sca-1 encodes a SR Ca^{2+} ATPase homolog that is required for development and muscle function. Strain carries a 205bp deletion in intron. The strain was obtained from Dr. Richmond.	Appendix C
CX8203	*kyIs140I; egl-19(n582)*;*unc-2(lj1)*	Strain carries two mutations: 1) 1547 bp deletion in *unc-2* gene (two exons are deleted) and 2)substitution (G->A) in *egl-19* gene, which results in a missence mutation. It also has a GFP marker for AWC (kyIs140I). Strain was obtained from Dr. Chiou-Fen, who initially requested it from Cori Bargmann's lab	Appendix B
PR1300	*ace-3(dc2)*	Strain carries 581 bp deletion in *ace-3* (two exons are deleted) and *ace-4* genes. *ace-3* encodes one of four C. elegans acetylcholinesterases (AChE). Completely deficient in Class C AChE activity.	3
GC201	*ace-2(g72)*; *ace-1(p1000)*	Strain carries a substitution (W99Opal) in coding exon in *ace-1* gene resulting in nonsense mutation and a substitution (G492E) in coding	3

		exon in *ace-2* gene resulting in a missense mutation. Strain is slow moving Unc. Cannot back. Hypercontracts when you tap nose. *ace-1* encodes a class A acetylcholinesterase that functions redundantly with ACE-2. *ace-2* is an acetylcholineesterase necessary for the termination of the transmission at the cholinergic neurons. It is expressed in motoneurons.	

7.10 Appendix J: List of genes identified in RNA-seq

Table XV: Genes differentially expressed in wild-type (Tg) vs wild-type (nTg)

Gene ID	Gene Name	logFC	Expression level	FDR
WBGene00000668	*col-93*	5.54150361	8.097588998	1.86492E-27
WBGene00000714	*col-141*	6.160283463	6.707630223	9.96996E-23
WBGene00000749	*col-176*	8.188117089	9.445629055	1.24526E-20
WBGene00000720	*col-147*	4.367960957	8.606098958	1.07623E-18
WBGene00021731		7.053086377	7.138216503	2.05464E-18
WBGene00000733	*col-160*	3.649242836	9.655152881	2.3621E-18
WBGene00000675	*col-101*	6.333796671	7.390526407	1.8203E-17
WBGene00018911		5.158522455	2.291204691	1.20766E-15
WBGene00000741	*col-168*	3.35498559	8.565844683	4.94876E-14
WBGene00011533		3.432691164	6.098545467	1.03033E-13
WBGene00000740	*col-167*	2.919058203	9.527891461	1.9801E-12
WBGene00000732	*col-159*	3.083082095	5.188350541	1.62338E-11
WBGene00000669	*col-94*	2.768850038	9.142493995	2.81207E-11
WBGene00022230		3.952744704	4.563956521	4.79034E-11
WBGene00000667	*col-92*	2.745535378	9.152052612	4.90142E-11
WBGene00021222	*irld-53*	4.385164033	1.392622866	2.61949E-10
WBGene00206464		4.751787252	5.770555804	2.68065E-10
WBGene00017496	*srbc-15*	3.458614543	2.28032688	3.17095E-10
WBGene00019046		6.936337818	3.135459852	6.80293E-10
WBGene00000742	*col-169*	2.405207987	7.00921372	1.29524E-09
WBGene00013980	*dos-1*	2.5252881	3.203582844	1.80085E-09
WBGene00010528		3.883920613	4.254123836	3.76092E-09
WBGene00000728	*col-155*	2.439459395	6.881907488	4.59695E-09
WBGene00000691	*col-117*	2.43428184	11.00391595	6.06962E-09
WBGene00045276		2.590621859	3.809013045	7.23805E-09
WBGene00000743	*col-170*	2.367115648	5.55989427	7.98286E-09
WBGene00006843	*unc-119*	2.374218911	5.163486179	9.10533E-09
WBGene00022093		2.806715542	5.854429085	1.07627E-08
WBGene00020873		3.297415084	2.694699138	1.56262E-08
WBGene00020497		2.169083338	7.01285754	2.21305E-08
WBGene00007857		2.262573347	5.015629805	2.36628E-08
WBGene00017567		3.309399348	3.843263081	3.74591E-08
WBGene00018939	*fbxa-190*	3.132308098	1.824516222	8.70727E-08
WBGene00044019		2.05893722	4.495358134	1.58895E-07
WBGene00000594	*col-3*	2.090348269	10.88346938	1.59161E-07
WBGene00045275		3.170798866	3.196533052	1.80481E-07
WBGene00000671	*col-96*	3.707757279	6.783360315	1.83058E-07
WBGene00016465		3.352799075	1.492878105	3.84628E-07
WBGene00019979		2.284045123	5.0407534	4.81489E-07

WBGene00007543	*fipr-7*	3.324534947	6.876509587	7.03212E-07
WBGene00008815	*srz-103*	2.812900958	1.880341669	9.4639E-07
WBGene00022665		1.865449503	5.547865998	1.08257E-06
WBGene00017704		3.026777352	1.981367456	1.11452E-06
WBGene00021977		2.149727643	4.577599797	1.72139E-06
WBGene00000715	*col-142*	2.628687771	5.239958066	1.72139E-06
WBGene00015281		2.136067375	3.037603099	1.83811E-06
WBGene00022406	*srsx-7*	3.405882722	1.315997642	1.89081E-06
WBGene00007634		3.326909047	0.977114134	1.89716E-06
WBGene00021743		3.372423021	2.454361679	1.94962E-06
WBGene00018424		2.085569579	6.001350059	2.00715E-06
WBGene00021224	*clec-209*	2.623620944	1.581552473	2.28721E-06
WBGene00000176	*aqp-8*	1.831682078	5.512201188	2.36636E-06
WBGene00018841		2.17419975	3.338743467	2.40515E-06
WBGene00019849	*oac-40*	3.216032102	1.437630799	2.60348E-06
WBGene00014116		1.804305106	5.530780745	2.85711E-06
WBGene00015483		2.06098394	5.280577874	2.92672E-06
WBGene00012088		2.922357991	1.541772014	3.18605E-06
WBGene00006092	*str-25*	3.358220092	0.633940101	3.2709E-06
WBGene00017962	*fbxa-72*	3.424005458	1.558705625	3.95868E-06
WBGene00007856		1.874091078	5.181127929	4.27363E-06
WBGene00007591		1.857166022	5.719615828	4.65226E-06
WBGene00007939		2.530997604	1.586844923	5.77022E-06
WBGene00016283		1.829042494	3.417252895	6.59154E-06
WBGene00011847	*chil-26*	2.985708191	1.577331306	6.59154E-06
WBGene00004877	*smf-2*	2.520378481	2.220962357	7.22676E-06
WBGene00021880		2.927397352	1.0779268	7.44064E-06
WBGene00010225	*ttr-31*	2.118495269	5.803550862	7.76705E-06
WBGene00000616	*col-39*	1.859196375	6.864885966	8.12427E-06
WBGene00010216		3.132339728	3.065857742	1.02999E-05
WBGene00013381	*cyp-31A5*	2.645809422	2.085765388	1.06741E-05
WBGene00012487		1.919666572	3.835156289	1.08086E-05
WBGene00007146		2.155507308	2.817887623	1.16625E-05
WBGene00013698		1.831459707	4.475440374	1.2899E-05
WBGene00000716	*col-143*	4.341970755	1.577743051	1.5673E-05
WBGene00194839		2.885009869	1.343356332	1.61293E-05
WBGene00006261	*str-230*	2.120969991	2.976220017	1.66616E-05
WBGene00020333	*sre-12*	2.795738798	1.370725298	1.68129E-05
WBGene00002264	*lec-1*	1.934734641	4.28348801	1.7499E-05
WBGene00000539	*cln-3.1*	1.754032598	3.699007006	1.92534E-05
WBGene00000656	*col-80*	1.997546666	6.34220741	1.98268E-05
WBGene00219378		1.84088597	3.05391405	2.13116E-05
WBGene00000666	*col-91*	2.15691079	3.325490386	2.45366E-05
WBGene00000272	*bro-1*	2.675769487	1.386707025	2.4848E-05
WBGene00006226	*str-182*	2.38039452	2.698258859	2.58801E-05

WBGene00018910		2.596835655	1.844960233	2.79226E-05
WBGene00008520		1.831125718	3.307296825	2.8118E-05
WBGene00005730	*srv-19*	2.869061155	1.230184927	3.02793E-05
WBGene00005091	*srd-13*	3.467968832	0.24138374	3.11335E-05
WBGene00010563		1.818039339	3.532267238	3.17854E-05
WBGene00017540		2.957164017	0.736731005	3.2271E-05
WBGene00009238		7.492502067	-0.72899213	3.43207E-05
WBGene00000058	*acr-19*	1.643818978	4.274482792	3.47633E-05
WBGene00020680		2.756665106	0.897247983	3.58917E-05
WBGene00020416		2.1858885	1.853472079	3.61421E-05
WBGene00008982	*srsx-2*	7.588200427	-0.672521972	3.63784E-05
WBGene00018682	*aagr-4*	1.908472504	4.833144245	3.65502E-05
WBGene00206378		2.640740118	1.50465218	3.6762E-05
WBGene00005614	*srj-26*	2.404145178	1.503089163	3.68571E-05
WBGene00021498		2.187183146	2.894588599	3.75331E-05
WBGene00014190	*irld-62*	2.72352002	1.075189882	4.08688E-05
WBGene00005070	*srb-5*	2.083488878	2.764102037	4.69782E-05
WBGene00018018		1.65830579	5.254882876	4.94487E-05
WBGene00007081		1.92877453	2.643754451	5.27147E-05
WBGene00014050		2.977518703	1.172887646	5.27854E-05
WBGene00006081	*str-13*	2.239382462	2.329461676	5.44397E-05
WBGene00043069		1.935771541	2.379317773	5.59163E-05
WBGene00004953	*spd-2*	1.754997796	3.047195713	5.83206E-05
WBGene00016437		1.930944632	2.975189404	5.94563E-05
WBGene00009345		2.639864049	1.235565199	5.99083E-05
WBGene00006200	*str-154*	2.542684876	1.050866148	6.03911E-05
WBGene00018915	*str-267*	2.597702434	1.288177317	6.26038E-05
WBGene00018380	*decr-1.1*	2.460434467	1.401390753	6.75082E-05
WBGene00001843	*hgo-1*	1.5836423	5.569758037	7.16742E-05
WBGene00077783		2.161895913	1.685347943	7.30225E-05
WBGene00016252		2.218219621	1.810299215	7.6697E-05
WBGene00013986		2.659783263	1.888091771	7.71415E-05
WBGene00008152		1.838729598	3.258392683	7.91436E-05
WBGene00011079		2.195148942	2.558837562	8.03951E-05
WBGene00018559	*srt-37*	2.561601384	1.259688382	8.17414E-05
WBGene00020144		2.347407644	1.575027948	8.20598E-05
WBGene00007818		2.464791583	6.156155755	8.55514E-05
WBGene00005334	*srh-115*	3.283665745	0.785751274	8.73517E-05
WBGene00013300	*lgc-7*	2.665010305	1.157235899	8.80685E-05
WBGene00022806		2.222165576	2.561097356	9.55829E-05
WBGene00023508	*srz-38*	1.879062461	2.73660832	9.56778E-05
WBGene00010915		2.315200076	2.666329938	9.7483E-05
WBGene00015836	*math-7*	2.541923581	1.617405053	0.000100869
WBGene00004157	*pqn-75*	1.709047771	5.799752277	0.00010528
WBGene00022292		2.337706843	1.545281802	0.000107995

WBGene00013074	*hmit-1.2*	1.603849979	3.449766205	0.000112602
WBGene00022245	*acp-6*	1.674998437	7.040678856	0.000112765
WBGene00003981	*pes-8*	1.737387479	3.847606572	0.000113821
WBGene00011177		3.64880928	0.044050488	0.000116265
WBGene00009385	*sas-5*	1.724692054	3.224946135	0.000121731
WBGene00014953		2.404145178	1.432188664	0.000122341
WBGene00005699	*sru-36*	2.405827459	1.712818864	0.000131507
WBGene00021978		1.870734155	2.732229961	0.000132806
WBGene00006256	*str-225*	2.365783859	2.062318785	0.000140664
WBGene00044035		1.446923529	4.165790698	0.00014171
WBGene00009386	*tag-290*	1.757340212	3.471195865	0.00014171
WBGene00015960	*srbc-9*	2.646772732	1.209870039	0.000147401
WBGene00017439		1.697555591	3.007758907	0.000152541
WBGene00011739		2.312741595	2.736330554	0.000153784
WBGene00005986	*srx-95*	2.469637605	1.223668918	0.00016288
WBGene00010206		3.049074233	0.936232689	0.000163462
WBGene00021403		2.011727154	2.512975593	0.000169657
WBGene00004010	*pha-1*	2.023010287	1.829707607	0.000172481
WBGene00006093	*str-27*	2.422420966	1.467939841	0.00017693
WBGene00005439	*srh-231*	3.248112921	0.725873374	0.000182381
WBGene00017333	*ugt-38*	3.693056396	0.085372093	0.000184577
WBGene00007450		1.716011216	4.086690321	0.000186999
WBGene00017957		2.361230473	1.564537213	0.000188455
WBGene00005700	*sru-37*	2.328634975	1.379260457	0.000196852
WBGene00006124	*str-60*	2.917940107	0.807764754	0.000197766
WBGene00003987	*pes-23*	2.257427439	1.617986643	0.000214217
WBGene00018590	*nlp-37*	1.552314308	6.020478752	0.000227853
WBGene00009479	*fcp-1*	1.397914932	6.916831219	0.00024636
WBGene00020605	*lgc-50*	1.698486306	3.724415126	0.000247088
WBGene00005941	*srx-50*	2.516407154	1.343280088	0.000249369
WBGene00018393	*msra-1*	1.79428661	2.456115971	0.000252756
WBGene00195164		2.152637113	1.922114723	0.0002535
WBGene00016435		1.602279384	8.871145074	0.000261161
WBGene00009199		4.511326215	-0.855058678	0.000263912
WBGene00006244	*str-211*	6.960049786	-1.160324678	0.000273075
WBGene00022782		1.536149588	7.053727451	0.000273641
WBGene00005476	*srh-270*	2.565717857	1.536314564	0.000280145
WBGene00009608	*nhr-265*	4.75312664	-0.734901729	0.000283099
WBGene00015720		2.107489673	2.284365501	0.000297928
WBGene00020138		2.258454446	1.202947466	0.000297928
WBGene00015904	*irld-22*	2.813435078	0.871109942	0.000297928
WBGene00194699		1.872553159	3.946372135	0.000304423
WBGene00000372	*cyp-13A7*	3.099935388	3.540421576	0.000306552
WBGene00006127	*str-64*	1.709740235	3.521704485	0.000314462
WBGene00017277		2.370066975	1.336574315	0.000328323

WBGene00012406	*srz-91*	1.884509032	2.789979758	0.000332129
WBGene00010967		1.613271222	7.122626298	0.000336178
WBGene00000717	*col-144*	1.409270254	9.305441845	0.00033995
WBGene00008251	*srsx-30*	2.204069697	1.348394507	0.000344629
WBGene00020434		2.417696688	1.796375281	0.00035369
WBGene00009992		1.466967892	5.566167862	0.000380899
WBGene00000785	*cpr-5*	1.575918054	6.515052176	0.000385117
WBGene00001429	*fkb-4*	1.843153358	3.957189064	0.000393732
WBGene00006271	*str-244*	2.532055678	1.120724566	0.000404803
WBGene00005411	*srh-200*	2.504155897	0.976227291	0.000410553
WBGene00016281		1.681727009	5.0525292	0.000412791
WBGene00008707		1.365318071	6.507098565	0.000412832
WBGene00007430		1.76004814	2.468494764	0.000426475
WBGene00002074	*ima-3*	1.534617807	6.193444676	0.000426475
WBGene00013263		1.486596638	6.734009978	0.000436849
WBGene00009475		1.395345212	5.031004973	0.000449131
WBGene00005337	*srh-118*	2.308410819	1.439032031	0.000463525
WBGene00011100	*nhr-209*	1.923950295	1.861583416	0.000464275
WBGene00017211	*fbxb-36*	1.561852343	3.5639323	0.000468954
WBGene00013122		2.109773437	1.658622299	0.000470076
WBGene00044174	*fipr-5*	3.117423493	2.457763776	0.000470328
WBGene00005533	*sri-21*	2.926913251	0.593971934	0.000491083
WBGene00006626	*tsn-1*	1.565406363	6.48097327	0.000513719
WBGene00000739	*col-166*	1.33992189	9.03168728	0.000529879
WBGene00011336	*ubxn-5*	2.200355272	1.292371151	0.00053374
WBGene00019405		1.652948869	3.422105361	0.000534687
WBGene00006012	*srx-121*	2.00434696	2.212087444	0.000539158
WBGene00004044	*plk-3*	1.507850125	3.009790935	0.000557128
WBGene00010706	*cyp-14A2*	1.963318689	2.201293083	0.000566378
WBGene00012083		2.161757079	2.341715255	0.000577264
WBGene00015706		1.966991962	2.917877725	0.000583627
WBGene00009569	*srz-66*	2.161337253	1.341725983	0.000588869
WBGene00000681	*col-107*	1.803059372	8.093932102	0.000592361
WBGene00016733	*phat-2*	4.365863587	2.204739517	0.000601503
WBGene00219315		3.246315613	0.014809981	0.000621092
WBGene00005035	*sra-9*	1.928756756	2.618164053	0.00065183
WBGene00019933		2.601407283	1.316494185	0.000685909
WBGene00017257		3.313050271	-0.233885567	0.000692837
WBGene00010814		1.67183255	2.54883215	0.000698004
WBGene00194654		1.831956859	3.265201408	0.000698004
WBGene00005610	*srj-22*	1.649974221	3.933746669	0.000700674
WBGene00011147		1.648251645	2.49476766	0.000707251
WBGene00022264	*sdz-34*	2.014567234	2.958314431	0.000707251
WBGene00020881		2.10248799	2.783666389	0.000710662
WBGene00014067		1.969618631	3.140223935	0.000724477

WBGene00004097	*pqm-96*	1.956276295	2.626512305	0.000725909
WBGene00005399	*srh-184*	2.40882992	1.34277969	0.000745518
WBGene00008056	*nhr-164*	2.382281735	0.61024808	0.000751153
WBGene00017602	*clec-211*	2.315031137	0.965883607	0.00075265
WBGene00015309		1.769692655	2.243054206	0.000755608
WBGene00009346		1.431678511	3.375780047	0.000762174
WBGene00000718	*col-145*	3.121516719	4.069823969	0.000808206
WBGene00009342	*fasn-1*	1.391062039	6.366394123	0.000820712
WBGene00005089	*srd-11*	2.822006374	0.428805953	0.000829863
WBGene00206417		3.804814992	0.136755681	0.000839365
WBGene00022608	*madf-9*	1.575244754	3.212411143	0.000840237
WBGene00016253		2.092117172	1.776766481	0.000853889
WBGene00000512	*ckb-2*	1.703955198	5.908330296	0.000858012
WBGene00007402	*ugt-60*	1.37443767	3.62941316	0.00087159
WBGene00000407	*cdk-5*	1.344576606	4.013863102	0.000871629
WBGene00008908		4.702786659	-0.744619121	0.000872517
WBGene00005339	*srh-120*	1.589149616	2.636999326	0.000874543
WBGene00045336		1.283689318	4.288210891	0.00087927
WBGene00020076		2.568210718	1.040449532	0.000883493
WBGene00044081		2.692752349	1.116579308	0.000909458
WBGene00007755		1.781105781	2.74099876	0.000914398
WBGene00015380		3.022122173	-0.176068732	0.000914398
WBGene00044551		3.022122173	-0.140187401	0.000914398
WBGene00007827		1.81073467	7.214438376	0.000920417
WBGene00015371		2.259941521	1.170178761	0.000921153
WBGene00015799		1.647631525	2.728671722	0.000958169
WBGene00011358	*lgc-16*	2.38054881	0.815834849	0.000966801
WBGene00015206		1.818225017	2.819349042	0.000987656
WBGene00019387		2.697595658	0.568998341	0.000998996
WBGene00011882	*nstp-9*	2.88835448	0.277702008	0.001001197
WBGene00012510		2.854308672	0.530251194	0.001012278
WBGene00007473	*chil-8*	1.929011718	1.670896719	0.001038036
WBGene00007308		6.76905912	-1.409508534	0.001074091
WBGene00000140	*anc-1*	1.531376068	10.51174148	0.001081462
WBGene00005363	*srh-147*	1.851448597	2.266008677	0.00108176
WBGene00007100		1.65397393	2.367337449	0.001086349
WBGene00007541	*fipr-4*	1.755980095	8.144609573	0.001086829
WBGene00007544	*fipr-6*	1.957996108	6.839740868	0.001091774
WBGene00021233		2.078713303	1.821035269	0.001092206
WBGene00006190	*str-143*	1.978311574	2.055123375	0.001093499
WBGene00011531	*rsbp-1*	1.27732547	7.561167613	0.00110152
WBGene00005612	*srj-24*	3.63028512	-0.372899229	0.001103136
WBGene00005682	*sru-19*	2.241120785	0.847832805	0.001106744
WBGene00013837	*fbxa-30*	1.956458588	1.696137538	0.001111843
WBGene00007646	*nkb-1*	1.3568646	7.219729822	0.001112773

WBGene00011744		2.322160366	1.375065465	0.00113422
WBGene00220257		1.754138212	2.521758603	0.001139297
WBGene00009494	*hrg-5*	2.837498595	0.154708611	0.001144035
WBGene00000476	*cfi-1*	1.503934707	3.557443929	0.001147605
WBGene00019566		2.102393872	0.951525247	0.001153395
WBGene00009524		1.955736223	1.100237064	0.00115405
WBGene00008723		1.848321362	2.307572749	0.001167245
WBGene00018969		1.467992851	5.291603366	0.001201766
WBGene00005955	*srx-64*	1.840718195	1.977326712	0.001225452
WBGene00020129		2.136640796	1.164537408	0.001226367
WBGene00003633	*nhr-43*	1.247105836	4.194274129	0.001245787
WBGene00017381	*ddr-2*	1.653488578	3.759205741	0.00125419
WBGene00009334		1.298213607	5.167568371	0.001256653
WBGene00044707		1.669715066	2.6313038	0.001275668
WBGene00019251		2.132550823	1.642915142	0.001334744
WBGene00010536		2.078176895	1.551505611	0.001336169
WBGene00005871	*srw-124*	1.758896718	2.746398185	0.001336431
WBGene00020675		2.1124169	1.939039866	0.001338988
WBGene00005711	*sru-48*	2.001305143	2.023042529	0.001343113
WBGene00003727	*nhr-137*	1.209924734	4.642883672	0.001345664
WBGene00001780	*gst-32*	1.92910878	1.605309298	0.001354778
WBGene00012162		1.480888054	3.696895257	0.001368677
WBGene00020608	*srab-22*	3.139950933	0.281697187	0.001369027
WBGene00015359		1.822826774	1.437830696	0.001370333
WBGene00018556	*srt-36*	2.141095565	1.37868505	0.00137348
WBGene00010129		2.882669369	0.135933008	0.001384451
WBGene00015708		2.337288643	0.846233489	0.001394206
WBGene00005148	*srd-71*	1.581532672	2.815031833	0.001418142
WBGene00008659	*clec-151*	1.987819126	2.278276675	0.00142272
WBGene00020696		1.323431473	7.338132532	0.001427428
WBGene00022674		1.706915763	2.589698836	0.001440914
WBGene00018398	*sptl-2*	1.228318562	4.817862773	0.001454568
WBGene00005364	*srh-148*	2.709635235	0.065171942	0.001464639
WBGene00003663	*nhr-73*	3.831452444	0.179231323	0.001485036
WBGene00005056	*sra-30*	2.197618227	0.886075263	0.001509847
WBGene00005072	*srb-7*	1.762375711	2.367861483	0.001515883
WBGene00020869		1.519709712	6.505436349	0.001516711
WBGene00022235	*sqd-1*	1.45923091	8.054827679	0.001558494
WBGene00013909	*srbc-44*	2.438916695	0.75298072	0.001572966
WBGene00015514		1.333058972	8.086558175	0.001586144
WBGene00012143		1.219006852	4.672577168	0.001590005
WBGene00000263		1.375698958	8.186156138	0.001599123
WBGene00043986	*fut-5*	2.113035351	1.185191779	0.001599123
WBGene00013716		1.335417493	4.956944873	0.001610023
WBGene00022029		2.343623807	1.54481618	0.001630141

WBGene00021319		1.197841147	4.797759234	0.001632953
WBGene00019372		1.764899941	2.139343442	0.001653822
WBGene00005475	*srh-269*	2.492724786	0.501845886	0.001653822
WBGene00005410	*srh-199*	2.942754854	-0.024351835	0.00166357
WBGene00005281	*srh-59*	2.136640796	1.247457047	0.001666599
WBGene00017141		2.127441587	1.427618666	0.001677965
WBGene00005254	*srh-31*	2.144360582	1.523386411	0.001708553
WBGene00022417		1.488353028	3.542451654	0.001727734
WBGene00019732		1.358495333	4.969217622	0.001744844
WBGene00021958		2.409304088	1.021751313	0.001755154
WBGene00010103		2.726251759	-0.009561687	0.001777534
WBGene00005356	*srh-139*	2.070902967	1.566244832	0.001784744
WBGene00019483		2.219210795	1.059547944	0.001785657
WBGene00007076		2.532010029	-0.070614979	0.001796933
WBGene00005716	*srv-5*	1.571275526	3.007512486	0.001838558
WBGene00015272		2.084018277	0.616771407	0.001843245
WBGene00009756		1.904882029	1.829963027	0.001878173
WBGene00022886		2.221667182	0.807955609	0.001885989
WBGene00010901		1.357378854	4.497204648	0.001913597
WBGene00009877		1.464664472	3.958789766	0.001915861
WBGene00010386		1.381824067	3.787531884	0.001927889
WBGene00015224		2.401766688	0.44606758	0.001938351
WBGene00001925	*his-51*	2.822006374	0.495176638	0.001984005
WBGene00005094	*srd-16*	3.076566732	0.257844377	0.001987574
WBGene00020947		1.73614972	4.402163331	0.002005938
WBGene00206486		2.135610269	1.760648031	0.002011005
WBGene00019222		2.287895609	0.506953709	0.002011005
WBGene00044131		1.911430422	1.068213623	0.002035849
WBGene00006308	*sul-1*	1.541292981	3.108161314	0.002048513
WBGene00022312	*clec-171*	2.359257779	0.556429052	0.002056875
WBGene00045056		1.493122632	2.394181168	0.002097621
WBGene00000727	*col-154*	1.279616918	5.431672296	0.002110814
WBGene00006209	*str-164*	2.037573484	0.935255085	0.002110963
WBGene00001927	*his-53*	3.269559741	-0.566839461	0.002125622
WBGene00012409		1.732713865	1.874704572	0.002131072
WBGene00043156		1.411880999	3.628732605	0.002143248
WBGene00002055	*ifc-1*	1.218381518	6.958999282	0.002143248
WBGene00003732	*nhx-4*	1.209669291	4.380216262	0.002143248
WBGene00012147		1.950178476	1.352813984	0.002144885
WBGene00018821		2.78218489	0.882567012	0.002166525
WBGene00002127	*inx-5*	1.442813213	5.292155906	0.002234338
WBGene00005669	*sru-6*	1.692958862	1.955963137	0.002234338
WBGene00011151		2.400268319	0.769560198	0.002247617
WBGene00015012	*bath-20*	1.69044983	1.714182061	0.002250573
WBGene00020139		1.353277255	5.200723785	0.002321867

WBGene00005762	*srw-15*	1.914475589	1.330128662	0.002324962
WBGene00009123		1.365911429	3.014584927	0.002339544
WBGene00007753		1.188625478	4.515855462	0.002372889
WBGene00005618	*srj-33*	2.439604759	1.030269036	0.00238043
WBGene00012177	*decr-1.2*	3.526931362	-0.470556235	0.00239851
WBGene00020120		1.307216233	4.092497225	0.002437385
WBGene00011108		1.165953857	4.173377488	0.00246983
WBGene00020666		3.243715358	-0.641957534	0.002470368
WBGene00006774	*unc-38*	1.387244451	3.236250415	0.002470986
WBGene00000599	*col-10*	1.228182516	9.54708327	0.002505352
WBGene00019537		1.320959617	8.071738434	0.00250913
WBGene00044422		2.12067522	1.541888088	0.00250938
WBGene00015665		1.935071642	1.533173131	0.002510842
WBGene00001568	*gei-11*	1.164794948	4.644512857	0.002562161
WBGene00003870	*ooc-5*	1.319812933	3.682694636	0.00256741
WBGene00020747		1.530122639	2.361491999	0.002639928
WBGene00015761		2.287633986	0.489024904	0.002639928
WBGene00011721		1.893319967	1.006917709	0.002649327
WBGene00195211		3.194930421	-0.379443417	0.002681665
WBGene00009341	*thoc-3*	1.233618056	3.656693178	0.002693183
WBGene00009097	*fipr-2*	1.190033433	7.814977756	0.002725776
WBGene00005665	*sru-2*	1.979596585	0.872075322	0.002730765
WBGene00009637	*nspc-13*	2.709205128	0.387416287	0.002733897
WBGene00003551	*nas-33*	1.836691101	1.659476384	0.002769993
WBGene00022511		1.885463416	2.692626186	0.002780472
WBGene00006525	*tax-2*	1.368122107	5.114898592	0.002780472
WBGene00017149		1.179246161	4.822934568	0.002783512
WBGene00006925	*vit-1*	1.471001979	2.39692126	0.002794426
WBGene00000772	*cpb-3*	1.578860142	2.768614324	0.002801405
WBGene00022291		3.762905973	-0.758829673	0.002809694
WBGene00009478	*syx-7*	1.576106812	2.258424218	0.002816039
WBGene00007456	*srz-29*	3.55602323	-0.17616634	0.002816269
WBGene00018404	*nhr-39*	2.038618336	0.765401965	0.00281725
WBGene00006144	*str-85*	2.550278073	1.202969516	0.002853314
WBGene00009938		1.497792807	3.265370409	0.002868501
WBGene00005629	*srj-50*	1.938176841	1.014551286	0.002903545
WBGene00020449	*fbxa-54*	1.288457983	3.859937719	0.002923804
WBGene00005849	*srw-102*	1.995884276	1.09637928	0.002934602
WBGene00009707	*srxa-16*	2.099092327	0.725433725	0.002956232
WBGene00022723		1.594649367	3.692755384	0.002960048
WBGene00021327	*mrpl-38*	1.333053311	9.327282163	0.002973217
WBGene00005119	*srd-41*	1.463139871	3.274484974	0.002973217
WBGene00012428		1.432972396	3.365906495	0.003061403
WBGene00009384		1.384035938	3.958601722	0.003078219
WBGene00020015	*nhr-210*	1.576568108	1.737985211	0.003079191

WBGene00009493	*hrg-4*	1.608769704	2.193576864	0.003090538
WBGene00003495	*mup-2*	1.564493551	8.544245323	0.003107173
WBGene00017869		2.125705824	1.673890734	0.003170793
WBGene00021572	*srd-72*	1.409594659	2.956227863	0.003201756
WBGene00009518	*clec-166*	1.303793596	6.431163599	0.003250164
WBGene00011668	*clec-47*	2.16335212	2.488045196	0.00325022
WBGene00015731		1.803250914	0.937396758	0.003286579
WBGene00016535		1.263403555	5.355453193	0.003309229
WBGene00010694		1.458990096	2.689261518	0.003331697
WBGene00009158		1.295810778	5.709951145	0.003332981
WBGene00010740		1.219746536	5.559524449	0.003337647
WBGene00001884	*his-10*	3.339101663	0.13085812	0.003395257
WBGene00044305	*rad-8*	1.263286992	3.556824669	0.00344206
WBGene00002348	*myo-1*	1.152618706	9.236592336	0.003459532
WBGene00007841		1.116402384	4.396447117	0.00350133
WBGene00005639	*srm-2*	1.723027994	1.828977235	0.00350133
WBGene00011486		1.817640728	1.867949164	0.003516989
WBGene00005219	*srg-62*	1.945098751	1.639880419	0.003557905
WBGene00005441	*srh-234*	2.119986911	0.406087252	0.003561651
WBGene00008961		1.84209185	1.489767062	0.003573255
WBGene00018021		1.459838897	2.665120085	0.003574367
WBGene00005323	*srh-104*	1.659076003	1.618554531	0.003602623
WBGene00010886		6.595678206	-1.615634312	0.003620794
WBGene00003093	*lys-4*	1.327327638	4.669372275	0.003714593
WBGene00011474	*aldo-1*	1.186999276	7.828172864	0.00371549
WBGene00008518	*irld-2*	1.791126822	1.611596402	0.003720276
WBGene00008780		1.15185548	5.384085917	0.003774409
WBGene00194706		1.172907973	4.022939382	0.003811114
WBGene00005053	*sra-27*	4.069958194	-1.263074203	0.003864916
WBGene00008973		1.207832309	5.791686357	0.003870785
WBGene00007290		1.600778071	2.011324289	0.00387968
WBGene00077756		2.126609492	1.488956017	0.003957839
WBGene00018219		1.231531011	3.607915397	0.003972133
WBGene00017564	*srxa-4*	2.371126096	0.397449751	0.00397605
WBGene00020383		1.172488165	5.813344949	0.004008929
WBGene00019296	*mcu-1*	1.231843095	3.547093783	0.004032025
WBGene00015763		6.344787393	-1.760650953	0.004061558
WBGene00019036	*irld-36*	2.106223768	0.382914874	0.004135819
WBGene00008867		1.712843425	1.772599558	0.004159749
WBGene00019214		1.580078619	2.390282393	0.004212435
WBGene00044088	*oac-2*	3.294949284	-0.692894219	0.004229082
WBGene00018501		2.041631182	0.944131282	0.00431254
WBGene00011290		1.592400382	2.358224081	0.004330376
WBGene00013699		1.364837925	3.462155672	0.004392533
WBGene00002050	*ifa-1*	1.311084012	6.514703333	0.004392533

WBGene00020533		3.243715358	-0.72254958	0.004410895
WBGene00008333		1.464951265	1.99326689	0.004418443
WBGene00015737	*srsx-12*	1.762211451	2.257367534	0.004430099
WBGene00020024		2.120307603	0.78962786	0.004442586
WBGene00219544		2.287895609	0.493878692	0.004489129
WBGene00017975		1.464685182	3.161127888	0.004525832
WBGene00021492	*comt-5*	1.46382278	2.403644444	0.004529239
WBGene00015340		3.875819702	6.859229653	0.004529393
WBGene00005508	*srh-304*	2.3715717	0.107590824	0.004552307
WBGene00017337		1.91659907	1.445876135	0.004558449
WBGene00006748	*unc-8*	1.496311018	2.449061705	0.004597729
WBGene00020804		1.836545672	1.390511514	0.004600332
WBGene00020169	*mmaa-1*	1.212820651	4.081489517	0.004602602
WBGene00000083	*adt-2*	1.149463388	5.924522783	0.004607539
WBGene00016479	*srab-6*	4.596509456	-0.924295689	0.004609255
WBGene00016317		1.200742955	4.810759774	0.00467732
WBGene00011098	*nhr-207*	1.564987207	1.976734702	0.004710601
WBGene00017355		1.155987313	5.076058561	0.004757165
WBGene00006897	*ver-4*	1.428244452	3.02362694	0.004757403
WBGene00013207		1.635891844	1.844813749	0.004765205
WBGene00219325		2.639821076	-0.456579455	0.004811962
WBGene00006111	*str-46*	1.800984223	1.067154444	0.004858576
WBGene00011157	*chil-15*	1.910655583	0.955912836	0.00489861
WBGene00005352	*srh-135*	1.650515493	2.462381233	0.005015475
WBGene00017404		2.387999016	0.099636318	0.005044265
WBGene00015765		2.758921446	-0.021028543	0.005046481
WBGene00020398		1.343931777	5.32545811	0.005106423
WBGene00206479		1.432257211	2.675479509	0.005134802
WBGene00012312		2.343729869	0.298387747	0.005134802
WBGene00005992	*srx-101*	2.288771564	0.874333209	0.00525141
WBGene00018615		1.425632911	2.034148166	0.005264583
WBGene00138718		2.343797777	-0.076414426	0.005289651
WBGene00004300	*ram-2*	1.641351579	8.847814715	0.005341866
WBGene00189955		2.1983554	0.218027711	0.005365929
WBGene00019930	*fbxc-35*	2.313788516	0.431774192	0.005372519
WBGene00010715		1.902403612	0.96201962	0.00542122
WBGene00044175	*fipr-9*	1.904123039	3.685350174	0.005480019
WBGene00007255		1.383845935	2.766072433	0.005511107
WBGene00005823	*srw-76*	1.780785185	2.015952519	0.005517276
WBGene00016223		3.469403599	-0.940080549	0.005559299
WBGene00013908	*srbc-43*	1.935939545	1.32813383	0.005561582
WBGene00005116	*srd-38*	1.812225489	2.056214539	0.00556915
WBGene00014195	*srz-10*	2.021219912	1.299514338	0.005647182
WBGene00019326		1.130392675	4.578350487	0.005749414
WBGene00012846	*srxa-14*	2.301634663	0.271118629	0.005768057

WBGene00010705	*cyp-14A1*	1.359537445	2.802384461	0.005866022
WBGene00005543	*sri-31*	1.695960062	1.656692321	0.005936605
WBGene00022616	*hsd-3*	2.276744645	0.537870075	0.005970921
WBGene00006286	*str-260*	1.37985108	3.328425188	0.006008265
WBGene00009983	*cut-2*	3.987730037	7.827287764	0.006052293
WBGene00015802	*flu-2*	1.101797271	4.975598177	0.006138925
WBGene00003530	*nas-11*	1.05720526	5.656033104	0.006290086
WBGene00008589		1.120791216	4.480787854	0.006306062
WBGene00006205	*str-160*	1.590485987	2.102555051	0.006361711
WBGene00016832	*sre-49*	1.41011781	2.813917767	0.006363704
WBGene00050880		1.623606357	1.611812326	0.006461719
WBGene00008281		1.270388566	3.007149538	0.006545024
WBGene00021755	*hpo-38*	1.278410152	2.533597506	0.006545024
WBGene00022601		1.52300867	1.530684642	0.006569169
WBGene00016412	*mrps-26*	1.087109685	5.293879645	0.006585946
WBGene00015391	*sdha-1*	1.078704539	7.794161187	0.006606514
WBGene00001538	*gcy-12*	1.052096912	5.928632626	0.006612199
WBGene00009343		1.20015496	3.584454372	0.006677792
WBGene00022694		1.280467056	3.565487301	0.006703233
WBGene00016261		1.06140619	3.908764185	0.006708722
WBGene00000602	*col-13*	1.956181232	1.401711104	0.006808069
WBGene00005965	*srx-74*	1.49441986	2.094864635	0.006864484
WBGene00020308		2.465756588	0.793118743	0.006900423
WBGene00000998	*dig-1*	1.257088093	8.818302169	0.006924069
WBGene00077751	*irld-27*	1.876638827	1.927042749	0.007040778
WBGene00005064	*sra-38*	3.294949284	-0.585223516	0.007090781
WBGene00009120		1.097244269	6.503477686	0.007221635
WBGene00004359	*rhr-2*	1.103059715	3.443348693	0.007235318
WBGene00044538		3.043665396	-0.507980316	0.00726086
WBGene00013720		1.314955792	3.530834407	0.00741459
WBGene00005540	*sri-28*	1.748533843	1.806156744	0.007579425
WBGene00011426		2.339477323	0.385314804	0.007594547
WBGene00016434		2.790867683	-0.046615729	0.007682203
WBGene00044423		1.653229298	1.228392993	0.007700611
WBGene00006593	*tol-1*	1.168596988	5.549292778	0.007710031
WBGene00019122		1.687835178	1.448557756	0.007718788
WBGene00005592	*srj-4*	1.337236563	3.490999845	0.007725356
WBGene00003729	*nhx-1*	1.424988028	2.508127439	0.007743972
WBGene00021577		1.518787289	2.287602519	0.007752116
WBGene00018244		2.774982988	-0.025533897	0.007768836
WBGene00016579	*sre-14*	1.377679411	2.012293899	0.007792033
WBGene00005317	*srh-98*	1.834309129	1.220379364	0.007792033
WBGene00011884	*enol-1*	1.150597132	8.535529455	0.007820493
WBGene00009620	*fip-5*	1.181373214	5.750093212	0.007843861
WBGene00010454		1.101968923	3.971302613	0.007895201

WBGene00008856		1.034055178	5.098942447	0.00794823
WBGene00018225	*nep-14*	1.371706529	2.430448165	0.007990544
WBGene00016950		3.018381362	-0.82664079	0.007993963
WBGene00044106	*srbc-84*	1.47846381	2.571324355	0.008022539
WBGene00018221		1.157467999	5.761069275	0.008061019
WBGene00013070		4.184445568	-1.314902846	0.008163979
WBGene00044708		1.520443441	1.680739633	0.008192749
WBGene00012176		1.6659654	2.184345111	0.008236908
WBGene00009934		2.228625843	0.262086505	0.008236908
WBGene00005233	*srh-7*	2.664500954	0.053262339	0.008506313
WBGene00017581		1.668914014	2.019982919	0.008522093
WBGene00077514		1.255526413	3.342835734	0.008563984
WBGene00023505	*srz-102*	1.808976166	1.351054062	0.008566282
WBGene00005698	*sru-35*	1.413295651	2.056045382	0.008626028
WBGene00011532	*chaf-1*	1.043263315	7.274109771	0.008674776
WBGene00013625	*srz-53*	1.694550901	1.455552594	0.008687151
WBGene00012242	*srt-39*	1.636327789	2.342047123	0.008996104
WBGene00009548		1.561473154	2.11502713	0.00900174
WBGene00012925	*wht-8*	1.643687873	1.716028325	0.009022394
WBGene00005168	*srg-10*	3.856302779	-1.499583151	0.009076691
WBGene00005707	*sru-44*	2.000493548	1.242965927	0.00908549
WBGene00004473	*rps-4*	1.264963982	10.464092	0.009089589
WBGene00008575	*scl-24*	1.079540265	5.50626196	0.009131398
WBGene00018811	*pmt-2*	1.146967253	6.154854891	0.009134995
WBGene00194746		1.399239453	1.94601001	0.009200171
WBGene00013749		3.135443249	-0.779248226	0.009503751
WBGene00003375	*mlp-1*	1.472105466	4.589126341	0.009536281
WBGene00044718		6.107002998	-1.955360328	0.009583919
WBGene00020302		1.489032803	1.804047686	0.009616585
WBGene00003514	*myo-2*	1.005075024	9.495357785	0.009616585
WBGene00004719	*sad-1*	1.310873634	2.97122767	0.009624009
WBGene00009190		1.099827217	4.115267557	0.009636468
WBGene00013390		1.794709926	1.611196568	0.009648926
WBGene00013396		2.120258406	0.683454635	0.009688726
WBGene00009960		2.425948417	0.391721589	0.009688726
WBGene00005889	*srw-142*	1.574968025	1.133854658	0.009688726
WBGene00017214		1.569548459	1.833839601	0.009735026
WBGene00015522		1.111967628	2.974678953	0.00981956
WBGene00018895		1.171147948	3.670190111	0.009935964
WBGene00206492		1.877233185	1.030667435	0.009935964
WBGene00007540		2.564954833	-0.542137604	0.010065573
WBGene00005067	*srb-2*	1.584643858	1.917741872	0.010102731
WBGene00011833		1.306675406	3.904480746	0.010174614
WBGene00001107	*dsl-5*	1.53252796	2.28071249	0.010202459
WBGene00009196		1.760042795	1.441474043	0.010265289

WBGene00007179		2.006020074	0.258270986	0.010300587
WBGene00001620	*glt-1*	1.039399412	6.319996014	0.010300587
WBGene00045385	*lgc-24*	1.657854996	1.536669704	0.010300587
WBGene00003511	*mxl-3*	1.024303007	5.797366845	0.010300587
WBGene00008917		1.362271284	2.640015801	0.010333571
WBGene00044676	*fbxa-42*	2.78888092	0.476275788	0.010363541
WBGene00011283		1.301209817	5.848064616	0.010389481
WBGene00010896		1.16056794	8.359575662	0.010409333
WBGene00000214	*asp-1*	1.030440542	11.48229304	0.010469547
WBGene00018533		1.039272823	5.011937076	0.010470651
WBGene00003571	*ncx-6*	1.256808381	3.700206201	0.010472515
WBGene00016928	*srb-19*	1.552334615	1.322002602	0.010472515
WBGene00020756		1.184585211	3.226263878	0.010515953
WBGene00019266		1.76902142	1.066234201	0.010525008
WBGene00022542		1.807176183	1.142531075	0.010543897
WBGene00018919		1.277651014	3.304095381	0.010577248
WBGene00007681		1.015613477	5.175194399	0.010614617
WBGene00008240		1.209153376	3.567157563	0.010614617
WBGene00001594	*glc-4*	1.046450819	4.802863346	0.010657654
WBGene00010565	*vacl-14*	1.31394322	3.583348229	0.01069985
WBGene00044754		1.328390221	5.053311945	0.010821029
WBGene00000644	*col-68*	1.804973249	1.294763103	0.010821029
WBGene00017198	*nhr-36*	1.220681804	2.968919924	0.010851851
WBGene00016682		1.285872125	3.441984245	0.010931986
WBGene00015442		1.92910878	1.323254799	0.010931986
WBGene00011220		2.487604521	-0.071203581	0.010931986
WBGene00006106	*str-41*	2.073008718	1.028903398	0.011020086
WBGene00007144		1.15507817	3.944283419	0.011046452
WBGene00006449	*tag-76*	2.39322791	-0.285571784	0.011265319
WBGene00005909	*srx-18*	1.639577928	2.011009381	0.01129131
WBGene00008977	*iglr-1*	1.297597974	2.88671804	0.011291793
WBGene00022807	*srab-25*	1.615658801	1.224905053	0.011482752
WBGene00012990	*sam-10*	1.313226658	5.902817018	0.011558842
WBGene00011742		1.030291074	5.215172729	0.011565244
WBGene00000265	*brd-1*	1.266363181	2.488156051	0.011581971
WBGene00012772	*srt-49*	2.054562127	1.1312643	0.011581971
WBGene00019382		1.783673929	2.223206532	0.011725111
WBGene00001158	*ech-9*	1.260063548	5.01078837	0.011776653
WBGene00007141	*pitr-4*	1.633490933	2.443209953	0.011776653
WBGene00015311		1.458054256	2.445150535	0.011797828
WBGene00019704	*fbxb-40*	1.604409046	1.167584079	0.011863359
WBGene00005897	*srx-6*	1.578100939	2.280590461	0.011866636
WBGene00015663		2.091843464	0.842362487	0.011873018
WBGene00010277		1.649531818	1.773844483	0.011928754
WBGene00007909		1.153037128	3.059930628	0.01200951

WBGene00044428		1.38368063	2.211588172	0.012078837
WBGene00019943		1.068749556	4.524445733	0.012181271
WBGene00018431		1.291185109	2.500627941	0.012198945
WBGene00020878		1.86125943	2.431289934	0.012204456
WBGene00014183		3.387413718	2.862551605	0.012383134
WBGene00009768		1.451910104	2.847006835	0.012383528
WBGene00007678	*srz-90*	2.120203124	0.621602129	0.012388432
WBGene00021501		2.23385799	0.318067998	0.012413927
WBGene00005860	*srw-113*	1.627564835	0.785111305	0.012515898
WBGene00007104		1.387603941	2.327486729	0.012565955
WBGene00021083		2.687145453	1.470099065	0.012621839
WBGene00003369	*mlc-1*	1.219099711	7.641054421	0.012646094
WBGene00007693		1.403891184	2.646758259	0.01266834
WBGene00044355		1.708314683	1.151379148	0.012706863
WBGene00015935		1.107152659	4.481393998	0.012716718
WBGene00001702	*grd-13*	1.543935331	5.439362585	0.012734419
WBGene00006677	*twk-24*	1.083179482	5.557049119	0.012734419
WBGene00006737	*ulp-2*	0.961039776	4.34130289	0.012752063
WBGene00009906	*clec-241*	3.294949284	-0.708763532	0.012801568
WBGene00012381		1.122459951	5.350111971	0.012900173
WBGene00022263		1.407730013	1.874986271	0.012935624
WBGene00001569	*gei-12*	1.359026366	2.269280579	0.012935743
WBGene00007859	*mrps-31*	1.328156904	3.335281833	0.012935743
WBGene00001900	*his-26*	2.176316168	1.166691088	0.012941053
WBGene00019393	*irld-45*	1.472984222	2.535459003	0.012941053
WBGene00020914	*sulp-6*	1.888013872	0.724258816	0.013042951
WBGene00014144		1.36738946	2.511528166	0.013100001
WBGene00003058	*lov-1*	1.305758532	2.903492902	0.013127968
WBGene00006592	*dpy-31*	0.945858229	5.963714393	0.013357386
WBGene00017307		2.897368519	3.548709924	0.013390887
WBGene00008969		1.217011092	4.525851747	0.013408458
WBGene00006759	*unc-22*	1.129725942	8.787676236	0.013413769
WBGene00009483		1.003021303	4.322571293	0.013421953
WBGene00020440		2.848818067	-0.626567417	0.013432764
WBGene00018994		1.388522667	2.843513386	0.013450335
WBGene00018379		1.590178422	2.104343205	0.013499456
WBGene00007773		1.377706249	3.648999984	0.013511441
WBGene00008642		1.160533318	3.278690583	0.013519579
WBGene00019361		1.043433462	5.205451343	0.013580318
WBGene00011736		0.982821206	8.255910868	0.013633665
WBGene00008772	*irld-4*	2.795697482	-0.715380163	0.013684508
WBGene00008097	*ugt-15*	1.184865375	4.26520946	0.01372114
WBGene00195210		1.501258519	1.42914353	0.013737375
WBGene00013853		1.031787968	6.738306484	0.01378466
WBGene00017228		1.354287431	1.976254067	0.013801058

WBGene00021708	*srbc-37*	1.619577419	1.586468945	0.013801058
WBGene00003161	*mdf-2*	1.096848167	3.674017673	0.014112733
WBGene00021574		1.874419879	0.385209549	0.014117802
WBGene00018648		1.382695646	2.690197284	0.014150959
WBGene00018917	*irld-35*	1.427488494	2.119355344	0.014156679
WBGene00009242	*sre-6*	1.296441682	2.853211627	0.014156679
WBGene00009119	*ndk-1*	1.166041329	10.22215589	0.014310189
WBGene00011622		1.747939321	1.594389635	0.014334323
WBGene00020686		2.360556025	0.610809866	0.014334323
WBGene00005280	*srh-57*	1.786079848	0.956719586	0.014334323
WBGene00005034	*sra-8*	1.952641509	1.106437624	0.014396369
WBGene00004442	*rpl-28*	1.167304723	10.30710121	0.014443383
WBGene00006438	*nrfl-1*	1.055860238	7.069261959	0.014450319
WBGene00044124	*srsx-15*	1.456593979	2.219789792	0.014554591
WBGene00009121		1.064180442	3.872313246	0.014562369
WBGene00020782		1.205115285	3.660605951	0.014562369
WBGene00010588	*srz-14*	1.618323666	2.130617124	0.014586202
WBGene00019617		1.257707853	6.213804869	0.01459028
WBGene00008790		3.243715358	-0.7508874	0.014598783
WBGene00008021		1.185857807	2.97306775	0.014628007
WBGene00011830	*cyp-29A2*	1.474002351	2.49972817	0.01474338
WBGene00007123	*srbc-79*	1.381513005	1.290956413	0.014744123
WBGene00007526		1.370487452	1.719311355	0.014806066
WBGene00000166	*apt-9*	1.18274888	2.785240857	0.014828207
WBGene00202500		1.556940477	1.320360506	0.014862308
WBGene00006958	*wve-1*	2.079580637	-0.077327161	0.014881395
WBGene00004391	*rnr-1*	0.972876055	4.753204808	0.015067047
WBGene00010703		0.980863276	7.848263365	0.015089215
WBGene00009266		1.380534589	4.319529367	0.015089215
WBGene00018478	*otpl-5*	1.246343162	3.262175823	0.015094775
WBGene00000907	*daf-11*	0.983069253	5.479651823	0.015095261
WBGene00005591	*srj-1*	2.225606243	0.367713272	0.015170279
WBGene00017023		1.004946507	4.780888944	0.015190621
WBGene00001752	*gst-4*	1.218101563	5.859292245	0.015190621
WBGene00017137	*pink-1*	1.051382342	4.426124018	0.015291424
WBGene00194916		1.230629798	3.150374818	0.015300077
WBGene00005844	*srw-97*	1.82404699	0.409142696	0.015337513
WBGene00020046	*best-16*	1.741676826	1.409875662	0.015393316
WBGene00019350		1.455878658	2.930419221	0.015407967
WBGene00018289		1.408838224	3.14480179	0.015511433
WBGene00023450		1.043056873	4.273951387	0.015545624
WBGene00015760		1.641391656	1.305265639	0.015583632
WBGene00017556		2.003997354	1.033820904	0.015605209
WBGene00009781		1.046470723	5.327064783	0.015614143
WBGene00004223	*ptr-9*	1.601719557	1.339031127	0.015644873

WBGene00006844	*unc-120*	1.027216944	5.316288367	0.015674907
WBGene00012179		1.247370906	7.35205628	0.015690264
WBGene00005097	*srd-19*	1.45292054	1.514651263	0.015741319
WBGene00009176	*nmat-2*	1.223398058	3.717441904	0.015773461
WBGene00044668		2.430838342	-0.635605557	0.015811191
WBGene00021741		1.724828165	0.507575824	0.015831532
WBGene00022170		0.974947569	9.52643245	0.01587215
WBGene00015034		1.270287777	2.232183397	0.015931514
WBGene00016753	*oac-9*	1.381882204	2.530551374	0.015955292
WBGene00006021	*srx-130*	1.480399144	1.716505611	0.015963219
WBGene00016626	*clhm-1*	1.157638065	2.835992151	0.01610319
WBGene00022097	*nhr-242*	2.028082905	0.379279337	0.016227386
WBGene00006409	*hdl-2*	1.473150596	2.384172949	0.016227896
WBGene00003535	*nas-16*	1.617452556	1.918361031	0.016227896
WBGene00000784	*cpr-4*	1.12372707	9.086790275	0.016240282
WBGene00009625		1.306797474	3.867151504	0.016269434
WBGene00013069		1.611285016	2.097337033	0.016364727
WBGene00008320		1.176587952	3.581928205	0.016396308
WBGene00006587	*tnt-2*	0.99674633	7.690871543	0.016452676
WBGene00016207		1.575131252	1.961290241	0.016514102
WBGene00019973		1.272207852	2.817131136	0.016685849
WBGene00007554	*pptr-2*	1.067644282	5.354211821	0.016747311
WBGene00010021	*srbc-49*	1.436064216	2.052296075	0.016747311
WBGene00011422		1.026415691	4.080549275	0.016748222
WBGene00005859	*srw-112*	2.997364718	-0.607007298	0.016752266
WBGene00017120	*tctn-1*	1.168449239	3.205544255	0.016763734
WBGene00022572		1.753600866	1.58105771	0.016773631
WBGene00009850		0.998990278	5.309252356	0.016818562
WBGene00008889		1.158420647	4.170663596	0.016818562
WBGene00008644		1.448019179	2.424386246	0.016880043
WBGene00001680	*gpb-2*	1.158558766	3.166849441	0.016880043
WBGene00003162	*mdh-2*	0.985017218	8.180241808	0.016913764
WBGene00000719	*col-146*	2.742062939	3.270027828	0.016927005
WBGene00008236		1.2545559	2.35991542	0.016927729
WBGene00009833		2.119891153	0.209056116	0.016953802
WBGene00006126	*str-63*	1.498268182	1.368375035	0.017002057
WBGene00015413	*pdhb-1*	0.939620158	5.312179366	0.017039973
WBGene00005159	*srg-1*	1.864565738	0.486995845	0.017133117
WBGene00015444		1.743792896	1.304304941	0.017272219
WBGene00000221	*atf-5*	1.068138853	6.04950324	0.017425391
WBGene00016809		1.150318077	3.753880157	0.017462532
WBGene00006728	*ubq-2*	1.13343683	10.11188054	0.017462532
WBGene00016708		5.971591026	-2.165131724	0.017494118
WBGene00015148	*hpo-28*	0.96781126	5.337829449	0.017590669
WBGene00008297	*cdr-3*	2.064128562	0.314200468	0.017610232

WBGene00014163	*rnh-1.2*	1.247315772	2.557803706	0.017625756
WBGene00015766		1.297680775	2.17799618	0.017720418
WBGene00018703	*sec-3*	1.052639286	3.887007734	0.01776346
WBGene00010059		1.03494857	4.840612449	0.017787739
WBGene00007243	*nspb-7*	1.979519953	0.991865777	0.017807129
WBGene00007509		1.446611506	1.375328724	0.017839736
WBGene00003499	*mut-2*	1.810283848	0.399068317	0.017839736
WBGene00010539	*ttr-2*	1.471868578	5.598123403	0.017998971
WBGene00005509	*srh-305*	1.708883644	0.839709936	0.018177424
WBGene00011552		2.028089467	0.180156835	0.018232071
WBGene00005247	*srh-22*	2.149237938	0.220475744	0.018388872
WBGene00001389	*far-5*	1.23828978	3.363580014	0.018472012
WBGene00022854	*cin-4*	1.244459964	2.007959984	0.018475621
WBGene00010999		2.387999016	-0.025112432	0.018812384
WBGene00006675	*twk-22*	1.257844498	3.918143524	0.018812524
WBGene00005529	*sri-17*	1.286940351	2.240011866	0.018834938
WBGene00009529		1.732883527	0.650669498	0.018887233
WBGene00002998	*lin-9*	0.958171354	4.079506463	0.018897471
WBGene00011183		1.708476445	1.00902335	0.018947109
WBGene00022528	*srt-13*	1.456780323	2.193667097	0.019032481
WBGene00015973		1.51424072	1.827242709	0.019092378
WBGene00044005		1.708663885	0.933703035	0.019112032
WBGene00016688	*srbc-18*	1.583823133	2.225610383	0.019118736
WBGene00016677		0.923928077	6.980675125	0.01914463
WBGene00007067		1.03471366	3.601834713	0.019146007
WBGene00001971	*hmg-1.1*	1.103783458	7.674285812	0.019217822
WBGene00007537	*fipr-8*	1.339797677	5.637904073	0.019222358
WBGene00017343		2.454347587	-0.248042079	0.019223568
WBGene00015018	*srz-85*	1.50351233	1.94141303	0.019223568
WBGene00015339		3.55928863	5.924074414	0.019342357
WBGene00020555	*nhr-219*	1.448536864	2.266392767	0.019373794
WBGene00006453	*tag-80*	1.278178647	5.468783035	0.019443385
WBGene00008998	*ncs-4*	1.006117689	3.362308852	0.019593206
WBGene00005207	*srg-50*	1.969885575	0.406338129	0.019642968
WBGene00008279		1.457283463	1.052810768	0.01970233
WBGene00016691	*srbc-23*	1.594100702	0.919402327	0.019710136
WBGene00010381		1.400337611	2.295452986	0.01976704
WBGene00005910	*srx-19*	2.246048444	-0.263667436	0.01976704
WBGene00006544	*tbx-7*	1.40923226	2.032939304	0.01976704
WBGene00007714		2.740545958	-0.761322594	0.019808099
WBGene00023284		1.498268182	1.380178439	0.019842622
WBGene00018322		5.898799959	-2.129972518	0.019867206
WBGene00003003	*lin-14*	1.106027268	5.443074337	0.019908506
WBGene00019420	*fbxb-46*	2.605704478	-0.199932742	0.020041055
WBGene00016222		3.182237707	-1.180919295	0.020097068

WBGene00015762		6.040885158	-2.106704961	0.02025118
WBGene00018955		1.191519302	3.829044272	0.020482372
WBGene00006278	*str-252*	1.57994195	1.993037383	0.020615698
WBGene00015723		3.809494207	-1.584522112	0.020643257
WBGene00017231		1.274279043	2.967227398	0.020725528
WBGene00004928	*soc-1*	1.037804876	3.952655258	0.020798791
WBGene00018015		1.094191455	3.29093818	0.020862867
WBGene00021908		1.782833711	0.805283663	0.020933804
WBGene00015568	*sre-3*	1.42460043	1.415810167	0.020933804
WBGene00077683		2.260996534	0.241573021	0.021107728
WBGene00013962		1.205947065	6.043023918	0.021131305
WBGene00013562		1.259654479	3.377681579	0.021154304
WBGene00009096	*fipr-1*	1.004731588	7.538649569	0.021157446
WBGene00008799		1.676059735	1.139959764	0.021159227
WBGene00007109		1.175465575	3.842945947	0.021181401
WBGene00005490	*srh-286*	1.444563816	2.424634402	0.021181658
WBGene00017063		1.030526149	5.182149328	0.02118959
WBGene00013661		1.67747939	0.805094974	0.021195828
WBGene00022224	*set-28*	1.813684068	1.478999912	0.021195828
WBGene00008432		1.088746215	4.057651188	0.021229474
WBGene00005416	*srh-206*	1.418268225	2.063384153	0.021229474
WBGene00016118		0.962542113	6.797023313	0.021401292
WBGene00010483		1.480918032	2.674816458	0.021550178
WBGene00001669	*gpa-7*	1.296400409	3.160558569	0.021597832
WBGene00005000	*spp-15*	1.984411374	0.063104338	0.021727665
WBGene00021873	*clec-82*	1.756092684	0.833506857	0.021765128
WBGene00011710		1.444901806	2.179538597	0.021778511
WBGene00019604		1.246747062	1.704196284	0.021836184
WBGene00006919	*vha-10*	1.147391525	6.910719547	0.021916818
WBGene00017845	*srsx-9*	4.029683693	-1.490623378	0.021965309
WBGene00007517	*gpx-3*	1.001650885	4.435232451	0.022044964
WBGene00019114	*nhr-194*	1.019840173	3.027364876	0.022044964
WBGene00138724		1.360814881	2.187133716	0.022076713
WBGene00010130	*vha-14*	1.201459301	7.170431333	0.022105139
WBGene00004764	*sel-7*	1.470509307	3.569026622	0.022129063
WBGene00021225		1.234606933	3.377422519	0.022163354
WBGene00021993		1.801420041	0.666969814	0.022266272
WBGene00004303	*ran-2*	0.928672604	4.79903383	0.022341834
WBGene00005296	*srh-75*	1.480544717	0.875315337	0.022368661
WBGene00008315		0.973306268	3.4649276	0.022405184
WBGene00016285		1.345974831	2.696661719	0.022503909
WBGene00044164		1.562424286	1.118051601	0.022636759
WBGene00018055		1.402147064	1.964957594	0.022690119
WBGene00018851		2.921773721	-1.41412753	0.022690119
WBGene00006134	*str-73*	2.232950705	-0.118114978	0.022690119

WBGene00021464	*ugt-31*	1.415065543	6.122322885	0.022690119
WBGene00012374		1.530662224	1.107540629	0.022797586
WBGene00010894		1.222937513	3.081056009	0.022799773
WBGene00017109	*clec-177*	2.588768506	-0.375219752	0.022799773
WBGene00020448	*fbxa-51*	2.154694122	-0.05304173	0.022799773
WBGene00005984	*srx-93*	2.151724489	0.104264759	0.022799773
WBGene00005803	*srw-56*	1.613629533	1.241034525	0.022842454
WBGene00008449		1.229793677	3.376227239	0.022846722
WBGene00010863		1.038664932	2.78275762	0.02288901
WBGene00022615		0.944893604	7.313746387	0.023012416
WBGene00206498		2.343729869	0.174221898	0.023226669
WBGene00006259	*str-228*	2.362577295	-0.157019369	0.023282126
WBGene00021438		1.587329791	1.232819166	0.023424434
WBGene00008595	*clec-56*	0.996234646	3.600844747	0.023424434
WBGene00022127	*yop-1*	0.998160183	6.091531945	0.023507644
WBGene00019552		2.997364718	-0.578043356	0.023515618
WBGene00004024	*php-3*	1.013009368	3.688609471	0.02351736
WBGene00016499		1.369002908	1.67623661	0.023710059
WBGene00008215		1.15439926	5.037278654	0.023841905
WBGene00013135	*rga-2*	1.512756512	3.077705074	0.023893435
WBGene00005415	*srh-204*	2.49607815	-0.884473149	0.023893435
WBGene00001428	*fkb-3*	1.014722614	4.047163546	0.023917091
WBGene00019099		2.056392673	0.902116783	0.023936161
WBGene00019346		0.993762549	4.458927029	0.023963613
WBGene00017656		2.409107814	-0.509833871	0.024073974
WBGene00011761		0.949095533	5.135556296	0.024164088
WBGene00013895		1.211946205	4.796794191	0.024164088
WBGene00017156		1.496387052	1.721022945	0.024175023
WBGene00016211	*sdz-3*	1.521119095	1.460233708	0.024184209
WBGene00021519		1.627282489	1.710504031	0.024273111
WBGene00003802	*npp-16*	2.360465284	-0.439484772	0.024418365
WBGene00013964		0.899960878	3.807284377	0.024489468
WBGene00022131		1.17737795	4.912991009	0.02454004
WBGene00013785	*nep-23*	1.778027189	0.46419171	0.02454004
WBGene00008463		1.378131966	3.447840325	0.024567216
WBGene00021453		2.070492041	0.08510233	0.024620273
WBGene00012172		1.092823256	3.760867085	0.024660026
WBGene00005810	*srw-63*	1.522413121	1.935862619	0.024748178
WBGene00004855	*sma-1*	1.106093368	7.565710389	0.024892811
WBGene00001002	*div-1*	0.938220648	5.087171601	0.024904995
WBGene00013037		0.925104151	5.003412486	0.025513884
WBGene00219243		2.282964185	-0.709436706	0.02553261
WBGene00009014		1.97990086	0.089715715	0.025550407
WBGene00000395	*cdh-3*	1.201663236	4.28371019	0.025557481
WBGene00001703	*grd-14*	3.073394125	2.416926299	0.025620752

WBGene00011625	*vps-39*	0.923395942	4.338552508	0.025639725
WBGene00007073	*ugt-2*	1.234960113	3.165559859	0.025706071
WBGene00022040		0.852868196	4.412268468	0.025820074
WBGene00020259		1.162093129	1.980810533	0.025914052
WBGene00005464	*srh-258*	2.683202006	-0.812462426	0.025932949
WBGene00012892		1.583823133	2.173870147	0.025956428
WBGene00001645	*gly-20*	0.885635638	5.143470904	0.026026551
WBGene00000080	*adr-2*	0.962133972	3.956708061	0.026039138
WBGene00022633		0.986314201	4.639138716	0.02616048
WBGene00001193	*egl-26*	1.203733169	4.100520485	0.026208017
WBGene00000246	*bcc-1*	1.010285381	3.330417627	0.026210244
WBGene00013705		2.155380448	0.471298621	0.02623076
WBGene00195241		2.50635787	0.14391959	0.026237255
WBGene00015938	*anat-1*	0.97349785	4.962344126	0.026238249
WBGene00022545		1.334732808	2.214197955	0.026343569
WBGene00001090	*drh-1*	1.179213151	2.588413251	0.026447524
WBGene00012296	*spe-46*	1.197221898	3.438831274	0.026658433
WBGene00003388	*moe-3*	1.306421201	2.475776653	0.026744199
WBGene00011070		1.116555441	5.56717291	0.026799045
WBGene00016196		1.160554696	3.426329161	0.026840474
WBGene00015652	*srz-79*	1.477434129	1.54754361	0.027060494
WBGene00010666		2.246048444	-0.264669408	0.027086048
WBGene00005888	*srw-141*	1.495931839	0.980078758	0.027130175
WBGene00022893		1.262794712	3.1558104	0.027146809
WBGene00008415	*mce-1*	1.028460154	6.114325116	0.02715689
WBGene00021950	*cutl-26*	1.071777892	3.648677833	0.027164033
WBGene00004130	*ketn-1*	0.951275257	7.699330421	0.02716597
WBGene00015077		1.212655379	2.907289982	0.027167326
WBGene00015774		1.883487991	0.54185866	0.027167326
WBGene00001953	*hlh-8*	1.413606524	1.262840089	0.02745711
WBGene00005301	*srh-80*	1.600590352	1.354733624	0.027517394
WBGene00044560		1.570919553	1.098764161	0.027518894
WBGene00007988	*best-8*	1.340132582	1.502659224	0.02755558
WBGene00017389	*lgc-38*	1.02345278	3.058284995	0.027737575
WBGene00021884		1.339685974	2.842611471	0.027956068
WBGene00016227	*nhr-280*	2.384991546	-0.435995068	0.027999508
WBGene00008593	*clec-227*	0.983548951	3.291864393	0.028005362
WBGene00005282	*srh-60*	1.807176183	1.094895838	0.028012284
WBGene00016436		0.915079945	3.955847392	0.028094074
WBGene00014162	*chil-9*	1.86602978	0.174877739	0.028304664
WBGene00016308		1.697255553	1.744790101	0.02843232
WBGene00021934	*cct-8*	1.15715246	2.544623589	0.028437522
WBGene00017699	*flcn-1*	1.004613867	5.370363797	0.02845074
WBGene00016322		1.386080214	1.489206704	0.028480436
WBGene00019845	*irld-13*	1.214942091	3.611451328	0.028487631

WBGene00005722	*srv-11*	1.242982685	1.945071689	0.028508588
WBGene00004978	*spg-7*	0.968236338	6.479924204	0.028563875
WBGene00015862	*srt-25*	1.35379903	2.354058172	0.0286789
WBGene00021023		1.824852548	0.021777316	0.028758203
WBGene00005150	*sre-2*	1.025639089	3.944404966	0.028775369
WBGene00016581		1.187340357	2.268090559	0.028798899
WBGene00009320		1.122998461	4.095732804	0.028828978
WBGene00194780		1.506405502	1.154558131	0.028953269
WBGene00021407		1.369836897	2.50690259	0.028964696
WBGene00000694	*col-120*	1.911646353	-0.009563934	0.029069118
WBGene00017071	*aagr-1*	0.927977849	5.006905732	0.029082303
WBGene00009959		1.417571169	0.965463027	0.029159473
WBGene00206468		1.231211597	3.1201009	0.029196464
WBGene00011912		0.965871543	4.425240078	0.029244149
WBGene00010497	*axl-1*	1.152873362	2.626235051	0.029256589
WBGene00020203		1.536534635	1.433854914	0.029384563
WBGene00194695		1.587761472	1.113007342	0.029384563
WBGene00000781	*cpr-1*	1.106872422	8.982573215	0.029414581
WBGene00015137		0.917826873	4.603134913	0.029545465
WBGene00012173		1.708476445	1.010125398	0.029613651
WBGene00006257	*str-226*	3.659202185	-1.731144402	0.029650623
WBGene00005735	*srv-24*	1.375416384	1.896704235	0.029669045
WBGene00009609	*oac-27*	1.371249102	2.07133121	0.02970122
WBGene00001555	*gcy-35*	1.435952883	2.017753447	0.029716577
WBGene00004497	*rps-28*	1.061424463	10.35674303	0.029864335
WBGene00022671		1.557408643	1.057644362	0.029904758
WBGene00010503		1.03125143	3.604540631	0.029979001
WBGene00000601	*col-12*	2.579775665	5.291835117	0.029994999
WBGene00020372		1.360247145	1.750069446	0.029999454
WBGene00010763		1.952805927	-0.109532425	0.029999454
WBGene00004490	*rps-21*	1.066337656	10.69732267	0.030098089
WBGene00022409	*srt-53*	1.14803058	2.978869712	0.030151938
WBGene00016869		1.708476445	1.036736267	0.030163876
WBGene00005648	*srp-7*	0.996508444	5.373338215	0.030165755
WBGene00009033		1.208744257	3.458135812	0.030184166
WBGene00138725		1.52707639	1.383233066	0.030184166
WBGene00023463	*srz-82*	1.282509263	2.930861127	0.030273806
WBGene00000388	*cdc-25.3*	2.857284875	-0.995098739	0.030312044
WBGene00007971	*rpb-3*	0.881306557	4.624754134	0.030319917
WBGene00011373		1.802142742	0.380553642	0.030401159
WBGene00014094		2.829666064	0.710193968	0.03043802
WBGene00001187	*egl-19*	0.994885616	7.461476838	0.03043802
WBGene00017792		0.923475167	3.839276871	0.030548643
WBGene00007026	*mdt-31*	0.872579463	4.773390072	0.030581213
WBGene00018640		1.275797399	3.436168018	0.030630567

WBGene00005474	*srh-268*	2.020768085	0.262907851	0.030679591
WBGene00007711		1.273328617	3.387972436	0.03094849
WBGene00008806	*mboa-7*	0.890063448	4.240270266	0.03109711
WBGene00018308		2.067777825	-0.448993557	0.031099077
WBGene00011973		1.448588376	0.703331118	0.031191466
WBGene00044663		1.472872443	1.756213815	0.03124258
WBGene00016952		2.049819384	0.251257724	0.031307744
WBGene00206477		1.213191791	2.935686114	0.031397194
WBGene00001667	*gpa-5*	2.017585352	-0.220639065	0.031516294
WBGene00007569		2.75121865	-1.064948102	0.031628862
WBGene00009395	*clec-64*	1.155001802	1.872090628	0.031755623
WBGene00007518	*del-8*	1.16201182	3.903813774	0.031755623
WBGene00006078	*str-10*	2.139021272	-0.175182723	0.031818363
WBGene00006192	*str-145*	1.295588699	2.157169986	0.031834782
WBGene00011175		1.783571923	1.900766592	0.031947365
WBGene00012521		1.623606357	1.523836799	0.031953317
WBGene00022758		1.433103131	1.532773327	0.03195856
WBGene00021571	*srbc-81*	1.457784983	0.939807438	0.031965418
WBGene00017655		2.246048444	-0.234837505	0.032291488
WBGene00005303	*srh-82*	1.350799859	2.479322764	0.032349406
WBGene00006121	*str-56*	1.333351572	2.374483947	0.032349406
WBGene00018348		1.205097113	1.956167327	0.032583161
WBGene00010546		1.238512236	1.341383311	0.032687748
WBGene00004483	*rps-14*	1.001572849	11.19747769	0.032694892
WBGene00015757		1.67390237	1.094326636	0.032813819
WBGene00235117		2.683202006	-0.672288358	0.032823781
WBGene00022122	*trap-1*	0.876716371	6.683311438	0.032823781
WBGene00015177	*tmc-2*	0.975815657	4.788314169	0.032933842
WBGene00006272	*str-245*	1.56262671	0.759357072	0.032979402
WBGene00015963		1.385023682	0.904436176	0.033009051
WBGene00010746		1.198312767	2.218704307	0.033056656
WBGene00007885	*ugt-21*	1.20403392	2.387819295	0.033056656
WBGene00050892	*ttr-57*	3.057875765	-1.460018734	0.03307976
WBGene00020246	*clic-1*	1.016859597	4.945264736	0.033153854
WBGene00007472	*chil-7*	1.533816117	1.134754502	0.033167706
WBGene00016833	*sre-51*	1.487539024	1.431774937	0.033173928
WBGene00016608	*cogc-5*	0.887026639	4.401181463	0.033385666
WBGene00015792		1.449984182	2.002393995	0.03340052
WBGene00007734		2.8227887	-0.87291091	0.03357252
WBGene00017415		2.923897167	-0.968654977	0.03357252
WBGene00043988		0.926797414	3.320011735	0.033622571
WBGene00015885	*fbxa-65*	0.919785132	3.576090777	0.033746784
WBGene00007792		2.318210399	0.024660366	0.033815028
WBGene00017983		1.123073965	2.746401377	0.033831068
WBGene00019582		1.479983279	2.048583981	0.033857604

WBGene00005771	*srw-24*	3.367627571	-1.807927453	0.033857604
WBGene00016152	*pho-12*	1.138084298	2.939809717	0.033996097
WBGene00005615	*srj-27*	2.923897167	-1.081892781	0.033996852
WBGene00022240	*shl-1*	1.023205083	4.379104391	0.034088904
WBGene00044158		1.759751119	0.827783815	0.034096925
WBGene00006122	*str-57*	6.288913698	-2.015484512	0.034211673
WBGene00014188		2.08568675	1.113564719	0.034213913
WBGene00019417	*fbxb-52*	1.758629756	1.056442836	0.034213913
WBGene00019208	*lips-14*	1.151686795	3.122809592	0.034221085
WBGene00002148	*gon-14*	1.071883903	6.609534314	0.034247999
WBGene00022576		1.334732808	2.227191551	0.034422098
WBGene00008249	*srsx-28*	1.110265096	3.522028216	0.034518094
WBGene00011880		0.980162665	6.781598003	0.034573055
WBGene00001224	*ehs-1*	0.984068997	6.441675037	0.034752187
WBGene00011066	*ztf-15*	0.949629307	3.666538238	0.034884986
WBGene00001430	*fkb-5*	0.991430636	5.85248232	0.034912137
WBGene00005688	*sru-25*	2.192604719	-0.443278855	0.03510808
WBGene00009482		1.05765933	5.773878724	0.035143698
WBGene00009982		1.88890902	8.232573049	0.035194395
WBGene00044208		1.430559751	1.890175248	0.035209824
WBGene00021867		1.361259845	1.642617444	0.035233316
WBGene00005694	*sru-31*	1.478335875	1.945293691	0.035533909
WBGene00020505		1.133342082	2.134509242	0.035539543
WBGene00018920		2.141191659	-0.303665918	0.035562734
WBGene00044785		1.85531221	0.214102128	0.035598886
WBGene00020048	*lgc-12*	1.435837959	1.96439525	0.035598886
WBGene00005138	*srd-61*	1.879565572	-0.465779899	0.035610863
WBGene00010625		0.793216384	4.560908709	0.035697369
WBGene00021838		1.250006991	1.772884728	0.035700974
WBGene00014051	*spv-1*	1.058204358	6.084969811	0.035739652
WBGene00003620	*nhr-21*	0.807459736	5.952037585	0.035748649
WBGene00008211		0.828410783	5.489242963	0.035789027
WBGene00012181	*srt-11*	2.257965103	-0.598189454	0.035840467
WBGene00007763		1.572936702	0.683131237	0.035981277
WBGene00017949		1.623606357	1.463732421	0.035981513
WBGene00017393	*nep-5*	1.263904185	1.81425981	0.036050719
WBGene00000133	*amt-1*	1.024760912	2.494072564	0.036079815
WBGene00077588		1.946857019	0.091427092	0.036111676
WBGene00020166		1.053522303	7.299013207	0.036187206
WBGene00007022	*mdt-22*	1.020114686	3.620102301	0.036189274
WBGene00003233	*mgl-2*	1.019543741	3.197765838	0.036235041
WBGene00017029		3.491413174	-1.867768769	0.036363726
WBGene00004037	*plc-2*	0.917527164	4.153389406	0.036593827
WBGene00004452	*rpl-38*	0.955033954	10.98869609	0.036648185
WBGene00018054		1.536634151	1.090686544	0.036789543

WBGene00010805		1.131647216	3.109044519	0.036931369
WBGene00020022		0.870244489	5.538627154	0.037242993
WBGene00012596	*nhr-234*	1.45292054	1.451561469	0.037508812
WBGene00012265		1.046085013	3.375678178	0.037628411
WBGene00009304	*eva-1*	1.12096812	5.297219191	0.037746715
WBGene00019116	*nhr-143*	0.915864338	3.718418271	0.037871584
WBGene00013889		1.769231813	-0.006834012	0.037972081
WBGene00003089	*ltd-1*	1.118405917	5.684592188	0.038014261
WBGene00015351		1.173258047	2.560218052	0.038022999
WBGene00009099		1.270587536	2.391316177	0.038022999
WBGene00017024		1.574568561	1.04937441	0.038022999
WBGene00019260		2.074412902	-0.347185324	0.038073554
WBGene00003891	*osm-11*	0.793755648	9.470819347	0.038244087
WBGene00022324	*fbxa-26*	1.316128365	2.07668844	0.038271032
WBGene00018410		1.143146325	2.141169712	0.038400601
WBGene00008536		1.044452373	4.096006019	0.038425924
WBGene00017245		0.960703144	3.712771492	0.038480728
WBGene00004408	*rla-0*	0.985322282	10.62217289	0.038523285
WBGene00000010	*aat-9*	1.132466201	2.241166093	0.038581606
WBGene00008328	*srz-43*	2.921773721	-1.439865686	0.038581606
WBGene00011713		1.000294362	3.873467583	0.038657449
WBGene00001918	*his-44*	2.310125302	-0.542716111	0.038764036
WBGene00008708		1.646209846	1.794480878	0.038804335
WBGene00007327		1.099094031	2.042625013	0.038817649
WBGene00018203		1.699615953	1.051105783	0.038879162
WBGene00012505		1.052893617	3.20934845	0.039123718
WBGene00006433	*sdhb-1*	0.86576997	7.302053934	0.039123718
WBGene00019371		1.572176437	0.570309134	0.039147945
WBGene00000271	*brf-1*	0.868073238	4.562862457	0.039147945
WBGene00019369		1.43736778	0.945135684	0.039181384
WBGene00005738	*srv-27*	1.534754007	1.840874008	0.039182656
WBGene00005300	*srh-79*	1.596109271	1.124633805	0.039204633
WBGene00022266	*srt-56*	1.247044702	2.408888675	0.039257893
WBGene00020176		1.596525346	0.677741254	0.039382204
WBGene00008875		1.441124268	2.327582043	0.039404303
WBGene00001077	*dpy-18*	0.807915812	6.428065012	0.039526441
WBGene00015655		2.271071568	-0.015570253	0.03953347
WBGene00018284		3.141963206	-1.325174766	0.039574092
WBGene00006826	*unc-97*	1.030287432	6.588022167	0.039574092
WBGene00004998	*spp-13*	1.509266536	2.881665609	0.039576439
WBGene00011743		0.897915813	5.616397107	0.03957777
WBGene00005920	*srx-29*	3.141963206	-1.430804333	0.039589057
WBGene00011234		0.797209501	4.24794318	0.039637598
WBGene00013919		0.848877231	5.185650355	0.039692458
WBGene00016491	*acdh-5*	1.959505716	-0.609003195	0.039703357

WBGene00003008	*lin-22*	1.269604851	1.647248466	0.03974927
WBGene00009808	*srm-4*	1.282359825	1.723335637	0.03977003
WBGene00015897	*nhr-156*	2.251479456	-0.838580499	0.039782402
WBGene00014115	*gld-4*	0.881723843	5.282365715	0.039839596
WBGene00005919	*srx-28*	1.445071972	2.058598116	0.039864381
WBGene00011025		1.226565711	2.687989141	0.039870813
WBGene00013920	*pssy-1*	0.863556787	5.680657478	0.039870813
WBGene00001539	*gcy-13*	1.257178731	2.564356842	0.039967284
WBGene00009081		0.906788005	3.834658476	0.040137063
WBGene00019047		1.084757829	2.58659372	0.040248407
WBGene00016914		1.028574831	2.668083225	0.040332784
WBGene00009327		1.76683512	1.040616841	0.040332784
WBGene00001400	*fax-1*	1.429477214	1.09699198	0.040482343
WBGene00001893	*his-19*	2.561187073	-0.786333844	0.040524975
WBGene00022435		1.116706479	2.614705025	0.040635213
WBGene00016540		1.043938777	2.337695428	0.040755119
WBGene00006239	*str-206*	1.454546101	1.223120508	0.040902507
WBGene00011398	*qdpr-1*	0.87018007	5.686713098	0.041003342
WBGene00018538		0.871490688	5.970520936	0.041120382
WBGene00006154	*str-97*	0.956381288	4.226719716	0.041140719
WBGene00007150	*acly-2*	1.021098588	3.483178522	0.041170356
WBGene00009359	*clec-102*	1.327359139	1.153384157	0.04132013
WBGene00017112		1.106891841	3.119632299	0.041330244
WBGene00015628	*best-6*	1.903977516	0.405410093	0.041330244
WBGene00003703	*nhr-113*	1.242195292	2.432966362	0.041471822
WBGene00019263		1.313227369	0.911682754	0.041510827
WBGene00010342		1.354512299	1.408947962	0.041518649
WBGene00011704	*sdz-31*	3.30150973	-1.941521499	0.041648814
WBGene00018008	*vpr-1*	0.935972135	5.560657862	0.041690636
WBGene00016172		0.880446549	5.35517439	0.041829363
WBGene00000040	*aco-1*	0.919835558	6.677562608	0.041893146
WBGene00004278	*rab-19*	0.93898922	5.297518434	0.042125354
WBGene00004417	*rpl-6*	0.967294718	10.09422574	0.042170339
WBGene00011509		1.247856896	2.573294065	0.042185801
WBGene00017670		1.710981469	0.055412594	0.042210119
WBGene00005767	*srw-20*	1.151916754	2.758661085	0.042371227
WBGene00016409		0.825776829	5.059306365	0.042537407
WBGene00005831	*srw-84*	1.804973249	1.227108227	0.042537407
WBGene00015082		1.808681298	0.19043011	0.042547421
WBGene00015266		0.78817076	4.057985777	0.042571006
WBGene00007325		1.744534777	0.573140767	0.04263849
WBGene00000233	*avr-15*	0.926770513	5.070336975	0.042713945
WBGene00007816		0.961247862	3.065202039	0.04278501
WBGene00009215	*thn-2*	2.039967786	1.653669496	0.04291428
WBGene00006102	*str-37*	1.62518312	1.842373917	0.042928979

WBGene00016329	*osr-1*	1.925107915	2.013975676	0.042986663
WBGene00000157	*aps-2*	1.088126025	3.636241106	0.043087147
WBGene00018715		0.907693405	3.722602698	0.043119759
WBGene00011485	*srbc-14*	1.786727083	0.462267437	0.043119759
WBGene00017800		0.855238729	4.772887717	0.043302679
WBGene00000670	*col-95*	1.438866367	1.694066234	0.043350244
WBGene00008359	*nspc-17*	1.004033561	4.533822199	0.043378974
WBGene00008921		0.833438311	4.824311583	0.043497043
WBGene00000902	*daf-6*	1.188857141	3.792739026	0.043533847
WBGene00005231	*srh-5*	1.116410096	2.558709557	0.043533847
WBGene00017944		1.888450729	0.293202789	0.043645825
WBGene00007876	*dct-19*	2.158302771	-0.181679301	0.043713427
WBGene00138719		2.059343603	0.075050763	0.043796744
WBGene00015642		0.969927352	4.550532458	0.043818746
WBGene00011418	*igdb-1*	1.447958188	0.821518907	0.043818746
WBGene00017864	*pcca-1*	0.796205547	7.599992221	0.043832696
WBGene00016169		1.170434267	2.542647831	0.044124431
WBGene00015707		1.717282851	0.971454644	0.044219503
WBGene00017223		1.772186579	0.247560558	0.044325736
WBGene00021637		0.78492088	5.350075367	0.04445842
WBGene00011144		0.869732462	3.300351958	0.04445842
WBGene00003656	*nhr-66*	1.032347442	4.418270764	0.04445842
WBGene00020952	*kel-8*	1.097929174	3.24732826	0.044472266
WBGene00009642		0.934828002	3.307943657	0.04452662
WBGene00016100		1.063077969	3.431206923	0.044657215
WBGene00012490		1.628209521	0.423692538	0.044657215
WBGene00044735		1.499745956	0.894056372	0.044792283
WBGene00006586	*tni-4*	0.832897489	6.493149227	0.044941089
WBGene00009090	*fipr-3*	1.620225984	5.790216756	0.044975199
WBGene00005160	*srg-2*	1.367855085	1.990584916	0.045004436
WBGene00011351		1.063382661	2.85571573	0.0450114
WBGene00016743	*srb-15*	1.469560445	1.296777003	0.045049627
WBGene00003848	*odr-1*	1.069958735	3.33249519	0.045049794
WBGene00010964		1.007813013	10.89929015	0.045053923
WBGene00010025	*srbc-54*	1.603383106	0.60537997	0.045067789
WBGene00010338		1.044533347	2.573247088	0.045154763
WBGene00006965	*xtr-1*	1.151309868	2.354502248	0.045203652
WBGene00012746		1.394967398	1.716549375	0.045263327
WBGene00021010		1.725333499	1.024556615	0.04535102
WBGene00005222	*srg-65*	1.708769223	0.800558785	0.04535102
WBGene00005260	*srh-37*	1.952805927	-0.302100719	0.04535102
WBGene00017388		1.862824058	0.777289671	0.04535792
WBGene00006006	*srx-115*	1.201351813	2.40657428	0.045379467
WBGene00008196		0.982793949	4.346333181	0.04560429
WBGene00004445	*rpl-31*	0.920226852	10.10104765	0.045653393

WBGene00009762		2.512794634	-0.732150787	0.045682558
WBGene00044602		1.666857534	0.721315036	0.045735285
WBGene00015277		1.39392439	1.116975241	0.04574382
WBGene00001536	*gcy-9*	1.034895724	3.324785863	0.045759114
WBGene00013646		1.729055183	0.115114559	0.045777551
WBGene00021533		0.881718132	5.332522011	0.045923239
WBGene00000064	*act-2*	1.02101431	6.740263422	0.045931884
WBGene00001773	*gst-25*	1.72744885	0.30462351	0.045931884
WBGene00077763		1.17422556	1.86642709	0.046092751
WBGene00012298	*prmt-7*	0.803698786	5.45072573	0.046092751
WBGene00012031		0.899524053	6.115865536	0.046118547
WBGene00005609	*srj-21*	1.528306514	0.556923433	0.046118547
WBGene00017985		1.096274861	2.900321067	0.046136735
WBGene00007490	*mks-5*	0.940949022	4.521631714	0.046148192
WBGene00004860	*sma-6*	0.912679776	4.215148072	0.046148192
WBGene00008306		1.466255306	0.974024765	0.046148691
WBGene00010417		1.575317738	1.104885236	0.046316249
WBGene00011320		1.499733218	1.085901454	0.046352687
WBGene00009227		1.547440654	0.826246391	0.04653088
WBGene00010152		1.188585932	2.711261236	0.046626722
WBGene00004449	*rpl-35*	0.937589581	11.20505522	0.046632048
WBGene00021631		1.907945095	-0.351620799	0.046703205
WBGene00003807	*npr-1*	1.114891607	3.39169359	0.046709773
WBGene00004489	*rps-20*	0.887528885	9.930254414	0.04674279
WBGene00003076	*lsm-1*	0.784699373	4.55719865	0.046797076
WBGene00018878	*glit-1*	0.793740507	4.248439659	0.046890213
WBGene00011181		0.87767105	4.814532144	0.046891052
WBGene00005802	*srw-55*	2.71769148	-1.630851597	0.046908469
WBGene00012771		1.108502808	1.958403344	0.047061318
WBGene00007605	*asp-10*	1.012732125	2.822862549	0.047061318
WBGene00020703		0.8788657	5.533498247	0.047197991
WBGene00020665		0.993557461	3.718107319	0.047197991
WBGene00013184		1.613820211	0.865028379	0.047197991
WBGene00005907	*srx-16*	1.387812302	1.77850618	0.04721375
WBGene00021268		0.843446898	3.016905968	0.047363218
WBGene00008527	*set-8*	2.319159309	-1.060252328	0.047363218
WBGene00016698		1.349708159	2.181987891	0.047371757
WBGene00011333	*nrde-2*	0.912361608	6.640010397	0.047371757
WBGene00012043	*irld-52*	1.673172606	0.59284657	0.047514684
WBGene00011206		1.037274872	3.029996151	0.047763242
WBGene00010383	*mpst-3*	0.874349143	3.752254871	0.047763242
WBGene00007451		1.429477214	1.112016525	0.047783138
WBGene00008805	*git-1*	1.084376307	2.376251014	0.047907363
WBGene00000053	*acr-14*	1.104400481	2.894662048	0.048041344
WBGene00044607		1.04415539	1.990486786	0.048096867

WBGene00019493	*catp-5*	0.855103347	4.204226286	0.048144283
WBGene00016619		1.167132792	3.106513748	0.04827674
WBGene00010107		5.898799959	-2.279779916	0.048300611
WBGene00021158		0.935691876	3.430183207	0.048366791
WBGene00019905		3.013919755	-1.489116048	0.04865867
WBGene00016146		2.523957553	5.762777906	0.0487113
WBGene00017894		0.832362409	5.194224776	0.048774079
WBGene00013411		2.162781576	-0.366885724	0.04883513
WBGene00022871		1.592952459	1.387350284	0.048842707
WBGene00044378		1.764331692	-0.385584452	0.04884691
WBGene00015258		0.880959386	2.93321914	0.048945381
WBGene00004459	*rpn-2*	0.800258031	5.819711896	0.048945381
WBGene00009531		0.846817925	4.648908783	0.049132348
WBGene00007912		0.919569971	4.617439602	0.049380554
WBGene00008330		0.921844613	3.648403363	0.049380554
WBGene00006734	*ufd-2*	1.053471222	2.61471139	0.049380554
WBGene00009875		2.409107814	-0.538970302	0.049401351
WBGene00018793	*mrpl-40*	0.75729761	5.840107175	0.049440117
WBGene00019938		0.881148212	4.234635825	0.049465241
WBGene00008209		2.051448297	-0.352228912	0.049703627
WBGene00016932		3.430847591	-1.926296334	0.049711697

Table XVI: Genes differentially expressed in wild-type (Tg) vs *ceh-28* (Tg)

Gene ID	Gene Name	logFC	Expression level	FDR
WBGene00000063	*act-1*	3.230020262	9.189241758	2.69898E-14
WBGene00006714	*ubc-19*	9.165242159	0.55687494	1.95817E-11
WBGene00008349		6.174619684	0.800452778	2.87247E-11
WBGene00018910		4.776956741	1.470144826	3.33211E-11
WBGene00018911		3.569338269	2.104574249	4.98202E-10
WBGene00021224	*clec-209*	4.2273432	1.218015607	9.27789E-10
WBGene00000450	*ceh-28*	9.059939646	0.253088489	1.59035E-09
WBGene00013482		2.243468878	2.971567916	1.38965E-05
WBGene00021222	*irld-53*	2.976696938	1.225235824	4.025E-05
WBGene00008350		3.953416184	0.158736972	0.000128604
WBGene00017496	*srbc-15*	2.48048582	2.136112514	0.000142008
WBGene00009983	*cut-2*	5.145329386	7.496584833	0.0002808
WBGene00001752	*gst-4*	1.813451101	5.564399594	0.00037215
WBGene00077455		5.737579057	-0.751844811	0.000374079
WBGene00022093		2.001311707	5.771351663	0.000754463
WBGene00044174	*fipr-5*	3.077704294	2.227836275	0.001028924
WBGene00016733	*phat-2*	4.89695706	1.919651495	0.001028924
WBGene00015340		4.64700525	6.553147311	0.001133538
WBGene00020039		4.258722826	4.5260937	0.001443988
WBGene00015398	*tag-293*	2.33986075	2.368489516	0.001873233
WBGene00012161		4.659551677	-0.871537736	0.002217123
WBGene00015339		4.585840634	5.59085107	0.002225589
WBGene00011537		3.946586743	3.452960441	0.003370454
WBGene00000678	*col-104*	3.616782988	4.130781118	0.003370454
WBGene00008477	*clec-17*	1.458746655	4.281529517	0.003551855
WBGene00044175	*fipr-9*	2.227623043	3.444561089	0.003551855
WBGene00001925	*his-51*	3.029260414	0.250461941	0.003790727
WBGene00016435		1.430122105	8.745790905	0.004012367
WBGene00022325	*fbxa-5*	3.026018457	0.038122339	0.004187209
WBGene00001714	*grl-5*	4.801096821	2.988176432	0.004299942
WBGene00010461		4.894814616	1.655574037	0.004505015
WBGene00017073		3.213723228	3.92910782	0.004797638
WBGene00010745	*dod-17*	2.076326945	2.860658795	0.004934977
WBGene00018292		3.150036578	3.452966098	0.005753729
WBGene00018297		3.862038293	8.432479282	0.005777698
WBGene00194699		1.872552537	3.780687375	0.005961577
WBGene00000672	*col-97*	3.631756255	5.125679744	0.006290339
WBGene00017307		3.451089266	3.255696743	0.006547629
WBGene00007806	*clec-230*	2.866627105	1.882224462	0.00708308
WBGene00022679		3.642136464	5.976376191	0.008037989
WBGene00011339		1.888875762	1.939087787	0.00819011
WBGene00001895	*his-21*	3.401785348	-0.119806583	0.00850017

WBGene00016146		3.255866704	5.439073262	0.008901011
WBGene00000603	*col-14*	3.395457167	5.263868271	0.01006994
WBGene00002264	*lec-1*	1.541837045	4.219231808	0.010211965
WBGene00044402		6.698636558	-2.025370757	0.010384886
WBGene00017835		2.925152126	1.953231037	0.011283244
WBGene00017305	*nspb-12*	3.093705838	3.981606779	0.011283244
WBGene00009964	*fip-6*	2.296054168	3.952775808	0.012388434
WBGene00011103		2.493940409	3.46193504	0.013455181
WBGene00010468		3.778730025	4.115249318	0.013455181
WBGene00005018	*sqt-3*	3.573176844	6.971275009	0.013596057
WBGene00010961		1.50426022	4.92901969	0.014820791
WBGene00008492		1.613169182	3.677356695	0.014820791
WBGene00012255	*lpr-6*	3.022406331	2.071213631	0.01484944
WBGene00018602		2.077890395	6.056690925	0.01549305
WBGene00077691		3.196297147	4.26171099	0.01549305
WBGene00000650	*col-74*	3.503952002	5.478935088	0.01549305
WBGene00016437		1.569639673	2.85281057	0.015922188
WBGene00015046	*nlp-34*	1.413006566	7.192582288	0.015991839
WBGene00020040		3.081208858	4.263583348	0.016419417
WBGene00014039		3.163841849	2.839879856	0.016419417
WBGene00007544	*fipr-6*	1.650532382	6.726300821	0.016840531
WBGene00012420		2.144300817	1.504834813	0.018080841
WBGene00019154	*glf-1*	3.459431619	2.146722767	0.020180732
WBGene00009261		3.608145229	1.428484782	0.020196969
WBGene00003375	*mlp-1*	1.636115736	4.424124911	0.0220928
WBGene00044724		3.061713132	3.867074663	0.023711318
WBGene00000704	*col-130*	3.40915902	4.250178824	0.023787648
WBGene00020803		2.96664967	3.550557202	0.024747114
WBGene00010123		1.390751703	2.091009546	0.026820269
WBGene00008899		2.240528808	-0.006934206	0.026820269
WBGene00009041	*cut-3*	3.5687038	3.408283802	0.026820269
WBGene00021625		3.376832711	6.322907239	0.026846287
WBGene00009608	*nhr-265*	2.969251098	-0.899068531	0.02974244
WBGene00044479		2.860762941	0.706607986	0.029950269
WBGene00006200	*str-154*	1.713255255	0.994312472	0.029950269
WBGene00001703	*grd-14*	3.239330066	2.156985255	0.031300688
WBGene00012540		3.558486008	2.836237648	0.031471283
WBGene00001900	*his-26*	2.449890058	0.937570312	0.031667934
WBGene00001076	*dpy-17*	3.305121263	6.093973708	0.031878305
WBGene00044024		3.486309518	2.2966673	0.033275483
WBGene00011536		3.892746525	-0.217631098	0.033275483
WBGene00020237	*phat-4*	2.596964428	4.4408636	0.033392766
WBGene00018489		3.001591141	3.151447996	0.03371837
WBGene00000738	*col-165*	3.133304009	6.652291905	0.03371837
WBGene00021085		3.02793793	2.718259607	0.034808877

WBGene00018726		2.552426475	2.102792337	0.035054215
WBGene00000140	*anc-1*	1.326984399	10.43419196	0.035054215
WBGene00001927	*his-53*	2.704032091	-0.748387502	0.035231789
WBGene00000625	*col-48*	2.843951554	4.148265146	0.035565255
WBGene00000372	*cyp-13A7*	2.419942982	3.460207136	0.036156178
WBGene00013980	*dos-1*	1.103506269	3.309085202	0.03630054
WBGene00007857		1.125407259	5.111524107	0.036440638
WBGene00010467		3.759053889	-0.006999309	0.037776918
WBGene00016732	*phat-1*	2.4005997	1.687358488	0.037776918
WBGene00021225		1.314702738	3.201335989	0.039454459
WBGene00014173		1.498048067	4.640082081	0.039459195
WBGene00021934	*cct-8*	1.304695928	2.347223803	0.040145975
WBGene00021975		1.340190669	3.187144183	0.040322852
WBGene00009058		1.123590078	5.366242161	0.042050381
WBGene00022029		1.862374727	1.445742404	0.042050381
WBGene00007543	*fipr-7*	1.694477112	6.920824006	0.042213629
WBGene00009573		2.820382549	2.404695971	0.042483198
WBGene00016598		3.119542825	1.229024494	0.044402248
WBGene00009386	*tag-290*	1.43610586	3.412878469	0.045114111
WBGene00004092	*ppt-1*	1.46584373	1.422819286	0.045202083
WBGene00018917	*irld-35*	1.494290973	1.905340058	0.046976503
WBGene00023417	*swm-1*	1.62665639	1.883219442	0.047811023
WBGene00010967		1.228238469	7.078578486	0.047854301
WBGene00000601	*col-12*	2.715495534	5.071018744	0.048545615

7.11 Appendix K: Custom Matlab scripts

7.11.1 Custom Matlab scripts to quantify GCaMP3 rise time in the isthmus muscles

```
a_extract_center_diff_peaks_for_loop
    x = numel(center_diff_peaks_time);
    for i = (1:x)
        y = center_diff_peaks_time(i);
        z = find(abs(time_minus-y) < 0.001);
        peak_index(i) = z;
        center_smooth_peak_times_extract{i} = time_minus(z - 4: z + 7);
        center_smooth_peak_mag_extract{i} = center_diff_smooth(z - 4: z + 7);
    end
    clear i x y z;
    figure;
    hold on;
    cellfun(@plot, center_smooth_peak_mag_extract);
    title('center diff smooth peaks')
    xlabel('index')
    ylabel('dF')
b_extract_posterior_diff_peaks_for_loop
    x = numel(posterior_diff_peaks_time);
    for i = (1:x)
        y = posterior_diff_peaks_time(i);
        z = find(abs(time_minus-y) < 0.001);
        peak_index(i) = z;
        posterior_smooth_peak_times_extract{i} = time_minus(z - 8: z + 6);
        posterior_smooth_peak_mag_extract{i} = posterior_diff_smooth(z - 8: z + 6);
    end
    clear i x y z;
    figure;
    hold on;
    cellfun(@plot, posterior_smooth_peak_mag_extract);
    title('posterior diff smooth peaks')
    xlabel('index')
    ylabel('dF')
c_extract_center_diff_peaks_approx_zero_for_loop
    x = numel(center_smooth_peak_mag_extract);
    center_smooth_peak_mag_extract_array = cell2mat(center_smooth_peak_mag_extract);
    center_smooth_peak_times_extract_array = cell2mat(center_smooth_peak_times_extract);
    y = numel(center_smooth_peak_mag_extract_array(:,1));
    center_diff_smooth_zero = zeros(y, x);
    for i = (1:x)
        s = abs(i);
        temp_mag = center_smooth_peak_mag_extract_array(:,s);
        for j = (1:y-1)
            t = abs(j);
            if [temp_mag(t) * temp_mag(t+1)] < 0
             center_diff_smooth_zero(t, s) = center_smooth_peak_times_extract_array(t, s);
            else center_diff_smooth_zero(t,s) = 0;
```

```
        end
      end
    end
    clear i j s t temp_mag x y
    clear center_smooth_peak_mag_extract center_smooth_peak_times_extract peak_index
d_extract_posterior_diff_peaks_approx_zero_for_loop
    x = numel(posterior_smooth_peak_mag_extract);
        posterior_smooth_peak_mag_extract_array =
    cell2mat(posterior_smooth_peak_mag_extract);
    posterior_smooth_peak_times_extract_array =
    cell2mat(posterior_smooth_peak_times_extract);
    y = numel(posterior_smooth_peak_mag_extract_array(:,1));
    posterior_diff_smooth_zero = zeros(y, x);
    for i = (1:x)
       s = abs(i);
       temp_mag = posterior_smooth_peak_mag_extract_array(:,s);
       for j = (1:y-1)
          t = abs(j);
          if [temp_mag(t) * temp_mag(t+1)] < 0
           posterior_diff_smooth_zero(t, s) = posterior_smooth_peak_times_extract_array(t, s);
          else posterior_diff_smooth_zero(t,s) = 0;
          end
       end
    end
    clear i j s t temp_mag x y
    clear posterior_smooth_peak_mag_extract posterior_smooth_peak_times_extract
    peak_index
```

7.11.2 Custom Matlab scripts to quantify GCaMP3 peak delay in the isthmus muscles

```
a_diff_smooth
    center_diff = diff(center);
    center_diff_smooth = smooth(center_diff, 5);
    posterior_diff = diff(posterior);
    posterior_diff_smooth = smooth(posterior_diff, 5);
    time_minus = time(2:end);
b_plot_diff_smooth
    plot(time_minus,center_diff_smooth,'DisplayName','center')
    hold on
    plot(time_minus,posterior_diff_smooth,'DisplayName','posterior')
    x=time_minus;
    xlabel('time,sec')
    y=center_diff_smooth;
    ylabel('Diff(F)')
    legend('show')
c_find_max
    [center_diff_peaks, center_diff_peaks_time]= findpeaks(center_diff_smooth, time_minus,
    'MinPeakHeight',20000);
    [posterior_diff_peaks, posterior_diff_peaks_time]= findpeaks(posterior_diff_smooth,
    time_minus, 'MinPeakHeight',20000);
```

```
d_plot_find_max
    plot(time_minus, center_diff_smooth,'b');
    hold on;
    plot(time_minus, posterior_diff_smooth,'r');
    plot(center_diff_peaks_time, center_diff_peaks, 'ob ');
    plot(posterior_diff_peaks_time, posterior_diff_peaks, '+r ');
    hold off
e_calc_time_delay
   time_delay_diff_posterior = posterior_diff_peaks_time - center_diff_peaks_time;
```

7.11.3 Custom Matlab scripts to quantify GCaMP3 peak delay in M4

```
a_diff_smooth
    anterior_diff = diff(anterior);
    anterior_diff_smooth = smooth(anterior_diff, 5);
    middle_diff = diff(middle);
    middle_diff_smooth = smooth(middle_diff, 5);
    posterior_diff = diff(posterior);
    posterior_diff_smooth = smooth(posterior_diff, 5);
    time_minus = time(2:end);
b_plot_diff_smooth
    plot(time_minus,anterior_diff_smooth,'DisplayName','anterior')
    hold on
    plot(time_minus,middle_diff_smooth,'DisplayName','middle')
    plot(time_minus,posterior_diff_smooth,'DisplayName','posterior')
    x=time_minus;
    xlabel('time,sec')
    y=anterior_diff_smooth;
    ylabel('Diff(F)')
    legend('show')
c_find_max
    [anterior_diff_peaks, anterior_diff_peaks_time]= findpeaks(anterior_diff_smooth, time_minus,
    'MinPeakHeight',0.1);
    [middle_diff_peaks, middle_diff_peaks_time]= findpeaks(middle_diff_smooth, time_minus,
    'MinPeakHeight',0.1);
    [posterior_diff_peaks, posterior_diff_peaks_time]= findpeaks(posterior_diff_smooth,
    time_minus, 'MinPeakHeight',0.1);
d_plot_find_max
    plot(time_minus, anterior_diff_smooth,'b');
    hold on;
    plot(time_minus, middle_diff_smooth,'g');
    plot(time_minus, posterior_diff_smooth,'r');
    plot(anterior_diff_peaks_time, anterior_diff_peaks, 'ob ');
    plot(middle_diff_peaks_time, middle_diff_peaks, '*g ');
    plot(posterior_diff_peaks_time, posterior_diff_peaks, '+r ');
    hold off
e_calc_time_delay_middle
    time_delay_diff_middle = middle_diff_peaks_time - anterior_diff_peaks_time;
f_calc_time_delay_posterior
   time_delay_diff_posterior = posterior_diff_peaks_time - anterior_diff_peaks_time;
```

7.12 Appendix L: Using CellProfiler and Fiji to straighten the pharynxes and register images

Straighten Pharynx

- Open CellProfiler
  - Set Input modules
    - Load the images which are needed to be straighten by dragging the image folder into the “Fil list” window
    - Set Extract metadata to “No”
    - Use NamesAndTypes to assign the name “RawData” to these images
  - Load Analysis modules
    - Use File>Import>Pipeline “straighten_pipeline_v7.cpproj ”from the file to load
    - This pipeline includes four modules: “ApplyThreshhold”, “IdentifyPrimaryObjects”, “StraightenWorms”, and “SaveImages”.
  - Set Output folder for straightened images
    - Click “View output settings”. Under Default Output Folder, choose or make a new folder “Output”
    - Start “Test Mode” and Run the first image to test if analysis pipeline is working
    - Exit Test Mode and hit “Analyze Images”

Rotate pharynx (if necessary)

- Look through the straighten images to see how most of them are pointed
- Open CellProfiler
  - Set Input modules
    - Load the straightened images by dragging the image folder into the “File list” window
    - Set Extract metadata to “No”
    - Use NamesAndTypes to assign the name “Output_temp” to these images
  - Load Analysis modules
    - Use File>Import>Pipeline “rotate_pharynx_save.cpproj” from file to load
  - Hit “Analyze Images”
    - A window will open to each images that will allow you to skip rotation or rotate 180 degrees
    - Click OK, and this will open overwrite the straightened images in the output folder

Register images

- Open straightened images in Fiji
  - These images are different sizes, so they cannot be imported as an image sequence
  - Drag straightened images onto the Fiji icon on the dock
  - Use Image>Stacks>Images to Stack to convert individual images to a stack
    - Use “Copy (center)” and check “Use Titles as Labels”
    - If the images load in the incorrect order, use the “Stack Sorter” to “Sort by Label”
  - Register using Plugins>Registration>StackReg using the transformation “Translation”
  - Save registered images in “Output registered” folder

Create a kymograph showing maximum fluorescence intensity in the isthmus

- The isthmus should be pretty straight, so draw a line thick enough to include the entire isthmus.

- Create Kymograph using "KymoResliceWide" Maximal intensity works best for localized increases in the fluorescence near the isthmus lumen, but average fluorescence could be also used.
- Save the kymograph image with the original image stack.

Generate a Profile Plot Maximum intensity from kymograph

- Rotate the kymograph on the x-axis using Plugins>Transform>TransformJ: Rotate
  - Rotate 90^{o} on the x-axis
- Select All
- Use the macro "Stack Profile Plot" to generate a stack of Profile plots
  - The intensity measurements probably need to be changed in the "Stack Profile Plot" macro text file. Use the Maximum and Minimum intensity measurements from the original kymograph to choose intensity values that bracket the Max and Min values.

Generate a Surface Profile of "isthmus crop" stack

- Crop pharyngeal isthmus
  - Rotate image until pharyngeal isthmus is horizontal using "Image>Transform-Rotate…"
  - Draw rectangular ROI that includes the entire isthmus in each frame I the stack and crop using "Image>crop".
  - Save images in a folder "isthmus crop"
- Adjust Brightness/Contrast (if you are only looking at temporal and spatial changes in fluorescence)
- False color using 'physics' LUT
- Generate a surface plot stack using "Analyze>Surface Plot"
- Save as movies or as RGB images

7.13 Appendix M: Copyright

JOHN WILEY AND SONS LICENSE
TERMS AND CONDITIONS
Oct 19, 2017

This Agreement between Alena Kozlova ("You") and John Wiley and Sons ("John Wiley and Sons") consists of your license details and the terms and conditions provided by John Wiley and Sons and Copyright Clearance Center.

License Number	4212780046103
License date	Oct 19, 2017
Licensed Content Publisher	John Wiley and Sons
Licensed Content Publication	Developmental Neurobiology
Licensed Content Title	Behavioral and synaptic defects in C. elegans lacking the NK-2 homeobox gene ceh-28
Licensed Content Author	Paramita Ray,Ralf Schnabel,Peter G. Okkema
Licensed Content Date	Dec 27, 2007
Licensed Content Pages	13
Type of use	Dissertation/Thesis
Requestor type	University/Academic
Format	Electronic
Portion	Figure/table
Number of figures/tables	3
Original Wiley figure/table number(s)	Figure 1, Figure 4, Figure 7
Will you be translating?	No
Title of your thesis / dissertation	Characterization of neuromuscular communications in the C.elegans pharynx during feeding
Expected completion date	Dec 2017
Expected size (number of pages)	1
Requestor Location	Alena Kozlova University of Illinois Biological Sciences 900 S. Ashland Avenue Chicago, IL 60607 United States Attn:
Publisher Tax ID	EU826007151
Billing Type	Invoice
Billing Address	Alena Kozlova University of Illinois Biological Sciences

900 S. Ashland Avenue
Chicago, IL 60607
United States
Attn: Alena Kozlova

Total 0.00 USD

Terms and Conditions

TERMS AND CONDITIONS

This copyrighted material is owned by or exclusively licensed to John Wiley & Sons, Inc. or one of its group companies (each a"Wiley Company") or handled on behalf of a society with which a Wiley Company has exclusive publishing rights in relation to a particular work (collectively "WILEY"). By clicking "accept" in connection with completing this licensing transaction, you agree that the following terms and conditions apply to this transaction (along with the billing and payment terms and conditions established by the Copyright Clearance Center Inc., ("CCC's Billing and Payment terms and conditions"), at the time that you opened your RightsLink account (these are available at any time at http://myaccount.copyright.com).

Terms and Conditions

- The materials you have requested permission to reproduce or reuse (the "Wiley Materials") are protected by copyright.

- You are hereby granted a personal, non-exclusive, non-sub licensable (on a stand-alone basis), non-transferable, worldwide, limited license to reproduce the Wiley Materials for the purpose specified in the licensing process. This license, **and any CONTENT (PDF or image file) purchased as part of your order,** is for a one-time use only and limited to any maximum distribution number specified in the license. The first instance of republication or reuse granted by this license must be completed within two years of the date of the grant of this license (although copies prepared before the end date may be distributed thereafter). The Wiley Materials shall not be used in any other manner or for any other purpose, beyond what is granted in the license. Permission is granted subject to an appropriate acknowledgement given to the author, title of the material/book/journal and the publisher. You shall also duplicate the copyright notice that appears in the Wiley publication in your use of the Wiley Material. Permission is also granted on the understanding that nowhere in the text is a previously published source acknowledged for all or part of this Wiley Material. Any third party content is expressly excluded from this permission.

- With respect to the Wiley Materials, all rights are reserved. Except as expressly granted by the terms of the license, no part of the Wiley Materials may be copied, modified, adapted (except for minor reformatting required by the new Publication), translated, reproduced, transferred or distributed, in any form or by any means, and no derivative works may be made based on the Wiley Materials without the prior permission of the respective copyright owner.**For STM Signatory Publishers clearing permission under the terms of the STM Permissions Guidelines only, the**

terms of the license are extended to include subsequent editions and for editions in other languages, provided such editions are for the work as a whole in situ and does not involve the separate exploitation of the permitted figures or extracts, You may not alter, remove or suppress in any manner any copyright, trademark or other notices displayed by the Wiley Materials. You may not license, rent, sell, loan, lease, pledge, offer as security, transfer or assign the Wiley Materials on a stand-alone basis, or any of the rights granted to you hereunder to any other person.

- The Wiley Materials and all of the intellectual property rights therein shall at all times remain the exclusive property of John Wiley & Sons Inc, the Wiley Companies, or their respective licensors, and your interest therein is only that of having possession of and the right to reproduce the Wiley Materials pursuant to Section 2 herein during the continuance of this Agreement. You agree that you own no right, title or interest in or to the Wiley Materials or any of the intellectual property rights therein. You shall have no rights hereunder other than the license as provided for above in Section 2. No right, license or interest to any trademark, trade name, service mark or other branding ("Marks") of WILEY or its licensors is granted hereunder, and you agree that you shall not assert any such right, license or interest with respect thereto

- NEITHER WILEY NOR ITS LICENSORS MAKES ANY WARRANTY OR REPRESENTATION OF ANY KIND TO YOU OR ANY THIRD PARTY, EXPRESS, IMPLIED OR STATUTORY, WITH RESPECT TO THE MATERIALS OR THE ACCURACY OF ANY INFORMATION CONTAINED IN THE MATERIALS, INCLUDING, WITHOUT LIMITATION, ANY IMPLIED WARRANTY OF MERCHANTABILITY, ACCURACY, SATISFACTORY QUALITY, FITNESS FOR A PARTICULAR PURPOSE, USABILITY, INTEGRATION OR NON-INFRINGEMENT AND ALL SUCH WARRANTIES ARE HEREBY EXCLUDED BY WILEY AND ITS LICENSORS AND WAIVED BY YOU.

- WILEY shall have the right to terminate this Agreement immediately upon breach of this Agreement by you.

- You shall indemnify, defend and hold harmless WILEY, its Licensors and their respective directors, officers, agents and employees, from and against any actual or threatened claims, demands, causes of action or proceedings arising from any breach of this Agreement by you.

- IN NO EVENT SHALL WILEY OR ITS LICENSORS BE LIABLE TO YOU OR ANY OTHER PARTY OR ANY OTHER PERSON OR ENTITY FOR ANY SPECIAL, CONSEQUENTIAL, INCIDENTAL, INDIRECT, EXEMPLARY OR PUNITIVE DAMAGES, HOWEVER CAUSED, ARISING OUT OF OR IN CONNECTION WITH THE DOWNLOADING, PROVISIONING, VIEWING OR USE OF THE MATERIALS REGARDLESS OF THE FORM OF ACTION, WHETHER FOR BREACH OF CONTRACT, BREACH OF WARRANTY, TORT, NEGLIGENCE, INFRINGEMENT OR OTHERWISE (INCLUDING, WITHOUT LIMITATION, DAMAGES BASED ON LOSS OF PROFITS, DATA, FILES, USE, BUSINESS OPPORTUNITY OR CLAIMS OF THIRD PARTIES), AND WHETHER

OR NOT THE PARTY HAS BEEN ADVISED OF THE POSSIBILITY OF SUCH DAMAGES. THIS LIMITATION SHALL APPLY NOTWITHSTANDING ANY FAILURE OF ESSENTIAL PURPOSE OF ANY LIMITED REMEDY PROVIDED HEREIN.

- Should any provision of this Agreement be held by a court of competent jurisdiction to be illegal, invalid, or unenforceable, that provision shall be deemed amended to achieve as nearly as possible the same economic effect as the original provision, and the legality, validity and enforceability of the remaining provisions of this Agreement shall not be affected or impaired thereby.

- The failure of either party to enforce any term or condition of this Agreement shall not constitute a waiver of either party's right to enforce each and every term and condition of this Agreement. No breach under this agreement shall be deemed waived or excused by either party unless such waiver or consent is in writing signed by the party granting such waiver or consent. The waiver by or consent of a party to a breach of any provision of this Agreement shall not operate or be construed as a waiver of or consent to any other or subsequent breach by such other party.

- This Agreement may not be assigned (including by operation of law or otherwise) by you without WILEY's prior written consent.

- Any fee required for this permission shall be non-refundable after thirty (30) days from receipt by the CCC.

- These terms and conditions together with CCC's Billing and Payment terms and conditions (which are incorporated herein) form the entire agreement between you and WILEY concerning this licensing transaction and (in the absence of fraud) supersedes all prior agreements and representations of the parties, oral or written. This Agreement may not be amended except in writing signed by both parties. This Agreement shall be binding upon and inure to the benefit of the parties' successors, legal representatives, and authorized assigns.

- In the event of any conflict between your obligations established by these terms and conditions and those established by CCC's Billing and Payment terms and conditions, these terms and conditions shall prevail.

- WILEY expressly reserves all rights not specifically granted in the combination of (i) the license details provided by you and accepted in the course of this licensing transaction, (ii) these terms and conditions and (iii) CCC's Billing and Payment terms and conditions.

- This Agreement will be void if the Type of Use, Format, Circulation, or Requestor Type was misrepresented during the licensing process.

- This Agreement shall be governed by and construed in accordance with the laws of the State of New York, USA, without regards to such state's conflict of law rules. Any legal action, suit or proceeding arising out of or relating to these Terms and Conditions

JOHN WILEY AND SONS LICENSE TERMS AND CONDITIONS

Oct 19, 2017

This Agreement between Alena Kozlova ("You") and John Wiley and Sons ("John Wiley and Sons") consists of your license details and the terms and conditions provided by John Wiley and Sons and Copyright Clearance Center.

License Number	4212781022961
License date	Oct 19, 2017
Licensed Content Publisher	John Wiley and Sons
Licensed Content Publication	FEBS Journal
Licensed Content Title	Muscle and neuronal nicotinic acetylcholine receptors
Licensed Content Author	Dimitra Kalamida,Konstantinos Poulas,Vassiliki Avramopoulou,Efrosini Fostieri,George Lagoumintzis,Konstantinos Lazaridis,Anastasia Sideri,Marios Zouridakis,Socrates J. Tzartos
Licensed Content Date	Jul 19, 2007
Licensed Content Pages	47
Type of use	Dissertation/Thesis
Requestor type	University/Academic
Format	Electronic
Portion	Figure/table
Number of figures/tables	1
Original Wiley figure/table number(s)	Figure 1
Will you be translating?	No
Title of your thesis / dissertation	Characterization of neuromuscular communications in the C.elegans pharynx during feeding
Expected completion date	Dec 2017
Expected size (number of pages)	1
Requestor Location	Alena Kozlova University of Illinois Biological Sciences 900 S. Ashland Avenue Chicago, IL 60607 United States Attn:
Publisher Tax ID	EU826007151
Billing Type	Invoice

Print This Page

» Copyright

Login

In this section

- Cost of Publication
- Authorship Changes
- Manuscript Formatting Requirements
- Manuscript Composition
- Preparing Figures
- Experimental Details to Report in Your Manuscript
- Data Repository Standards
- Data Supplements
- Special Instructions for Physiological Reviews
- Special Instructions for Physiology in Medicine
- Peer Review Policy
- Special Instructions for Advances in Physiology Education
- Promoting Transparent Reporting in APS Publications to Enhance Data Reproducibility
- Open Access
- Policy on Depositing Articles in PMC
- Copyright
- Permissions
- Policy on Use of Previously Published Data in Illustrations
- APS Ethics Policy
- Human Fetuses, Fetal Tissue, Embryos, and Embryonic Cells
- Guiding Principles for

Copyright

The APS Journals are copyrighted for the protection of authors and the Soc as the Society's official copyright transfer form.

Rights of Authors of APS Articles

- For educational purposes only:
  - Authors may republish parts of their final-published version articles and without requesting permission, provided that full acknowledger work.
  - Authors may use their articles (in whole or in part) for presentations These presentations may be reproduced on any type of media in n conference such as the proceedings of a meeting or conference. A charge to the user or if the materials arising are directly or indirectl

Research Involving Animals and Human Beings
Ethics Posters

Information For...

Advertising / Marketing
Advocacy and Outreach
Authors
Chapters
Committees
Early Career Professionals
Graduate/Professional Students
Groups
K-12 Education
Minority Scientists
Postdoctoral Fellows
Public / Press
Sections
Subscription / Help Information
Undergraduate Students

- Posting of the accepted or final version of articles or parts of articles is
below:
  - ***Theses and dissertations.*** APS permits whole published articles
dissertations and posted to thesis repositories. Full citation is requi
  - ***Open courseware.*** Articles, or parts of articles, may be posted to
Permission must be requested from the APS. A copyright fee will a
article's publication by the APS. Full citation is required.
  - ***Websites.*** Authors may not post a PDF of the accepted or final ver
website including social and research networking platforms; instea
the APS journal website (see exception to authors' own institution's
  - ***Institutional repositories (non-theses).*** Authors may deposit thei
into an institutional repository providing:
    - the APS retains copyright to the article[1]
    - a 12 month embargo period from the date of final publication o
institutional repository and the author
    - a link to the published article on the APS website is prominentl
institutional repository
    - the article is not used for commercial purposes
    - Self-archived articles posted to repositories are without warran

[1]Unless it is published under the APS *AuthorChoice* open access
public access under a Creative Commons license (CC BY)

(See also the APS Policy on Depositing Articles in PMC.)

9650 Rockville Pike | Bethesda, MD | 20814-3991 | +1 (301) 634-7164 | Fax: 301.634.7241 Privacy Po

Copyright Clearance Center

Note: Copyright.com supplies permissions but not the copyrighted content itself.

1 PAYMENT 2 REVIEW 3 CONFIRMATION

Step 3: Order Confirmation

Thank you for your order! A confirmation for your order will be sent to your account email address. If you have questions about your order, you can call us 24 hrs/day, M-F at +1.855.239.3415 Toll Free, or write to us at info@copyright.com. This is not an invoice.

Confirmation Number: 11674484
Order Date: 10/06/2017

If you paid by credit card, your order will be finalized and your card will be charged within 24 hours. If you choose to be invoiced, you can change or cancel your order until the invoice is generated.

Payment Information

Alena Kozlova
akozlo7@uic.edu
+1 (312) 996-9111
Payment Method: n/a

Order Details

The journal of neuroscience : the official journal of the Society for Neuroscience

Order detail ID:	70736901
Order License Id:	4203141442191
ISSN:	1529-2401
Publication Type:	e-Journal
Volume:	
Issue:	
Start page:	
Publisher:	SOCIETY FOR NEUROSCIENCE
Author/Editor:	Society for Neuroscience

Permission Status:	Granted
Permission type:	Republish or display content
Type of use:	Republish in a thesis/dissertation
Requestor type	Academic institution
Format	Print
Portion	image/photo
Number of images/photos requested	1
The requesting person/organization	Alena Kozlova
Title or numeric reference of the portion(s)	Figure 5
Title of the article or chapter the portion is from	Mutations in the Caenorhabditis elegans Na,K-ATPase alpha-subunit gene, eat-6, disrupt

Note: This item will be invoiced or charged separately through CCC's **RightsLink** service. More info **$ 0.00**

Confirmation Number: 11674484

Special Rightsholder Terms & Conditions

The following terms & conditions apply to the specific publication under which they are listed

The journal of neuroscience : the official journal of the Society for Neuroscience
Permission type: Republish or display content
Type of use: Republish in a thesis/dissertation

TERMS AND CONDITIONS

The following terms are individual to this publisher:

None

Other Terms and Conditions:

STANDARD TERMS AND CONDITIONS

1. Description of Service; Defined Terms. This Republication License enables the User to obtain licenses for republication of one or more copyrighted works as described in detail on the relevant Order Confirmation (the "Work(s)"). Copyright Clearance Center, Inc. ("CCC") grants licenses through the Service on behalf of the rightsholder identified on the Order Confirmation (the "Rightsholder"). "Republication", as used herein, generally means the inclusion of a Work, in whole or in part, in a new work or works, also as described on the Order Confirmation. "User", as used herein, means the person or entity making such republication.

2. The terms set forth in the relevant Order Confirmation, and any terms set by the Rightsholder with respect to a particular Work, govern the terms of use of Works in connection with the Service. By using the Service, the person transacting for a republication license on behalf of the User represents and warrants that he/she/it (a) has been duly authorized by the User to accept, and hereby does accept, all such terms and conditions on behalf of User, and (b) shall inform User of all such terms and conditions. In the event such person is a "freelancer" or other third party independent of User and CCC, such party shall be deemed jointly a "User" for purposes of these terms and conditions. In any event, User shall be deemed to have accepted and agreed to all such terms and conditions if User republishes the Work in any fashion.

3. Scope of License; Limitations and Obligations.

3.1 All Works and all rights therein, including copyright rights, remain the sole and exclusive property of the Rightsholder. The license created by the exchange of an Order Confirmation (and/or any invoice) and payment by User of the full amount set forth on that document includes only those rights expressly set forth in the Order Confirmation and in these terms and conditions, and conveys no other rights in the Work(s) to User. All rights not expressly granted are hereby reserved.

3.2 General Payment Terms: You may pay by credit card or through an account with us payable at the end of the month. If you and we agree that you may establish a standing account with CCC, then the following terms apply: Remit Payment to: Copyright Clearance Center, 29118 Network Place, Chicago, IL 60673-1291. Payments Due: Invoices are payable upon their delivery to you (or upon our notice to you that they are available to you for downloading). After 30 days, outstanding amounts will be subject to a service charge of 1-1/2% per month or, if less, the maximum rate allowed by applicable law. Unless otherwise specifically set forth in the Order Confirmation or in a separate written agreement signed by CCC, invoices are due and payable on "net 30" terms. While User may exercise the rights licensed immediately upon issuance of the Order Confirmation, the license is automatically revoked and is null and void, as if it had never been issued, if complete payment for the license is not received on a timely basis either from User directly or through a payment agent, such as a credit card company.

3.3 Unless otherwise provided in the Order Confirmation, any grant of rights to User (i) is "one-time" (including the editions and product family specified in the license), (ii) is non-exclusive and non-transferable and (iii) is subject to any and all limitations and restrictions (such as, but not limited to, limitations on duration of use or circulation) included in the Order Confirmation or invoice and/or in these terms and conditions. Upon completion of the licensed use, User shall either secure a new permission for further use of the Work(s) or immediately cease any new use of the Work(s) and shall render inaccessible (such as by deleting or by removing or severing links or other locators) any further copies of the Work (except for copies printed on paper in accordance with this license and still in User's stock at the end of such period).

3.4 In the event that the material for which a republication license is sought includes third party materials (such as photographs, illustrations, graphs, inserts and similar materials) which are identified in such material as having been used by permission, User is responsible for identifying, and seeking separate licenses (under this Service or otherwise)

for, any of such third party materials; without a separate license, such third party materials may not be used.

3.5 Use of proper copyright notice for a Work is required as a condition of any license granted under the Service. Unless otherwise provided in the Order Confirmation, a proper copyright notice will read substantially as follows: "Republished with permission of [Rightsholder's name], from [Work's title, author, volume, edition number and year of copyright]; permission conveyed through Copyright Clearance Center, Inc. " Such notice must be provided in a reasonably legible font size and must be placed either immediately adjacent to the Work as used (for example, as part of a by-line or footnote but not as a separate electronic link) or in the place where substantially all other credits or notices for the new work containing the republished Work are located. Failure to include the required notice results in loss to the Rightsholder and CCC, and the User shall be liable to pay liquidated damages for each such failure equal to twice the use fee specified in the Order Confirmation, in addition to the use fee itself and any other fees and charges specified.

3.6 User may only make alterations to the Work if and as expressly set forth in the Order Confirmation. No Work may be used in any way that is defamatory, violates the rights of third parties (including such third parties' rights of copyright, privacy, publicity, or other tangible or intangible property), or is otherwise illegal, sexually explicit or obscene. In addition, User may not conjoin a Work with any other material that may result in damage to the reputation of the Rightsholder. User agrees to inform CCC if it becomes aware of any infringement of any rights in a Work and to cooperate with any reasonable request of CCC or the Rightsholder in connection therewith.

4. Indemnity. User hereby indemnifies and agrees to defend the Rightsholder and CCC, and their respective employees and directors, against all claims, liability, damages, costs and expenses, including legal fees and expenses, arising out of any use of a Work beyond the scope of the rights granted herein, or any use of a Work which has been altered in any unauthorized way by User, including claims of defamation or infringement of rights of copyright, publicity, privacy or other tangible or intangible property.

5. Limitation of Liability. UNDER NO CIRCUMSTANCES WILL CCC OR THE RIGHTSHOLDER BE LIABLE FOR ANY DIRECT, INDIRECT, CONSEQUENTIAL OR INCIDENTAL DAMAGES (INCLUDING WITHOUT LIMITATION DAMAGES FOR LOSS OF BUSINESS PROFITS OR INFORMATION, OR FOR BUSINESS INTERRUPTION) ARISING OUT OF THE USE OR INABILITY TO USE A WORK, EVEN IF ONE OF THEM HAS BEEN ADVISED OF THE POSSIBILITY OF SUCH DAMAGES. In any event, the total liability of the Rightsholder and CCC (including their respective employees and directors) shall not exceed the total amount actually paid by User for this license. User assumes full liability for the actions and omissions of its principals, employees, agents, affiliates, successors and assigns.

6. Limited Warranties. THE WORK(S) AND RIGHT(S) ARE PROVIDED "AS IS". CCC HAS THE RIGHT TO GRANT TO USER THE RIGHTS GRANTED IN THE ORDER CONFIRMATION DOCUMENT. CCC AND THE RIGHTSHOLDER DISCLAIM ALL OTHER WARRANTIES RELATING TO THE WORK(S) AND RIGHT(S), EITHER EXPRESS OR IMPLIED, INCLUDING WITHOUT LIMITATION IMPLIED WARRANTIES OF MERCHANTABILITY OR FITNESS FOR A PARTICULAR PURPOSE. ADDITIONAL RIGHTS MAY BE REQUIRED TO USE ILLUSTRATIONS, GRAPHS, PHOTOGRAPHS, ABSTRACTS, INSERTS OR OTHER PORTIONS OF THE WORK (AS OPPOSED TO THE ENTIRE WORK) IN A MANNER CONTEMPLATED BY USER; USER UNDERSTANDS AND AGREES THAT NEITHER CCC NOR THE RIGHTSHOLDER MAY HAVE SUCH ADDITIONAL RIGHTS TO GRANT.

7. Effect of Breach. Any failure by User to pay any amount when due, or any use by User of a Work beyond the scope of the license set forth in the Order Confirmation and/or these terms and conditions, shall be a material breach of the license created by the Order Confirmation and these terms and conditions. Any breach not cured within 30 days of written notice thereof shall result in immediate termination of such license without further notice. Any unauthorized (but licensable) use of a Work that is terminated immediately upon notice thereof may be liquidated by payment of the Rightsholder's ordinary license price therefor; any unauthorized (and unlicensable) use that is not terminated immediately for any reason (including, for example, because materials containing the Work cannot reasonably be recalled) will be subject to all remedies available at law or in equity, but in no event to a payment of less than three times the Rightsholder's ordinary license price for the most closely analogous licensable use plus Rightsholder's and/or CCC's costs and expenses incurred in collecting such payment.

8. **Miscellaneous.**

8.1 User acknowledges that CCC may, from time to time, make changes or additions to the Service or to these terms and conditions, and CCC reserves the right to send notice to the User by electronic mail or otherwise for the purposes of notifying User of such changes or additions; provided that any such changes or additions shall not apply to permissions already secured and paid for.

8.2 Use of User-related information collected through the Service is governed by CCC's privacy policy, available online here: http://www.copyright.com/content/cc3/en/tools/footer/privacypolicy.html.

8.3 The licensing transaction described in the Order Confirmation is personal to User. Therefore, User may not assign or transfer to any other person (whether a natural person or an organization of any kind) the license created by the Order Confirmation and these terms and conditions or any rights granted hereunder; provided, however, that User may assign such license in its entirety on written notice to CCC in the event of a transfer of all or substantially all of User's rights in the new material which includes the Work(s) licensed under this Service.

8.4 No amendment or waiver of any terms is binding unless set forth in writing and signed by the parties. The Rightsholder and CCC hereby object to any terms contained in any writing prepared by the User or its principals, employees, agents or affiliates and purporting to govern or otherwise relate to the licensing transaction described in the

Order Confirmation, which terms are in any way inconsistent with any terms set forth in the Order Confirmation and/or in these terms and conditions or CCC's standard operating procedures, whether such writing is prepared prior to, simultaneously with or subsequent to the Order Confirmation, and whether such writing appears on a copy of the Order Confirmation or in a separate instrument.

8.5 The licensing transaction described in the Order Confirmation document shall be governed by and construed under the law of the State of New York, USA, without regard to the principles thereof of conflicts of law. Any case, controversy, suit, action, or proceeding arising out of, in connection with, or related to such licensing transaction shall be brought, at CCC's sole discretion, in any federal or state court located in the County of New York, State of New York, USA, or in any federal or state court whose geographical jurisdiction covers the location of the Rightsholder set forth in the Order Confirmation. The parties expressly submit to the personal jurisdiction and venue of each such federal or state court.If you have any comments or questions about the Service or Copyright Clearance Center, please contact us at 978-750-8400 or send an e-mail to info@copyright.com.

v 1.1

Confirmation Number: 11674484

Citation Information

Order Detail ID: 70736901

The journal of neuroscience : the official journal of the Society for Neuroscience by Society for Neuroscience Reproduced with permission of SOCIETY FOR NEUROSCIENCE in the format Republish in a thesis/dissertation via Copyright Clearance Center.

CITED LITERATURE

Adams, D.J., Nutter, T.J., 1992. Calcium permeability and modulation of nicotinic acetylcholine receptor-channels in rat parasympathetic neurons. J Physiol Paris 86, 67-76.

Akerboom, J., Carreras Calderon, N., Tian, L., Wabnig, S., Prigge, M., Tolo, J., Gordus, A., Orger, M.B., Severi, K.E., Macklin, J.J., Patel, R., Pulver, S.R., Wardill, T.J., Fischer, E., Schuler, C., Chen, T.W., Sarkisyan, K.S., Marvin, J.S., Bargmann, C.I., Kim, D.S., Kugler, S., Lagnado, L., Hegemann, P., Gottschalk, A., Schreiter, E.R., Looger, L.L., 2013. Genetically encoded calcium indicators for multi-color neural activity imaging and combination with optogenetics. Front Mol Neurosci 6, 2.

Akerboom, J., Rivera, J.D., Guilbe, M.M., Malave, E.C., Hernandez, H.H., Tian, L., Hires, S.A., Marvin, J.S., Looger, L.L., Schreiter, E.R., 2009. Crystal structures of the GCaMP calcium sensor reveal the mechanism of fluorescence signal change and aid rational design. J Biol Chem 284, 6455-6464.

Albertson, D.G., Thomson, J.N., 1976. The pharynx of Caenorhabditis elegans. Philos Trans R Soc Lond B Biol Sci 275, 299-325.

Albuquerque, E.X., Pereira, E.F., Alkondon, M., Rogers, S.W., 2009. Mammalian nicotinic acetylcholine receptors: from structure to function. Physiol Rev 89, 73-120.

Albuquerque, E.X., Pereira, E.F., Castro, N.G., Alkondon, M., Reinhardt, S., Schroder, H., Maelicke, A., 1995. Nicotinic receptor function in the mammalian central nervous system. Ann N Y Acad Sci 757, 48-72.

Alfonso, A., Grundahl, K., Duerr, J.S., Han, H.P., Rand, J.B., 1993. The Caenorhabditis elegans unc-17 gene: a putative vesicular acetylcholine transporter. Science 261, 617-619.

Altun, Z.F., Chen, B., Wang, Z.W., Hall, D.H., 2009. High resolution map of Caenorhabditis elegans gap junction proteins. Dev Dyn 238, 1936-1950.

Anders, S., McCarthy, D.J., Chen, Y., Okoniewski, M., Smyth, G.K., Huber, W., Robinson, M.D., 2013. Count-based differential expression analysis of RNA sequencing data using R and Bioconductor. Nat Protoc 8, 1765-1786.

Anders, S., Pyl, P.T., Huber, W., 2015. HTSeq--a Python framework to work with high-throughput sequencing data. Bioinformatics 31, 166-169.

Araya, R., Noguchi, T., Yuhki, M., Kitamura, N., Higuchi, M., Saido, T.C., Seki, K., Itohara, S., Kawano, M., Tanemura, K., Takashima, A., Yamada, K., Kondoh, Y., Kanno, I., Wess, J., Yamada, M., 2006. Loss of M5 muscarinic acetylcholine receptors leads to cerebrovascular and neuronal abnormalities and cognitive deficits in mice. Neurobiol Dis 24, 334-344.

Ardiel, E.L., Rankin, C.H., 2010. An elegant mind: learning and memory in Caenorhabditis elegans. Learn Mem 17, 191-201.

Armstrong, C.M., Hille, B., 1998. Voltage-gated ion channels and electrical excitability. Neuron 20, 371-380.

Augustine, G.J., Charlton, M.P., Smith, S.J., 1987. Calcium action in synaptic transmitter release. Annu Rev Neurosci 10, 633-693.

Ausubel, F.M., 1990. Current protocols in molecular biology. Greene Pub. Associates and Wiley-Interscience : J. Wiley, New York.

Avery, L., 1993a. The genetics of feeding in Caenorhabditis elegans. Genetics 133, 897-917.

Avery, L., 1993b. Motor neuron M3 controls pharyngeal muscle relaxation timing in Caenorhabditis elegans. J Exp Biol 175, 283-297.

Avery, L., Horvitz, H.R., 1987. A cell that dies during wild-type C. elegans development can function as a neuron in a ced-3 mutant. Cell 51, 1071-1078.

Avery, L., Horvitz, H.R., 1989. Pharyngeal pumping continues after laser killing of the pharyngeal nervous system of C. elegans. Neuron 3, 473-485.

Avery, L., Horvitz, H.R., 1990. Effects of starvation and neuroactive drugs on feeding in Caenorhabditis elegans. J Exp Zool 253, 263-270.
Avery, L., Raizen, D., Lockery, S., 1995. Electrophysiological methods. Methods Cell Biol 48, 251-269.
Avery, L., Shtonda, B.B., 2003. Food transport in the C. elegans pharynx. J Exp Biol 206, 2441-2457.
Avery, L., Thomas, J.H., 1997. Feeding and Defecation, in: Riddle, D.L., Blumenthal, T., Meyer, B.J., Priess, J.R. (Eds.), C. elegans II. Cold Spring Harbor Laboratory Press, Cold Spring Harbor, NY, p. 679716.
Avery, L., You, Y.J., 2012. C. elegans feeding. WormBook : the online review of C. elegans biology, 1-23.
Bargmann, C.I., 1998. Neurobiology of the Caenorhabditis elegans genome. Science 282, 2028-2033.
Bargmann, C.I., 2006. Chemosensation in C. elegans. WormBook : the online review of C. elegans biology, 1-29.
Beaster-Jones, L., Okkema, P.G., 2004. DNA binding and in vivo function of C. elegans PEB-1 require a conserved FLYWCH motif. J Mol Biol 339, 695-706.
Beker, F., Weber, M., Fink, R.H., Adams, D.J., 2003. Muscarinic and nicotinic ACh receptor activation differentially mobilize Ca2+ in rat intracardiac ganglion neurons. J Neurophysiol 90, 1956-1964.
Berchtold, M.W., Brinkmeier, H., Muntener, M., 2000. Calcium ion in skeletal muscle: its crucial role for muscle function, plasticity, and disease. Physiol Rev 80, 1215-1265.
Bergamasco, C., Bazzicalupo, P., 2006. Chemical sensitivity in Caenorhabditis elegans. Cellular and molecular life sciences : CMLS 63, 1510-1522.
Bers, D.M., 2002. Cardiac excitation-contraction coupling. Nature 415, 198-205.
Brenner, S., 1974. The genetics of Caenorhabditis elegans. Genetics 77, 71-94.
Brodde, O.E., Michel, M.C., 1999. Adrenergic and muscarinic receptors in the human heart. Pharmacol Rev 51, 651-690.
Burdine, R.D., Branda, C.S., Stern, M.J., 1998. EGL-17(FGF) expression coordinates the attraction of the migrating sex myoblasts with vulval induction in C. elegans. Development 125, 1083-1093.
Burgoyne, R.D., 2007. Neuronal calcium sensor proteins: generating diversity in neuronal Ca2+ signalling. Nat Rev Neurosci 8, 182-193.
Cappelletti, G., Surrey, T., Maci, R., 2005. The parkinsonism producing neurotoxin MPP+ affects microtubule dynamics by acting as a destabilising factor. FEBS Lett 579, 4781-4786.
Cartelli, D., Casagrande, F., Busceti, C.L., Bucci, D., Molinaro, G., Traficante, A., Passarella, D., Giavini, E., Pezzoli, G., Battaglia, G., Cappelletti, G., 2013. Microtubule alterations occur early in experimental parkinsonism and the microtubule stabilizer epothilone D is neuroprotective. Sci Rep 3, 1837.
Castro, N.G., Albuquerque, E.X., 1995. alpha-Bungarotoxin-sensitive hippocampal nicotinic receptor channel has a high calcium permeability. Biophys J 68, 516-524.
Catterall, W.A., 2000. Structure and regulation of voltage-gated Ca2+ channels. Annual review of cell and developmental biology 16, 521-555.
Caulfield, M.P., 1993. Muscarinic receptors--characterization, coupling and function. Pharmacol Ther 58, 319-379.
Caulfield, M.P., Birdsall, N.J., 1998. International Union of Pharmacology. XVII. Classification of muscarinic acetylcholine receptors. Pharmacol Rev 50, 279-290.

Chakrapani, B.P., Kumar, S., Subramaniam, J.R., 2008. Development and evaluation of an in vivo assay in Caenorhabditis elegans for screening of compounds for their effect on cytochrome P450 expression. J Biosci 33, 269-277.

Chalasani, S.H., Chronis, N., Tsunozaki, M., Gray, J.M., Ramot, D., Goodman, M.B., Bargmann, C.I., 2007. Dissecting a circuit for olfactory behaviour in Caenorhabditis elegans. Nature 450, 63-70.

Chan, J.P., Staab, T.A., Wang, H., Mazzasette, C., Butte, Z., Sieburth, D., 2013. Extrasynaptic muscarinic acetylcholine receptors on neuronal cell bodies regulate presynaptic function in Caenorhabditis elegans. J Neurosci 33, 14146-14159.

Changeux, J., Edelstein, S.J., 2001. Allosteric mechanisms in normal and pathological nicotinic acetylcholine receptors. Curr Opin Neurobiol 11, 369-377.

Chen, B.L., Hall, D.H., Chklovskii, D.B., 2006. Wiring optimization can relate neuronal structure and function. Proc Natl Acad Sci U S A 103, 4723-4728.

Chen, T.W., Wardill, T.J., Sun, Y., Pulver, S.R., Renninger, S.L., Baohan, A., Schreiter, E.R., Kerr, R.A., Orger, M.B., Jayaraman, V., Looger, L.L., Svoboda, K., Kim, D.S., 2013. Ultrasensitive fluorescent proteins for imaging neuronal activity. Nature 499, 295-300.

Chen, X., Chalfie, M., 2014. Modulation of C. elegans Touch Sensitivity Is Integrated at Multiple Levels. J Neurosci 34, 6522-6536.

Chiang, J.T., Steciuk, M., Shtonda, B., Avery, L., 2006. Evolution of pharyngeal behaviors and neuronal functions in free-living soil nematodes. J Exp Biol 209, 1859-1873.

Chuang, C.F., Vanhoven, M.K., Fetter, R.D., Verselis, V.K., Bargmann, C.I., 2007. An innexin-dependent cell network establishes left-right neuronal asymmetry in C. elegans. Cell 129, 787-799.

Combes, D., Fedon, Y., Grauso, M., Toutant, J.P., Arpagaus, M., 2000. Four genes encode acetylcholinesterases in the nematodes Caenorhabditis elegans and Caenorhabditis briggsae. cDNA sequences, genomic structures, mutations and in vivo expression. J Mol Biol 300, 727-742.

Consortium, C.e.D.M., 2012. large-scale screening for targeted knockouts in the Caenorhabditis elegans genome. G3 (Bethesda) 2, 1415-1425.

Conti-Fine, B.M., Milani, M., Kaminski, H.J., 2006. Myasthenia gravis: past, present, and future. J Clin Invest 116, 2843-2854.

Culetto, E., Combes, D., Fedon, Y., Roig, A., Toutant, J.P., Arpagaus, M., 1999. Structure and promoter activity of the 5' flanking region of ace-1, the gene encoding acetylcholinesterase of class A in Caenorhabditis elegans. J Mol Biol 290, 951-966.

Dajas-Bailador, F.A., Mogg, A.J., Wonnacott, S., 2002. Intracellular Ca2+ signals evoked by stimulation of nicotinic acetylcholine receptors in SH-SY5Y cells: contribution of voltage-operated Ca2+ channels and Ca2+ stores. Journal of neurochemistry 81, 606-614.

Dani, J.A., Bertrand, D., 2007. Nicotinic acetylcholine receptors and nicotinic cholinergic mechanisms of the central nervous system. Annu Rev Pharmacol Toxicol 47, 699-729.

Davis, M.W., Fleischhauer, R., Dent, J.A., Joho, R.H., Avery, L., 1999. A mutation in the C. elegans EXP-2 potassium channel that alters feeding behavior. Science 286, 2501-2504.

Davis, M.W., Somerville, D., Lee, R.Y., Lockery, S., Avery, L., Fambrough, D.M., 1995. Mutations in the Caenorhabditis elegans Na,K-ATPase alpha-subunit gene, eat-6, disrupt excitable cell function. J Neurosci 15, 8408-8418.

de Bono, M., Maricq, A.V., 2005. Neuronal substrates of complex behaviors in C. elegans. Annu Rev Neurosci 28, 451-501.

Dennis, M., Giraudat, J., Kotzyba-Hibert, F., Goeldner, M., Hirth, C., Chang, J.Y., Lazure, C., Chretien, M., Changeux, J.P., 1988. Amino acids of the Torpedo marmorata acetylcholine receptor alpha subunit labeled by a photoaffinity ligand for the acetylcholine binding site. Biochemistry 27, 2346-2357.

Dent, J.A., Davis, M.W., Avery, L., 1997. avr-15 encodes a chloride channel subunit that mediates inhibitory glutamatergic neurotransmission and ivermectin sensitivity in Caenorhabditis elegans. EMBO J 16, 5867-5879.
Diamond, J.S., 2002. A broad view of glutamate spillover. Nature neuroscience 5, 291-292.
Dittman, J.S., Kaplan, J.M., 2008. Behavioral impact of neurotransmitter-activated G-protein-coupled receptors: muscarinic and GABAB receptors regulate Caenorhabditis elegans locomotion. J Neurosci 28, 7104-7112.
Dodge, F.A., Jr., Rahamimoff, R., 1967. Co-operative action a calcium ions in transmitter release at the neuromuscular junction. J Physiol 193, 419-432.
Doncaster, C.C., 1962. Nematode feeding mechanisms. I. Observations of Rhabditis and Pelodera. Nematologica 8, 313-320.
Doyle, D.A., Morais Cabral, J., Pfuetzner, R.A., Kuo, A., Gulbis, J.M., Cohen, S.L., Chait, B.T., MacKinnon, R., 1998. The structure of the potassium channel: molecular basis of K+ conduction and selectivity. Science 280, 69-77.
Duerr, J.S., Han, H.P., Fields, S.D., Rand, J.B., 2008. Identification of major classes of cholinergic neurons in the nematode Caenorhabditis elegans. The Journal of comparative neurology 506, 398-408.
Duman, R.S., Aghajanian, G.K., 2012. Synaptic dysfunction in depression: potential therapeutic targets. Science 338, 68-72.
Dunlap, K., Luebke, J.I., Turner, T.J., 1995. Exocytotic Ca2+ channels in mammalian central neurons. Trends Neurosci 18, 89-98.
Dutar, P., Nicoll, R.A., 1988. Classification of muscarinic responses in hippocampus in terms of receptor subtypes and second-messenger systems: electrophysiological studies in vitro. J Neurosci 8, 4214-4224.
Eglen, R.M., 2005. Muscarinic receptor subtype pharmacology and physiology. Prog Med Chem 43, 105-136.
Eglen, R.M., Choppin, A., Dillon, M.P., Hegde, S., 1999. Muscarinic receptor ligands and their therapeutic potential. Curr Opin Chem Biol 3, 426-432.
Eglen, R.M., Hegde, S.S., Watson, N., 1996. Muscarinic receptor subtypes and smooth muscle function. Pharmacol Rev 48, 531-565.
Eglen, R.M., Nahorski, S.R., 2000. The muscarinic M(5) receptor: a silent or emerging subtype? Br J Pharmacol 130, 13-21.
Eldar-Finkelman, H., 2002. Glycogen synthase kinase 3: an emerging therapeutic target. Trends Mol Med 8, 126-132.
Engel, A.G., Lambert, E.H., Gomez, M.R., 1977. A new myasthenic syndrome with end-plate acetylcholinesterase deficiency, small nerve terminals, and reduced acetylcholine release. Ann Neurol 1, 315-330.
Engel, A.G., Lambert, E.H., Mulder, D.M., Torres, C.F., Sahashi, K., Bertorini, T.E., Whitaker, J.N., 1982. A newly recognized congenital myasthenic syndrome attributed to a prolonged open time of the acetylcholine-induced ion channel. Ann Neurol 11, 553-569.
Engel, A.G., Shen, X.M., Selcen, D., Sine, S.M., 2015. Congenital myasthenic syndromes: pathogenesis, diagnosis, and treatment. Lancet Neurol 14, 420-434.
Espada, S., Rojo, A.I., Salinas, M., Cuadrado, A., 2009. The muscarinic M1 receptor activates Nrf2 through a signaling cascade that involves protein kinase C and inhibition of GSK-3beta: connecting neurotransmission with neuroprotection. Journal of neurochemistry 110, 1107-1119.
Faludi, G., Mirnics, K., 2011. Synaptic changes in the brain of subjects with schizophrenia. Int J Dev Neurosci 29, 305-309.
Fatt, P., 1954. Biophysics of junctional transmission. Physiol Rev 34, 674-710.

Felder, C.C., 1995. Muscarinic acetylcholine receptors: signal transduction through multiple effectors. FASEB J 9, 619-625.
Felder, C.C., Bymaster, F.P., Ward, J., DeLapp, N., 2000. Therapeutic opportunities for muscarinic receptors in the central nervous system. J Med Chem 43, 4333-4353.
Feng, H., Hope, I.A., 2013. The Caenorhabditis elegans homeobox gene ceh-19 is required for MC motorneuron function. Genesis 51, 163-178.
Finney, M., Ruvkun, G., 1990. The unc-86 gene product couples cell lineage and cell identity in C. elegans. Cell 63, 895-905.
Fisher, A., Heldman, E., Gurwitz, D., Haring, R., Karton, Y., Meshulam, H., Pittel, Z., Marciano, D., Brandeis, R., Sadot, E., Barg, Y., Pinkas-Kramarski, R., Vogel, Z., Ginzburg, I., Treves, T.A., Verchovsky, R., Klimowsky, S., Korczyn, A.D., 1996. M1 agonists for the treatment of Alzheimer's disease. Novel properties and clinical update. Ann N Y Acad Sci 777, 189-196.
Fleming, J.T., Squire, M.D., Barnes, T.M., Tornoe, C., Matsuda, K., Ahnn, J., Fire, A., Sulston, J.E., Barnard, E.A., Sattelle, D.B., Lewis, J.A., 1997. Caenorhabditis elegans levamisole resistance genes lev-1, unc-29, and unc-38 encode functional nicotinic acetylcholine receptor subunits. J Neurosci 17, 5843-5857.
Francis, M.M., Evans, S.P., Jensen, M., Madsen, D.M., Mancuso, J., Norman, K.R., Maricq, A.V., 2005. The Ror receptor tyrosine kinase CAM-1 is required for ACR-16-mediated synaptic transmission at the C. elegans neuromuscular junction. Neuron 46, 581-594.
Gally, C., Eimer, S., Richmond, J.E., Bessereau, J.L., 2004. A transmembrane protein required for acetylcholine receptor clustering in Caenorhabditis elegans. Nature 431, 578-582.
Galzi, J.L., Changeux, J.P., 1995. Neuronal nicotinic receptors: molecular organization and regulations. Neuropharmacology 34, 563-582.
Gassmann, M., Bettler, B., 2012. Regulation of neuronal GABA(B) receptor functions by subunit composition. Nat Rev Neurosci 13, 380-394.
Ghai, V., Smit, R.B., Gaudet, J., 2012. Transcriptional regulation of HLH-6-independent and subtype-specific genes expressed in the Caenorhabditis elegans pharyngeal glands. Mech Dev 129, 284-297.
Gilhus, N.E., 2016. Myasthenia Gravis. N Engl J Med 375, 2570-2581.
Golden, J.W., Riddle, D.L., 1982. A pheromone influences larval development in the nematode Caenorhabditis elegans. Science 218, 578-580.
Goodman, M.B., Hall, D.H., Avery, L., Lockery, S.R., 1998. Active currents regulate sensitivity and dynamic range in C. elegans neurons. Neuron 20, 763-772.
Gotti, C., Clementi, F., 2004. Neuronal nicotinic receptors: from structure to pathology. Prog Neurobiol 74, 363-396.
Hall, D.H., Hedgecock, E.M., 1991. Kinesin-related gene unc-104 is required for axonal transport of synaptic vesicles in C. elegans. Cell 65, 837-847.
Hall, D.H., Lints, R., Altun, Z., 2006. Nematode neurons: anatomy and anatomical methods in Caenorhabditis elegans. Int Rev Neurobiol 69, 1-35.
Hanger, D.P., Mann, D.M., Neary, D., Anderton, B.H., 1992. Molecular pathology of Alzheimer's disease in sporadic and familial Alzheimer's disease with mutations in the amyloid precursor protein. Biochemical Society transactions 20, 642-645.
Hao, L., Johnsen, R., Lauter, G., Baillie, D., Burglin, T.R., 2006. Comprehensive analysis of gene expression patterns of hedgehog-related genes. BMC Genomics 7, 280.
Harfe, B.D., Fire, A., 1998. Muscle and nerve-specific regulation of a novel NK-2 class homeodomain factor in Caenorhabditis elegans. Development 125, 421-429.
Helmchen, F., Imoto, K., Sakmann, B., 1996. Ca2+ buffering and action potential-evoked Ca2+ signaling in dendrites of pyramidal neurons. Biophys J 70, 1069-1081.

Hersch, S.M., Gutekunst, C.A., Rees, H.D., Heilman, C.J., Levey, A.I., 1994. Distribution of m1-m4 muscarinic receptor proteins in the rat striatum: light and electron microscopic immunocytochemistry using subtype-specific antibodies. J Neurosci 14, 3351-3363.

Hobert, O., 2005. Specification of the nervous system. WormBook : the online review of C. elegans biology, 1-19.

Hobson, R.J., Geng, J., Gray, A.D., Komuniecki, R.W., 2003. SER-7b, a constitutively active Galphas coupled 5-HT7-like receptor expressed in the Caenorhabditis elegans M4 pharyngeal motorneuron. Journal of neurochemistry 87, 22-29.

Hodgkin, A.L., Huxley, A.F., 1952. A quantitative description of membrane current and its application to conduction and excitation in nerve. J Physiol 117, 500-544.

Horikawa, K., Yamada, Y., Matsuda, T., Kobayashi, K., Hashimoto, M., Matsu-ura, T., Miyawaki, A., Michikawa, T., Mikoshiba, K., Nagai, T., 2010. Spontaneous network activity visualized by ultrasensitive Ca(2+) indicators, yellow Cameleon-Nano. Nat Methods 7, 729-732.

Huang da, W., Sherman, B.T., Lempicki, R.A., 2009. Systematic and integrative analysis of large gene lists using DAVID bioinformatics resources. Nat Protoc 4, 44-57.

Huang, D.W., Sherman, B.T., Tan, Q., Collins, J.R., Alvord, W.G., Roayaei, J., Stephens, R., Baseler, M.W., Lane, H.C., Lempicki, R.A., 2007. The DAVID Gene Functional Classification Tool: a novel biological module-centric algorithm to functionally analyze large gene lists. Genome Biol 8, R183.

Huganir, R.L., Greengard, P., 1990. Regulation of neurotransmitter receptor desensitization by protein phosphorylation. Neuron 5, 555-567.

Hulme, S.E., Shevkoplyas, S.S., Apfeld, J., Fontana, W., Whitesides, G.M., 2007. A microfabricated array of clamps for immobilizing and imaging C. elegans. Lab Chip 7, 1515-1523.

Hutchinson, D.O., Walls, T.J., Nakano, S., Camp, S., Taylor, P., Harper, C.M., Groover, R.V., Peterson, H.A., Jamieson, D.G., Engel, A.G., 1993. Congenital endplate acetylcholinesterase deficiency. Brain 116 (Pt 3), 633-653.

Hwang, J.M., Chang, D.J., Kim, U.S., Lee, Y.S., Park, Y.S., Kaang, B.K., Cho, N.J., 1999. Cloning and functional characterization of a Caenorhabditis elegans muscarinic acetylcholine receptor. Receptors Channels 6, 415-424.

Ishii, M., Kurachi, Y., 2006. Muscarinic acetylcholine receptors. Curr Pharm Des 12, 3573-3581.

Iversen, S.D., 1997. Behavioural evaluation of cholinergic drugs. Life Sci 60, 1145-1152.

Jin, Y., 2005. Synaptogenesis. WormBook : the online review of C. elegans biology, 1-11.

Johnson, C.D., Russell, R.L., 1983. Multiple molecular forms of acetylcholinesterase in the nematode Caenorhabditis elegans. Journal of neurochemistry 41, 30-46.

Johnstone, I.L., Barry, J.D., 1996. Temporal reiteration of a precise gene expression pattern during nematode development. EMBO J 15, 3633-3639.

Jones, A.K., Sattelle, D.B., 2004. Functional genomics of the nicotinic acetylcholine receptor gene family of the nematode, Caenorhabditis elegans. Bioessays 26, 39-49.

Jones, C.K., Byun, N., Bubser, M., 2012. Muscarinic and nicotinic acetylcholine receptor agonists and allosteric modulators for the treatment of schizophrenia. Neuropsychopharmacology 37, 16-42.

Kage-Nakadai, E., Imae, R., Yoshina, S., Mitani, S., 2014. Methods for single/low-copy integration by ultraviolet and trimethylpsoralen treatment in Caenorhabditis elegans. Methods 68, 397-402.

Kalamida, D., Poulas, K., Avramopoulou, V., Fostieri, E., Lagoumintzis, G., Lazaridis, K., Sideri, A., Zouridakis, M., Tzartos, S.J., 2007. Muscle and neuronal nicotinic acetylcholine receptors. Structure, function and pathogenicity. FEBS J 274, 3799-3845.

Kamentsky, L., Jones, T.R., Fraser, A., Bray, M.A., Logan, D.J., Madden, K.L., Ljosa, V., Rueden, C., Eliceiri, K.W., Carpenter, A.E., 2011. Improved structure, function and compatibility for CellProfiler: modular high-throughput image analysis software. Bioinformatics 27, 1179-1180.

Karlin, A., Cox, R.N., Dipaola, M., Holtzman, E., Kao, P.N., Lobel, P., Wang, L., Yodh, N., 1986. Functional domains of the nicotinic acetylcholine receptor. Ann N Y Acad Sci 463, 53-69.

Katz, B., 2003. Neural transmitter release: from quantal secretion to exocytosis and beyond. J Neurocytol 32, 437-446.

Katz, B., Miledi, R., 1967. Ionic requirements of synaptic transmitter release. Nature 215, 651.

Katz, B., Miledi, R., 1970. Further study of the role of calcium in synaptic transmission. J Physiol 207, 789-801.

Kerr, R.A., 2006. Imaging the activity of neurons and muscles. WormBook : the online review of C. elegans biology, 1-13.

Kim, K., Li, C., 2004. Expression and regulation of an FMRFamide-related neuropeptide gene family in Caenorhabditis elegans. The Journal of comparative neurology 475, 540-550.

Kramer, J.M., French, R.P., Park, E.C., Johnson, J.J., 1990. The Caenorhabditis elegans rol-6 gene, which interacts with the sqt-1 collagen gene to determine organismal morphology, encodes a collagen. Mol Cell Biol 10, 2081-2089.

Kubo, T., Bujo, H., Akiba, I., Nakai, J., Mishina, M., Numa, S., 1988. Location of a region of the muscarinic acetylcholine receptor involved in selective effector coupling. FEBS Lett 241, 119-125.

Kunitomo, H., Uesugi, H., Kohara, Y., Iino, Y., 2005. Identification of ciliated sensory neuron-expressed genes in Caenorhabditis elegans using targeted pull-down of poly(A) tails. Genome Biol 6, R17.

Lakowski, B., Hekimi, S., 1998. The genetics of caloric restriction in Caenorhabditis elegans. Proc Natl Acad Sci U S A 95, 13091-13096.

Lee, J.S., Min, D.S., Park, C., Park, C.S., Cho, N.J., 2001. Phytosphingosine and C2-phytoceramide induce cell death and inhibit carbachol-stimulated phospholipase D activation in Chinese hamster ovary cells expressing the Caenorhabditis elegans muscarinic acetylcholine receptor. FEBS Lett 499, 82-86.

Lee, R.Y., Lobel, L., Hengartner, M., Horvitz, H.R., Avery, L., 1997. Mutations in the alpha1 subunit of an L-type voltage-activated Ca2+ channel cause myotonia in Caenorhabditis elegans. EMBO J 16, 6066-6076.

Lee, R.Y., Sawin, E.R., Chalfie, M., Horvitz, H.R., Avery, L., 1999. EAT-4, a homolog of a mammalian sodium-dependent inorganic phosphate cotransporter, is necessary for glutamatergic neurotransmission in caenorhabditis elegans. J Neurosci 19, 159-167.

Lee, Y.S., Park, Y.S., Nam, S., Suh, S.J., Lee, J., Kaang, B.K., Cho, N.J., 2000. Characterization of GAR-2, a novel G protein-linked acetylcholine receptor from Caenorhabditis elegans. Journal of neurochemistry 75, 1800-1809.

Leiers, B., Kampkotter, A., Grevelding, C.G., Link, C.D., Johnson, T.E., Henkle-Duhrsen, K., 2003. A stress-responsive glutathione S-transferase confers resistance to oxidative stress in Caenorhabditis elegans. Free Radic Biol Med 34, 1405-1415.

Levey, A.I., 1993. Immunological localization of m1-m5 muscarinic acetylcholine receptors in peripheral tissues and brain. Life Sci 52, 441-448.

Levey, A.I., Edmunds, S.M., Koliatsos, V., Wiley, R.G., Heilman, C.J., 1995. Expression of m1-m4 muscarinic acetylcholine receptor proteins in rat hippocampus and regulation by cholinergic innervation. J Neurosci 15, 4077-4092.

Lewis, J.A., Fleming, J.T., 1995. Basic Culture Methods, Methods in Cell Biology-Caenorhabditis elegans: Modern Biological Analysis of an Organism. Academic Press, San Diego, CA, pp. 4-30.

Li, S., Dent, J.A., Roy, R., 2003. Regulation of intermuscular electrical coupling by the Caenorhabditis elegans innexin inx-6. Molecular biology of the cell 14, 2630-2644.

Lindstrom, J., 1997. Nicotinic acetylcholine receptors in health and disease. Mol Neurobiol 15, 193-222.

Liu, Y., LeBeouf, B., Guo, X., Correa, P.A., Gualberto, D.G., Lints, R., Garcia, L.R., 2011. A cholinergic-regulated circuit coordinates the maintenance and bi-stable states of a sensory-motor behavior during Caenorhabditis elegans male copulation. PLoS genetics 7, e1001326.

Liu, Y., Padgett, D., Takahashi, M., Li, H., Sayeed, A., Teichert, R.W., Olivera, B.M., McArdle, J.J., Green, W.N., Lin, W., 2008. Essential roles of the acetylcholine receptor gamma-subunit in neuromuscular synaptic patterning. Development 135, 1957-1967.

Lutcke, H., Murayama, M., Hahn, T., Margolis, D.J., Astori, S., Zum Alten Borgloh, S.M., Gobel, W., Yang, Y., Tang, W., Kugler, S., Sprengel, R., Nagai, T., Miyawaki, A., Larkum, M.E., Helmchen, F., Hasan, M.T., 2010. Optical recording of neuronal activity with a genetically-encoded calcium indicator in anesthetized and freely moving mice. Front Neural Circuits 4, 9.

Mandelkow, E.M., Drewes, G., Biernat, J., Gustke, N., Van Lint, J., Vandenheede, J.R., Mandelkow, E., 1992. Glycogen synthase kinase-3 and the Alzheimer-like state of microtubule-associated protein tau. FEBS Lett 314, 315-321.

Mank, M., Griesbeck, O., 2008. Genetically encoded calcium indicators. Chem Rev 108, 1550-1564.

Mank, M., Santos, A.F., Direnberger, S., Mrsic-Flogel, T.D., Hofer, S.B., Stein, V., Hendel, T., Reiff, D.F., Levelt, C., Borst, A., Bonhoeffer, T., Hubener, M., Griesbeck, O., 2008. A genetically encoded calcium indicator for chronic in vivo two-photon imaging. Nat Methods 5, 805-811.

Marino, M.J., Rouse, S.T., Levey, A.I., Potter, L.T., Conn, P.J., 1998. Activation of the genetically defined m1 muscarinic receptor potentiates N-methyl-D-aspartate (NMDA) receptor currents in hippocampal pyramidal cells. Proc Natl Acad Sci U S A 95, 11465-11470.

Mathews, E.A., Garcia, E., Santi, C.M., Mullen, G.P., Thacker, C., Moerman, D.G., Snutch, T.P., 2003. Critical residues of the Caenorhabditis elegans unc-2 voltage-gated calcium channel that affect behavioral and physiological properties. J Neurosci 23, 6537-6545.

McKay, J.P., Raizen, D.M., Gottschalk, A., Schafer, W.R., Avery, L., 2004. eat-2 and eat-18 are required for nicotinic neurotransmission in the Caenorhabditis elegans pharynx. Genetics 166, 161-169.

McKay, S.J., Johnsen, R., Khattra, J., Asano, J., Baillie, D.L., Chan, S., Dube, N., Fang, L., Goszczynski, B., Ha, E., Halfnight, E., Hollebakken, R., Huang, P., Hung, K., Jensen, V., Jones, S.J., Kai, H., Li, D., Mah, A., Marra, M., McGhee, J., Newbury, R., Pouzyrev, A., Riddle, D.L., Sonnhammer, E., Tian, H., Tu, D., Tyson, J.R., Vatcher, G., Warner, A., Wong, K., Zhao, Z., Moerman, D.G., 2003. Gene expression profiling of cells, tissues, and developmental stages of the nematode C. elegans. Cold Spring Harb Symp Quant Biol 68, 159-169.

Mellanby, H., 1955. The identification and estimation of acetylcholine in three parasitic nematodes (Ascaris lumbricoides, Litomosoides carinii, and the microfilariae of Dirofilaria repens). Parasitology 45, 287-294.

Mello, C., Fire, A., 1995. DNA Transformation, in: Epstein, H.F., Shakes, D.C. (Eds.), Caenorhabditis elegans: Modern Biological Analysis of an Organism. Academic Press, San Diego, CA, pp. 451-482.

Migeon, J.C., Thomas, S.L., Nathanson, N.M., 1995. Differential coupling of m2 and m4 muscarinic receptors to inhibition of adenylyl cyclase by Gi alpha and G(o)alpha subunits. J Biol Chem 270, 16070-16074.

Min, D.S., Cho, N.J., Yoon, S.H., Lee, Y.H., Hahn, S.J., Lee, K.H., Kim, M.S., Jo, Y.H., 2000. Phospholipase C, protein kinase C, Ca(2+)/calmodulin-dependent protein kinase II, and tyrosine phosphorylation are involved in carbachol-induced phospholipase D activation in Chinese hamster ovary cells expressing muscarinic acetylcholine receptor of Caenorhabditis elegans. Journal of neurochemistry 75, 274-281.

Mishina, M., Takai, T., Imoto, K., Noda, M., Takahashi, T., Numa, S., Methfessel, C., Sakmann, B., 1986. Molecular distinction between fetal and adult forms of muscle acetylcholine receptor. Nature 321, 406-411.

Moll, P., Ante, M., Seitz, A., Reda, T., 2014. QuantSeq 3' mRNA sequencing for RNA quantification. Nat. Meth., i-iii.

Mongan, N.P., Baylis, H.A., Adcock, C., Smith, G.R., Sansom, M.S., Sattelle, D.B., 1998. An extensive and diverse gene family of nicotinic acetylcholine receptor alpha subunits in Caenorhabditis elegans. Receptors Channels 6, 213-228.

Mongan, N.P., Jones, A.K., Smith, G.R., Sansom, M.S., Sattelle, D.B., 2002. Novel alpha7-like nicotinic acetylcholine receptor subunits in the nematode Caenorhabditis elegans. Protein Sci 11, 1162-1171.

Nagai, T., Yamada, S., Tominaga, T., Ichikawa, M., Miyawaki, A., 2004. Expanded dynamic range of fluorescent indicators for Ca(2+) by circularly permuted yellow fluorescent proteins. Proc Natl Acad Sci U S A 101, 10554-10559.

Nagel, G., Brauner, M., Liewald, J.F., Adeishvili, N., Bamberg, E., Gottschalk, A., 2005. Light activation of channelrhodopsin-2 in excitable cells of Caenorhabditis elegans triggers rapid behavioral responses. Curr Biol 15, 2279-2284.

Nagel, G., Szellas, T., Huhn, W., Kateriya, S., Adeishvili, N., Berthold, P., Ollig, D., Hegemann, P., Bamberg, E., 2003. Channelrhodopsin-2, a directly light-gated cation-selective membrane channel. Proc Natl Acad Sci U S A 100, 13940-13945.

Nakai, J., Ohkura, M., Imoto, K., 2001. A high signal-to-noise Ca(2+) probe composed of a single green fluorescent protein. Nat Biotechnol 19, 137-141.

Nakata, K., Abrams, B., Grill, B., Goncharov, A., Huang, X., Chisholm, A.D., Jin, Y., 2005. Regulation of a DLK-1 and p38 MAP kinase pathway by the ubiquitin ligase RPM-1 is required for presynaptic development. Cell 120, 407-420.

Neher, E., 1995. The use of fura-2 for estimating Ca buffers and Ca fluxes. Neuropharmacology 34, 1423-1442.

Ohno, K., Hutchinson, D.O., Milone, M., Brengman, J.M., Bouzat, C., Sine, S.M., Engel, A.G., 1995. Congenital myasthenic syndrome caused by prolonged acetylcholine receptor channel openings due to a mutation in the M2 domain of the epsilon subunit. Proc Natl Acad Sci U S A 92, 758-762.

Okkema, P.G., Ha, E., Haun, C., Chen, W., Fire, A., 1997. The Caenorhabditis elegans NK-2 homeobox gene ceh-22 activates pharyngeal muscle gene expression in combination with pha-1 and is required for normal pharyngeal development. Development 124, 3965-3973.

Okkema, P.G., Harrison, S.W., Plunger, V., Aryana, A., Fire, A., 1993. Sequence requirements for myosin gene expression and regulation in Caenorhabditis elegans. Genetics 135, 385-404.

Okouchi, M., Ekshyyan, O., Maracine, M., Aw, T.Y., 2007. Neuronal apoptosis in neurodegeneration. Antioxid Redox Signal 9, 1059-1096.

Palmer, A.E., Giacomello, M., Kortemme, T., Hires, S.A., Lev-Ram, V., Baker, D., Tsien, R.Y., 2006. Ca2+ indicators based on computationally redesigned calmodulin-peptide pairs. Chem Biol 13, 521-530.

Park, Y.S., Kim, S., Shin, Y., Choi, B., Cho, N.J., 2003. Alternative splicing of the muscarinic acetylcholine receptor GAR-3 in Caenorhabditis elegans. Biochemical and biophysical research communications 308, 961-965.

Park, Y.S., Lee, Y.S., Cho, N.J., Kaang, B.K., 2000. Alternative splicing of gar-1, a Caenorhabditis elegans G-protein-linked acetylcholine receptor gene. Biochemical and biophysical research communications 268, 354-358.

Payandeh, J., Scheuer, T., Zheng, N., Catterall, W.A., 2011. The crystal structure of a voltage-gated sodium channel. Nature 475, 353-358.

Pereira, L., Kratsios, P., Serrano-Saiz, E., Sheftel, H., Mayo, A.E., Hall, D.H., White, J.G., LeBoeuf, B., Garcia, L.R., Alon, U., Hobert, O., 2015. A cellular and regulatory map of the cholinergic nervous system of C. elegans. Elife 4.

Perez-Reyes, E., 2003. Molecular physiology of low-voltage-activated t-type calcium channels. Physiol Rev 83, 117-161.

Peters, M.A., Teramoto, T., White, J.Q., Iwasaki, K., Jorgensen, E.M., 2007. A calcium wave mediated by gap junctions coordinates a rhythmic behavior in C. elegans. Curr Biol 17, 1601-1608.

Petrov, K.A., Girard, E., Nikitashina, A.D., Colasante, C., Bernard, V., Nurullin, L., Leroy, J., Samigullin, D., Colak, O., Nikolsky, E., Plaud, B., Krejci, E., 2014. Schwann cells sense and control acetylcholine spillover at the neuromuscular junction by alpha7 nicotinic receptors and butyrylcholinesterase. J Neurosci 34, 11870-11883.

Phelan, P., Starich, T.A., 2001. Innexins get into the gap. Bioessays 23, 388-396.

Plazas, P.V., Katz, E., Gomez-Casati, M.E., Bouzat, C., Elgoyhen, A.B., 2005. Stoichiometry of the alpha9alpha10 nicotinic cholinergic receptor. J Neurosci 25, 10905-10912.

Pocklington, A.J., O'Donovan, M., Owen, M.J., 2014. The synapse in schizophrenia. Eur J Neurosci 39, 1059-1067.

Pocock, R., Hobert, O., 2010. Hypoxia activates a latent circuit for processing gustatory information in C. elegans. Nature neuroscience 13, 610-614.

Raftery, M.A., Hunkapiller, M.W., Strader, C.D., Hood, L.E., 1980. Acetylcholine receptor: complex of homologous subunits. Science 208, 1454-1456.

Raizen, D.M., Avery, L., 1994. Electrical activity and behavior in the pharynx of Caenorhabditis elegans. Neuron 12, 483-495.

Raizen, D.M., Lee, R.Y., Avery, L., 1995. Interacting genes required for pharyngeal excitation by motor neuron MC in Caenorhabditis elegans. Genetics 141, 1365-1382.

Ramakrishnan, K., 2014. CEH-28 and ZAG-1 function in regulating defferentiation of C. elegans M4 pharyngeal neuron, Biological Sciences. Universty of Illinois at Chicago, p. 203.

Ramakrishnan, K., Okkema, P.G., 2014. Regulation of C. elegans neuronal differentiation by the ZEB-family factor ZAG-1 and the NK-2 homeodomain factor CEH-28. PLoS One 9, e113893.

Ramakrishnan, K., Ray, P., Okkema, P.G., 2014. CEH-28 activates dbl-1 expression and TGF-beta signaling in the C. elegans M4 neuron. Dev Biol 390, 149-159.

Rand, J.B., 1989. Genetic analysis of the cha-1-unc-17 gene complex in Caenorhabditis. Genetics 122, 73-80.

Rand, J.B., Russell, R.L., 1985. Properties and partial purification of choline acetyltransferase from the nematode Caenorhabditis elegans. Journal of neurochemistry 44, 189-200.

Rathouz, M.M., Berg, D.K., 1994. Synaptic-type acetylcholine receptors raise intracellular calcium levels in neurons by two mechanisms. J Neurosci 14, 6935-6945.

Ray, P., Schnabel, R., Okkema, P.G., 2008. Behavioral and synaptic defects in C. elegans lacking the NK-2 homeobox gene ceh-28. Dev Neurobiol 68, 421-433.
Rice, M.E., Cragg, S.J., 2008. Dopamine spillover after quantal release: rethinking dopamine transmission in the nigrostriatal pathway. Brain Res Rev 58, 303-313.
Richmond, J.E., Broadie, K.S., 2002. The synaptic vesicle cycle: exocytosis and endocytosis in Drosophila and C. elegans. Curr Opin Neurobiol 12, 499-507.
Richmond, J.E., Jorgensen, E.M., 1999. One GABA and two acetylcholine receptors function at the C. elegans neuromuscular junction. Nature neuroscience 2, 791-797.
Riddle, D.L., Blumenthal, T., Meyer, B.J., Priess, J.R., 1997. Introduction to C. elegans, in: Riddle, D.L., Blumenthal, T., Meyer, B.J., Priess, J.R. (Eds.), C. elegans II, 2nd ed, Cold Spring Harbor (NY).
Rostaing, P., Weimer, R.M., Jorgensen, E.M., Triller, A., Bessereau, J.L., 2004. Preservation of immunoreactivity and fine structure of adult C. elegans tissues using high-pressure freezing. J Histochem Cytochem 52, 1-12.
Rotundo, R.L., 2003. Expression and localization of acetylcholinesterase at the neuromuscular junction. J Neurocytol 32, 743-766.
Rouse, S.T., Marino, M.J., Potter, L.T., Conn, P.J., Levey, A.I., 1999. Muscarinic receptor subtypes involved in hippocampal circuits. Life Sci 64, 501-509.
Ruaud, A.F., Bessereau, J.L., 2006. Activation of nicotinic receptors uncouples a developmental timer from the molting timer in C. elegans. Development 133, 2211-2222.
Saur, T., DeMarco, S.E., Ortiz, A., Sliwoski, G.R., Hao, L., Wang, X., Cohen, B.M., Buttner, E.A., 2013. A genome-wide RNAi screen in Caenorhabditis elegans identifies the nicotinic acetylcholine receptor subunit ACR-7 as an antipsychotic drug target. PLoS genetics 9, e1003313.
Schafer, W.R., 2005. Deciphering the neural and molecular mechanisms of C. elegans behavior. Curr Biol 15, R723-729.
Schafer, W.R., Kenyon, C.J., 1995. A calcium-channel homologue required for adaptation to dopamine and serotonin in Caenorhabditis elegans. Nature 375, 73-78.
Schindelin, J., Arganda-Carreras, I., Frise, E., Kaynig, V., Longair, M., Pietzsch, T., Preibisch, S., Rueden, C., Saalfeld, S., Schmid, B., Tinevez, J.Y., White, D.J., Hartenstein, V., Eliceiri, K., Tomancak, P., Cardona, A., 2012. Fiji: an open-source platform for biological-image analysis. Nat Methods 9, 676-682.
Seymour, M.K., Wright, K.A., Doncaster, C.C., 1983. The action of the anterior feeding apparatus of *C. elegans* (Nematoda: Rhabditida). Journal of Zoological Society of London 201, 527-539.
Sharma, G., Vijayaraghavan, S., 2001. Nicotinic cholinergic signaling in hippocampal astrocytes involves calcium-induced calcium release from intracellular stores. Proc Natl Acad Sci U S A 98, 4148-4153.
Shimozono, S., Fukano, T., Kimura, K.D., Mori, I., Kirino, Y., Miyawaki, A., 2004. Slow Ca2+ dynamics in pharyngeal muscles in Caenorhabditis elegans during fast pumping. EMBO Rep 5, 521-526.
Shoop, R.D., Chang, K.T., Ellisman, M.H., Berg, D.K., 2001. Synaptically driven calcium transients via nicotinic receptors on somatic spines. J Neurosci 21, 771-781.
Shtonda, B., Avery, L., 2005. CCA-1, EGL-19 and EXP-2 currents shape action potentials in the Caenorhabditis elegans pharynx. J Exp Biol 208, 2177-2190.
Sieburth, D., Ch'ng, Q., Dybbs, M., Tavazoie, M., Kennedy, S., Wang, D., Dupuy, D., Rual, J.F., Hill, D.E., Vidal, M., Ruvkun, G., Kaplan, J.M., 2005. Systematic analysis of genes required for synapse structure and function. Nature 436, 510-517.
Skaper, S.D., Facci, L., Zusso, M., Giusti, P., 2017. Synaptic Plasticity, Dementia and Alzheimer Disease. CNS Neurol Disord Drug Targets 16, 220-233.

Song, B.M., Avery, L., 2012. Serotonin activates overall feeding by activating two separate neural pathways in Caenorhabditis elegans. J Neurosci 32, 1920-1931.
Spooren, W., Lindemann, L., Ghosh, A., Santarelli, L., 2012. Synapse dysfunction in autism: a molecular medicine approach to drug discovery in neurodevelopmental disorders. Trends Pharmacol Sci 33, 669-684.
Stanchev, D., Sargent, P.B., 2011. alpha7-Containing and non-alpha7-containing nicotinic receptors respond differently to spillover of acetylcholine. J Neurosci 31, 14920-14930.
Starich, T.A., Lee, R.Y., Panzarella, C., Avery, L., Shaw, J.E., 1996. eat-5 and unc-7 represent a multigene family in Caenorhabditis elegans involved in cell-cell coupling. J Cell Biol 134, 537-548.
Starr, D.A., Han, M., 2002. Role of ANC-1 in tethering nuclei to the actin cytoskeleton. Science 298, 406-409.
Steger, K.A., Avery, L., 2004. The GAR-3 muscarinic receptor cooperates with calcium signals to regulate muscle contraction in the Caenorhabditis elegans pharynx. Genetics 167, 633-643.
Steger, K.A., Shtonda, B.B., Thacker, C., Snutch, T.P., Avery, L., 2005. The C. elegans T-type calcium channel CCA-1 boosts neuromuscular transmission. J Exp Biol 208, 2191-2203.
Stuyvers, B.D., Boyden, P.A., ter Keurs, H.E., 2000. Calcium waves: physiological relevance in cardiac function. Circ Res 86, 1016-1018.
Suh, S.J., Park, Y.S., Lee, Y.S., Cho, T.J., Kaang, B.K., Cho, N.J., 2001. Three functional isoforms of GAR-2, a Caenorhabditis elegans G-protein-linked acetylcholine receptor, are produced by alternative splicing. Biochemical and biophysical research communications 288, 1238-1243.
Sulston, J.E., Horvitz, H.R., 1977. Post-embryonic cell lineages of the nematode, Caenorhabditis elegans. Dev Biol 56, 110-156.
Sulston, J.E., Schierenberg, E., White, J.G., Thomson, J.N., 1983. The embryonic cell lineage of the nematode Caenorhabditis elegans. Dev Biol 100, 64-119.
Sutphin, G.L., Kaeberlein, M., 2009. Measuring Caenorhabditis elegans life span on solid media. J Vis Exp.
Takayama, J., Faumont, S., Kunitomo, H., Lockery, S.R., Iino, Y., 2010. Single-cell transcriptional analysis of taste sensory neuron pair in Caenorhabditis elegans. Nucleic Acids Res 38, 131-142.
Talesa, V., Culetto, E., Schirru, N., Bernardi, H., Fedon, Y., Toutant, J.P., Arpagaus, M., 1995. Characterization of a null mutation in ace-1, the gene encoding class A acetylcholinesterase in the nematode Caenorhabditis elegans. FEBS Lett 357, 265-268.
Tang, Z.Z., Yarotskyy, V., Wei, L., Sobczak, K., Nakamori, M., Eichinger, K., Moxley, R.T., Dirksen, R.T., Thornton, C.A., 2012. Muscle weakness in myotonic dystrophy associated with misregulated splicing and altered gating of Ca(V)1.1 calcium channel. Human molecular genetics 21, 1312-1324.
Tedford, H.W., Zamponi, G.W., 2006. Direct G protein modulation of Cav2 calcium channels. Pharmacol Rev 58, 837-862.
Thestrup, T., Litzlbauer, J., Bartholomaus, I., Mues, M., Russo, L., Dana, H., Kovalchuk, Y., Liang, Y., Kalamakis, G., Laukat, Y., Becker, S., Witte, G., Geiger, A., Allen, T., Rome, L.C., Chen, T.W., Kim, D.S., Garaschuk, O., Griesinger, C., Griesbeck, O., 2014. Optimized ratiometric calcium sensors for functional in vivo imaging of neurons and T lymphocytes. Nat Methods 11, 175-182.
Thevenaz, P., Ruttimann, U.E., Unser, M., 1998. A pyramid approach to subpixel registration based on intensity. IEEE Trans Image Process 7, 27-41.
Tian, L., Hires, S.A., Mao, T., Huber, D., Chiappe, M.E., Chalasani, S.H., Petreanu, L., Akerboom, J., McKinney, S.A., Schreiter, E.R., Bargmann, C.I., Jayaraman, V., Svoboda,

K., Looger, L.L., 2009. Imaging neural activity in worms, flies and mice with improved GCaMP calcium indicators. Nat Methods 6, 875-881.
Touroutine, D., Fox, R.M., Von Stetina, S.E., Burdina, A., Miller, D.M., 3rd, Richmond, J.E., 2005. acr-16 encodes an essential subunit of the levamisole-resistant nicotinic receptor at the Caenorhabditis elegans neuromuscular junction. J Biol Chem 280, 27013-27021.
Trapnell, C., Roberts, A., Goff, L., Pertea, G., Kim, D., Kelley, D.R., Pimentel, H., Salzberg, S.L., Rinn, J.L., Pachter, L., 2012. Differential gene and transcript expression analysis of RNA-seq experiments with TopHat and Cufflinks. Nat Protoc 7, 562-578.
Unwin, N., Miyazawa, A., Li, J., Fujiyoshi, Y., 2002. Activation of the nicotinic acetylcholine receptor involves a switch in conformation of the alpha subunits. J Mol Biol 319, 1165-1176.
Vallejo-Illarramendi, A., Toral-Ojeda, I., Aldanondo, G., Lopez de Munain, A., 2014. Dysregulation of calcium homeostasis in muscular dystrophies. Expert Rev Mol Med 16, e16.
Varoqui, H., Diebler, M.F., Meunier, F.M., Rand, J.B., Usdin, T.B., Bonner, T.I., Eiden, L.E., Erickson, J.D., 1994. Cloning and expression of the vesamicol binding protein from the marine ray Torpedo. Homology with the putative vesicular acetylcholine transporter UNC-17 from Caenorhabditis elegans. FEBS Lett 342, 97-102.
Vilaro, M.T., Mengod, G., Palacios, J.M., 1993. Advances and limitations of the molecular neuroanatomy of cholinergic receptors: the example of multiple muscarinic receptors. Prog Brain Res 98, 95-101.
Von Stetina, S.E., Watson, J.D., Fox, R.M., Olszewski, K.L., Spencer, W.C., Roy, P.J., Miller, D.M., 3rd, 2007. Cell-specific microarray profiling experiments reveal a comprehensive picture of gene expression in the C. elegans nervous system. Genome Biol 8, R135.
Walker, R.H., Jung, H.H., Dobson-Stone, C., Rampoldi, L., Sano, A., Tison, F., Danek, A., 2007. Neurologic phenotypes associated with acanthocytosis. Neurology 68, 92-98.
Weimer, R.M., Jorgensen, E.M., 2003. Controversies in synaptic vesicle exocytosis. J Cell Sci 116, 3661-3666.
Wess, J., 1996. Molecular biology of muscarinic acetylcholine receptors. Crit Rev Neurobiol 10, 69-99.
Wess, J., 2004. Muscarinic acetylcholine receptor knockout mice: novel phenotypes and clinical implications. Annu Rev Pharmacol Toxicol 44, 423-450.
Wheeler, S.V., Jane, S.D., Cross, K.M., Chad, J.E., Foreman, R.C., 1994. Membrane clustering and bungarotoxin binding by the nicotinic acetylcholine receptor: role of the beta subunit. Journal of neurochemistry 63, 1891-1899.
White, J.G., Southgate, E., Thomson, J.N., Brenner, S., 1976. The structure of the ventral nerve cord of Caenorhabditis elegans. Philos Trans R Soc Lond B Biol Sci 275, 327-348.
White, J.G., Southgate, E., Thomson, J.N., Brenner, S., 1986. The Structure of the Nervous System of the Nematode Caenorhabditis elegans. Philosophical Transactions of the Royal Society of London. B, Biological Sciences 314, 1-340.
Wijesekera, L.C., Leigh, P.N., 2009. Amyotrophic lateral sclerosis. Orphanet J Rare Dis 4, 3.
Witzemann, V., Barg, B., Nishikawa, Y., Sakmann, B., Numa, S., 1987. Differential regulation of muscle acetylcholine receptor gamma- and epsilon-subunit mRNAs. FEBS Lett 223, 104-112.
Wolfe, B.B., Yasuda, R.P., 1995. Development of selective antisera for muscarinic cholinergic receptor subtypes. Ann N Y Acad Sci 757, 186-193.
Yamada, M., Lamping, K.G., Duttaroy, A., Zhang, W., Cui, Y., Bymaster, F.P., McKinzie, D.L., Felder, C.C., Deng, C.X., Faraci, F.M., Wess, J., 2001a. Cholinergic dilation of cerebral blood vessels is abolished in M(5) muscarinic acetylcholine receptor knockout mice. Proc Natl Acad Sci U S A 98, 14096-14101.

Yamada, M., Miyakawa, T., Duttaroy, A., Yamanaka, A., Moriguchi, T., Makita, R., Ogawa, M., Chou, C.J., Xia, B., Crawley, J.N., Felder, C.C., Deng, C.X., Wess, J., 2001b. Mice lacking the M3 muscarinic acetylcholine receptor are hypophagic and lean. Nature 410, 207-212.

Yasuda, R., Nimchinsky, E.A., Scheuss, V., Pologruto, T.A., Oertner, T.G., Sabatini, B.L., Svoboda, K., 2004. Imaging calcium concentration dynamics in small neuronal compartments. Sci STKE 2004, pl5.

Zhang, S., Banerjee, D., Kuhn, J.R., 2011. Isolation and culture of larval cells from C. elegans. PLoS One 6, e19505.

Zhen, M., Jin, Y., 2004. Presynaptic terminal differentiation: transport and assembly. Curr Opin Neurobiol 14, 280-287.

Zhou, Z., Neher, E., 1993. Mobile and immobile calcium buffers in bovine adrenal chromaffin cells. J Physiol 469, 245-273.

Zucker, R.S., Regehr, W.G., 2002. Short-term synaptic plasticity. Annu Rev Physiol 64, 355-405.

Zwaal, R.R., Van Baelen, K., Groenen, J.T., van Geel, A., Rottiers, V., Kaletta, T., Dode, L., Raeymaekers, L., Wuytack, F., Bogaert, T., 2001. The sarco-endoplasmic reticulum Ca2+ ATPase is required for development and muscle function in Caenorhabditis elegans. J Biol Chem 276, 43557-43563.

VITA

ALENA KOZLOVA

PROFESSIONAL SUMMARY

- Knowledgeable innovator and problem solver with advanced skills in developmental, molecular biology, neurobiology, immunology and genetics as evidenced by 3 publications (and 2 papers in preparation) and discovery of a novel cellular mechanism of neuromuscular communication.
- Self-motivated and thorough researcher with a meticulous and rigorous approach to experiment accuracy as demonstrated by performance of technically challenging experiments, which led to $20,000 grant funding.
- Excellent speaker with ability to organize and communicate ideas effectively to small and large groups as evidenced by 5 poster and 2 oral presentations at the local and international conferences.
- Strong leader and relationship builder with organizational skills as evidenced by being a founder of Journal and Troubleshooting Club, Writing Club and organizer of career panel for the Graduate Students.
- Highly dedicated analyst with ability to define a problem and identify possible causes as well as comprehend large amounts of information.
- Inspiring mentor with strong ability to teach skills or concepts and motivate others to complete projects as demonstrated by teaching 4 different Biological sciences Lab courses at UIC and successful mentorship a number of undergraduate students.

PROFESSIONAL EXPERIENCE

Doctoral Research **August 2011 – December 2017**

University of Illinois at Chicago, Chicago IL
Department of Biological Sciences
Advisor: Peter G. Okkema, Ph.D.
Dissertation: Characterization of neuromuscular communication in *C. elegans* pharynx.

Research focused on understanding the mechanisms of neuromuscular disorders (myotonic dystrophy, myasthenic syndrome) on molecular level using *C. elegans* as a model organism. Functional relationship between two acetylcholine receptors was shown to be important for proper communication between a neuron and a muscle cell.

Research Technician **October 2008 – April 2011**

University of Chicago, Chicago, IL
Department of Microbiology
Advisor: Tatyana V. Golovkina, Ph.D.
Research project: Identification of host cell proteins interacting with the Gag protein of MMTV in murine mammary tumors.

Undergraduate Honors Thesis Research **June 2007 – June 2008**

Institute of Bioorganic Chemistry, Moscow, Russia
Russian Academy of Science
Advisor: Tatyana Azhikina, Ph.D.
Thesis: Development of malignant tissue prognosis approach based on the level of methylation heterogeneity.

Undergraduate Researcher **June 2006 – June 2007**
Institute of Bioorganic Chemistry, Moscow, Russia
Russian Academy of Science
Advisor: Tatyana Azhikina, Ph.D.
Research Project: Analysis of non-methylated CpG-sites distribution in ATP4A-UPK1A (Chr19) locus in 293T cell line.

TECHNICAL SKILLS

Molecular Biology and Biochemistry	Plasmid and genomic DNA isolation, RNA isolation
	Gene cloning, Gateway and TOPO cloning
	PCR, RT-PCR, qPCR,
	Colony lifting
	FACS analysis
	Immunostaining, Immunofluorescent microscopy
	Fluorescent microscopy, time-lapse microscopy
	Ca^{2+} (GCaMP3) imaging
	Northern blotting, Southern blotting
	DNA sequence analysis
	Bisulfate sequencing
	Next Generation mRNA sequencing
	Protein isolation from cell culture and tissue samples
	Protein coimmunoprecipitation (co-IP), mRNA co-IP
	Western blotting, ELISA
	Mass spec data analysis
Cell culture	Human cell line maintenance
	Plasmid transfection, viral transfection
Animal models	Drosophila, *C. elegans*
	Mouse handling and techniques
	Fine tissue dissections
	Generation of transgenic animals
	Behavioral assays, genotyping
Software	MATLAB, MXPro-Mx3000P, Original Pro 7.5
	Gel-Pro Analyzer 3.1, VisionWorksLS, Gene Runner
	Photoshop CS6, Microsoft Office, Adobe Illustrator
	BLAST, BLAT, Bisearch, Lasergene 8.0, FlowJo 7.5, Zenn
	MacVector, ImageJ, FiJi, Pymol

EDUCATION

University of Illinois at Chicago, Chicago, IL, USA **December 2017**
Doctor of Philosophy in Molecular, Cellular, and Developmental Biology
Area of Specialization: Developmental Biology, Genetics and Neurobiology

Lomonosov Moscow State University, Moscow, Russia **June 2008**
Bachelor of Science in Biology
Diploma with Highest Honors, Department of Biochemistry

PEER-REVIEWED PUBLICATIONS

Kane M, Case LK, Kopaskie K, **Kozlova A**, MacDearmid C, Chervonsky AV, Golovkina TV. *Successful transmission of a retrovirus depends on the commensal microbiota.* Science. 2011 Oct; 14;334(6053):245-9.

Bulanenkova SS, **Kozlova AA**, Kotova ES, Snezhkov EV, Azhikina TL, Akopov SB, Nikolaev LG, Sverdlov ED. *Dam methylase accessibility as an instrument for analysis of mammalian chromatin structure. Epigenetics*. 2011 Sep; 1;6(9):1078-84.

Azhikina T, **Kozlova A**, Skvortsov T, Sverdlov E. *Heterogeneity and degree of TIMP4, GATA4, SOX18, and EGFL7 gene promoter methylation in non-small cell lung cancer and surrounding tissues.* Cancer Genet. 2011 Sep; 204(9):492-500

MANUSCRIPTS IN PREPARATION

Kozlova, A.A. and **Okkema, P.G.** *Crosstalk between acetylcholine receptors affects signaling at the neuromuscular junction in the Caenorhabditis elegans pharynx*. (Submitted)

Kozlova, A.A. and **Okkema, P.G.** *CEH-28 affects neuromuscular communication in C. elegans pharynx*. (In preparation)

CONFERENCES PRESENTATIONS

Alena Kozlova, Michelle Lotfi and Peter Okkema. July 2016. The EAT-2 and GAR-3 acetylcholine receptors have distinct effects on pharyngeal muscle peristalsis. Genetics Society of America. The Allied Genetics 2016 Conference, Orlando, FL. (**Poster presentation**)

Alena Kozlova, Michelle Lotfi and Peter Okkema. April 2016. Unexpected and antagonistic function for the EAT-2 and GAR-3 acetylcholine receptors during pharyngeal muscle peristalsis. 4th annual Midwest *C. elegans* meeting, Van Andel Research Institute in Grand Rapids, MI. (**Oral presentation**)

Alena Kozlova, Kalpana Ramakrishnan and Peter Okkema. June 2015. Using optical and molecular approaches to understand M4 neuronal defects in *ceh-28* mutants. Genetics Society of America. 20th International *C. elegans* meeting, UCLA, Los Angeles, CA. (**Poster presentation**)

Alena Kozlova, Michelle Lotfi and Peter Okkema. June 2015. The EAT-2 and GAR-3 acetylcholine receptors have distinct effects on pharyngeal muscle peristalsis. Genetics Society of America. 20th International *C. elegans* meeting, UCLA, Los Angeles, CA. (**Poster presentation**)

Alena Kozlova, Sana Hussain and Peter Okkema. June 2013. Characterization of Ca^{2+} dynamics in the M4 neuron using GCaMP3. Genetics Society of America. 19th International *C. elegans* meeting, UCLA, Los Angeles, CA. (**Poster presentation**)

Alena Kozlova and Tatyana Azhikina. August 2007. Development of malignant tissue prognosis approach based on the level of methylation heterogeneity. Spetses International Summer School 2007, Federation of European Biochemical Societies (FEBS), Island of Spetses, Greece. (**Poster presentation**)

LEADERSHIP EXPERIENCE

Organized Journal and Troubleshooting Club for Graduate students in the Department of Biological Sciences at UIC — **Fall 2013 – Spring 2015**

Organized a career panel "Jobs outside academia" for Graduate students at UIC — **Spring 2016**

Organized Writing Club for Graduate students in the Department of Biological Sciences at UIC — **Summer, Fall 2017**

AWARDS

Graduate College Student Presenter Award	University of Illinois at Chicago Biological Sciences	**2013, 2016**
Department of Biological Sciences Travel Award	University of Illinois at Chicago Biological Sciences	**2013, 2015, 2016**
PhD Student Travel Award	University of Illinois at Chicago Liberal Arts and Sciences	**2013, 2016**
Graduate Student Council Travel Award	University of Illinois at Chicago Graduate School	**2016**

TEACHING EXPERIENCE

University of Illinois at Chicago

Teaching Assistant: Cell Biology Laboratory	**Fall 2015, Spring 2017**
Teaching Assistant: Molecular Biology Laboratory	**Fall 2016, 2017**
Teaching Assistant: Developmental Biology Laboratory	**Spring 2014, 2015, 2016**
Teaching Assistant: Microbiology Laboratory	**Fall 2011 - Spring 2013**

MENTORSHIP EXPERIENCE

Sana Hussain	Undergraduate Honors Program, UIC	**Fall 2012 – Spring 2013**
Michelle Lotfi	Undergraduate Honors Program, UIC	**Fall 2013 – Spring 2015**
Zhihua Li	Undergraduate Honors Program, UIC	**Fall 2015 – Spring 2017**
Arjun Balyan	Graduate Researcher	**Fall 2013**
Lorna Cohen	Graduate Researcher	**Fall 2013**

PROFESSIONAL ASSOCIATIONS

Genetic Society of America (GSA)	**since March 2015**
Graduate Women In Science (GWIS), Eta Chapter, Chicago	**since May 2015**
C. elegans Worm Club, Chicago	**since January 2015**

INTERESTS

Baking, knitting, crafting, mediatation, playing piano.